

Atmospheric Degradation of Amines (ADA)

Summary report from atmospheric chemistry
studies of amines, nitrosamines, nitramines
and amides



CLIMIT project no. 208122

C.J. Nielsen, B. D'Anna, R. Bossi, A.J.C. Buncan, L. Dithmer, M. Glasius,
M. Hallquist, A.M.K. Hansen, A. Lutz, K. Salo, M.M. Maguta, Q. Nguyen, T. Mikoviny,
M. Müller, H. Skov, E. Sarrasin, Y. Stenstrøm, Y. Tang, J. Westerlund and A. Wisthaler

About the Atmospheric Degradation of Amines project

CLIMIT has awarded CTCC three contracts (2009 – 193438; 2010 – 201604; 2011 – 208122) for the project “Atmospheric Degradation of Amines - ADA”. The project was supported by industrial partners:

- StatoilHydro (2009).
- Statoil ASA (2010-11).
- Masdar (2009-10).
- Vattenfall AB (2010-11).
- Shell (2011).

CTCC has entered consortium agreements with universities and research institutions to carry out the project:

- Norwegian University of Life Sciences, UMB (2009-11). Norway.
- Universität Innsbruck, II (2009-11). Austria
- IRCELYON (2009-11). France.
- Norwegian Institute for Air Research, NILU (2009-10). Norway
- NERI (2010-11). Denmark
- Gothenburg University, GAC (2010-11). Sweden.
- Aarhus University, AC3 (2011). Denmark.

Quality Assurance

The data and results in this report have been quality controlled and verified according to generally accepted principles for publication in internationally recognised scientific journals.

Prof. Claus Jørgen Nielsen
University of Oslo.
Department of Chemistry

Oslo,
29.02.2012

ISBN 978-82-992954-7-5

Atmospheric Degradation of Amines (ADA)

Summary report from atmospheric chemistry studies of amines, nitrosamines, nitramines and amides

Claus Jørgen Nielsen, Barbara D'Anna, Rossana Bossi, Arne Joakim Coldvin Bunkan, Line Dithmer, Marianne Glasius, Mattias Hallquist, Anne Maria K. Hansen, Anna Lutz, Kent Salo, Mihayo Musabila Maguta, Quynh Nguyen, Tomas Mikoviny, Markus Müller, Henrik Skov, Emmanuel Sarrasin, Yngve Stenstrøm, Yizhen Tang, Jonathan Westerlund and Armin Wisthaler

This page is intentionally left blank

Preface

An investment decision concerning the building of a full-scale post-combustion CO₂ capture plant at Mongstad is scheduled in 2016. It is possible that the plant will employ amine technology, which at the time of writing is considered the more mature technology available within the defined time frame for start-up of the plant. Given the scale of implementation of post-combustion Carbon Capture and Storage, it is likely that there will be relatively small but still significant discharges of amines to the atmosphere during operation. Studies on the emission from amine-based CO₂ capture mimic facilities indicate the simple alkane-amines as process degradation products of the more complex amines used in CO₂ capture. These small amines will therefore always be present in the cleaned flue gas, no matter which parent amine is used in the absorber, and they may present the major environment and human health problem linked to the implementation of amine-based CO₂ capture. Quantitative knowledge about the atmospheric fate of simple alkane-amines such as CH₃CH₂NH₂ (ethylamine), (CH₃CH₂)₂NH (diethylamine) and (CH₃CH₂)₃N (triethylamine), including their partitioning to particles and droplets and their contribution to the formation of new particles, is therefore important to an Environmental Impact Assessment of amine-based CO₂ capture.

The overall objective of the ADA-2011 project is to contribute to the understanding of the atmospheric degradation of amines emitted to the atmosphere from CO₂ capture plants. The specific objectives are:

- To use the EUPHORE outdoor photochemical chamber to identify and quantify the gas phase photo-oxidation products resulting from amines under natural atmospheric conditions.
- To use the Oslo and Innsbruck photochemical chambers to obtain information on the kinetics of the OH reaction with primary products and information on secondary products of the amine photo-oxidation.
- To verify/update/develop atmospheric photo-oxidation schemes for amines to account for all products formed under natural conditions, and to develop gas phase chemistry models for implementation in dispersion models.
- To characterize the aerosol formed during the atmospheric photo-oxidation of amines.
- To identify possible toxic constituents in the aerosol.

The present report summarises the progress in the ADA project on the study of the atmospheric photo-oxidation of amines.

The project has achieved its targets.

This page is intentionally left blank

Table of Contents

Preface.....	1
Executive Summary	5
HSE	7
1. Experimental facilities and instrumentation	9
1.1 The Innsbruck and Oslo photo-chemistry reactors	9
1.2 The EUPHORE photo-chemical reactor.....	9
1.3 On-line and <i>in situ</i> analytical instrumentation at EUPHORE	10
1.3.1 PTR-TOF-MS	10
1.3.2 VTDMA.....	11
1.3.3 AMS.....	11
1.3.4 FT-IR	12
1.4 Off-line analytical methods	12
1.4.1 QTOF-MS analysis of aerosol samples	12
1.4.2 Nitrosamines and nitramines.....	13
1.4.3 LC-MS analysis of DNPH-cartridge samples	14
1.4.4 GC-FID analyses of SPME samples	14
2. Results from kinetic experiments	15
2.1 Amine + OH	15
2.1.1 Structure Activity Relationship for OH reactions with amines	18
2.2 Nitramine + OH.....	21
2.2.1 Quantum chemical study of nitramine + OH reactions.....	25
2.2.2 Structure Activity Relationship for OH reactions with nitramines.....	26
3. Results from gas phase photo-oxidation studies.....	27
3.1 Estimates of nitrosamine and nitramine formation in the Mongstad area.....	28
3.2 Ethylamine.....	36
3.2.1 Branching ratios in the photo-oxidation of ethylamine.....	40
3.3 Diethylamine	45
3.3.1 Branching ratios in the photo-oxidation of diethylamine.....	48
3.3.2 NO ₃ radical chemistry	53
3.4 Triethylamine	56
3.4.1 O ₃ chemistry	59
3.4.2 OH chemistry	62
3.4.3 Branching ratios in the photo-oxidation of triethylamine	63
3.5 Piperazine.....	67
3.6 Amides.....	72
3.6.1 N-ethylacetamide	72
3.6.2 N,N-diethylacetamide.....	74
3.7 Nitramines.....	76
3.7.1 N-nitro methylamine	76
3.7.2 N-nitro dimethylamine	77
3.7.3 N-nitro ethylamine.....	77
3.7.4 N-nitro diethylamine.....	78
4. Results from nitrosamine photolysis experiments	80
4.1 Interpretation of photolysis results.....	81
4.2 Retrieval of OH radical concentration during photolysis of nitrosamines.....	83
4.3 Retrieval of NO _x from FTIR spectra	85
4.4 Actinic flux data – j_{NO_2}	86
4.5 Numerical model of the EUPHORE photolysis experiments.....	86
4.6 N-Nitroso dimethylamine gas phase photolysis	88
4.7 N-Nitroso diethylamine gas phase photolysis	93
4.8 N-Nitroso morpholine gas phase photolysis	96
4.9 N-Nitroso piperazine gas phase photolysis	99

4.10	<i>N</i> -Nitroso piperidine gas phase photolysis	101
4.11	<i>N</i> -Nitroso pyrrolidine gas phase photolysis	103
4.12	Nitrosamine relative photolysis rate experiment	104
5.	Results from aerosol formation studies	106
5.1	General	107
5.1.1	Composition	108
5.1.2	Thermal properties and ageing of particles	109
5.2	Photo-oxidation of ethylamine under low NO _x conditions (03.06.2011)	109
5.2.1	Aerosol Yield	110
5.2.2	Aerosol composition	111
5.2.3	Thermal properties and ageing	114
5.2.4	Atmospheric implications	116
6.	Literature	117
	ANNEX	122
A.	Monitor calibration and data analysis	122
B.	NO₂ Photolysis frequency determination and inter-calibration	130
C.	Amine + OH Relative-Rate Experiments	137
D.	Additional results from Aerosol Studies	146
E.	Infrared absorption cross-sections	163
F.	Dipole moments and isotropic polarizabilities from Quantum Chemical Calculations	165
G.	PTR-TOF-MS data validation	166
H.	Chemical formulas, compound names, structures and CAS numbers	169

Executive Summary

The atmospheric gas phase photo-oxidation of ethylamine, diethylamine, triethylamine and piperazine has been studied under relevant NO_x conditions at EUPHORE – the European Photochemical Reactor in Valencia, Spain. Atmospheric photo-oxidation of amines is dominated by the OH radical that reacts with amines by abstracting a hydrogen atom from either the alkyl or from the amino group. Kinetic measurements of OH radical reactions with diethylamine, triethylamine and other amines have been carried out allowing determination of their atmospheric lifetimes; diethylamine and triethylamine are estimated to have lifetimes with respect to reaction with OH radicals around 4 h in the Mongstad area, while the lifetimes of ethylamine and piperazine will be respectively 10-12 h and 2 h. Triethylamine also reacts fast with ozone and its lifetime with respect to reaction with O₃ is estimated to be only 2 h in the Mongstad area.

All major products in the photo-oxidation of ethylamine, diethylamine and triethylamine have been identified and quantified, and detailed photo-oxidation schemes including branching ratios obtained. Based on the results from on-line and *in situ* instrumentation it is found that around 9% of the reaction between ethylamine and OH radicals takes place at the amino group (–NH₂), and that the potentially carcinogenic nitramine, CH₃CH₂NHNO₂, is formed directly as a result of this reaction. For diethylamine the study shows that around 60% of the reaction with OH radicals takes place at the amino group (>NH), and that the carcinogenic nitrosamine, (CH₃CH₂)₂NNO, and the potentially carcinogenic nitramine, (CH₃CH₂)₂NNO₂, are formed as a result of this reaction. For triethylamine the study shows that around 35% of the reaction with OH radicals has the potential to form the nitrosamine, (CH₃CH₂)₂NNO, and the nitramine, (CH₃CH₂)₂NNO₂. The nitramines, CH₃CH₂NHNO₂ and (CH₃CH₂)₂NNO₂, have estimated atmospheric lifetimes with respect to reaction with OH radicals of more than 1 day in the Mongstad area. These compounds are therefore expected to be deposited before undergoing further atmospheric photo-oxidation.

It was not possible to quantify the piperazine photo-oxidation products; *N*-nitroso piperazine and *N*-nitro piperazine are formed but they rapidly undergo further photo-oxidation.

Photolysis experiments with *N*-nitroso dimethylamine, *N*-nitroso diethylamine, *N*-nitrosomorpholine, *N*-nitroso piperazine, *N*-nitroso piperidine and *N*-nitroso pyrazine were carried out under natural sunlight conditions at EUPHORE. All nitrosamines studied undergo rapid photolysis with rates of 0.30 – 0.35 times that of NO₂. The actinic flux varies throughout the year and the atmospheric lifetime of nitrosamines with respect to photolysis varies accordingly from a few minutes in mid-summer to several hours in mid-winter. The yearly average atmospheric lifetime of nitrosamines with respect to photolysis (day and night) will be around 40 minutes in the Mongstad area ($\langle j_{\text{NO}_2} \rangle_{\text{year}} \sim 1.3 \times 10^{-3} \text{ s}^{-1}$).

The amount of nitrosamines and nitramines that will be formed in the atmospheric photo-oxidation of amines depends upon the mixing ratio of NO_x. Assuming $\langle \text{NO} \rangle_{\text{year}} = 0.3$, $\langle \text{NO}_2 \rangle_{\text{year}} = 4$ ppbV and $\langle \text{O}_3 \rangle_{\text{year}} = 69$ ppbV, respectively, as mimicking upper limit conditions in the Mongstad area, less than 0.3% of ethylamine that is photo-oxidized will result in the nitramine (CH₃CH₂NHNO₂). For diethylamine less than 1.5% of photo-oxidized diethylamine will end up as nitramine ((CH₃CH₂)₂NNO₂), and for triethylamine less than 0.3% of photo-oxidized triethylamine will end up as nitramine ((CH₃CH₂)₂NNO₂).

The amounts of nitrosamines present in air during photo-oxidation of amines depend not only on the ambient amounts of NO and NO₂, but also on the amount of oxidizing radicals and the actinic flux. The conditions vary during the time of day and throughout year, and because nitrosamines are constantly formed and destroyed by photolysis the amount may be derived from steady-state considerations. Taking an annual average oxidant activity corresponding to $\langle \text{OH} \rangle_{\text{year}} = 9.6 \times 10^5 \text{ cm}^{-3}$ and an annual average actinic flux corresponding to $\langle j_{\text{NO}_2} \rangle_{\text{year}} \sim 1.3 \times 10^{-3} \text{ s}^{-1}$ as mimicking the

conditions in the Mongstad area results in an average steady-state nitrosamine concentration of less than 0.13% of diethylamine and triethylamine present in the air mass.

The major primary products in atmospheric photo-oxidation of ethylamine, diethylamine and triethylamine are imines (ethanimine and *N*-ethyl ethanimine) and amides (acetamide, *N*-ethyl acetamide and *N,N*-diethyl acetamide). The atmospheric fate of imines is not yet completely understood; hydrolysis in the atmospheric aqueous phase is most likely a dominant sink, in which ethanimine and *N*-ethyl ethanimine hydrolyse to acetaldehyde and ammonia, and acetaldehyde and ethylamine, respectively. The atmospheric photo-oxidation of acetamide leads to isocyanic acid, while the major products from atmospheric photo-oxidation of *N*-ethyl acetamide and *N,N*-diethyl acetamide are *N*-formyl acetamide, *N*-acetyl acetamide, *N*-ethyl-*N*-formyl acetamide and *N*-acetyl-*N*-ethyl acetamide. As the atmospheric lifetimes of these amides are around 1 day in the Mongstad area, they will be sufficiently dispersed that concentrations of secondary products from the amine photo-oxidation will be insignificant.

The aerosol generated upon OH radical initiated photo-oxidation of ethylamine, diethylamine, triethylamine and piperazine was studied using both on-line and off-line techniques. Aerosol yields varied from 6 to 64% depending on both the NO_x concentration and the type of amine. Under high NO_x more HNO₃ is formed in the gas phase which readily reacts with the amine forming the corresponding aminium salt. Aminium nitrate salt represented by far the major aerosol constituent during photo-oxidation of ethylamine and diethylamine. Triethylamine degradation was very different and independent of the NO_x conditions, the aerosol mass was dominated by secondary organic products and the ratio organic/nitrate increased with time. In general, particles formed under low NO_x are less volatile than the corresponding aerosol formed under high NO_x conditions, where the contribution of the primary aminium salt is more important. Ageing of particles produced a less volatile aerosol with time. In an exhaust plume, salt formation from amines will necessarily compete with NH₃. The process will depend on the available ammonia concentration and the possibility of atmospheric transformation of the amine salt by ammonia exchange. The ammonia exchange was evaluated in selected experiments and even when amine and ammonia were present at similar concentrations, only trace levels of ammonium (0.7 μg/m³) were observed in the aerosol. Nevertheless in an exhaust plume, the concentration of ammonia will most probably be 10 to 100 times larger than those of the amines and exchange cannot be neglected. Once the primary aminium salt has been formed in a plume, the aerosol could partly evaporate upon dilution. The fresh aerosol is semi-volatile for the first few hours. Dilution tests suggested that the aerosol formed from piperazine and triethylamine was not affected by this dilution while the aerosol formed during from ethylamine and diethylamine did partly evaporate. The evaporated amines could further react with available radicals as OH. The outcome of this process might potentially produce lower volatility products able to partition back into the condensed phase. Recent publications report that amines released to the atmosphere in addition take part in new particle formation and increase both the nucleation and growth rates. The photo-oxidation studies of amines were performed in a dry atmosphere, while in an exhaust plume the partial pressure of water will be much higher. It is expected that water will play a crucial role enhancing aerosol formation, and will be changing solubility of oxidants and amine precursors in the aerosol phase.

HSE

The project involved handling of hazardous chemicals and was carried out as required by statutes and regulations.

Safety precautions, synthesis: All synthetic work at UMB has been done in an inert atmosphere (N₂) in a well-ventilated fume hood. Usual precautions have been implemented when working with organic synthesis, *i.e.* use of gloves, laboratory coat and safety goggles. Compounds suspected to be cancer promoting or explosive are treated wet and destroyed according to standard laboratory practice. All chemical waste has been sealed in special flasks and sent to authorized companies for destruction of such materials.

The Standard Operational Procedure (SOP) in the CEAM (EUPHORE) laboratories is that all compounds studied, including possible degradation products, are treated as toxic/potentially carcinogenic. The SOP also includes that all toxic/carcinogenic and/or suspected explosive compounds are handled in well-ventilated fume hoods using gloves, laboratory coats and safety goggles. A Safe Job Analysis has been conducted, and a participant meeting arranged and documented.

The SOP in the UiO laboratory is that all compounds studied, including possible degradation products, are treated as potentially carcinogenic unless other information is available. The SOP also includes that all toxic/carcinogenic compounds are handled on vacuum lines. The compounds have been studied in a closed reactor where they were completely oxidized through reaction with OH radicals.

UiO is not required to produce HSE data sheets for compounds synthesized for research purpose.

The University of Oslo is a Governmental institution that follows HSE rules and regulations according to Norwegian Law. The HSE-manual can be found here:

<http://www.kjemi.uio.no/intern/organisasjonsutvikling/hms/hse-manual/>

Activities in the UIBK laboratories were conducted in compliance with Austrian HSE regulations and laws: <http://www.uibk.ac.at/arbeitsicherheit/rechtsbasis/> see, Chemikaliengesetz (ChemG) and Chemikalienverordnung (ChemV).

No accidents, near accidents or spillage occurred during the project lifetime.

This page is intentionally left blank

Gas Phase Atmospheric Chemistry of Amines, Nitrosamines, Nitramines and Amides

1. Experimental facilities and instrumentation

The ADA-2011 project included several experimental activities: photo-oxidation studies in the Innsbruck, Oslo and at EUPHORE chambers; chemical kinetic studies, organic synthesis of reactants and reference compounds including *N*-nitroso and *N*-nitro amines, recording of absolute UV and infrared absorption cross-sections, development of on-line analytical instrumentation, development of off-line analytical methods and analytical software development.

1.1 The Innsbruck and Oslo photo-chemistry reactors

The “Oslo reactor” reactor is a 2.2 m long, 250 L electro-polished stainless steel chamber equipped with a White type multiple reflection mirror system aligned with an optical path length of 128 m for rovibrationally resolved infrared spectroscopy. The reaction chamber is equipped with UV photolysis lamps mounted in a quartz tube inside the chamber. Infrared spectra were recorded with a Bruker IFS 66vs FTIR instrument employing LN₂-cooled MCT and InSb detectors, and the light intensity was reduced to ensure linear detector response.

The “Innsbruck-reactor” is a 480 L Teflon coated reaction chamber made of glass and surrounded by 18 UV/VIS lamps ($\lambda \geq 300$ nm) to simulate sunlight. Analytical instrumentation included a high-resolution proton-transfer-reaction time-of-flight mass spectrometer (PTR-TOF-MS 8000, Ionicon Analytik GmbH) for VOC measurements, a chemiluminescence NO-detection instrument (CLD770 AL ppt, ECO PHYSICS) combined with a photolytic converter (PLC 760 MH, ECO PHYSICS) for NO₂ detection, a UV photometric ozone analyser (49i, Thermo Scientific) and a temperature / relative humidity sensor (UFT75-AT, MELTEC).

1.2 The EUPHORE photo-chemical reactor

The European Photochemical Reactor, EUPHORE, in Valencia, Spain (longitude -0.5, latitude 39.5) is an “open access” large-scale facility established in 1991 as part of the CEAM Centre of Applied Research with financial support from EU, http://www.ceam.es/html/index_i.htm. There are two ~200 m³ hemispherical chambers for photochemical studies. The chambers are constructed from Teflon film, which have a uniform transmission of sunlight, and are protected by steel canopies, which are opened during the photo-oxidation experiments. After the experiments, the chambers are closed and flushed overnight with scrubbed air. The floors of the chambers are cooled to ensure a stable temperature in the chambers during the experiments.

A typical EUPHORE experiment started around 06:00 UT when reagents were added to the chamber. The canopy of the chamber was opened after the reagents were considered to be well mixed, and the first air samples had been collected. Some experiments lasted up to 12 hours after which the canopy was closed, and a large-volume collection of aerosol carried out. The chamber was then flushed overnight with scrubbed air.

Unlike the typical laboratory smog chamber, purified air is constantly added to compensate for leakage, loss through connections, sampling on filters and continuous sampling by ozone, NO_x and other monitors, and by the on-line instruments. This is corrected for in the data analysis: SF₆ was added to measure the apparent dilution rate by FT-IR.

The EUPHORE facility offers a large variety of analytical instrumentation for *in situ* and on-line detection of chemical components and particles in the chamber (FT-IR, GC-MS, SMPS, TEOM, and

monitors for actinic flux, CH₂O, NO_x, NO_y, CO, H₂O, O₃, HONO). A detailed description of the EUPHORE facility and the existing analytical instruments is available in the literature.¹⁻⁵

To complement the in-house instrumentation, users may attach their own instruments and sample collection devices. The ADA-2011 project provided three additional on-line instruments: an Aerosol Mass Spectrometer (AMS), a High-Resolution Proton-Transfer-Reaction Time-of-Flight Mass Spectrometer (PTR-TOF-MS) and a Volatility Tandem Differential Mobility Analysers (VTDMA) system. These instruments are further described below. The high mass resolution of the PTR-TOF-MS instrument allows an (almost) unambiguous determination of the sum formulae of ions detected – structural isomers, however, cannot be distinguished. In addition, reactor air was sampled several times a day employing various adsorbents for subsequent analysis (nitrosamines, nitramines, carbonyls, amides).

1.3 On-line and *in situ* analytical instrumentation at EUPHORE

1.3.1 PTR-TOF-MS

The experimental set-up and procedures of the 2010 EUPHORE experiments have been described in the in the ADA-2010 Project Summary Report.⁶

In the 2011 experiments, a commercial proton-transfer-reaction time-of-flight mass spectrometer (PTR-TOF-MS, model PTR-TOF 8000, Ionicon Analytik GmbH, Innsbruck, Austria) was deployed for real-time analysis of the amines and their volatile oxidation products.⁷

In the EUPHORE experiments, the instrument was operated at $E/N = 88$ Td, E being the electric field strength and N the buffer gas density ($1 \text{ Td} = 10^{-17} \text{ V cm}^2$). The PTR-TOF-MS inlet capillary and the reaction chamber were temperature-controlled at 75°C. The PTR-TOF-MS was interfaced to the EUPHORE chamber via a Sulfinert[®]-passivated stainless steel tube (length: 125 cm; inner diameter: 5.33 mm; temperature: 75°C; flow: 11 lpm). A flow of 0.16 lpm was branched off from this main inlet flow into a shortened PEEK inlet capillary (length: 10 cm). Subsequently, a sample flow of 0.025 lpm was branched off into the PTR-TOF-MS reaction chamber for analysis.

Experiments in the Innsbruck photo-reactor were conducted in duplicates, with the PTR-TOF-MS operating at $E/N = 88$ Td and $E/N = 52$ Td, respectively. The low E/N -mode was used for optimized detection of peroxy-nitrate-type compounds. The PTR-TOF 8000 standard PEEK capillary inlet was used during the Innsbruck experiments. This inlet was interfaced to the chamber via a Teflon PFA tube (length: 20 cm, outer diameter: 2.66 mm).

PTR-TOF-MS raw data were corrected for instrumental effects such as the detector dead time and Poisson counting statistics and analysed using custom-made peak searching and fitting software routines.^{8,9} A mass accuracy of < 8 ppm and 2- σ detection limits in the range of 9-to-39 pptV were inferred from an analysis of calibration measurements with a multi-component VOC gas mixture (Apel-Riemer Environmental Inc., Denver, USA). The obtained calibration data were used to correct for instrumental mass discrimination effects induced by mass-dependent ion extraction efficiencies and detector aging.

The obtained data were normalized to the hydronium ion signals (H₃O⁺ and H₃O⁺•H₂O) and filtered to isolate the main photo-oxidation products. For filtering, normalized signal count rates were summed over the time of reaction and only signals with a count-rate yield > 1% (> 3% for some experiments) (relative to the signal decrease observed for the reagent species) was selected. The automated output was visually inspected and all signals not relevant for further analysis (*e.g.* fragment ions, ¹³C-containing ions, instrument-intrinsic ions, ions arising from side reactions) were discarded.

Instrument sensitivities for the target compounds of this study were derived from theories for calculation of ion-molecule capture rates using quantum chemically calculated molecular properties

(see ANNEX F, page 165). The combined error from mass discrimination determination (10%), reaction rate coefficient calculations (10%) and reference calibrations (5%) is $\pm 15\%$ for the PTR-TOF data. Examples of PTR-TOF-MS data validation are summarized in ANNEX G, page 166.

1.3.2 VTDMA

A volatility tandem differential mobility analysers (VTDMA) system has been developed for measuring the thermal characteristics of SOA particles¹⁰ or fundamental thermal properties of pure compounds.¹¹ The VTDMA system is useful for observing changes in particle size/volume when exposed to heat.¹²⁻¹⁴ The system comprises three main parts: *a*) a DMA, selecting particles of a known size, *b*) an “exposure unit”, where the potential size change occurs due to heating *c*) an SMPS system, measuring the residual particle size distribution (Figure 1.1). The heating unit consists of four or eight parallel ovens having a temperature range from 298 to well above 573 K, enabling rapid change of the temperature. The VTDMA has been proven to detect very small changes in volatility that can be attributed to changes in chemical composition.

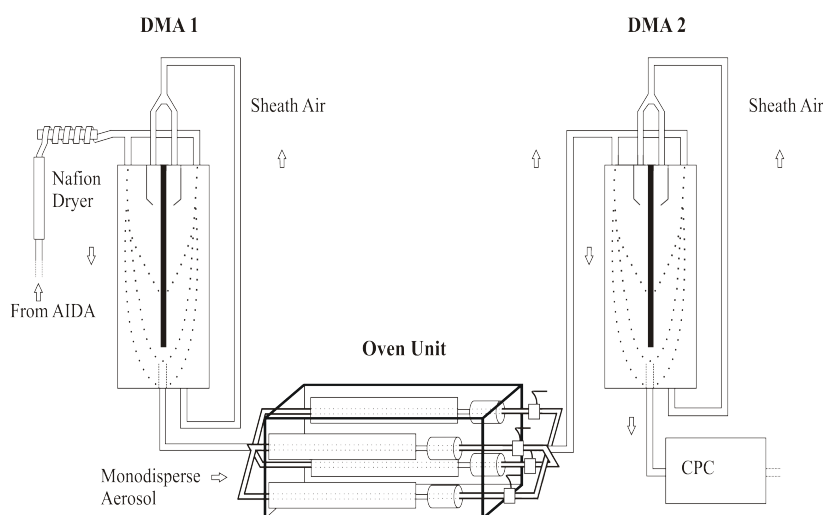


Figure 1.1. Schematic of the VTDMA set-up. (From Jonsson *et al.* Ref. ¹⁰)

1.3.3 AMS

The time-of-flight Aerodyne Aerosol Mass Spectrometer (AMS) is an innovative instrument that allows real-time and *in situ* analysis of fine and ultrafine particles. The instrument investigates size distribution and chemical composition of particles between 0.03 to 1.0 μm on a 1 min basis. The methodology used within c-TOF AMS is fully described in Drewnick *et al.*¹⁵ The particles are sampled through a critical orifice (diameter 100 μm) at 80 $\text{cm}^3 \text{min}^{-1}$ and focused by an aerodynamic lens which blocks all particles larger than 1 μm in diameter. Then they enter a vacuum chamber where a mechanical chopper allows a packet of particles (beam chopped) to be accelerated according to their vacuum aerodynamic diameter (D_{va}) and thereby giving size distribution data. The particles are then sent to the vaporization-ionization chamber where the non-refractory (NR) components of the particles are flash-vaporized on a hot surface ($\sim 600^\circ\text{C}$) and ionized by electron impact (70 eV). Resultant positively charged ions are guided into the time-of-flight mass spectrometer. The collected mass spectra (m/z from 4 to >350 in a minute scale) give information on the chemical composition (i.e., nitrate, sulphate, chloride, potassium, ammonium, aliphatic organic, PAHs) using a “fragmentation table”. Using default parameters (70 eV for the electron impact ionization) fragmentation of the aliphatic organic fraction is important. During the ADA project we tried to

develop and optimize data acquisition at 30 eV in an attempt reduce the fragmentation of the amines and their degradation products.

High Resolution data analysis by Cumulative Function Distribution. Quantification and identification of the aerosol components is often complicated due to the low resolution ($m/\Delta m=800-1000$) of the Compact-Time of Flight MS of the AMS. In the aerosol formed upon amine degradation several signals are often associated to multiple ion fragments. It is the case for m/z 30 (NO^+ fragment at 29.99 and CNH_4^+ 30.04) and m/z 44 (which can contain up to 3 fragments m/z 43.985 CO_2^+ , m/z 44.027 $\text{C}_2\text{H}_4\text{O}^+$ and m/z 44.050 $\text{C}_2\text{H}_6\text{N}^+$, respectively). Routine analysis does not allow the separation of these fragments.

1.3.4 FT-IR

The EUPHORE Chamber B is equipped with a Nicolet 6700 FTIR spectrometer coupled with White multi-reflection mirror system for in situ analysis adjusted to give an optical path length of 553.5 m. FTIR spectra were recorded every ten minutes by co-adding 370 or 202 interferograms with a resolution of 0.5 respectively 0.25 cm^{-1} . Boxcar apodization was used in the Fourier transformation. The interferograms were saved for possible later re-processing.

Retrieval of trace gas volume mixing ratios was carried out semi-automatically employing the MALT program.¹⁰⁶ This method simulates the spectrum of the mixture of absorbing species from a set of initial concentrations and reference spectra and then varies the concentrations iteratively to minimize the residual between the measured and simulated spectrum. In the spectrum calculation, true absorption coefficients are used if available, otherwise high-resolution spectra can be used as a good approximation. The spectral data needed in the fitting procedure were taken from the HITRAN 2008 database (H_2O , CO , NO , NO_2 , CO_2 , CH_4);¹⁶ for other compounds such as ethyl-, diethyl- and triethylamine experimental IR spectra were used. Retrieval of chemical components from the FT-IR spectra is sensitive to detector non-linearity and interference of compounds with overlapping spectra. For compounds whose spectra only show *PQR*-structure the retrieval procedure has an estimated uncertainty of $\pm 10\%$. For compounds showing rotational fine structure the retrieval procedure has an estimated uncertainty of $\pm 5\%$.

1.4 Off-line analytical methods

Many off-line techniques used in this project collect both gas phase and particulate matter (aerosols). For this reason the off-line analysis results may not be directly comparable with the on-line measurement results. Off-line techniques often enable definitive confirmation of chemical compounds tentatively identified by the on-line techniques. The analytical methodologies are briefly outlined in the following.

1.4.1 QTOF-MS analysis of aerosol samples

Aerosol sample filters were extracted in acetonitrile in a cooled ultrasonic bath. The solution was filtered into a small beaker and evaporated in a gentle N_2 -flow. 1 mL of a 5% acetonitrile solution with 10 mM ammonium acetate was added to the beaker and then transferred to a sample vial. To ensure that all compounds in the glass beaker were dissolved additional 1 mL acetonitrile was added to the beaker and transferred to a sample vial. In addition to the sample filters, three clean quartz filters were extracted as well, and used as blanks.

Amine aerosol composition was analysed on a quadrupole time-of-flight mass spectrometer (QTOF-MS, Bruker microTOFq) at Aarhus University, Dep. of Chemistry. Aerosol filter extracts were injected directly through an Atmospheric Pressure Chemical Ionisation (APCI) inlet operated in positive mode. The instrument was calibrated before and after each analysis.

1.4.2 Nitrosamines and nitramines

For sampling of nitrosamines and nitramines Thermosorb/N cartridges (Cambridge Scientific Instruments Ltd., UK) were employed. Thermosorb/N cartridges are designed and patented for collection of nitrosamines from tobacco smoke (NIOSH, 1994). The solid phase contained in these cartridges has a special coating, which avoids degradation of nitrosamines during collection and thus sampling artefacts. During the first EUPHORE campaign (March 2010) collection on Thermosorb/N has been performed with and without an ozone scrubber (MnO₂) in order to evaluate the possible effect of ozone degradation of the target compounds. For Thermosorb/N cartridges a sampling flow of 1 L min⁻¹ has been used.

Thermosorb/N and charcoal cartridges were extracted with solvent.

Analysis of nitroso- and nitramines by GC-MS. A method has been developed for quantitative analysis of the following target compounds: *N*-nitrosodimethylamine, *N*-nitro dimethylamine, *N*-nitro methylamine and *N*-ethyl nitrosamine. The compounds have been provided by The Norwegian University of Life Sciences as pure standards (>99%).

The compounds were dissolved in acetonitrile to a concentration of about 1 mg/mL. Individual solutions at 10 µg/mL in dichloromethane were prepared in order to determine the full scan spectrum and the chromatographic retention time for each compound.

Individual solutions were analysed in full scan by GC-MS (Agilent 5975C MSD) with chemical ionization (CI) in both positive (PCI) and negative mode (NCI). Methane was used as ionisation agent. The compounds were separated on an RTX-1701 capillary column (30 m, 0.32 mm I.D., 1 µm film) from Restek. The oven was programmed to start at 45°C for 5 minutes, then 5°C/min to 160 °C for 1 minute and 25 °C/min to 260 °C for 5 minutes. The injection volume was 1 µL and the injector temperature 200 °C.

The NCI full scan spectrum showed *m/z* 46 (NO₂) as the most intense ion for the three nitramines. In full scan PCI all compounds displayed the protonated molecular ion as the most intense ion. *N*-nitroso dimethylamine could only be analysed by PCI. In Table 1.1 the ions used in selected ion monitoring (SIM) are shown.

Table 1.1. SIM ions for nitroso- and nitramines in PCI and NCI GC-MS

Compound	Acronym	Molecular Weight	PCI (m/z)	ions (m/z)	NCI (m/z)	ions
Nitrosodimethylamine	Me ₂ NNO	74	75	-	-	-
Nitromethylamine	MeNNO ₂	76	77	46	46	
Methylethylnitrosoamine	MeEthNNO	88	89	-	-	
Methylethylnitroamine	MeEthNNO ₂	104	105	46	46	
Dimethylnitroamine	Me ₂ NNO ₂	90	91	46	46	
Nitroethylamine	EthNNO ₂	90	91	46	46	
Diethylnitrosamine	Eth ₂ NNO	102	103	-	-	

A better sensitivity was obtained for the three nitramines by NCI. However, PCI was used for confirmation purposes for nitramines and for determination of *N*-nitrosodimethylamine.

Quantification was performed by linear regression with external calibration (standard concentrations ranging from 5 ng mL⁻¹ to 400 ng mL⁻¹).

Extraction of Thermosorb/N cartridges. The manufacturer recommends elution of Thermosorb/N with 2 mL methylene chloride/methanol (3:1, v/v) for the analysis of nitrosamines. Before elution of the samples, the elution efficiency was evaluated by spiking Thermosorb/N cartridges with the target compounds (100 ng) and eluting the cartridges with three times 2 mL aliquots of methylene chloride or methylene chloride/methanol (3:1, v/v). The three eluates were analysed separately. Methylene

chloride/methanol (3:1, v/v) resulted to be the solvent with the best elution efficiency. However, it was necessary to use 4 mL for complete elution of the compounds. The solvent extract was then evaporated under a gentle stream of nitrogen and reconstituted to an exact volume of 1 ml for GC-MS analysis. Unspiked Thermosorb/N cartridges were also eluted in order to determine the laboratory background level of the target compounds. No target compounds were found in the laboratory blank. The recovery of the four target compounds was the following: N-nitrosodimethylamine 65%, N-nitro dimethylamine 85%, N-nitro methylamine 76% and N-ethyl nitramine 93%.

In the final method spiking of the cartridges with $^{13}\text{C}_2$, D₆-nitrosoamine (100 ng) was introduced for controlling that the cartridge was properly eluted. Concentrations of the target analytes were not corrected for $^{13}\text{C}_2$, D₆-nitrosoamine recovery.

1.4.3 LC-MS analysis of DNPH-cartridge samples

Gas phase carbonyls were sampled for 30 min using DNPH derivatization. Compounds were retained in DNPH-silica charged cartridges, supplied by Waters. After elution with 2 ml of acetonitrile and left reacting overnight, the samples were injected into a LC-MS instrument. Mass spectra were obtained using APCI- and full scan mode.

1.4.4 GC-FID analyses of SPME samples

Solid phase micro-extraction (SPME) was employed for the sampling and subsequent analysis by gas chromatography – flame ionization detector (GC-FID) of amine compounds (precursors) and their degradation products. SPME (PDMS / DVB with Film Thickness of 65 μm) was directly exposed to the smog chamber for 10 minutes. Then, it was directly desorbed into an Agilent Technologies GC-FID system model 6890.

2. Results from kinetic experiments

The relative-rate method, in which the removal rates of the reacting species are measured simultaneously as a function of reaction time, have been employed in studies of OH kinetics with amines and nitramines. Assuming that the compounds react solely with the same radical and that none of the reactants are reformed in any side reactions, the relative rate coefficient, k_{rel} , is obtained from the following expression:

$$\ln\left\{\frac{[S]_0}{[S]_t}\right\} = k_{rel} \cdot \ln\left\{\frac{[R]_0}{[R]_t}\right\} \quad ; \quad k_{rel} = \frac{k_S}{k_R}$$

where $[S]_0$, $[R]_0$, $[S]_t$ and $[R]_t$ are concentrations of the substrate (nitramine) and the reference compound at start and at the time t , respectively, and k_S and k_R are the corresponding rate coefficients. A plot of $\ln\{[S]_0/[S]_t\}$ vs. $\ln\{[R]_0/[R]_t\}$ will thus give the relative reaction rate coefficient $k_{rel} = k_S/k_R$ as the slope.

2.1 Amine + OH

Five experiments have been carried out at EUPHORE to determine the OH rate coefficients for reaction with amines. The results from one experiment are presented in this section; the results from the other experiments are presented in ANNEX C, page 137.

A relative rate kinetics study of 4 amines ($(\text{CH}_3)_2\text{NH}$, $(\text{CH}_3)_3\text{N}$, $(\text{CH}_3\text{CH}_2)_2\text{NH}$ and $(\text{CH}_3\text{CH}_2)_3\text{N}$) was carried out after a day with NO/NO₂ calibration making use of the NO_x in the chamber (experiment #1). There are no previous kinetic data for the OH reaction with diethyl- and triethylamine. The results, shown in Figure 2.1, illustrate the amine gas phase loss during the experiment.

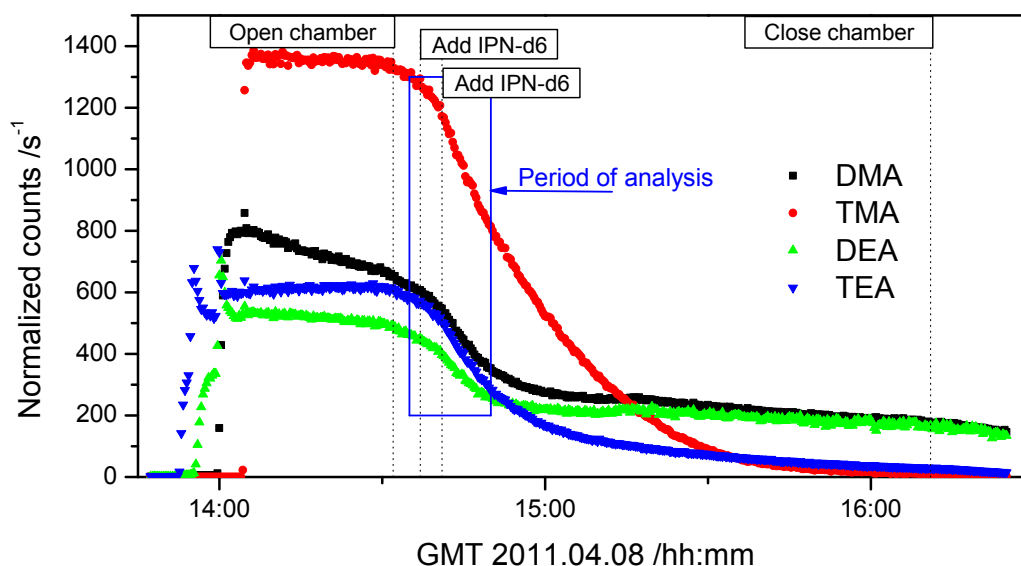


Figure 2.1. PTR-TOF-MS ion signals observed during the kinetic experiment with $(\text{CH}_3)_2\text{NH}$ (DMA), $(\text{CH}_3)_3\text{N}$ (TMA), $(\text{CH}_3\text{CH}_2)_2\text{NH}$ (DEA) and $(\text{CH}_3\text{CH}_2)_3\text{N}$ (TEA) on 2011.04.08.

The experiment was hampered by a high amount of nitric acid in the chamber causing massive particle formation and exchange of amines in the particles as can be seen from the injection and mixing period in Figure 2.1. Deuterated isopropyl nitrite ($\text{CD}_3\text{CH}(\text{ONO})\text{CD}_3$, nitrous acid, 1-(methyl- d_3)-ethyl-2,2,2- d_3 ester, IPN- d_6) was injected as an additional OH precursor (see Section 3.2) and, focusing on the period after injection of IPN- d_6 , the amine gas phase loss was dominated by reaction with OH.

The decays of $(\text{CH}_3)_2\text{NH}$, $(\text{CH}_3)_3\text{N}$, $(\text{CH}_3\text{CH}_2)_2\text{NH}$ and $(\text{CH}_3\text{CH}_2)_3\text{N}$ in the presence of OH radicals are plotted as $\ln\{[\text{Amine}]_0/[\text{Amine}]_t\}$ vs. $\ln\{[(\text{CH}_3)_2\text{NH}]_0/[(\text{CH}_3)_2\text{NH}]_t\}$ in Figure 2.2. Least-squares fitting of the data from the time-span 14:35 to 14:50 resulted in the following relative rate coefficients (2σ statistical error limits): $k_{\text{OH}+(\text{CH}_3)_3\text{N}}/k_{\text{OH}+(\text{CH}_3)_2\text{NH}} = 0.824 \pm 0.008$, $k_{\text{OH}+(\text{CH}_3\text{CH}_2)_2\text{NH}}/k_{\text{OH}+(\text{CH}_3)_2\text{NH}} = 1.036 \pm 0.016$ and $k_{\text{OH}+(\text{CH}_3\text{CH}_2)_3\text{N}}/k_{\text{OH}+(\text{CH}_3)_2\text{NH}} = 1.206 \pm 0.018$.

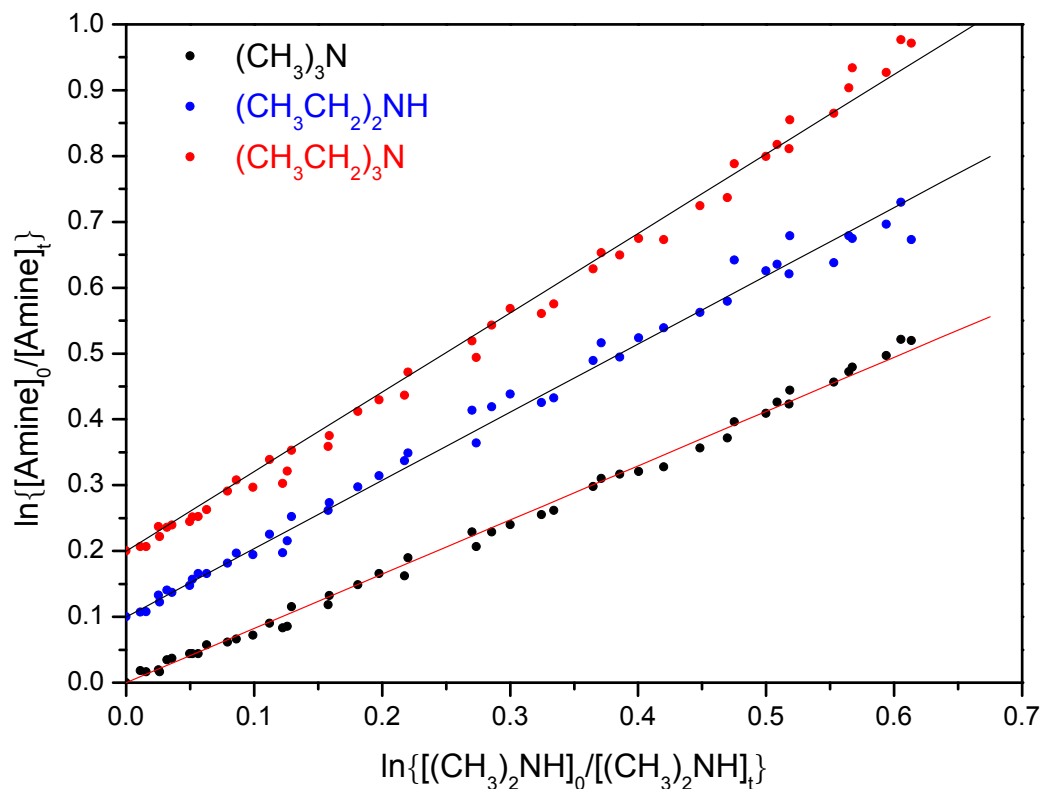


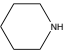
Figure 2.2. Relative rate plots showing the decays of $(\text{CH}_3)_2\text{NH}$, $(\text{CH}_3)_3\text{N}$, $(\text{CH}_3\text{CH}_2)_2\text{NH}$ and $(\text{CH}_3\text{CH}_2)_3\text{N}$ at 1013 hPa and 298 K in the presence of OH radicals. For the sake of clarity the data points for $(\text{CH}_3\text{CH}_2)_2\text{NH}$ and $(\text{CH}_3\text{CH}_2)_3\text{N}$ have been shifted by 0.1 and 0.2, respectively.

Kinetic data for the OH reaction with dimethylamine and trimethylamine have previously been reported. Atkinson *et al.*¹⁷ studied the kinetics of the OH radical reaction with $(\text{CH}_3)_2\text{NH}$ over the temperature range 299 – 426 K and reported $k_{\text{OH}}(T) = 2.89 \times 10^{-11} \times \exp\{(245 \pm 150)\text{K}/T\}$ and $k_{\text{OH}} = (6.54 \pm 0.66) \times 10^{-11} \text{ cm}^3 \text{ molecule}^{-1} \text{ s}^{-1}$ at 298 K. Carl and Crowley¹⁸ reported a room temperature value in perfect agreement with the results of Atkinson *et al.*, $k_{\text{OH}} = (6.49 \pm 0.64) \times 10^{-11} \text{ cm}^3 \text{ molecule}^{-1} \text{ s}^{-1}$. Atkinson *et al.*¹⁷ also studied the kinetics of the OH radical reaction with $(\text{CH}_3)_3\text{N}$ over the temperature range 299 – 426 K and reported $k_{\text{OH}}(T) = 2.62 \times 10^{-11} \times \exp\{(250 \pm 150)\text{K}/T\}$ and $k_{\text{OH}} = (6.09 \pm 0.61) \times 10^{-11} \text{ cm}^3 \text{ molecule}^{-1} \text{ s}^{-1}$ at 298 K. Carl and Crowley¹⁸ presented a room temperature value for $k_{\text{OH}} = (3.58 \pm 0.22) \times 10^{-11}$ which differ by a factor of 2. The absolute value of Atkinson *et al.*¹⁷ depends on a calibrated gas whereas Carl and Crowley¹⁸ used the UV cross section of the amine for calibration, and the latter authors suggest that the earlier results suffer from a calibration error.

Taking $k_{\text{OH}+(\text{CH}_3)_2\text{NH}} = (6.50 \pm 0.65) \times 10^{-11} \text{ cm}^3 \text{ molecule}^{-1} \text{ s}^{-1}$ at 298 K, places the other rate coefficients on an absolute scale at: $k_{\text{OH}+(\text{CH}_3)_3\text{N}} = (5.36 \pm 0.54) \times 10^{-11}$, $k_{\text{OH}+(\text{CH}_3\text{CH}_2)_2\text{NH}} = (6.73 \pm 0.67) \times 10^{-11}$ and $k_{\text{OH}+(\text{CH}_3\text{CH}_2)_3\text{N}} = (7.84 \pm 0.78) \times 10^{-11} \text{ cm}^3 \text{ molecule}^{-1} \text{ s}^{-1}$, respectively. The presently derived rate coefficient $k_{\text{OH}+(\text{CH}_3)_3\text{N}}$ falls between the two previously reported values.

Results from the other four relative-rate experiments carried out at EUPHORE and the weighted average values are included in Table 2.1. The table includes estimated atmospheric lifetimes with respect to reaction with OH radicals in the Mongstad area where $\langle \text{OH} \rangle_{\text{year}} = 9.6 \times 10^5 \text{ cm}^{-3}$.¹⁹

Table 2.1. Experimental rate coefficients at 295-300 K for the reactions of OH radicals with amines, and estimated lifetimes of amines with respect to gas phase reaction with OH in the Mongstad area.

Compound	Exp.	k_{rel}	$k_{OH} / 10^{-11} \text{ cm}^3 \text{ molecule}^{-1} \text{ s}^{-1}$	Reference	τ_{OH}^a	
CH ₃ NH ₂			2.20 ± 0.22	20	13-17 h	
			1.73 ± 0.11	18		
(CH ₃) ₂ NH	2	6.10 ± 0.37 ^b	9.2 ± 3.0			
	2	1.532 ± 0.034 ^c	8.0 ± 0.8			
	3	4.65 ± 0.10 ^b	7.0 ± 2.3			
	3	1.394 ± 0.022 ^c	7.3 ± 0.7			
	4	5.116 ± 0.048 ^b	7.7 ± 2.6			
	4	1.2355 ± 0.0077 ^c	6.5 ± 0.6			
	5	4.94 ± 0.32 ^b	7.4 ± 2.5			
	5	1.320 ± 0.015 ^c	6.9 ± 0.7	7.1 ± 0.6 ^e	This work	
				6.54 ± 0.66	17	
				6.49 ± 0.64	18	4 h
(CH ₃) ₃ N	1	0.824 ± 0.008 ^d	5.4 ± 0.5			
	2	3.6 ± 0.20 ^b	5.4 ± 1.8			
	2	0.902 ± 0.017 ^c	4.7 ± 0.5	5.1 ± 0.5 ^e	This work	
				6.09 ± 0.61	17	5-8 h
				3.58 ± 0.22	18	
CH ₃ CH ₂ NH ₂			2.77 ± 0.28	17	10-12 h	
			2.38 ± 0.5/-0.15	18		
(CH ₃ CH ₂) ₂ NH	1	1.036 ± 0.016 ^a	6.7 ± 0.7			
	2	6.16 ± 0.35 ^b	9.2 ± 3.1			
	2	1.534 ± 0.028 ^c	8.1 ± 0.8	7.4 ± 0.7 ^e	This work	4 h
(CH ₃ CH ₂) ₃ N	1	1.206 ± 0.018 ^a	7.8 ± 0.8			
	2	5.69 ± 0.29 ^b	8.5 ± 2.8			
	2	1.424 ± 0.019 ^c	7.5 ± 0.8	7.7 ± 0.8 ^e		4 h
CH ₃ (CH ₃ CH ₂)NH	4	5.711 ± 0.047 ^b	8.6 ± 2.9			
	4	1.4668 ± 0.0051 ^c	7.7 ± 0.7			
	5	4.92 ± 0.32 ^b	7.4 ± 2.5			
	5	1.315 ± 0.017 ^c	6.9 ± 0.7	7.3 ± 0.7 ^e	This work	4 h
CH ₃ (CH ₃ CH ₂ CH ₂)NH	3	6.36 ± 0.15 ^b	9.5 ± 3.1			
	3	1.910 ± 0.029 ^c	9.6 ± 3.2			
	4	6.419 ± 0.055 ^b	10.0 ± 1.0			
	4	1.6487 ± 0.0042 ^c	8.6 ± 0.9			
	5	5.11 ± 0.33 ^b	7.7 ± 2.6			
	5	1.364 ± 0.018 ^c	7.1 ± 0.7	8.3 ± 0.9 ^e	This work	4 h
NH ₂ CH ₂ CH ₂ OH (MEA)			9.2 ± 1.1	21	3 h	
Piperidine, 	3	4.76 ± 0.16 ^b	7.1 ± 2.3			
	3	1.428 ± 0.034 ^c	7.4 ± 0.7	7.4 ± 0.7 ^e	This work	4 h
(CH ₃ CH ₂) ₂ NOH			1.0 × 10 ⁻¹⁰	22	3 h	
(CH ₃) ₂ NCH ₂ CH ₂ OH			4.7 ± 1.2	23	3-6 h	
			9.0 ± 2.0	24		
(CH ₃) ₂ C(NH ₂)CH ₂ OH			2.8 ± 0.5	23	10 h	
(CH ₃) ₃ CNH ₂ (TBA)			1.2	25	24 h	
CF ₃ CH ₂ NH ₂ (TFEA)			0.09	25	14 d	
N(CH ₂ CH ₂) ₃ N (DABCO)			2.2	25	13 h	

^a The lifetimes in the Mongstad area are estimated assuming $\langle OH \rangle_{year} = 9.6 \times 10^5 \text{ cm}^{-3}$. ^b Reference compound tetrahydrofuran, $k_{ref} = (1.50 \pm 0.5) \times 10^{-11} \text{ cm}^3 \text{ molecule}^{-1} \text{ s}^{-1}$ at 298 K.²⁶ ^c Reference compound 1,3,5-trimethylbenzene, $k_{ref} = (5.24 \pm 0.52) \times 10^{-11} \text{ cm}^3 \text{ molecule}^{-1} \text{ s}^{-1}$ at 298 K.²⁷ ^d Reference compound (CH₃)₂NH, $k_{ref} = (6.50 \pm 0.65) \times 10^{-11} \text{ cm}^3 \text{ molecule}^{-1} \text{ s}^{-1}$ at 298 K. ^e Weighted average.

2.1.1 Structure Activity Relationship for OH reactions with amines

Atkinson established a general Structure-Activity Relationship (SAR) for OH radical reaction with organics²⁶ that later was extended to nitrosamines and nitramines.²⁸ In this SAR the total OH radical reaction rate coefficient is given by:

$$\begin{aligned}
 k_{total} = & k(\text{H-atom abstraction from C-H and O-H bonds}) \\
 & + k(\text{OH radical addition to } >\text{C}=\text{C}< \text{ and } -\text{C}\equiv\text{C}- \text{ bonds}) \\
 & + k(\text{OH radical addition to aromatic rings}) \\
 & + k(\text{OH radical interaction with } -\text{NH}_2, >\text{NH}, >\text{N}-, >\text{NNO}, -\text{SH} \text{ and } -\text{S}- \text{ groups})
 \end{aligned}$$

The calculation of overall H-atom abstraction rate coefficients is based upon the estimation of $-\text{CH}_3$, $-\text{CH}_2-$, $>\text{CH}-$, and $-\text{OH}$ group rate constants. The $-\text{CH}_3$, $-\text{CH}_2-$, and $>\text{CH}-$ group rate coefficients depend on the identity of the substituents around those groups, with

$$\begin{aligned}
 k(\text{CH}_3\text{-X}) &= k_{\text{prim}} \cdot F(\text{X}) \\
 k(\text{X-CH}_2\text{-Y}) &= k_{\text{sec}} \cdot F(\text{X}) \cdot F(\text{Y}) \\
 k(\text{X-CH}(\text{Y})\text{-Z}) &= k_{\text{tert}} \cdot F(\text{X}) \cdot F(\text{Y}) \cdot F(\text{Z})
 \end{aligned}$$

where k_{prim} , k_{sec} , and k_{tert} are the rate coefficients per $-\text{CH}_3$, $-\text{CH}_2-$, and $>\text{CH}-$ group for a “standard” substituent, X , Y , Z are the substituent groups; and $F(\text{X})$, $F(\text{Y})$, and $F(\text{Z})$ are the corresponding substituent factors. The standard substituent group is chosen to be $X = Y = Z = -\text{CH}_3$, $F(-\text{CH}_3) = 1.00$ by definition.²⁶ It was assumed that the majority of the initial OH radical reaction proceeds via OH radical addition to the N-atom, followed by a number of decomposition reactions of the adduct leading to products. In the recent update of the SAR²⁹ the following parameters relevant to amines, nitrosamines and nitramines are presented in Table 2.2.

Table 2.2. SAR-parameters for OH radical reaction with amines, nitrosamines and nitramines.

Group	$k_{298} / 10^{-12} \text{ cm}^3 \text{ molecule}^{-1} \text{ s}^{-1}$	Substituent Group X	$F(\text{X})$
$-\text{CH}_3$ (k_{prim})	0.136	$-\text{NH}_2, >\text{NH}, >\text{N}-, >\text{NNO}, >\text{NNO}_2^{\text{a}}$	9.3
$>\text{CH}_2$ (k_{sec})	0.934	$-\text{CH}_3$	1.0
$>\text{CH}-$ (k_{tert})	1.94	$-\text{CH}_2-, >\text{CH}-, >\text{C}<$	1.23
$-\text{OH}$	0.14	$-\text{OH}$	3.5
RNH_2	21	$-\text{NO}_2$	0
R_2NH	63		
R_3N	66		
R_2NNO	0		
R_2NNO_2	1.3		

^a Constrained to the same value in the SAR, Ref. 29.

Koch *et al.*²⁵ studied 3 simple, commercially available amines (TBA, TFEA and DABCO, see Table 2.1) with different structural specialties to test the predictions of the Atkinson SAR²⁸ and to explore the ground for improvements. The discrepancy between observed and predicted rate constants was more than a factor of 20 for TFEA and a factor of 6 for DABCO. On this basis the authors concluded that the predictive power of the SAR for amines appears to be extremely poor. In particular the SAR does not give a sound indication to where the hydrogen abstraction actually takes place in the molecule.

A somewhat similar problem with the SAR predictions is encountered for aldehydes. In this class of compounds, however, the bond enthalpy of the aldehydic hydrogen is significantly lower than those of the other C-H bonds and abstraction of the aldehydic hydrogen is completely dominant.³⁰ The inadequacy of the SAR is in both cases linked to “negative activation energies”.

Examples of SAR²⁹ estimation of rate coefficients for the reaction of amines with OH radicals (in units of $10^{-12} \text{ cm}^3 \text{ molecule}^{-1} \text{ s}^{-1}$):

CH₃NH₂:

$$k_{\text{tot}} = k_{\text{prim}} \times F(-\text{NH}_2) + k_{\text{RNH}_2} = 0.136 \times F(-\text{NH}_2) + k_{\text{RNH}_2}$$

CH₃CH₂NH₂:

$$k_{\text{tot}} = k_{\text{prim}} \times F(-\text{CH}_2) + k_{\text{sec}} \times F(-\text{CH}_3) \times F(-\text{NH}_2) + k_{\text{RNH}_2} = 0.136 + 0.934 \times F(-\text{NH}_2) + k_{\text{RNH}_2}$$

(CH₃)₂NH:

$$k_{\text{tot}} = 2 k_{\text{prim}} \times F(-\text{NH}_2) + k_{\text{RNH}_2} = 0.272 \times F(>\text{NH}) + k_{\text{R}_2\text{NH}}$$

(CH₃CH₂)₂NH:

$$k_{\text{tot}} = 2 k_{\text{prim}} \times F(-\text{CH}_2) + 2 k_{\text{sec}} \times F(-\text{CH}_3) \times F(-\text{NH}) + k_{\text{RNH}} = 0.335 + 1.868 \times F(>\text{NH}) + k_{\text{R}_2\text{NH}}$$

(CH₃)₃NH:

$$k_{\text{tot}} = 3 k_{\text{prim}} \times F(>\text{N-}) + k_{\text{R}_3\text{N}} = 0.408 \times F(>\text{N-}) + k_{\text{R}_3\text{N}}$$

(CH₃CH₂)₃NH:

$$k_{\text{tot}} = 3 k_{\text{prim}} \times F(-\text{CH}_2) + 3 k_{\text{sec}} \times F(-\text{CH}_3) \times F(>\text{N-}) + k_{\text{R}_3\text{N}} = 0.408 + 2.802 \times F(>\text{N-}) + k_{\text{R}_3\text{N}}$$

Assuming that the amine + OH reactivity can be described by the SAR as outlined in the example box, one may extract the 6 parameters $F(-\text{NH}_2)$, $F(>\text{NH})$, $F(>\text{N-})$, k_{RNH_2} , $k_{\text{R}_2\text{NH}}$, and $k_{\text{R}_3\text{N}}$ from the available data by a least squares fit of the observed rate coefficients presented in Table 2.1 (omitting the “special amines” $(\text{CH}_3\text{CH}_2)_2\text{NOH}$, $(\text{CH}_3)_3\text{CNH}_2$, $\text{CF}_3\text{CH}_2\text{NH}_2$ and $\text{N}(\text{CH}_2\text{CH}_2)_3\text{N}$). Figure 2.3 shows a comparison between observed and estimated rate coefficients from a model in which $F(-\text{NH}_2) = F(>\text{NH}) = F(>\text{N-})$.

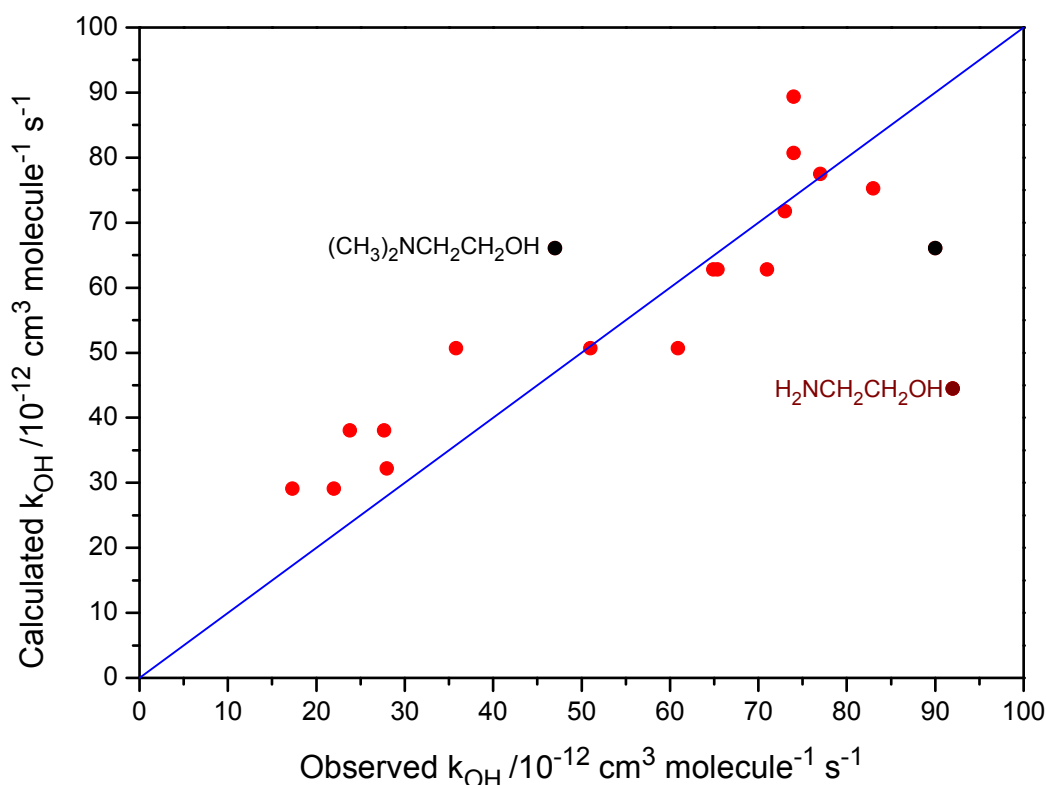


Figure 2.3. Comparison of experimental and calculated rate coefficients at 298 K for the reactions of the OH radical with aliphatic amines.

It can be seen from Figure 2.3 that, according to the SAR model, the rate coefficient of OH reaction with $\text{H}_2\text{NCH}_2\text{CH}_2\text{OH}$ (MEA)²¹ may be an outlier, and that the rate coefficient for $(\text{CH}_3)_2\text{NCH}_2\text{CH}_2\text{OH}$ (DMAE) reaction with OH might be around the average value of the two determinations.^{23,24} Further, there is a tilt in the modelled data set caused by MEA. Treating MEA as an outlier results in a much

more pleasing agreement between modelled and observed rate coefficients for the amine reactions with OH radicals, Figure 2.4. The fact that the rate coefficients for MEA and DMAE reactions with OH do not concord with the SAR model does not necessarily imply that the experimental results are in error. The OH groups in MEA and DMAE are H-bonded to the respective amino groups making these two molecules different from the other amines in the data set. This implies that other groups should undertake additional kinetic studies on these two molecules. The derived SAR parameters are summarized in Table 2.3.

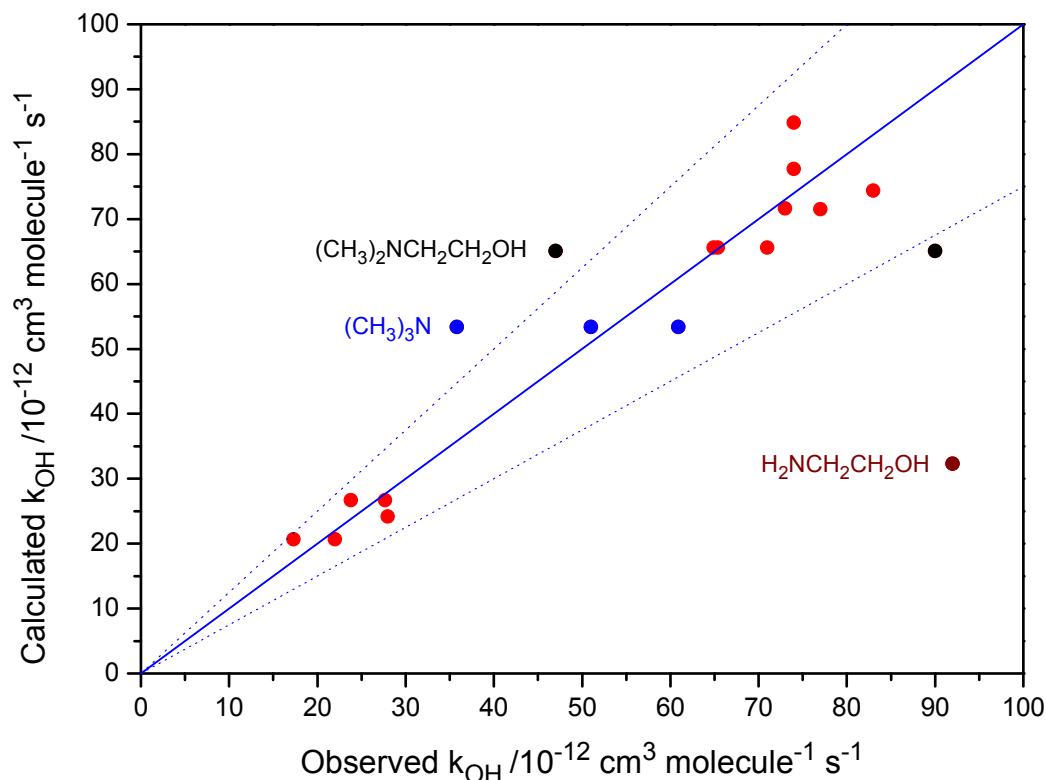


Figure 2.4. Comparison of experimental and calculated rate coefficients at 298 K for the reactions of the OH radical with aliphatic amines. The solid line denotes perfect agreement, and the dashed lines denote disagreement by 25%.

Table 2.3. SAR-parameters for OH radical reaction with aliphatic amines.

Group	$k_{298} / 10^{-12} \text{ cm}^3 \text{ molecule}^{-1} \text{ s}^{-1}$	Substituent Group X	$F(X)$
-CH ₃ (k_{prim})	0.136	-NH ₂ , >NH, >N- ^a	7.4 (9.3) ^b
>CH ₂ (k_{sec})	0.934	-CH ₃	1.0
>CH- (k_{tert})	1.94	-CH ₂ -, >CH-, >C<	1.23
-OH	0.14	-OH	3.5
RNH ₂	20 (21) ^b		
R ₂ NH	64 (63) ^b		
R ₃ N	50 (66) ^b		

^a Constrained to the same value. ^b Values in parentheses are from Kwok and Atkinson, Ref. 29.

From the updated SAR the rate coefficient for OH reaction with piperazine is estimated to be $1.3 \times 10^{-10} \text{ cm}^3 \text{ molecule}^{-1} \text{ s}^{-1}$, and the average lifetime, τ_{OH} , to be around 2 h in the Mongstad region.

A final note of caution: The SAR parameters for OH reactions with aliphatic amines should not be used for estimating rate coefficients of molecules with structures differing from those in the data set employed in deriving the SAR. Further, the SAR does not allow estimating the C-H:N-H branching ratio in the initial abstraction reaction.

2.2 Nitramine + OH

The ADA-2010 project reported kinetic data for the OH reaction with methylnitramine, CH_3NHNO_2 , and dimethylnitramine, $(\text{CH}_3)_2\text{NNO}_2$.⁶ Additional, relative-rate experiments employing other reference compounds have been carried out as part of ADA-2011.

The kinetics analysis according to eq.(I) assumes that only one loss process is taking place: other loss processes such as gas-phase or surface reactions with the radical precursors (H_2 and O_3) will give rise to systematic errors in the relative rates. The OH experiments generally lasted 1 – 2 h including spectral recording and waiting time between photolysis periods, during which >90% of the initial nitramine reacted. The lifetimes of CH_3NHNO_2 , $(\text{CH}_3)_2\text{NNO}_2$ and CH_3OCH_3 with respect to reaction with O_3 in the chamber in relation to the time span of the relative rate experiments are such that the systematic errors introduced by neglecting the additional loss processes are almost negligible. For CH_3OH the additional loss due to reaction with O_3 may be significant and the relative rate experiments were therefore analysed according to:

$$\ln\left\{\frac{[S]_0}{[S]_t}\right\} - k_{\text{O}_3+S} \cdot \int_0^t [\text{O}_3] \cdot dt = k_{\text{rel}} \cdot \left\{ \ln\left\{\frac{[R]_0}{[R]_t}\right\} - k_{\text{O}_3+R} \cdot \int_0^t [\text{O}_3] \cdot dt \right\} ; \quad k_{\text{rel}} = \frac{k_S}{k_R} \quad (\text{II})$$

The lifetimes of CH_3NHNO_2 , $(\text{CH}_3)_2\text{NNO}_2$, CH_3OCH_3 and CH_3OH in the Oslo chamber, when diluted in purified air, are on the order of days and therefore negligible in the present context. When mixed with H_2 and O_3 in purified air the lifetimes are shorter. Assuming that the increased decays can be attributed to reaction with O_3 , the following rate coefficients for O_3 reaction were determined: $k_{\text{O}_3+\text{CH}_3\text{NHNO}_2} = 3 \times 10^{-22}$, $k_{\text{O}_3+(\text{CH}_3)_2\text{NNO}_2} = 2 \times 10^{-22}$, $k_{\text{O}_3+\text{CH}_3\text{OCH}_3} = 5 \times 10^{-22}$ and $k_{\text{O}_3+\text{CH}_3\text{OH}} = 2 \times 10^{-21}$ $\text{cm}^3 \text{ molecule}^{-1} \text{ s}^{-1}$.

Examples of the FTIR spectra obtained from the kinetic studies of the $\text{CH}_3\text{NHNO}_2/\text{CH}_3\text{OCH}_3$ reaction with OH radicals and the resulting residuals from the non-linear least squares spectral analyses are shown in Figure 2.5. The only product band appearing in the spectra during the reaction stem from methylformate, which stems from the oxidation of dimethyl ether. For the sake of brevity, only spectra from the $\text{CH}_3\text{NHNO}_2/\text{CH}_3\text{OH} + \text{OH}$ experiments are shown here.

The decays of CH_3NHNO_2 and the reference compounds CH_3OCH_3 and CH_3OH in the presence of OH radicals are plotted as $\ln\{[\text{CH}_3\text{NHNO}_2]_0/[\text{CH}_3\text{NHNO}_2]_t\}$ vs. $\ln\{[\text{Ref}]_0/[\text{Ref}]_t\}$ in Figure 2.6.

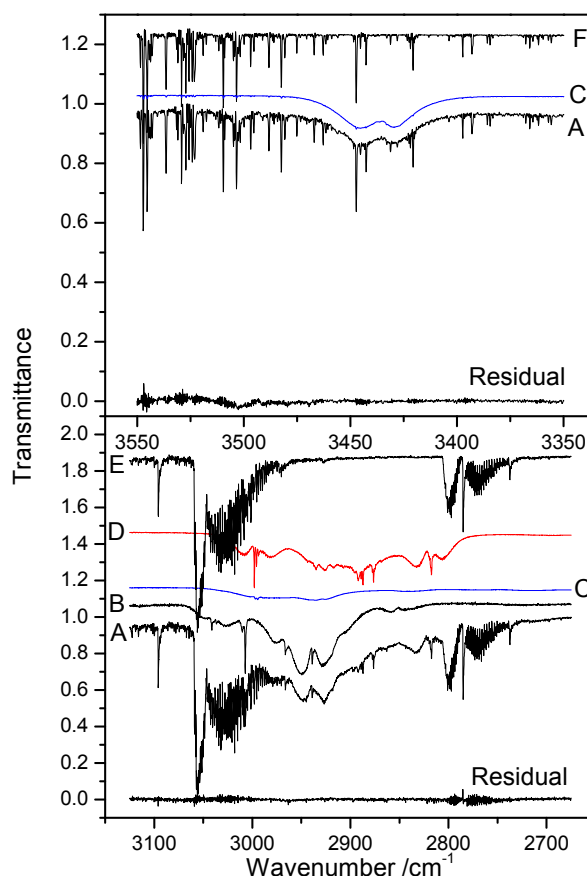


Figure 2.5. Infrared transmission spectra of (A) the $\text{CH}_3\text{NHNO}_2/\text{CH}_3\text{OCH}_3/\text{H}_2/\text{O}_3$ reaction mixture after 15 min photolysis, (B) CH_3OCHO , (C) CH_3NHNO_2 , (D) CH_3OCH_3 , (E) O_3 and (F) H_2O . The spectra (B)-(F) have been shifted for the sake of clarity.

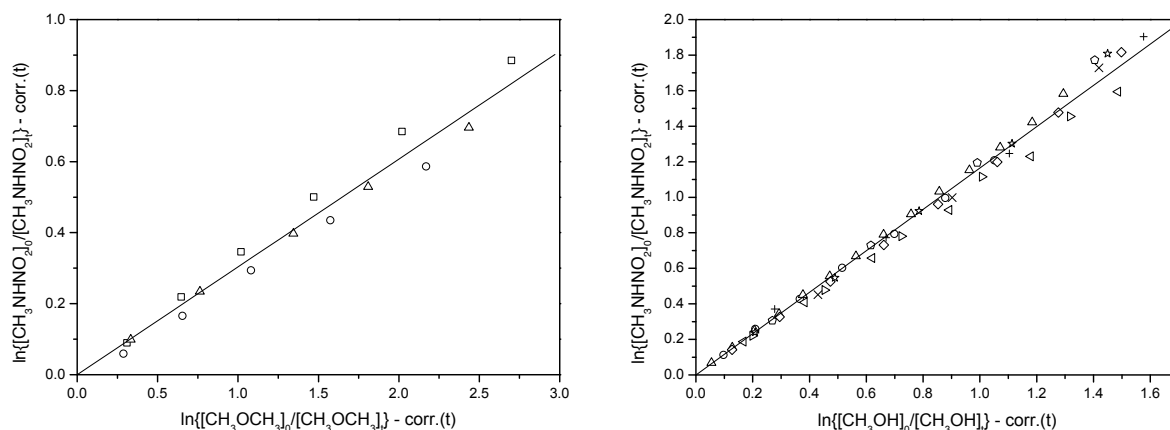


Figure 2.6. (Left) Relative rate plot showing the decay of CH_3NHNO_2 relative to CH_3OCH_3 at 1013 hPa and 298 K in the presence of OH radicals; $k_{\text{rel}} = 0.304 \pm 0.014$ (2σ) determined from 16 data points from 3 independent experiments. The data have been corrected for loss due to reaction with O_3 . (Right) Relative rate plot showing the decay of CH_3NHNO_2 vs. CH_3OH at 1013 hPa and 298 K in the presence of OH radicals; $k_{\text{rel}} = 0.823 \pm 0.023$ (2σ) determined from 49 data points from 9 independent experiments. The data have been corrected for loss due to reaction with O_3 , see text.

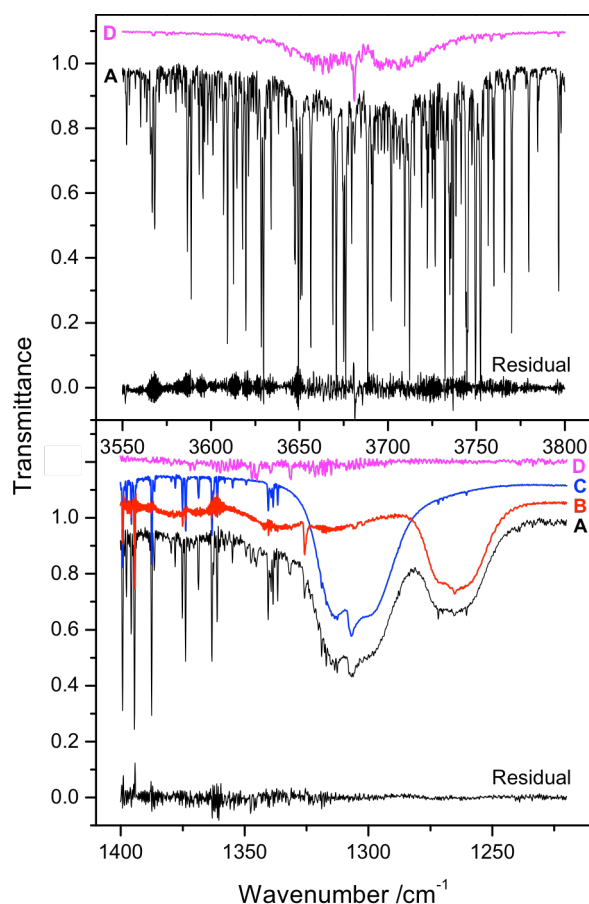


Figure 2.7. Infrared transmission spectra of (A) the *N*-nitro dimethylamine/methanol/ O_3/H_2 reaction mixture after 12 minutes photolysis, (B) *N*-nitro,*N*-methyl formamide, (C) *N*-nitro dimethylamine, (D) methanol, and the residual after spectral fitting. The spectra (B)-(D) have been shifted for the sake of clarity.

Taking recommended values for $k_{\text{OH}+\text{CH}_3\text{OCH}_3} = 2.8 \times 10^{-12}$ and $k_{\text{OH}+\text{CH}_3\text{OH}} = 9.0 \times 10^{-13}$ $\text{cm}^3 \text{ molecule}^{-1} \text{ s}^{-1}$ (both having uncertainty factors of 1.20),³¹ places $k_{\text{OH}+\text{CH}_3\text{NHNO}_2}$ at 0.85 ± 0.17 and 1.05 ± 0.21 $\times 10^{-12}$ $\text{cm}^3 \text{ molecule}^{-1} \text{ s}^{-1}$, respectively, at 298 K. Assuming no additional molecule specific systematic errors this suggests a best value from the present experiments of $k_{\text{OH}+\text{CH}_3\text{NHNO}_2} = (9.5 \pm 1.9) \times 10^{-13}$ $\text{cm}^3 \text{ molecule}^{-1} \text{ s}^{-1}$ at 298 K.

Examples of the FTIR spectra obtained from the kinetic studies of the $(\text{CH}_3)_2\text{NNO}_2/\text{CH}_3\text{OH}$ reaction with OH radicals and the resulting residuals from the non-linear least squares spectral analyses are shown in Figure 2.7. For the sake of brevity, spectra from the $(\text{CH}_3)_2\text{NNO}_2/\text{CH}_3\text{OCH}_3 + \text{OH}$ experiments are not included here. The decays of $(\text{CH}_3)_2\text{NNO}_2$ and the reference compounds CH_3OCH_3 and CH_3OH in the presence of OH radicals are plotted as $\ln\{[(\text{CH}_3)_2\text{NNO}_2]_0/[(\text{CH}_3)_2\text{NNO}_2]_t\}$ vs. $\ln\{[\text{Ref}]_0/[\text{Ref}]_t\}$ in Figure 2.8.

Assuming no other molecule specific systematic errors and including the uncertainty factors in the reference rate coefficient values then suggests a best value from the present experiments of $k_{\text{OH}+(\text{CH}_3)_2\text{NNO}_2} = (3.5 \pm 0.7) \times 10^{-12}$ $\text{cm}^3 \text{ molecule}^{-1} \text{ s}^{-1}$ at 298 K in excellent agreement with the previous result of Tuazon *et al.*,³² $(3.6 \pm 0.7) \times 10^{-12}$ $\text{cm}^3 \text{ molecule}^{-1} \text{ s}^{-1}$.

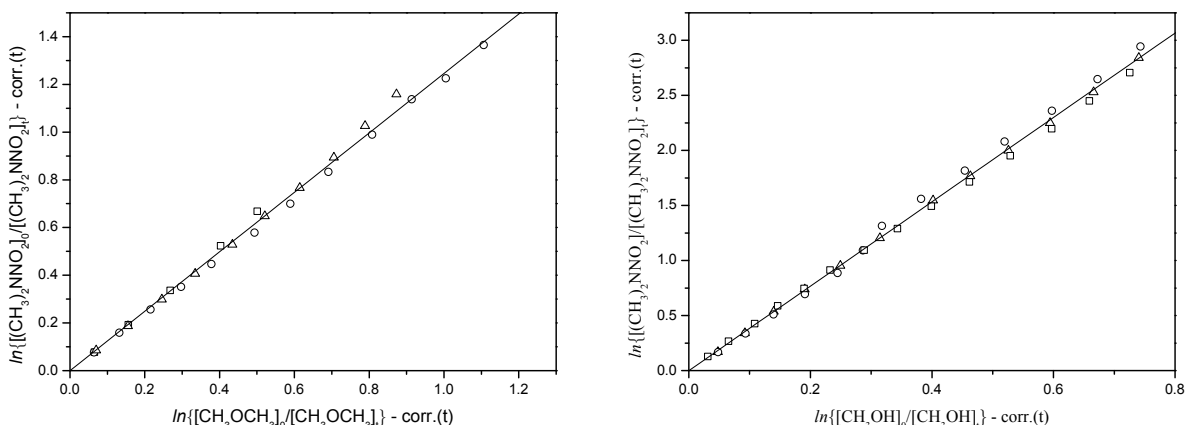


Figure 2.8. (Left) Relative rate plot showing the decay of $(\text{CH}_3)_2\text{NNO}_2$ vs. CH_3OCH_3 at 1013 hPa and 298 K in the presence of OH radicals; $k_{\text{rel}} = 1.246 \pm 0.015$ (2σ) determined from 29 data points from 3 independent experiments. The data have been corrected for loss due to reaction with O_3 , see text. (Right) Relative rate plot showing the decay of $(\text{CH}_3)_2\text{NNO}_2$ vs. CH_3OH at 1013 hPa and 298 K in the presence of OH radicals; $k_{\text{rel}} = 3.83 \pm 0.04$ (2σ) determined from 39 data points from 3 independent experiments. The data have been corrected for loss due to reaction with O_3 , see text.

The rate coefficients for the OH radical reactions with ethylnitramine ($\text{CH}_3\text{CH}_2\text{NHNO}_2$) and dimethylnitramine ($(\text{CH}_3\text{CH}_2)_2\text{NNO}_2$) were determined in relative-rate experiments employing ethylacetate ($\text{CH}_3\text{C}(\text{O})\text{OCH}_2\text{CH}_3$) as reference compound. The rate coefficient of OH radical reaction with ethylacetate has been determined by Picquet *et al.*,³³ Campbell *et al.*,³⁴ Wallington *et al.*³⁵ and by El Boudali *et al.*³⁶ to be $(1.7 \pm 0.3) \times 10^{-12} \text{ cm}^3 \text{ molecule}^{-1} \text{ s}^{-1}$.

Preliminary data from the experiments are shown in the form $\ln\{[\text{nitramine}]_0/[\text{nitramine}]_t\}$ vs. $\ln\{[\text{Reference}]_0/[\text{Reference}]_t\}$ in Figure 2.9 and Figure 2.10; the derived relative rate coefficients are collected in Table 2.4.

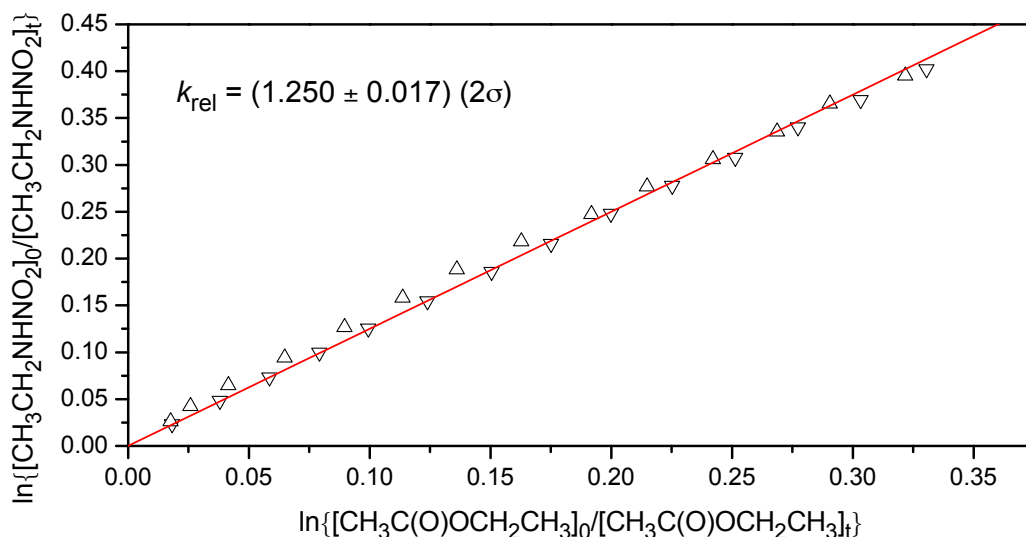


Figure 2.9. Decays of EtNHNO_2 and EtOAc in the presence of OH radicals plotted as $\ln\{[\text{EtNHNO}_2]_0/[\text{EtNHNO}_2]_t\}$ vs. $\ln\{[\text{EtOAc}]_0/[\text{EtOAc}]_t\}$.

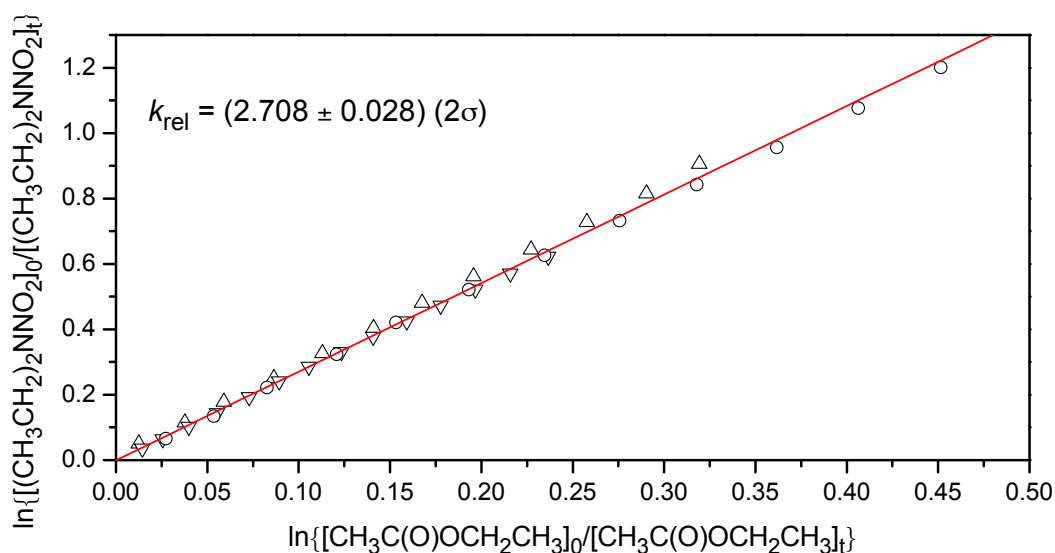


Figure 2.10. Decays of Et₂NNO₂ and EtOAc in the presence of OH radicals plotted as $\ln\{[\text{Et}_2\text{NNO}_2]_0/[\text{Et}_2\text{NNO}_2]_t\}$ vs. $\ln\{[\text{EtOAc}]_0/[\text{EtOAc}]_t\}$.

Table 2.4. Experimental rate constants at 295-300 K for the reactions of OH radicals with nitramines, and estimated lifetimes of nitramines with respect to reaction with OH in the Mongstad area.

Compound	k_{rel}	$k_{\text{OH}}/10^{-12} \text{ cm}^3 \text{ molecule}^{-1} \text{ s}^{-1}$	Reference	$\tau_{\text{OH}}^{\text{a}}$
CH ₃ NHNO ₂	$0.304 \pm 0.014^{\text{a}}$	0.85 ± 0.17	This work	12 d
	$0.823 \pm 0.023^{\text{b}}$	1.05 ± 0.21		
(CH ₃) ₂ NNO ₂	$1.246 \pm 0.015^{\text{a}}$	3.85 ± 0.70	This work 32	3 d
	$3.83 \pm 0.04^{\text{b}}$	3.45 ± 0.70		
		3.5 ± 0.7		
CH ₃ CH ₂ NHNO ₂	$1.250 \pm 0.017^{\text{c}}$		This work	6 d
(CH ₃ CH ₂) ₂ NNO ₂	$2.708 \pm 0.028^{\text{c}}$		This work	3 d

^a Reference compound CH₃OCH₃, $k_{\text{OH}+\text{CH}_3\text{OCH}_3} = 2.8 \times 10^{-12} \text{ cm}^3 \text{ molecule}^{-1} \text{ s}^{-1}$. ^b Reference compound CH₃OH, $k_{\text{OH}+\text{CH}_3\text{OH}} = 9.0 \times 10^{-13} \text{ cm}^3 \text{ molecule}^{-1} \text{ s}^{-1}$. ^c Reference compound CH₃C(O)OCH₂CH₃, $k_{\text{OH}+\text{CH}_3\text{C(O)OCH}_2\text{CH}_3} = 1.7 \times 10^{-12} \text{ cm}^3 \text{ molecule}^{-1} \text{ s}^{-1}$. The lifetimes are estimated for an average OH concentration in the Mongstad area of $9.6 \times 10^5 \text{ cm}^{-3}$.

It can be seen from Table 2.4 that the atmospheric lifetimes of nitramines with respect to reaction with OH radicals are expected to be in the order of days.

2.2.1 Quantum chemical study of nitramine + OH reactions

A systematic comparative study of OH radical reactions with methylamine, dimethylamine, *N*-nitro methylamine and *N*-nitro dimethylamine was undertaken to elucidate the difference in amine and nitramine reactivity. The potential energy surfaces (PES) of the reaction systems were probed in BHandH/aug-cc-pVDZ calculations using Gaussian-09.³⁷ The energies of the stationary states were refined in CCSD(T)/ 6-311++g(2d,2p) calculations. The transition states were verified by intrinsic reaction coordinate (IRC) calculations to connect the designated reactants and products at the same computational levels. Figure 2.11 compares energies of stationary points on the potential energy surfaces for the systems $\text{CH}_3\text{NH}_2/\text{CH}_3\text{NHNO}_2 + \text{OH}$ and $(\text{CH}_3)_2\text{NH}/(\text{CH}_3)_2\text{NNO}_2 + \text{OH}$.

In short, the reactions involve in all cases the formation of pre-reaction adduct complexes (RMC's) in which the OH radicals are H-bonded to the nitro groups, Figure 2.12. Further, the effect of the electron withdrawing nitro group is to increase the barriers to hydrogen abstraction from the neighbouring groups. In the case *N*-nitro methylamine, the barrier to N-H abstraction is calculated to be much higher than that to C-H abstraction ($E_{\text{TS2N}} > E_{\text{TS2C}}$). In the case *N*-nitro dimethylamine, the barrier to C-H abstraction becomes higher than in dimethylamine. Consequently, the theoretical study confirms that the reactivity of nitramines to reaction with OH radicals is lower than that of the corresponding amine, and that hydrogen abstraction from the alkyl chain will be the dominant route for OH reaction with primary nitramines.

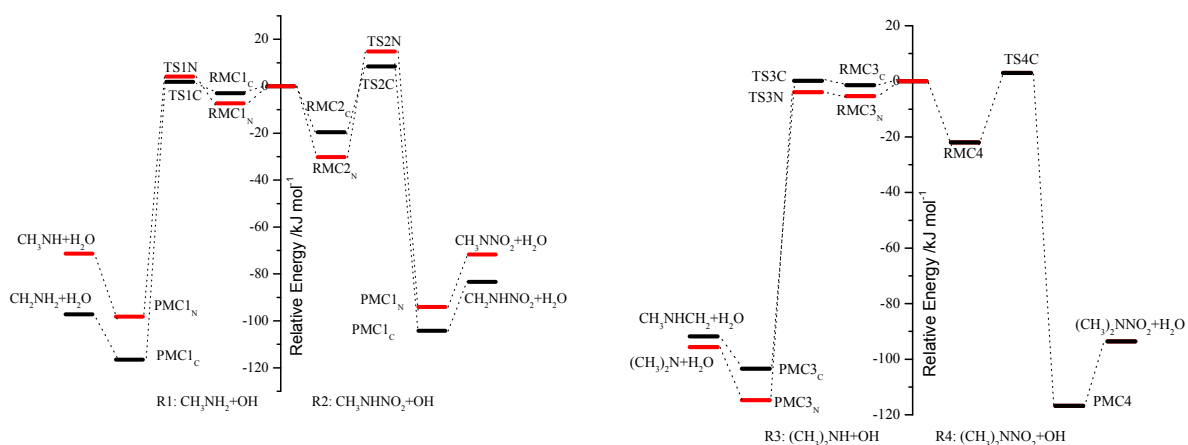


Figure 2.11. Sketch of potential energy surfaces for the reactions of OH radicals with (left) methylamine and *N*-nitro methylamine, and (right) dimethylamine and *N*-nitro dimethylamine.

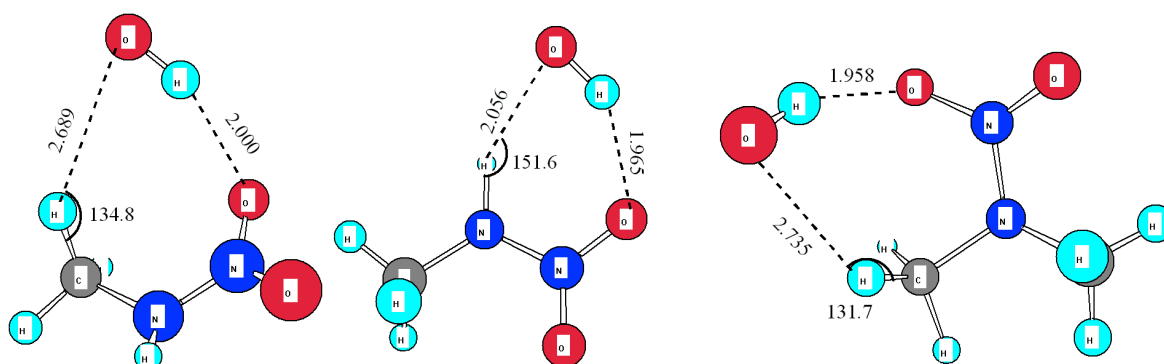


Figure 2.12. Pre-reaction adducts in the reactions of OH radicals with (left) *N*-nitro methanimine and (right) *N*-nitro dimethylamine.

2.2.2 Structure Activity Relationship for OH reactions with nitramines

The OH-SAR of Kwok and Atkinson,²⁹ includes parameters for estimation of the reactivity of nitrosamines and nitramines, Table 2.2. The relevant parameters, group rate constants $k(\text{R}_2\text{NNO}_2)$ and $k(\text{R}_2\text{NNO}_2)$, and a common substituent factor $F(\text{R}_2\text{NNO}) = F(\text{R}_2\text{NNO}_2)$, are based on kinetic data for one nitrosamine, $(\text{CH}_3)_2\text{NNO}$, and one nitramine, $(\text{CH}_3)_2\text{NNO}_2$.

Assuming a common substituent factor for primary and secondary nitramines, $F(\text{RNHNO}_2) = F(\text{R}_2\text{NNO}_2)$, the rate coefficients (in units of $10^{-12} \text{ cm}^3 \text{ molecule}^{-1} \text{ s}^{-1}$ at 298 K) for OH reactions with CH_3NHNO_2 ($(\text{CH}_3)_2\text{NNO}_2$), $\text{CH}_3\text{CH}_2\text{NHNO}_2$ and $(\text{CH}_3\text{CH}_2)_2\text{NNO}_2$ can then, according to the OH-SAR, be written as:

Nitramine		k_{Obs}
CH_3NHNO_2 :	$k_{\text{OH}} = k_{\text{prim}} \times F(\text{RNHNO}_2) + k(\text{RNHNO}_2)$ $= 0.136 \times 9.3 + k(\text{RNHNO}_2) = 1.3 + k(\text{RNHNO}_2)$	0.95
$(\text{CH}_3)_2\text{NNO}_2$:	$k_{\text{OH}} = 2 \times (k_{\text{prim}} \times F(\text{R}_2\text{NNO}_2)) + k(\text{R}_2\text{NNO}_2)$ $= 2 \times (0.136 \times 9.3) + 1.3 = 3.8$	3.55
$\text{CH}_3\text{CH}_2\text{NHNO}_2$:	$k_{\text{OH}} = k_{\text{prim}} \times F(-\text{CH}_2-) + k_{\text{sec}} \times F(-\text{CH}_3) \times F(\text{RNHNO}_2) + k(\text{RNHNO}_2)$ $= 0.136 \times 1.23 + 0.934 \times 1 \times 9.3 + k(\text{RNHNO}_2) = 8.9 + k(\text{RNHNO}_2)$	2.1
$(\text{CH}_3\text{CH}_2)_2\text{NNO}_2$:	$k_{\text{OH}} = 2 \times (k_{\text{prim}} \times F(-\text{CH}_2-) + k_{\text{sec}} \times F(-\text{CH}_3) \times F(\text{R}_2\text{NNO}_2)) + k(\text{R}_2\text{NNO}_2)$ $= 2 \times (0.136 \times 1.23 + 0.934 \times 1.0 \times 9.3) + 1.3 = 19.0$	4.6

It is obvious from the above that the existing SAR parameters for nitramines first of all do not predict the observed OH reactivity of $(\text{CH}_3\text{CH}_2)_2\text{NNO}_2$, and, second, that $F(\text{RNHNO}_2)$ cannot be equal to $F(\text{R}_2\text{NNO}_2)$. The $-\text{NO}_2$ group is electron withdrawing to the extent that the substituent factor $F(-\text{NO}_2)$ has been found to be zero for other organics, *i.e.* there is essentially no reactivity towards OH radicals of a substituted CH_2 -group ($\text{R}-\text{CH}_2-\text{NO}_2$). It is therefore unrealistic to constrain the substituent factors of $-\text{CNHNO}_2$, $-\text{R}_2\text{NNO}_2$ to be the same as those of $-\text{NH}_2$, $>\text{NH}$ and $>\text{N}-$ as implemented in the OH-SAR of Kwok and Atkinson (see Table 2.2),²⁹ It is therefore suggested to modify the OH-SAR for nitramines such that the reactivity of this class of compounds be described in terms of 4 parameters: $F(\text{RNHNO}_2)$, $k(\text{RNHNO}_2)$, $F(\text{R}_2\text{NNO}_2)$ and $k(\text{R}_2\text{NNO}_2)$; the substituent factors express the electron donating/withdrawing properties of the substituents, the group rate constants express the effect of pre-reaction adduct formation in the reaction ($k(\text{RNHNO}_2)$ also includes the contribution from direct H-abstraction from the $>\text{NH}$ group).

The available data suggest the following values ($/10^{-12} \text{ cm}^3 \text{ molecule}^{-1} \text{ s}^{-1}$ at 298 K): $F(\text{RNHNO}_2) = 1.2$, $F(\text{R}_2\text{NNO}_2) = 0.4$; $k(\text{RNHNO}_2) = 0.8$ and $k(\text{R}_2\text{NNO}_2) = 3.4$. Although the values appear sensible one should not put too much trust in them (4 parameters extracted from the 4 linear equations). In summary, the existing data is insufficient to determine a unique set of SAR parameters describing the nitramine reactivity towards OH radicals; more data are needed to develop a reliable SAR for this class of compounds.

3. Results from gas phase photo-oxidation studies

23 ethylamine, dimethylamine, triethylamine and piperazine photo-oxidation experiments were carried out at EUPHORE as part of the ADA-2011 project during July 2010, and during the periods March-April 2011 and May-June 2011. Sections 3.1 through 3.4 summarise the gas phase results obtained and the conclusions drawn from analyses of the experiments. Reaction enthalpies quoted in the text refer to 298 K (kJ mol^{-1}) and stem from G3 calculations.³⁸

The experimental protocols and monitored data from all experiments are summarized as Supplementary Information in: *ADA-2011: Protocols and monitor data*. This information can be downloaded from the ADA-project web portal: <http://www.mn.uio.no/ada>

All major products in the photo-oxidation of ethylamine, diethylamine and triethylamine have been identified and quantified, and detailed photo-oxidation schemes are presented below. Based on the results from the on-line and *in situ* instrumentation it is found that $9 \pm 1\%$ of the reaction between ethylamine and OH radicals takes place at the amino group ($-\text{NH}_2$), and that the nitramine, $\text{CH}_3\text{CH}_2\text{NHNO}_2$, is formed directly as a result of this reaction. It is emphasized that the derived value for the initial branching in the OH radical reaction with ethylamine is based on the assumption that branching of the ethylamino radical reactions with O_2 , NO and NO_2 is the same as that of the diethylamino radical. This assumption does not influence the validity in the extrapolation of laboratory results to ambient conditions. The analysis of the ethylamine photo-oxidation experiments is presented in section 3.2.

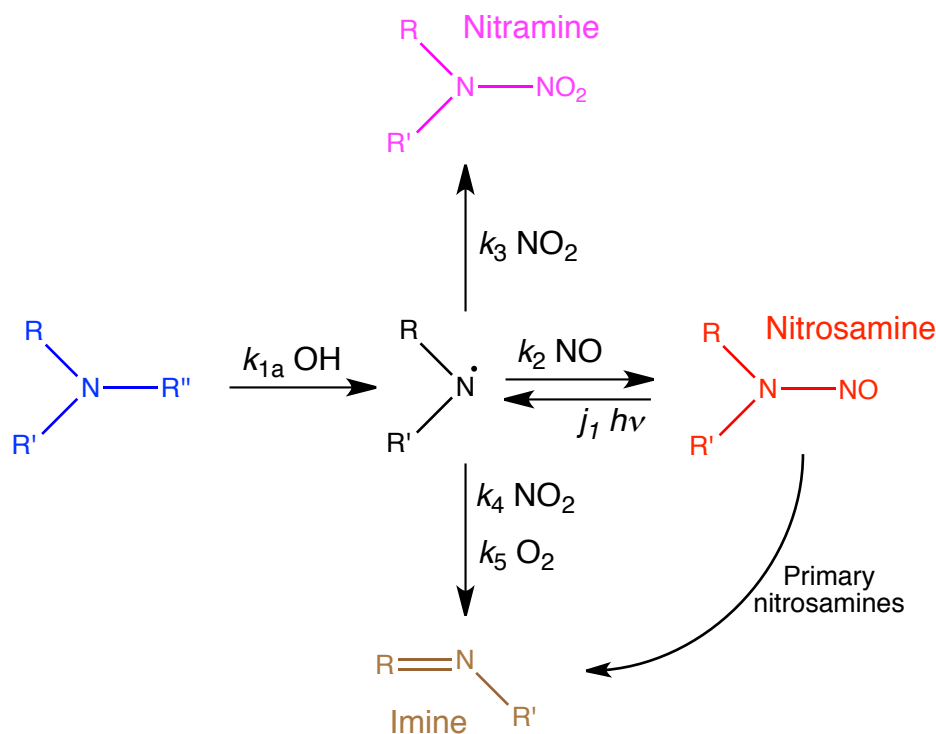
For diethylamine, the data show that $60 \pm 10\%$ of the reaction with OH radicals takes place at the amino group ($>\text{NH}$), and that the nitrosamine, $(\text{CH}_3\text{CH}_2)_2\text{NNO}$, and the nitramine, $(\text{CH}_3\text{CH}_2)_2\text{NNO}_2$, are formed as a result of this reaction. The analysis of the diethylamine photo-oxidation experiments is presented in section 3.3.

For triethylamine, the data show that around $35 \pm 5\%$ of the reaction with OH radicals has the potential to form the nitrosamine, $(\text{CH}_3\text{CH}_2)_2\text{NNO}$, and the nitramine, $(\text{CH}_3\text{CH}_2)_2\text{NNO}_2$. The analysis of the triethylamine photo-oxidation experiments is presented in section 3.4.

It has not been possible to quantify the piperazine photo-oxidation products; *N*-nitroso piperazine and *N*-nitro piperazine are formed but they rapidly undergo further photo-oxidation. The analysis of the piperazine photo-oxidation experiments is presented in section 3.5.

3.1 Estimates of nitrosamine and nitramine formation in the Mongstad area

Estimates of nitrosamine and nitramine formation yields from OH radical reaction with amines are based on the mechanism shown in Scheme 3.1, in which nitrosamine formation from primary amines has been included for completeness. Primary nitrosamines do, however, isomerize and react with O₂ within seconds to give the corresponding imines.⁶



Scheme 3.1. Atmospheric photo-oxidation scheme for amines showing the routes to imines, nitramines and nitrosamines.

The initial amine reaction with OH radicals constitutes the rate-limiting step in the formation of nitrosamines, nitramines and imines. Because nitrosamines are constantly formed and destroyed through photolysis, it makes little sense to quantify the yield as such. The yield (Y) depends on the NO and NO₂ mixing ratios and is given by: $Y = (k_{1a}/k_1) \cdot k_2 \cdot [\text{NO}] / (k_2 \cdot [\text{NO}] + (k_3 + k_4) \cdot [\text{NO}_2] + k_5 \cdot [\text{O}_2])$, where k_1 is the rate coefficient for the initial OH radical reaction with the amine. It is the amount of nitrosamine present in the atmosphere that is relevant, and this can be estimated from steady-state considerations leading to the following expression:^{6,39}

$$\frac{[\text{RR}'\text{NNO}]_{SS}}{[\text{RR}'\text{R}'\text{N}]} = \frac{k_{1a}}{j_1} \cdot \frac{k_2/k_3 \cdot X_{\text{NO}} \cdot X_{\text{OH}}}{(1 + k_4/k_3) \cdot X_{\text{NO}_2} + k_5/k_3 \cdot X_{\text{O}_2}} \quad ; \quad \text{where } X_i \text{ is the mixing ratio of } i$$

The amount of nitramine formed in the atmospheric oxidation of amines depends on the rate coefficient of the initial hydrogen abstraction reaction, the branching ratio in the reaction (here: k_{1a}/k_1), and the branching in the subsequent amino radical reactions (here: $k_3 \cdot [\text{NO}_2] / (k_2 \cdot [\text{NO}] + k_3 \cdot [\text{NO}_2] + k_4 \cdot [\text{NO}_2] + k_5 \cdot [\text{O}_2])$).

Figures 3.1-3.3 shows model simulations of the OH radical concentration (Cl atoms and NO₃ radicals are not considered here), the NO₂-photolysis rate, and the NO and NO₂ mixing ratios in the Mongstad area for September 2006,¹⁹ the results are based on simulations employing the COSMO-MUSCAT model.^{40,41} The Mongstad area is characterized by low NO_x-levels and O₃-levels in the region 30-50 ppbV,⁴² which is also reflected in the NO₂:NO ratio, Table 3.1.

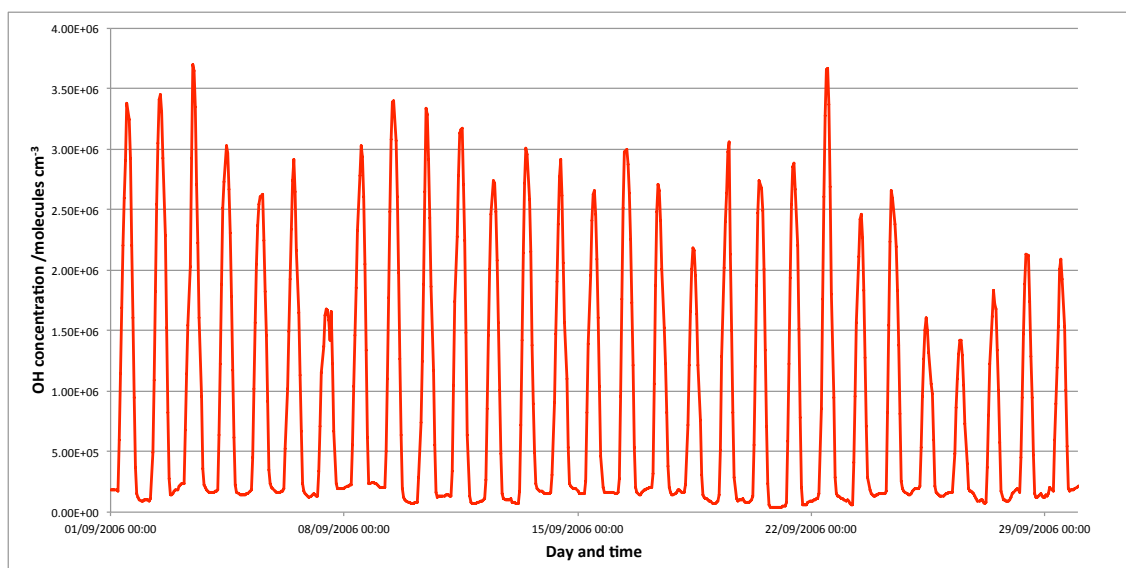


Figure 3.1. Model simulation of the OH radical concentration in the Mongstad area, September 2006.

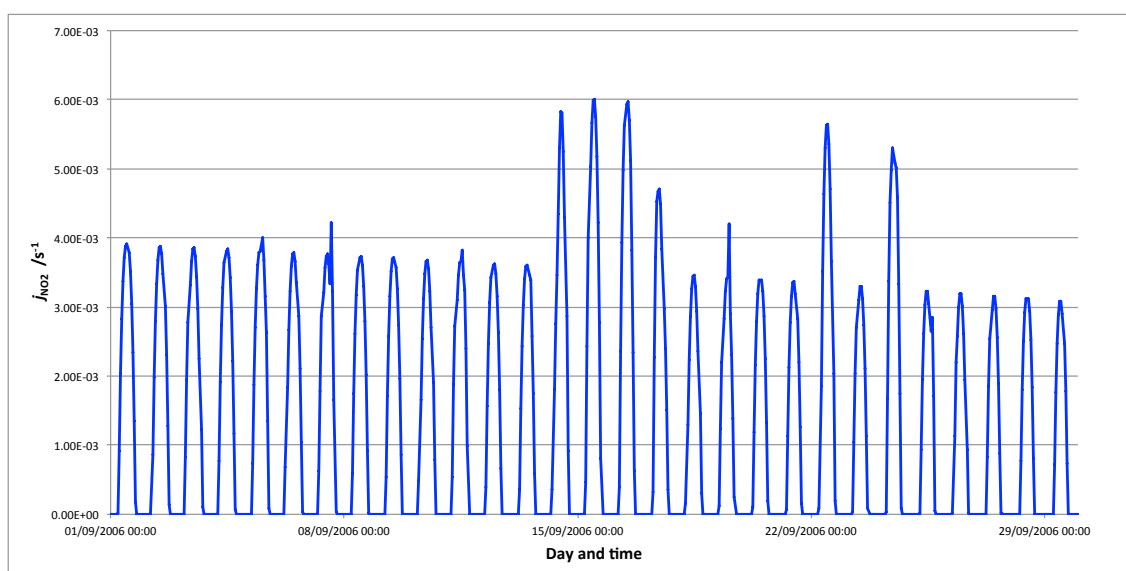


Figure 3.2. Model simulation of the NO₂ photolysis rate in the Mongstad region, September 2006.

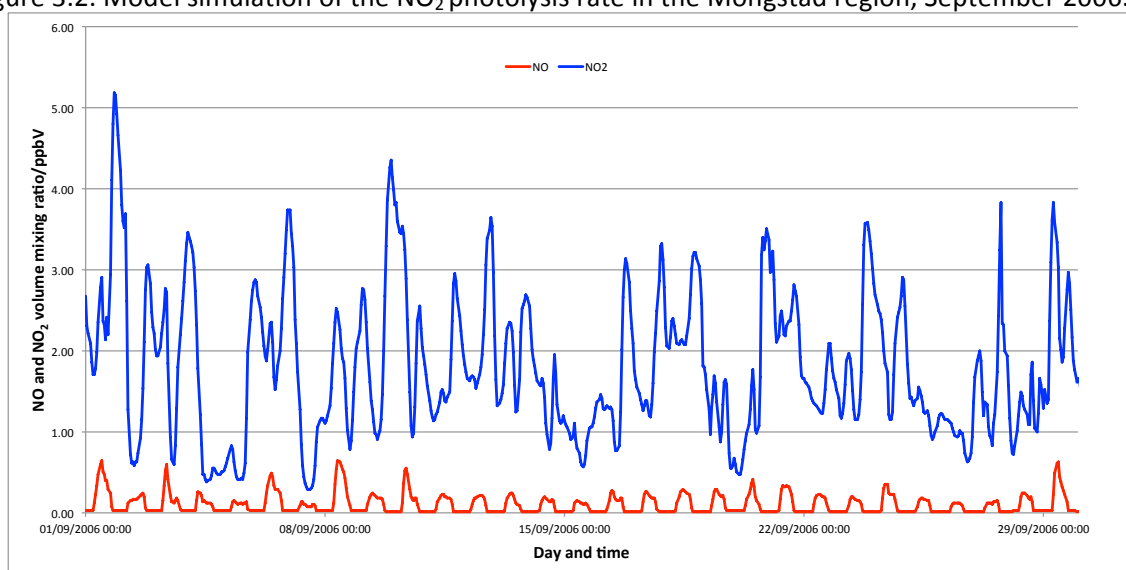


Figure 3.3. Model simulation of the NO and NO₂ mixing ratios in the Mongstad area, September 2006.

There is no reason that 2006 should differ from other years with respect to average values of OH, j_{NO_2} , NO and NO₂. The daily values, however, should only be used as part of larger time series. The average values of OH, j_{NO_2} , NO, NO₂ and O₃ during the months of March, June, September and December are summarized in Table 3.1; the annual average values of OH, j_{NO_2} , NO, NO₂ and O₃ in the Mongstad area are close to those for the month of September. It is obvious from Figure 3.1-Figure 3.3 and Table 3.1 that there will be large annual and daily variations in the nitramine yield and the nitrosamine steady-state mixing ratios. Yields in atmospheric photo-oxidation of compounds are not necessarily linear in terms of reactant mixing ratios.

It is stressed that employing average values of OH, j_{NO_2} , NO, NO₂ and O₃ to estimate nitrosamine and nitramine formation in atmospheric amine photo-oxidation is only a first approximation. Chemical Transport Models are needed to find the diurnal variations and, ultimately, average mixing ratios.

Table 3.1. Average values of NO₂ photolysis rate, OH radical concentration, and NO, NO₂ and O₃ volume mixing ratios in the Mongstad region.^a

	March	June	September	December	Average
j_{NO_2} /s ⁻¹	1.22×10^{-3}	2.76×10^{-3}	1.32×10^{-3}	2.82×10^{-5}	1.32×10^{-3}
OH /molecules cm ⁻³	3.90×10^5	2.57×10^6	8.88×10^5	6.77×10^5	9.58×10^5
NO /ppbV	0.228	0.212	0.106	0.268	0.139
NO ₂ /ppbV	1.70	1.95	1.83	1.43	1.99
O ₃ /ppbV	55	74	85	63	69

^a Data from Ref. 19.

Table 3.2 summarises the molecule specific parameters used in estimating annual average nitramine yield and nitrosamine steady-state mixing ratios. For the sake of completeness, Table 3.2 also includes literature parameters for MEA (aminoethanol),⁴³ methylamine and dimethylamine.⁶

Table 3.2. Reaction rate coefficients and branching ratios for formation of the corresponding amino radical and its reactions with NO, O₂ and NO₂. See Scheme 3.1 for definition of rate coefficients.

Amine	$k_{\text{Amine+OH}}$ ^a	$k_{\text{Nitramine+OH}}$ ^a	j_1/j_{NO_2}	k_{1a}/k_1	k_2/k_3	k_4/k_3	k_5/k_3	Nitramine yield	
								2h	∞
CH ₃ NH ₂ ^b	2.0×10^{-11}	9.5×10^{-13}	N.A.	0.25	0.75	4.0	2.0×10^{-6}	0.04%	0.34%
(CH ₃) ₂ NH ^b	6.5×10^{-11}	3.6×10^{-12}	0.25	0.42	0.75	0.10	3.0×10^{-7}	1.3%	3.8%
CH ₃ CH ₂ NH ₂	2.6×10^{-11}	2.1×10^{-12}	N.A.	0.09	0.70	0.0	11.2×10^{-7}	0.04%	0.23%
(CH ₃ CH ₂) ₂ NH	7.4×10^{-11}	4.6×10^{-12}	0.30	0.60	0.70	0.0	11.2×10^{-7}	0.60%	1.5%
(CH ₃ CH ₂) ₃ N ^d	7.7×10^{-11}	4.6×10^{-12}	0.30	0.35	0.70	0.0	11.2×10^{-7}	0.23%	0.30%
MEA ^c	3.1×10^{-11}	3.5×10^{-12}	N.A.	0.08	0.26	0.22	3.9×10^{-7}	0.10%	0.57%

^a Unit: cm³ molecule⁻¹ s⁻¹. ^b From Ref. 6. ^c From Ref. 43. ^d See section 3.4.3 for details. Reaction with O₃ included in calculation, $k_{\text{O}_3+(\text{CH}_3\text{CH}_2)_3\text{N}} = 8.2 \times 10^{-17}$ cm³ molecule⁻¹ s⁻¹.

Two scenarios are considered:

1. $\langle \text{NO} \rangle_a = 0.14$ ppbV, $\langle \text{NO}_2 \rangle_a = 2.0$ ppbV and $\langle \text{O}_3 \rangle_a = 69$ ppbV
2. $\langle \text{NO} \rangle_a = 0.42$ ppbV, $\langle \text{NO}_2 \rangle_a = 6.0$ ppbV and $\langle \text{O}_3 \rangle_a = 69$ ppbV (three times higher NO_x-levels).

The results for scenario 2, with NO_x-levels 3 times those from the COSMO-MUSCAT model simulations of the Mongstad area, are considered to represent upper limits to the amounts of nitrosamines and nitramines that may result from an amine emission. The average wind speed in the Mongstad area is around 4 m s⁻¹.⁴² During 2 hours an air parcel will therefore, on average, travel 30 km. It is therefore of interest to know not only the theoretical maximum nitramine yield, but also the nitramine yield during the first hours after emission. Table 3.2 includes the calculated nitramine yield 2 hours after emission as well as the maximal yield (100% photo-oxidized amine). Figure 3.4-Figure 3.6 illustrate the results from box-model calculations of the atmospheric photo-oxidation of amines plotted as a function of time after emission. The calculations are based on annual average values of OH, NO and NO₂ in the Mongstad area, and the branching data given in Table 3.2.

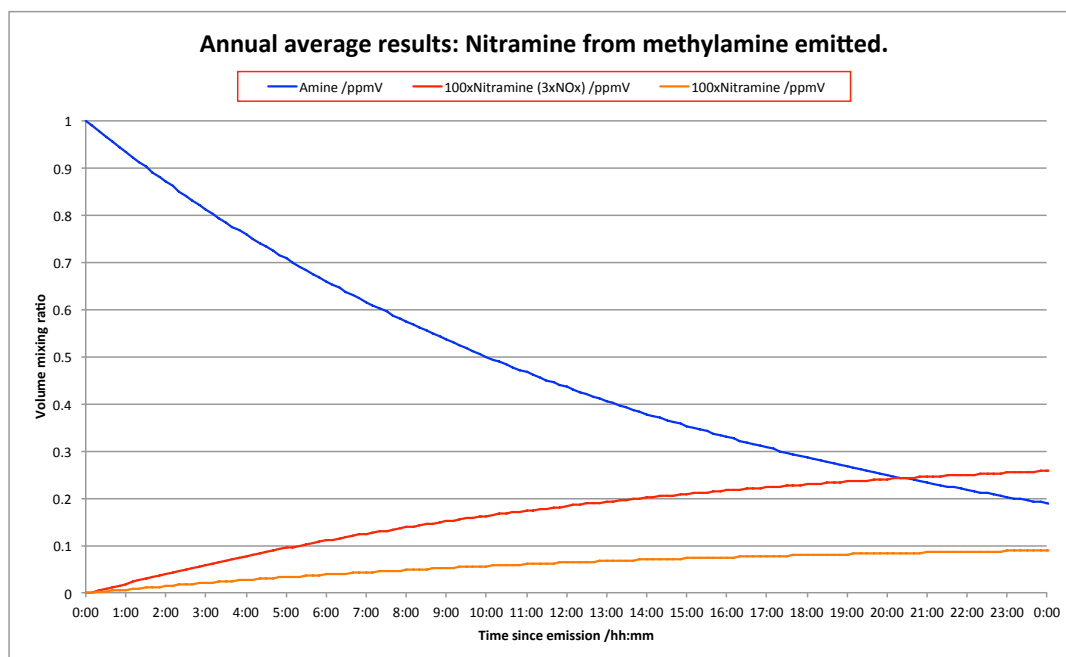


Figure 3.4. Results from a box model simulation of *N*-nitro methylamine formation in a closed air parcel with 1 ppmV initial methylamine mixing ratio. Results for annual average conditions in the Mongstad area.

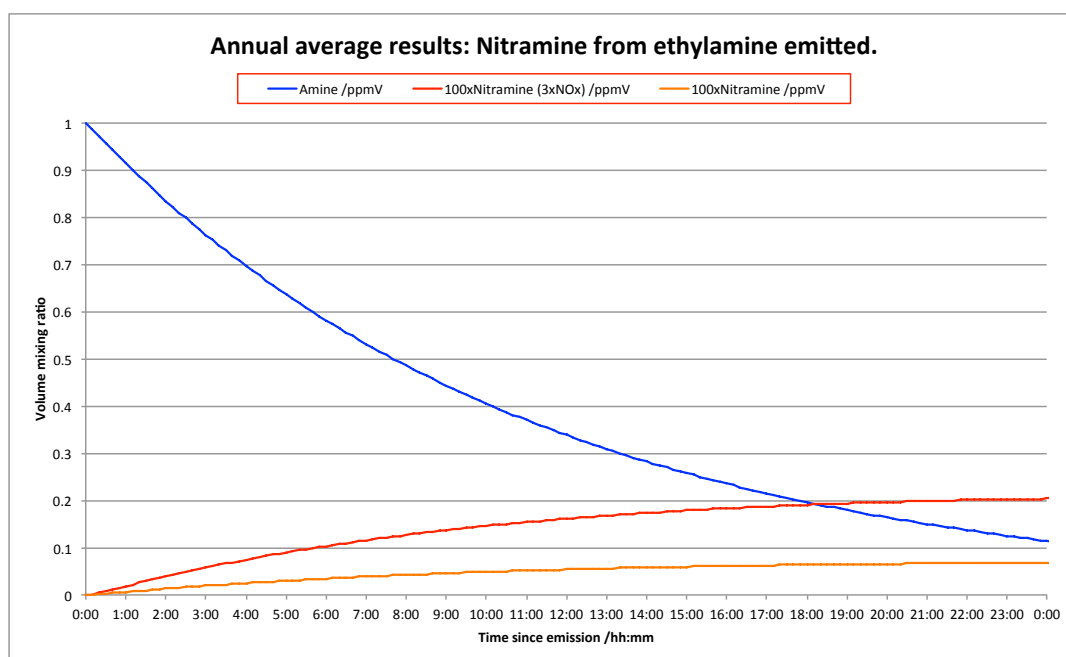


Figure 3.5. Results from a box model simulation of *N*-nitro ethylamine formation in a closed air parcel with 1 ppmV initial ethylamine mixing ratio. Results for annual average conditions in the Mongstad area.

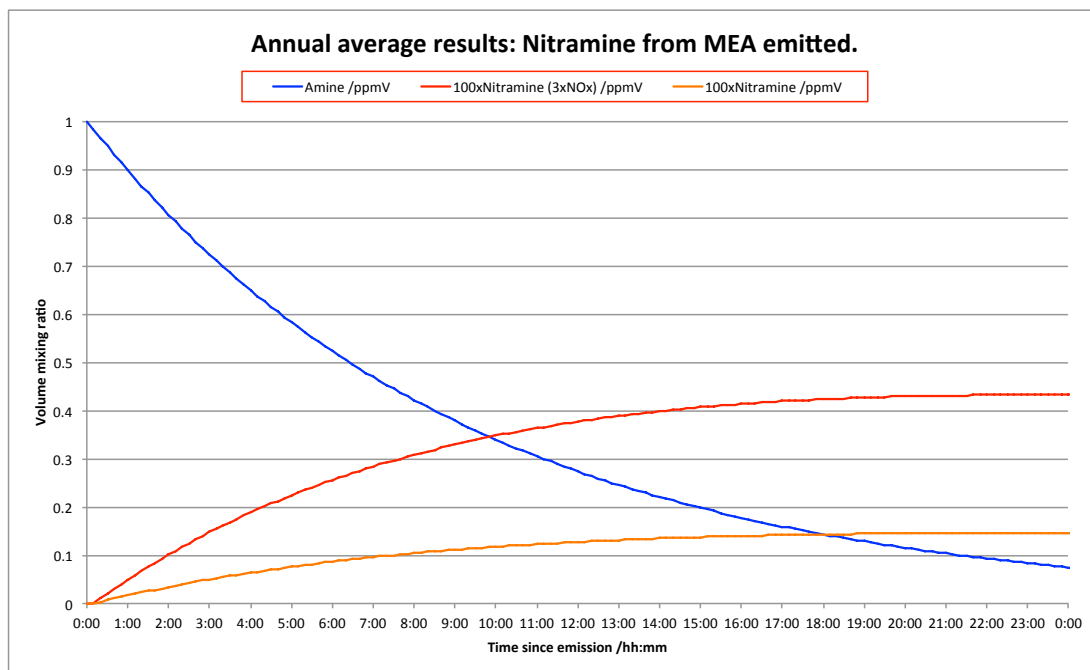


Figure 3.6. Results from a box model simulation of *N*-nitro aminoethanol formation in a closed air parcel with 1 ppmV initial aminoethanol mixing ratio. Results for annual average conditions in the Mongstad area.

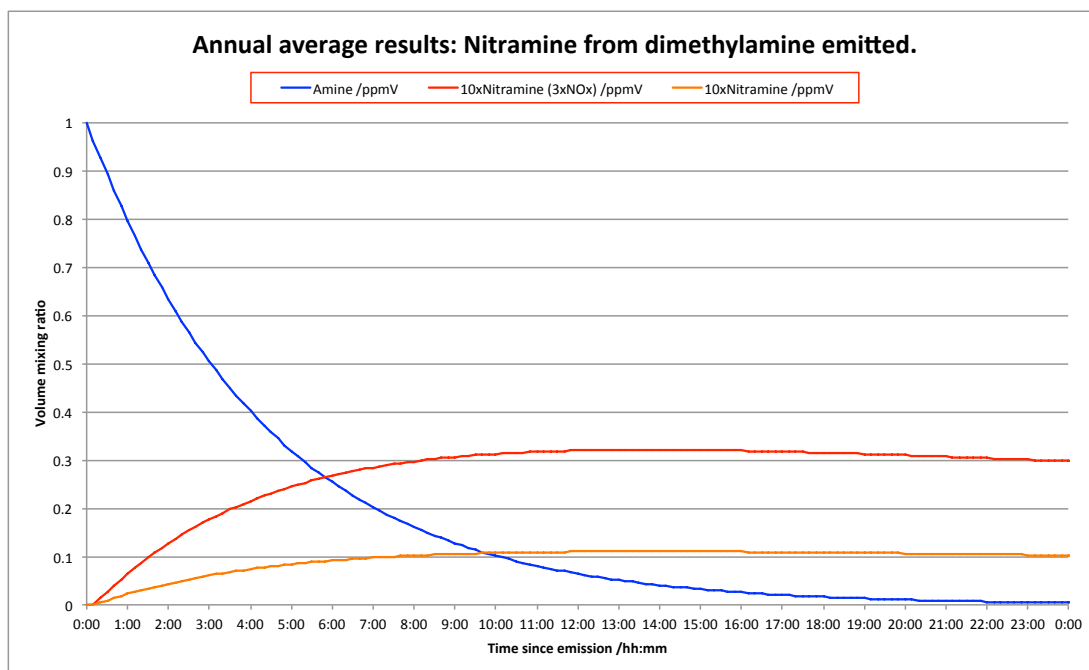


Figure 3.7. Results from a box model simulation of *N*-nitro ethylamine formation in a closed air parcel with 1 ppmV initial ethylamine mixing ratio. Results for annual average conditions in the Mongstad area.

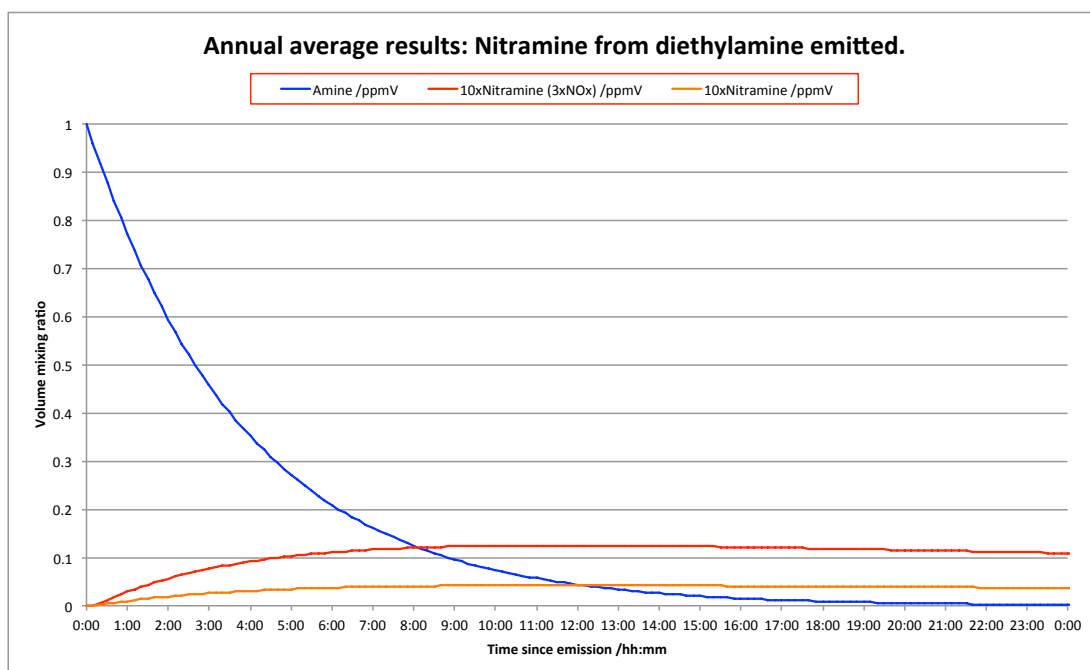


Figure 3.8. Results from a box model simulation of *N*-nitro diethylamine formation in a closed air parcel with 1 ppmV initial diethylamine mixing ratio. Results for annual average conditions in the Mongstad area.

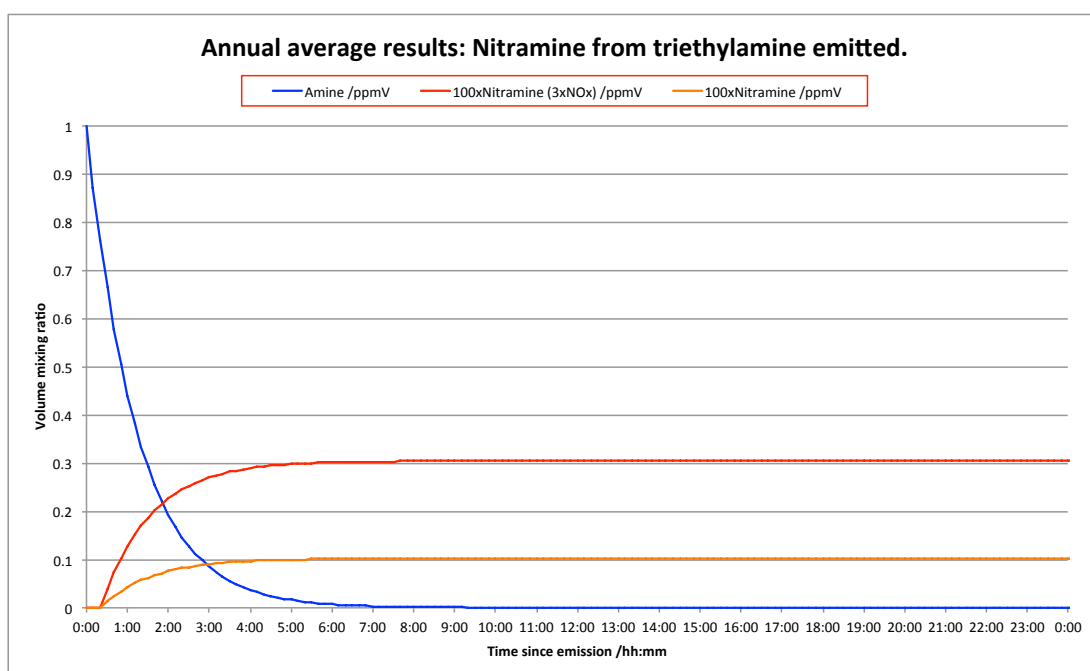


Figure 3.9. Results from a box model simulation of *N*-nitro diethylamine formation in a closed air parcel with 1 ppmV initial triethylamine mixing ratio. Results for annual average conditions in the Mongstad area.

The estimated amount of nitrosamine present in an amine containing closed air parcel as a function of time since emission is shown in Figure 3.10 for dimethylamine and in Figure 3.11 for diethylamine. The calculations are based on annual average values of OH, NO and NO₂ in the Mongstad area, and the branching data given in Table 3.2. It can be seen that the maximum nitrosamine mixing ratios under average conditions are found between 1 and 2 hours after emission. For dimethylamine the maximum amount is 0.26 ‰ of the emitted amine; for diethylamine and triethylamine the maximum amounts are 0.1 and 0.12 ‰, respectively. Under average conditions, the steady-state nitrosamine:amine ratio is estimated to be 0.34 ‰ for dimethylamine and 0.13 ‰ for diethylamine.

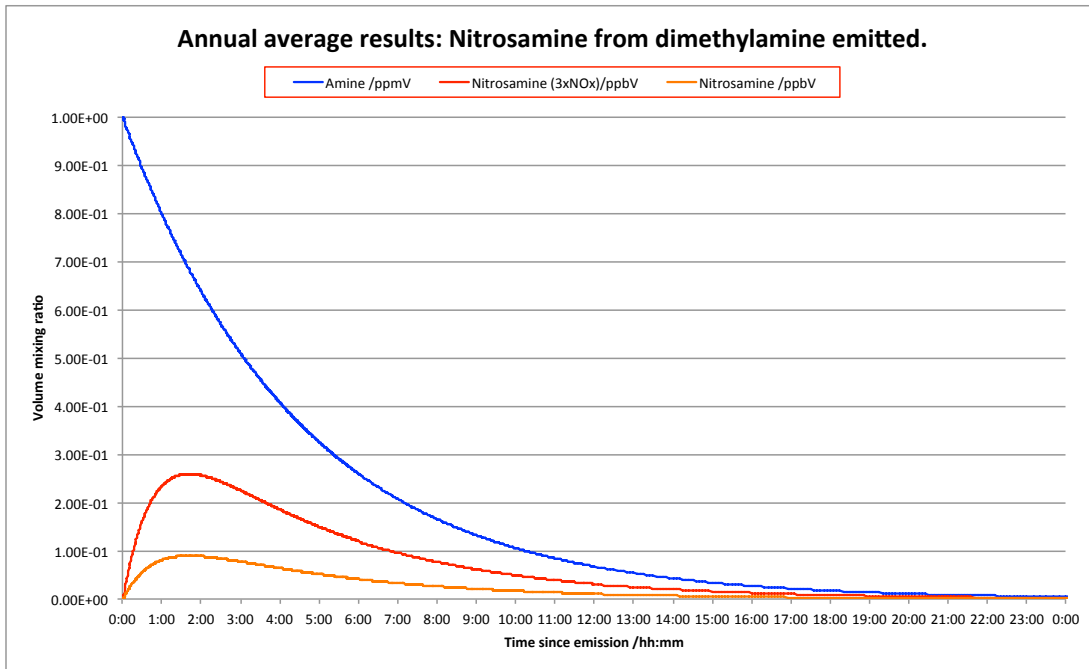


Figure 3.10. Results from a box model simulation of *N*-nitroso dimethylamine formation in a closed air parcel with 1 ppmV initial dimethylamine mixing ratio. Results for annual average conditions in the Mongstad area.

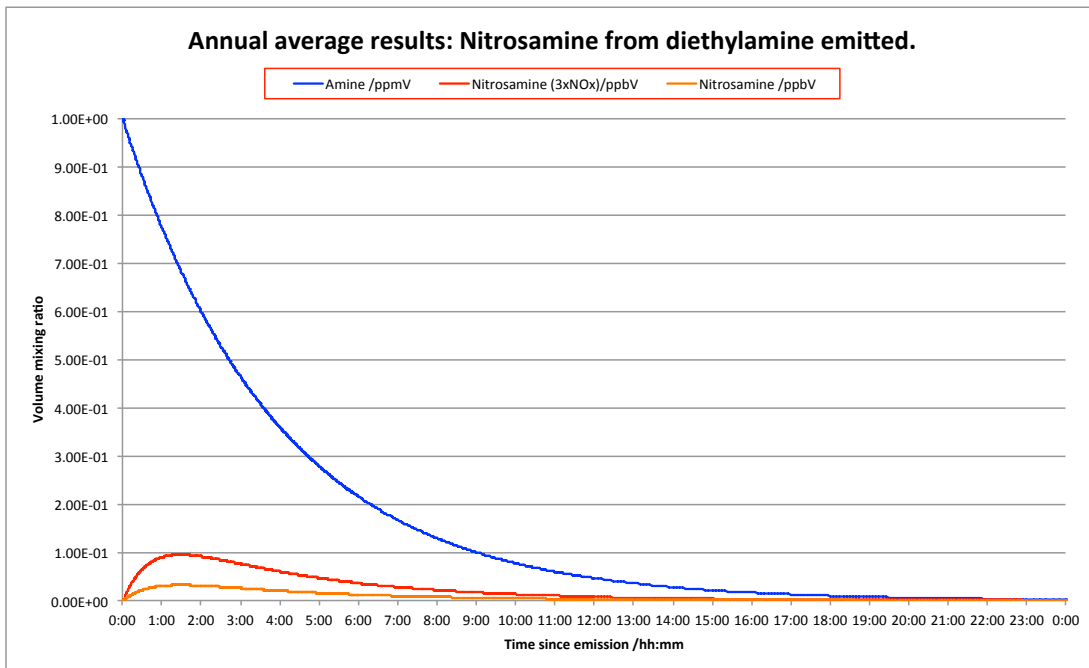


Figure 3.11. Results from a box model simulation of *N*-nitroso diethylamine formation in a closed air parcel with 1 ppmV initial diethylamine mixing ratio. Results for annual average conditions in the Mongstad area.

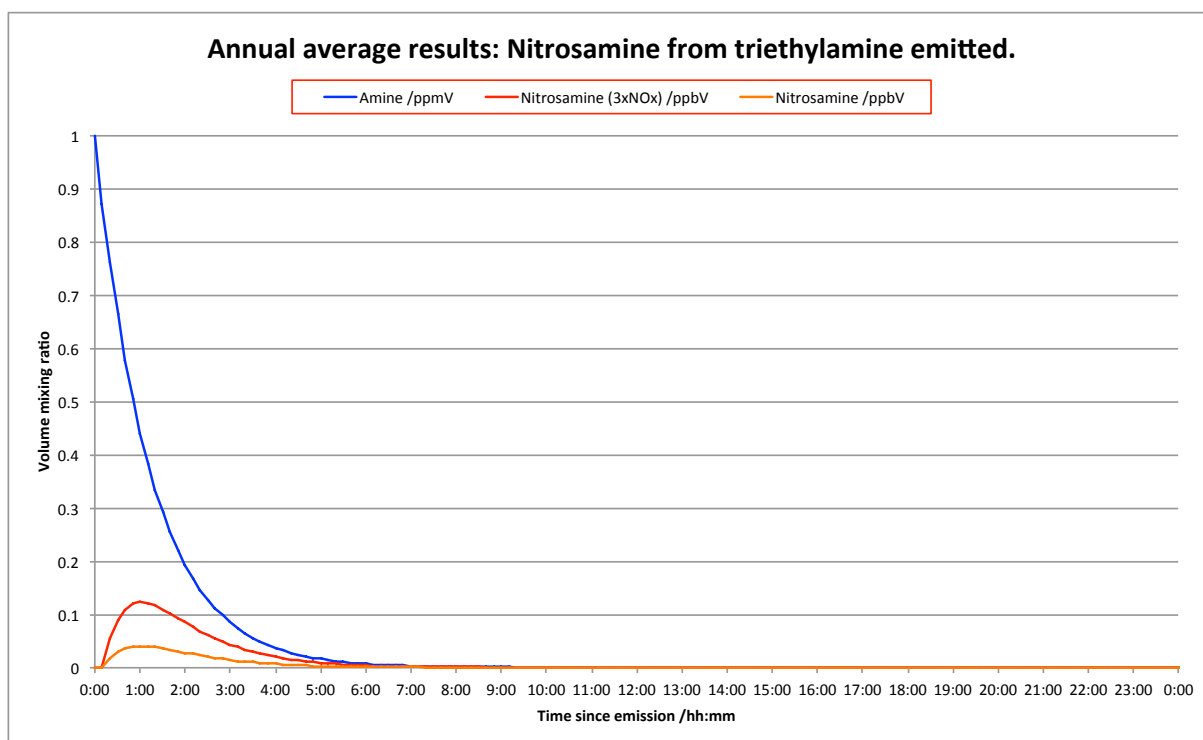


Figure 3.12. Results from a box model simulation of *N*-nitroso diethylamine formation in a closed air parcel with 1 ppmV initial triethylamine mixing ratio. Results for annual average conditions in the Mongstad area.

3.2 Ethylamine

Previous studies. The only experimental data on products formed in the atmospheric photo-oxidation of ethylamine stem from the ADA-2009 project, in which $\text{CH}_3\text{CH}_2\text{NHNO}_2$ (*N*-nitro ethylamine, ethylnitramine) was identified as one of the products in the OH-initiated photo-oxidation under high-NO_x conditions.⁴³ Atkinson *et al.*²⁰ determined the rate coefficient for the reaction of OH radicals with $\text{CH}_3\text{CH}_2\text{NH}_2$ over the temperature range 299 – 426 K and reported a negative Arrhenius activation energy, $k_{\text{OH}}(T) = 1.47 \times 10^{-11} \times \exp\{(190 \pm 150)\text{K}/T\}$ and $k_{\text{OH}} = (2.77 \pm 0.28) \times 10^{-11} \text{ cm}^3 \text{ molecule}^{-1} \text{ s}^{-1}$ at 298 K. Carl and Crowley¹⁸ reported a room temperature value that agreed to within 10%, $k_{\text{OH}} = (2.38 \pm 0.5 / -0.15) \times 10^{-11} \text{ cm}^3 \text{ molecule}^{-1} \text{ s}^{-1}$. Atkinson and Pitts⁴⁴ determined the rate coefficient of the $\text{O}(^3\text{P})$ atom reaction with ethylamine in the temperature range 298 – 440 K and reported a positive activation energy, $k_{\text{O}(^3\text{P})}(T) = 1.13 \times 10^{-11} \times \exp\{-(1275 \pm 200)/RT\}$ and $k_{\text{O}(^3\text{P})} = (1.33 \pm 0.14) \times 10^{-12} \text{ cm}^3 \text{ molecule}^{-1} \text{ s}^{-1}$ at 298 K. Slagle *et al.*⁴⁵ employed photo-ionization mass spectrometry and identified $\text{C}_2\text{H}_5\text{N}$ and $\text{C}_2\text{H}_6\text{N}$ as products in the $\text{O}(^3\text{P})$ reaction with ethylamine.

Galano and Alvarez-Idaboy⁴⁶ carried out a theoretical study of the OH reaction with ethylamine and calculated the rate coefficient at the CCSD(T)/6-311++G(2d,2p)//BH&HLYP/6-311++G(2d,2p) level of theory. Their result is $k_{\text{OH}}(T) = 1.39 \times 10^{-11} \times \exp(-49/RT) \text{ cm}^3 \text{ molecule}^{-1} \text{ s}^{-1}$ and $k_{\text{OH}} = 5.20 \times 10^{-12}$ at 298 K; they predict a *positive* Arrhenius activation energy. They also predict a branching ratio for H-abstraction from the CH_3 , CH_2 and NH_2 groups to be 0.004 : 0.977 : 0.019 at 298 K.

Murphy *et al.*⁴⁷ studied aerosol formation following NO_3 radical reaction with $\text{CH}_3\text{CH}_2\text{NH}_2$. The particles formed in their experiment consisted almost exclusively of ethylamminium nitrate - the contribution from non-salt organics was negligible.

Present studies. Four ethylamine experiments were carried out – two under high-NO_x conditions during the spring campaign 2011, and two under low-NO_x conditions during the summer campaign 2011. IPN-d6, $\text{CD}_3\text{CH}(\text{ONO})\text{CD}_3$, was added as an extra OH precursor in the spring experiments:

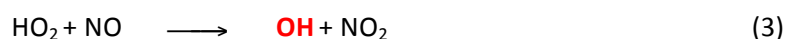
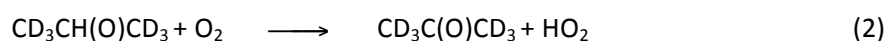
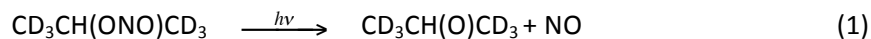


Table 3.3 summarises the ion signals above 1% of the ethylamine ion signal loss detected by PTR-TOF-MS during the photo-oxidation experiments; the 8 largest ion signals are highlighted in boldface type in the table. Figure 3.13 illustrates the data from the 2011.03.25 afternoon experiment; it can be seen that the signals divide into 4 groups.

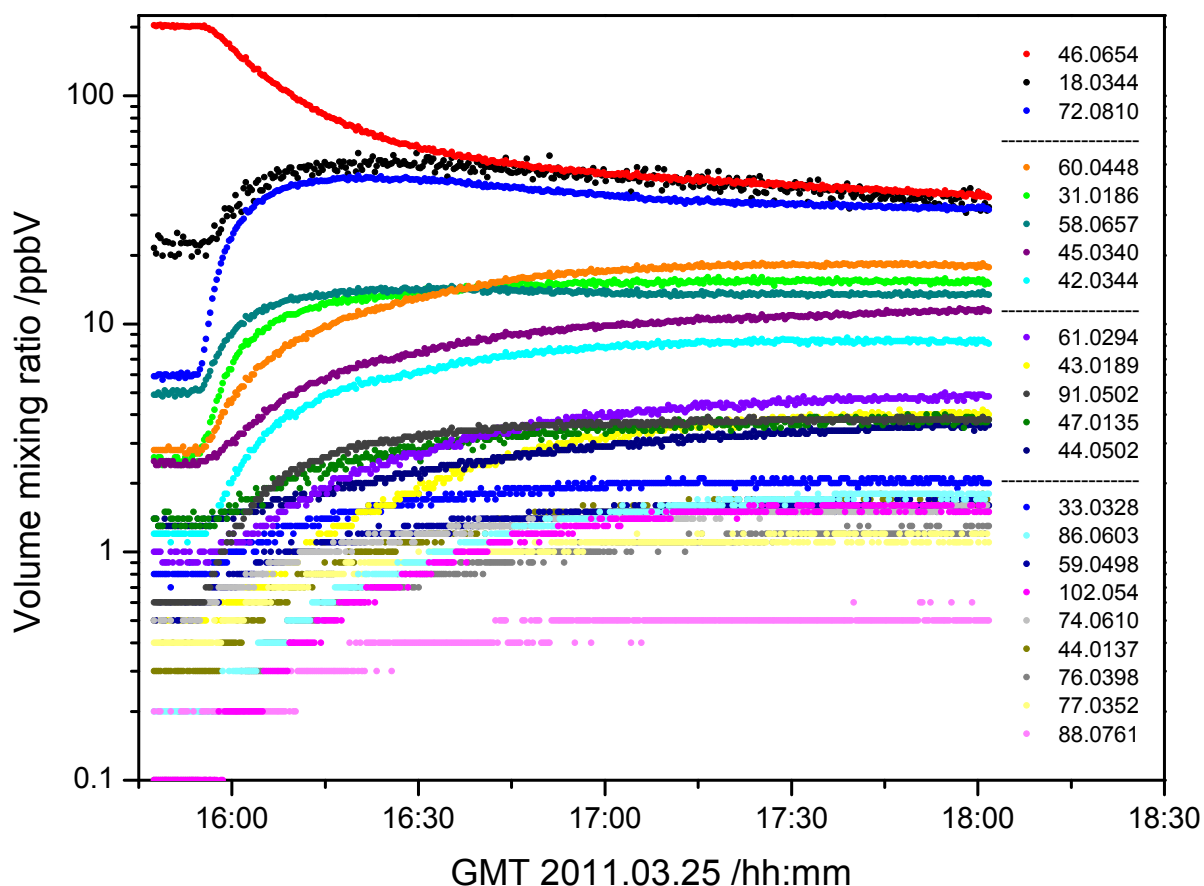
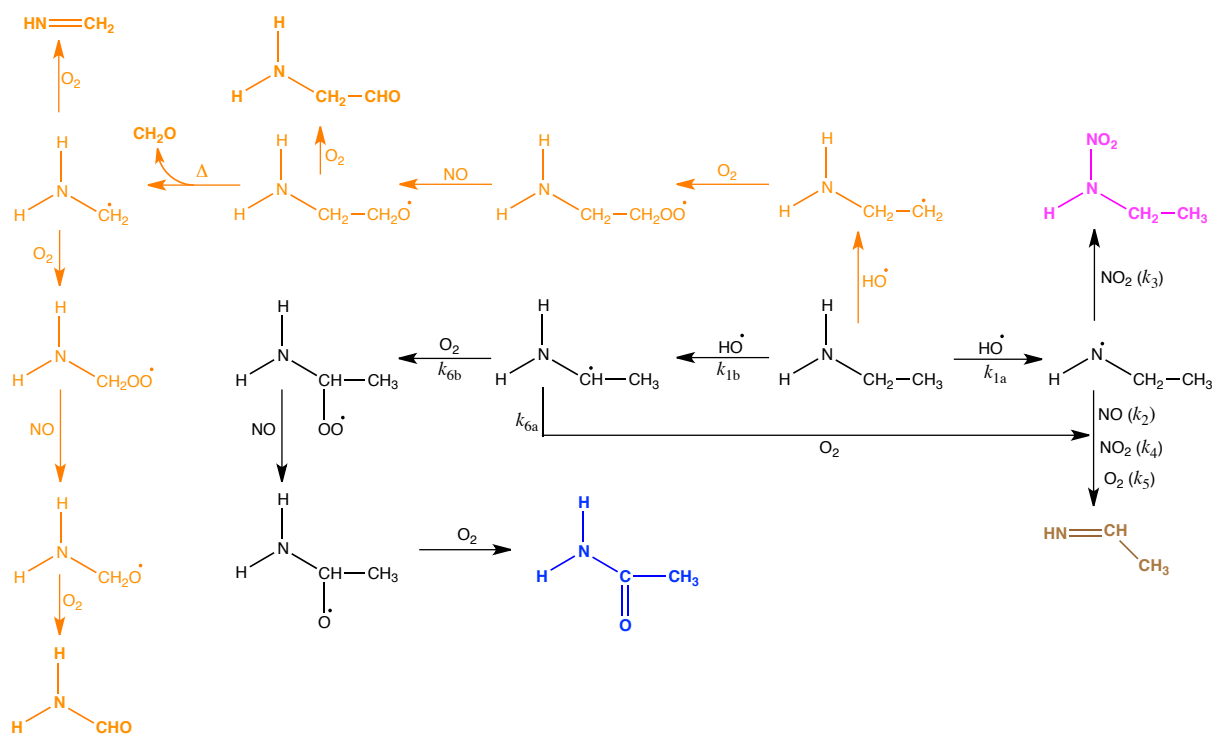


Figure 3.13. Observed ion signals and ion precursor volume mixing ratios during the ethylamine photo-oxidation experiment in the afternoon on 2011.03.25.

Of the 24 ion signals, registered by PTR-TOF-MS and with intensities above 1% of the ethylamine ion signal drop, only 1 of the 8 major ion signals corresponds exactly to that of the theoretically predicted products, Scheme 3.2. Further, the ion signal m/z 44.0502, corresponding to an expected major product, $\text{CH}_3\text{CH}=\text{NH}$ (ethanimine), falls in the lower end of the third bundle of signals detected above the 1%-level.

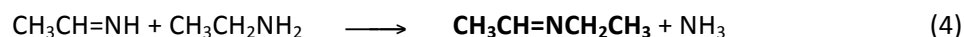
The low- NO_x experiments were affected by a diethylamine impurity from previous experiments giving rise to two additional ion signals m/z 74.0971 and 119.0608, corresponding to protonated $(\text{CH}_3\text{CH}_2)_2\text{NH}$ and $(\text{CH}_3\text{CH}_2)_2\text{NNO}_2$, respectively.

Six of the observed product ion signals stem from N-containing C_3 and C_4 compounds. These signals are highlighted in red colour in Table 3.3 and are explained by condensation reactions between aldehydes, ketones, carboxylic acids and imines on chamber and instrument inlet surfaces. Layer reviewed the chemistry of imines nearly 50 years ago and reported condensation reactions between amines and imines.⁴⁸ A more recent *in situ* study demonstrates a fast surface-catalysed reaction between 2,2-dimethylpropanal and methylamine.⁴⁹ Similar observations of products with more carbon atoms than the reactant was also made by Pitts *et al.* in their photo-oxidation study of diethylamine,⁵⁰ by Tuazon *et al.* in their study kinetics and product studies of O_3 reactions with amines⁵¹ and by Nielsen and co-workers in photo-oxidation studies of MEA,⁴³ and of methyl-, dimethyl- and trimethylamine.⁵²

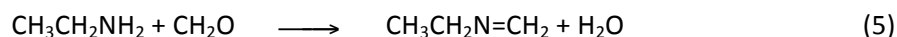


Scheme 3.2. Theoretical atmospheric photo-oxidation scheme for ethylamine. The orange coloured route is expected to be of minor importance.

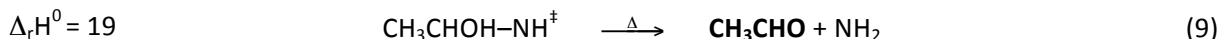
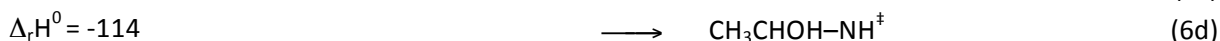
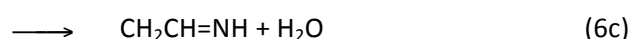
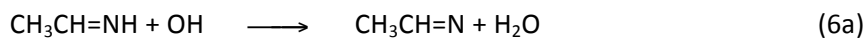
In the present experiments, the m/z 18.0344 (protonated NH_3) and m/z 72.0814 ($\text{C}_4\text{H}_{10}\text{N}^+$) ions may be explained by the condensation reaction between ethanimine and ethylamine:



The m/z 58.0657 ion signal ($\text{C}_3\text{H}_8\text{N}^+$, $\text{CH}_3\text{CH}_2\text{N}=\text{CH}_2$) may be explained by the condensation reaction between ethylamine and formaldehyde:



The m/z 42.0344 ion signal ($\text{C}_2\text{H}_3\text{N}^+$, protonated acetonitrile) may result from photo-oxidation of ethanimine. This process may also, in part, explain the m/z 60.0448 ion signal (protonated $\text{NH}_2\text{C}(\text{O})\text{CH}_3$ and/or $\text{NH}_2\text{CH}_2\text{CHO}$):



Formaldehyde is often a "chamber artefact"; the m/z 31.0186 signal (protonated CH_2O) is, however, unusually high and not a chamber artefact in this experiment. In fact it is one of the major ion signals showing a time-profile similar to that of $\text{CH}_3\text{CH}=\text{NCH}_2\text{CH}_3$ and may therefore, in part, have the same origin. The vibrationally excited 2-oxo ethylamine radical (9) may also undergo an exothermic C-C

bond scission forming the NH₂ radical and acetaldehyde – the last of the major products observed in the experiment (m/z 45.0342, protonated CH₃CHO).

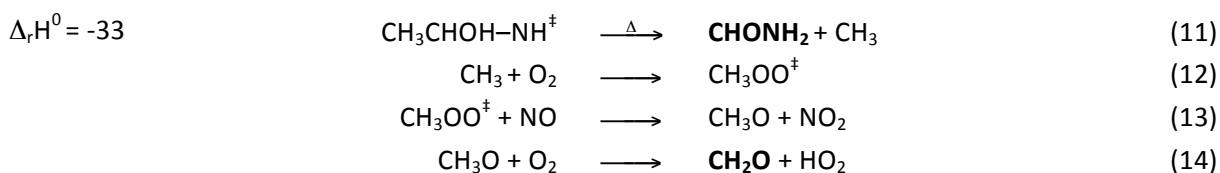


Table 3.3. Ion signals above 1% of the ethylamine ion signal loss observed in CH₃CH₂NH₂ photo-oxidation experiments. Major ion signals are highlighted in boldface types. Ion signals corresponding to compounds with more than 2 carbon atoms are typeset in red colour.

High-NOx		Low-NOx		ion sum formula	ion precursor and comments
2011.03.25 morning	2011.03.25 afternoon	2011.06.02	2011.06.03		
18.0344	18.0344	18.0334	18.0334	NH₄⁺	NH ₃ , from condensation reaction #
31.0186	31.0186	31.0186	31.0186	CH₃O⁺	CH ₂ O
33.0328	33.0328	33.0328	33.0328	CH ₅ O ⁺	CH ₃ OH, chamber artefact
42.0344	42.0344	42.0344	42.0344	C₂H₃N⁺	CH ₃ CN
43.0189	43.0189	43.0189	43.0189	C ₂ H ₃ O ⁺	CH ₃ COOH, fragment ion
44.0137	44.0137	44.0137	44.0137	HNCO ⁺	HNCO
44.0502	44.0502	44.0502	44.0502	C ₂ H ₆ N ⁺	CH ₃ N=CH ₂ , CH ₃ CH=NH
45.0342	45.0342	45.0342	45.0342	C₂H₅O⁺	CH ₃ CHO
46.0654	46.0654	46.0654	46.0654	C₂H₈N⁺	CH ₃ CH ₂ NH ₂ , parent amine
47.0135	47.0135	47.0135	47.0135	CH ₃ O ₂ ⁺	HCOOH, chamber artefact
58.0657	58.0657	58.0657	58.0657	C₃H₈N⁺	CH ₃ N=CHCH ₃ , from condensation reaction #
59.0498	59.0498	59.0498	59.0498	C ₃ H ₇ O ⁺	CH ₃ C(O)CH ₃ , chamber artefact
60.0448	60.0448	60.0448	60.0448	C₂H₆NO⁺	NH ₂ C(O)CH ₃ , NH ₂ CH ₂ CHO
61.0294	61.0294	61.0294	61.0294	C ₂ H ₅ O ₂ ⁺	CH ₃ COOH
72.0814	72.0814	72.0814	72.0814	C₄H₁₀N⁺	CH ₃ CH ₂ N=CHCH ₃ , from condensation reaction #
74.0605	74.0612	74.0605	74.0605	C₃H₈NO⁺	CH ₃ NHC(O)CH ₃ ? From CH ₃ N=CHCH ₃ ?
		74.0971	74.0971	C ₄ H ₁₂ N ⁺	(CH ₃ CH ₂)NH, impurity from previous experiment
76.0398	76.0398	76.0398	76.0398	C ₂ H ₆ NO ₂ ⁺	CH ₃ CH ₂ NO ₂ ?
77.0352	77.0352	77.0352	77.0352	CH ₅ N ₂ O ₂ ⁺	CH ₃ NHNO ₂ , from CH ₃ NH ₂
86.0603	86.0603	86.0603	86.0603	C₄H₈NO⁺	CH ₃ C(O)N=CHCH ₃ ? From CH ₃ N=CHCH ₃ ?
88.0761	88.0761	88.0761	88.0761	C₄H₁₀NO⁺	CH ₃ CH ₂ NHC(O)CH ₃ from CH ₃ CH ₂ N=CHCH ₃
91.0502	91.0502	91.0502	91.0502	C ₂ H ₇ N ₂ O ₂ ⁺	CH ₃ CH ₂ NHNO ₂
102.0540	102.0540	102.0540	102.0540	C₄H₈NO₂⁺	CH ₃ C(O)NHC(O)CH ₃ from CH ₃ CH ₂ N=CHCH ₃
		119.0808	119.0608	C ₄ H ₁₁ N ₂ O ₂ ⁺	(CH ₃ CH ₂)NNO ₂ , from (CH ₃ CH ₂)NH impurity

CH₃CH=NH + CH₃NH₂ → CH₃CH=NCH₃ + NH₃; CH₃CH=NH + CH₃CH₂NH₂ → CH₃CH=NCH₂CH₃ + NH₃; CH₃CH₂NH₂ + CH₂O → CH₃CH₂N=CH₂ + NH₃

A significant amount of aerosol was formed during the 2011.03.25 experiment. Figure 3.14 shows the derived aerosol mass from on-line SMPS measurements. The gas phase carbon balance is around 80% (see later) and starting with 210 ppbV ethylamine the remaining 20% (≈40 ppbV carbon) was transferred to the aerosol phase in the experiment. This is in good agreement with the 150 μg m⁻³ (≈25 ppbV for <M> = 150 g mol⁻¹) determined by SMPS, Figure 3.14. Aerosol formation and composition in ethylamine photo-oxidation is discussed in section 5.2, page 109.

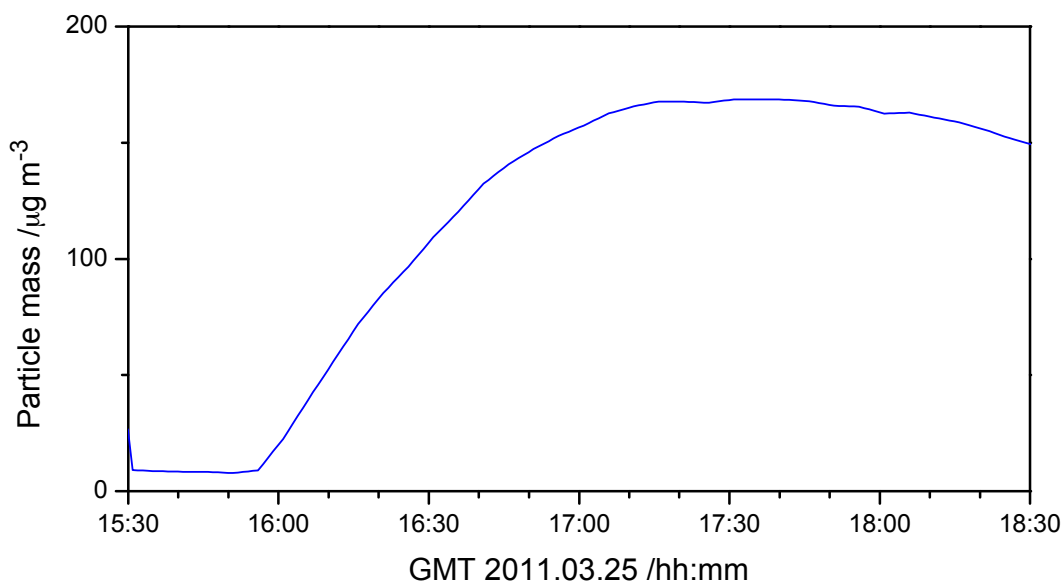


Figure 3.14. Particle mass as determined by SMPS during the ethylamine photo-oxidation experiment on 2011.03.25.

3.2.1 Branching ratios in the photo-oxidation of ethylamine

The initial H-abstraction by OH radicals may take place at three sites: $-\text{NH}_2$, $-\text{CH}_2-$ and $-\text{CH}_3$. The amino group is electron donating and therefore activates the neighbouring CH_2 -group, which, according to the SAR for OH reaction with organics,²⁹ in the outset is already around 7 times more reactive towards OH radicals than the CH_3 -group. The theoretical study of OH reaction with $\text{CH}_3\text{CH}_2\text{NH}_2$ by Galano and Alvarez-Idaboy⁴⁶ confirms this, although their predicted branching ratio for H-abstraction from the NH_2 group is too small, see above.

It has already been indicated in Scheme 3.2 that H-abstraction from the CH_3 -group in ethylamine is expected to be of minor importance. The predicted major products resulting from H-abstraction from the CH_3 -group are $\text{CHOCH}_2\text{NH}_2$ (amino acetaldehyde), CH_2O (formaldehyde), $\text{CH}_2=\text{NH}$ (methanimine) and CHONH_2 (formamide). Of these, formamide is the only compound that is a unique marker of this route. Amino acetaldehyde is an isomer of acetamide ($\text{CH}_3\text{C}(\text{O})\text{NH}_2$) and these compounds cannot be distinguished by PTR-MS. However, there are no indications of amino acetaldehyde in DNPH cartridges collected during the ethylamine photo-oxidation experiments. Methanimine, the major product of methylamine photo-oxidation, is known to undergo extremely fast photo-oxidation and condensation reactions[#] such that it was only observed in trace amounts in methylamine photo-oxidation experiments.⁶ It is therefore not expected to be detectable in the present experiments.

It can be concluded that H-abstraction from the CH_3 -group in ethylamine is a minor route in the OH-initiated photo-oxidation of ethylamine. Considering that there are two additional branching steps to the only unique marker of the route, formamide, a conservative upper limit to the branching ratio will be $k_{1c}/k_1 < 0.1$.

The various condensation reactions of ethylamine and ethanimine make it difficult to extract the CH_2/NH_2 branching ratio in the initial H-abstraction by OH radicals. The challenges/problems are in part masked in Figure 3.13, but become obvious when only including the expected primary gas phase photo-oxidation products and using a linear scale for the volume mixing ratio in the time profile plot, Figure 3.15.

[#] *i.e.* $\text{CH}_2=\text{NH} + \text{CH}_3\text{CH}_2\text{NH}_2 \rightarrow \text{CH}_2=\text{NCH}_2\text{CH}_3 + \text{NH}_3$; *N*-ethyl methanimine is detected, but it may also result from ethylamine condensation with CH_2O .

[#] The curves termed "Mass balance" in the figures correspond to ethylamine gas phase removal due to dilution,

There is an obvious mismatch between reactant loss and formation of the main products ($\text{CH}_3\text{CH}=\text{NH}$ reacts fast with $\text{CH}_3\text{CH}_2\text{NH}_2$ to give $\text{CH}_3\text{CH}_2\text{N}=\text{CHCH}_3$ and NH_3). The imine condensation reaction accounts for 2 ethylamine molecules removed from the gas phase, such that imine and amide formation alone explain around 80 of the 170 ppbV ethylamine removed from the gas phase. Including all the other compounds detected in the experiments results in a gas phase carbon balance of 80-90% and a nitrogen balance of 65-80% based upon the PTR-TOF MS results. Correcting for the PTR-TOF underestimation of NH_3 mixing ratios above 20 ppbV, see ANNEX G, brings the nitrogen balance up to 80-90%. The missing 10-20% in the mass balance is then accounted for by aerosol formation, see Figure 3.14. The right-hand side of Figure 3.15 illustrates the carbon and nitrogen balance in the ethylamine photo-oxidation experiment in the morning of 2011.03.25. The figure further includes the amine loss curve, corrected for condensation reactions (open circles), and a product curve representing the sum of the major primary products (purple curve). The figure clearly demonstrates that substantial secondary chemistry is taking place during the experiment.

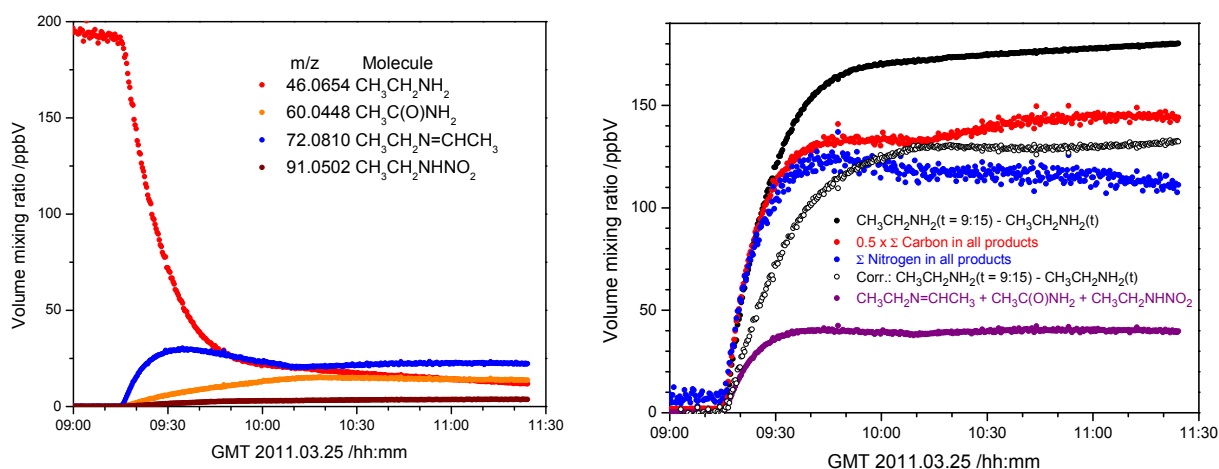


Figure 3.15. (Left): Selected ion signals and ion precursor volume mixing ratios during the ethylamine photo-oxidation experiment in the morning of 2011.03.25. (Right): Ethylamine loss curve (\bullet), carbon accounting curve (\bullet), nitrogen accounting curve (\bullet), growth curve for the major primary products(\circ).

In the analysis of the experimental data from the 4 ethylamine photo-oxidation experiments the following assumptions have been made:

1. H-abstraction from the CH_3 -group can be neglected.

This assumption does not influence the derived branching ratio k_{1a}/k_1 .

2. Branching ratios for the diethylamino radical reactions with NO , NO_2 and O_2 from the *N*-nitroso diethylamine photolysis study (section 4.7) are applicable to the ethylamino radical: $k_2/k_3 = 0.95$, $k_4/k_3 = 0$, $k_5/k_3 = 9.85 \times 10^{-7}$. It is further assumed that *N*-nitroso ethylamine undergoes fast isomerization and reaction with O_2 resulting in ethylamine in analogy to the reactions of *N*-nitroso methylamine.⁶

These assumptions will influence the derived branching ratio k_{1a}/k_1 . The assumptions will, however, not influence the validity of the extrapolation of the laboratory results to ambient conditions (the parameters constitute a self consistent set).

3. $k_{\text{EA}+\text{OH}} = 2.6 \times 10^{-11} \text{ cm}^3 \text{ molecule}^{-1} \text{ s}^{-1}$ at 298 K (see section 2.1), $k_{\text{EA}+\text{NO}_2+\text{OH}} = 2.1 \times 10^{-12} \text{ cm}^3 \text{ molecule}^{-1} \text{ s}^{-1}$ at 298 K (see section 2.2), and $k_{\text{imine}+\text{OH}} = 2 \times 10^{-11} \text{ cm}^3 \text{ molecule}^{-1} \text{ s}^{-1}$ at 298 K.

These assumptions have very little influence (< 1%) on the derived branching ratio k_{1a}/k_1 .

4. Mass balance is obtained by introducing a continuous 7% loss of ethylamine to aerosol (see section 5.2) in addition to that caused by dilution and wall loss. The remaining organic aerosol constituents are assumed to stem from other compounds than *N*-nitro ethylamine.

*These assumptions will influence the derived branching ratio k_{1a}/k_1 . Should the amount of ethylamine lost to aerosol be 20 instead of 7%, the derived branching will increase from 0.09 to 0.10. Further, should 10% of the *N*-nitro diethylamine that is formed in the photo-oxidation experiments be transferred to the aerosol, the determined initial branching ratio would be 10% too low. It is noted that *N*-nitro ethylamine has not been detected in the aerosol.*

The results from a best-balanced fit of the data from the 2 high-NO_x and 2 low-NO_x ethylamine photo-oxidation experiments are summarized in Figure 3.16 through Figure 3.18. An almost perfect agreement between observed and modelled time-profiles of *N*-nitro ethylamine is obtained for a branching ratio $k_{1a}/k_1 = 0.09 \pm 0.01$. For comparison the corresponding branching ratio in MEA (aminoethanol) has been reported to be 0.08 ± 0.03 ⁵³ and 0.15.²¹

It was difficult to determine the branching k_{6a}/k_6 from the acetamide time-profiles. A value of 0.85 has been employed in figures shown.

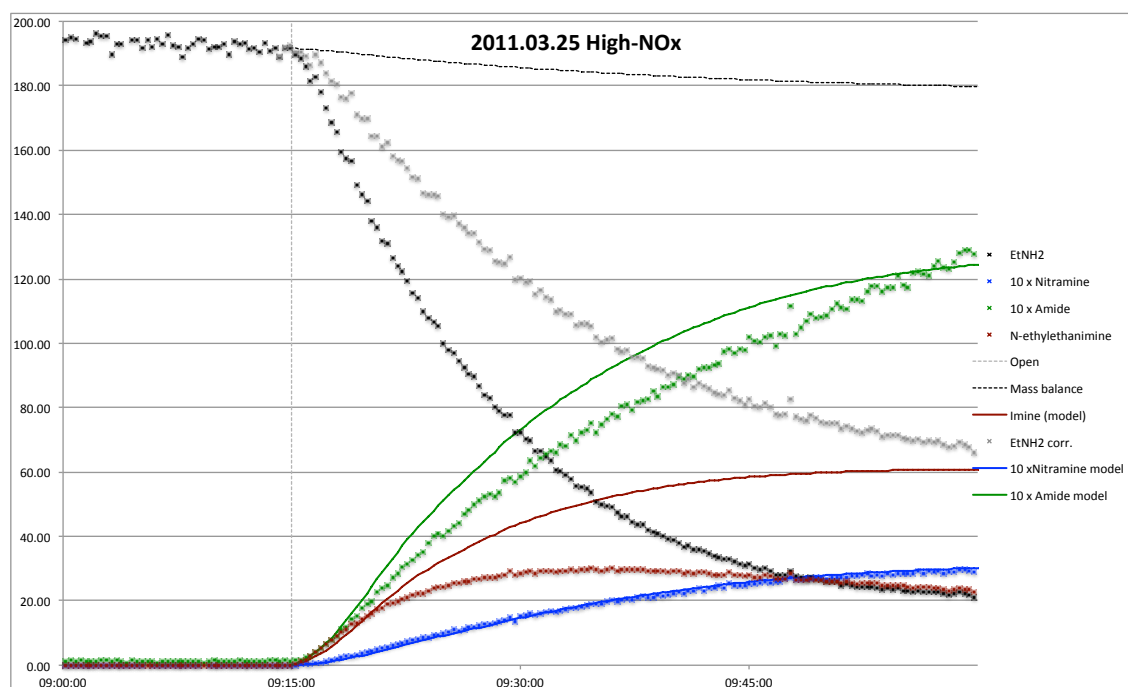


Figure 3.16. Observed and modelled volume mixing ratios of ethylamine, *N*-ethyl ethanimine, acetamide and *N*-nitro ethylamine during the photo-oxidation experiment in the morning of 2011.03.25.[#]

[#] The curves termed “Mass balance” in the figures correspond to ethylamine gas phase removal due to dilution, wall loss and loss to aerosol as nitrate.

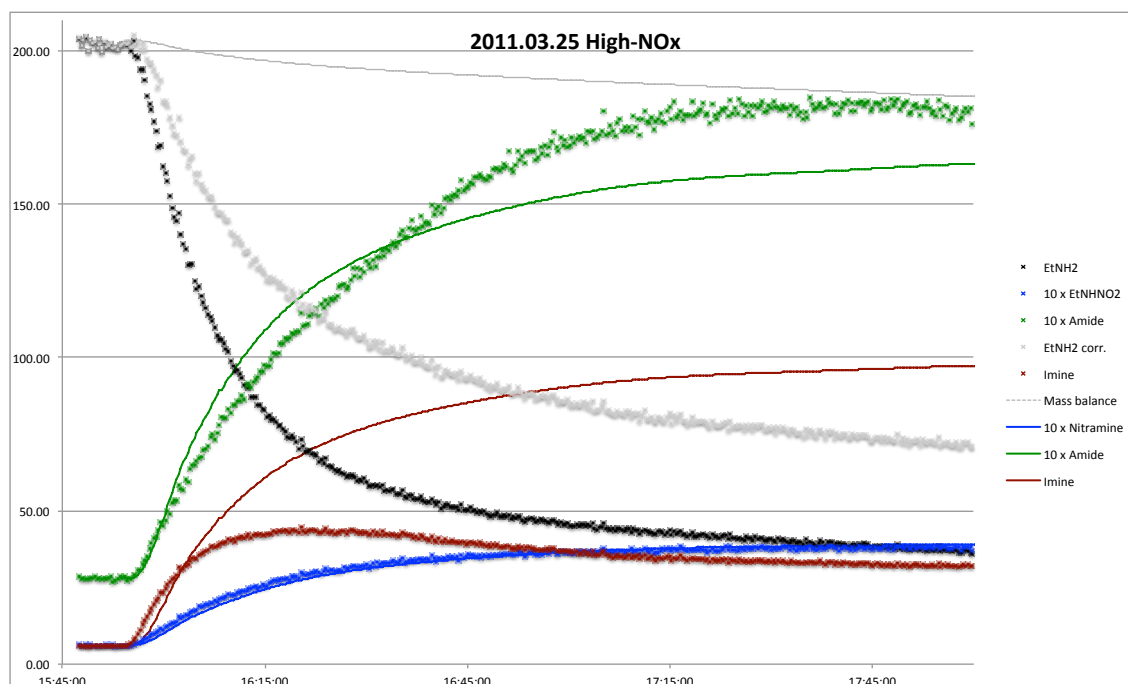


Figure 3.17. Observed and modelled volume mixing ratios of ethylamine, *N*-ethyl ethanimine, acetamide and *N*-nitro ethylamine during the photo-oxidation experiment in the afternoon on 2011.03.25.

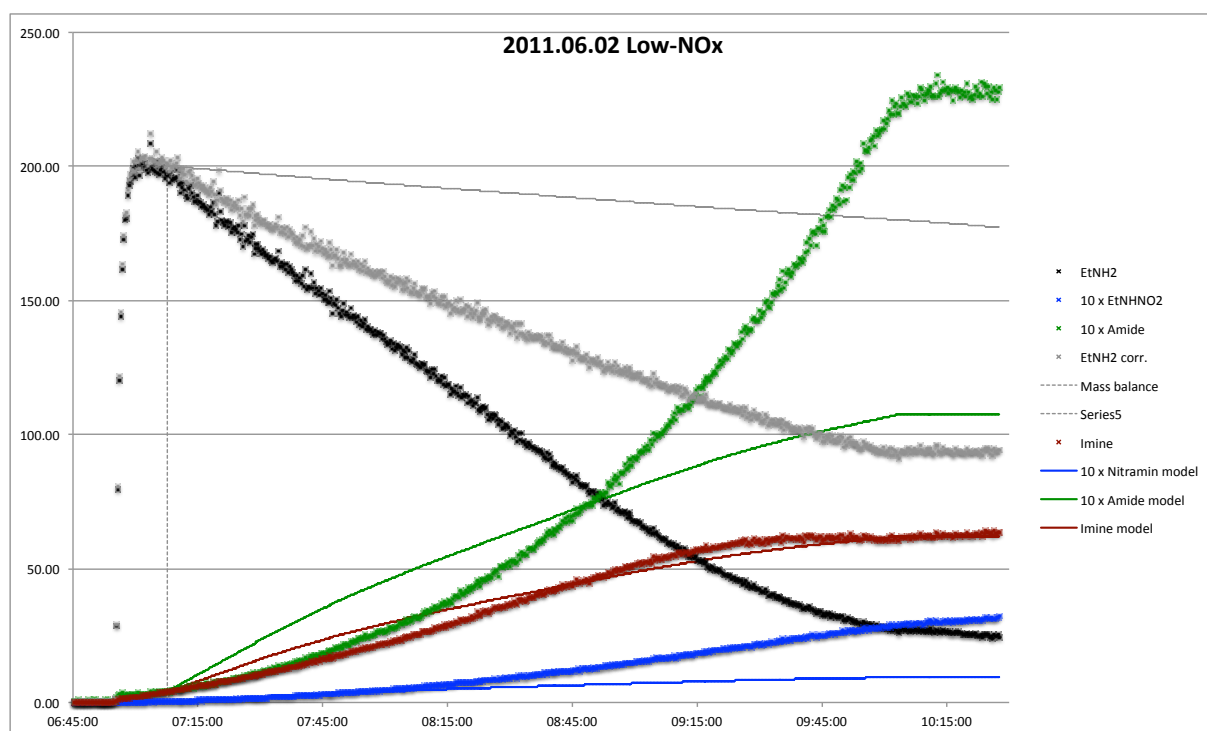


Figure 3.18. Observed and modelled volume mixing ratios of ethylamine, *N*-ethyl ethanimine, acetamide and *N*-nitro ethylamine during the photo-oxidation experiment on 2011.06.02.

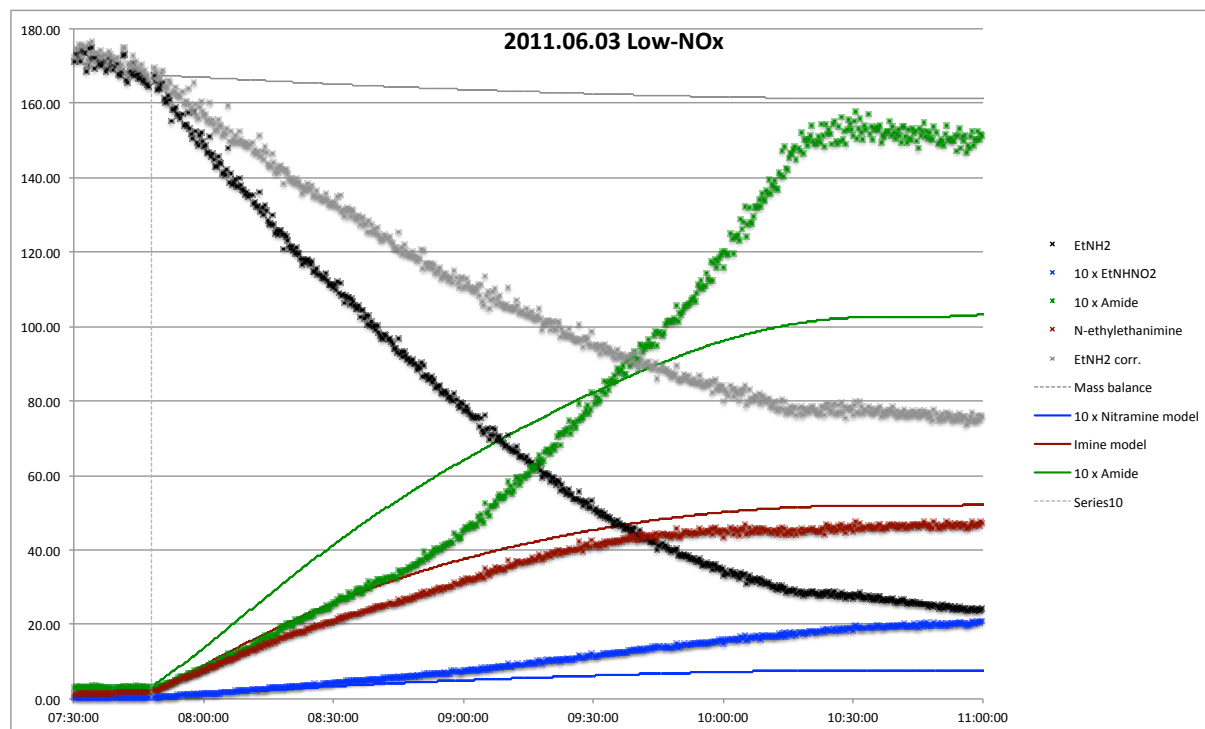


Figure 3.19. Observed and modelled volume mixing ratios of ethylamine, *N*-ethyl ethanimine, acetamide and *N*-nitro ethylamine during the photo-oxidation experiment on 2011.06.02.

The experimental low-NO_x data are only reproduced well during the first hour of the experiments after which there appears to be unaccounted for processes contributing to the *N*-nitro ethylamine and acetamide production (the curves change curvature). The latter parts of these two experiments were therefore not considered in the analysis.

3.3 Diethylamine

Previous studies. Pitts *et al.*⁵⁰ carried out a study of the products formed when a mixture of 500 ppb $(\text{CH}_3\text{CH}_2)_2\text{NH}$ + 80 ppb NO + 160 ppb NO_2 was subjected to natural sunlight conditions. They found the following molar product yields (taking into account the number of ethyl groups): 30% CH_3CHO (acetaldehyde), 4% $\text{CH}_3\text{CO}(\text{OO})\text{NO}_2$ (PAN), 32% $(\text{CH}_3\text{CH}_2)_2\text{NNO}_2$ (diethyl nitramine), 2.4% $\text{CH}_3\text{CH}_2\text{NC}(\text{O})\text{CH}_3$ (*N*-ethyl acetamide), 1.4% $(\text{CH}_3\text{CH}_2)_2\text{NCHO}$ (*N,N*-diethyl formamide), and 0.2% $(\text{CH}_3\text{CH}_2)_2\text{NC}(\text{O})\text{CH}_3$ (*N,N*-diethyl acetamide) in the gas phase. In the course of the experiment up to 290 ppbV O_3 and $60 \mu\text{g m}^{-3}$ aerosol was registered; small amounts of CH_3CONH_2 (acetamide) were found in the aerosol phase, which otherwise mainly consisted of nitrate. The mass balance reported was 46% for nitrogen and 69% for carbon. Pitts *et al.* also reported the formation of $(\text{CH}_3\text{CH}_2)_2\text{NNO}$ under dark, humid conditions when diethylamine was mixed with NO and NO_2 in air. Slagle *et al.*⁴⁵ employed photo-ionization mass spectrometry and identified the C_2H_5 radical and $\text{C}_3\text{H}_6/\text{C}_2\text{H}_4\text{N}/\text{C}_2\text{H}_2\text{O}$, $\text{C}_3\text{H}_7/\text{C}_2\text{H}_5\text{N}/\text{C}_2\text{H}_3\text{O}$, $\text{C}_2\text{H}_6\text{N}$, $\text{C}_2\text{H}_6\text{O}/\text{CH}_4\text{NO}$, $\text{C}_3\text{H}_6\text{N}$, $\text{C}_4\text{H}_9/\text{C}_3\text{H}_7\text{N}$, $\text{C}_2\text{H}_7\text{NO}$, $\text{C}_4\text{H}_9\text{N}$, $\text{C}_4\text{H}_{10}\text{N}$ and $\text{C}_4\text{H}_{11}\text{NO}$ as products in the $\text{O}(^3\text{P})$ reaction with diethylamine. The rate coefficient for O_3 reaction with diethylamine is reported to be $k_{\text{O}_3} = (1.33 \pm 0.15) \times 10^{-17} \text{ cm}^3 \text{ molecule}^{-1} \text{ s}^{-1}$ at 298 K.⁵⁴ Grosjean speculated on the atmospheric chemistry of diethylamine and outlined a simplified scheme for reaction with OH radicals.⁵⁵

In a recent investigation of the NO_3 radical initiated gas phase atmospheric oxidation of diethylamine Price⁵⁶ suggests the following interpretation of the major PTR-MS ion signals $[\text{MH}]^+$: m/z 31, CH_2O (formaldehyde); m/z 45, CH_3CHO (acetaldehyde); m/z 47, HCOOH (formic acid and/or $\text{C}_2\text{H}_5\text{OH}$ (ethanol)); m/z 58, $\text{CH}_3\text{CH}_2\text{NCH}_2$ (ethyl methanimine); m/z 60, $(\text{CH}_3)_3\text{N}$ (trimethylamine) and/or $\text{CH}_3\text{CH}_2\text{NO}$ (nitrosoethane); m/z 61, CH_3COOH (acetic acid) and/or $\text{CH}_3\text{CH}_2\text{CH}_2\text{OH}$ (propanol); m/z 72, $\text{CH}_3\text{CH}_2\text{NCHCH}_3$ (ethyl ethanimine); m/z 74, $\text{CH}_3\text{CH}_2\text{NHCHO}$ (*N*-ethyl formamide); m/z 88, $\text{CH}_3\text{CH}_2\text{NHCH}_2\text{CHO}$ (*N*-ethyl acetamide); m/z 119, $(\text{CH}_3\text{CH}_2)_2\text{NNO}_2$ (*N*-nitro diethylamine).

Murphy *et al.*⁴⁷ reported rapid particle formation during photo-oxidation experiments with $(\text{CH}_3\text{CH}_2)_2\text{NH}$ and, similar to the oxidation of CH_3NH_2 , that the aerosol formed mainly is nitrate salt. Yields of non-salt organic aerosol were negligible. Price analyzed the aerosol formed in the $(\text{CH}_3\text{CH}_2)_2\text{NH}/\text{O}_3/\text{NO}_x$ oxidation experiments by HR-TOF-AMS.⁵⁶ The major ion peaks observed from the aerosol included the amine backbone m/z 30.034 (CH_4N^+), m/z 44.050 ($\text{C}_2\text{H}_6\text{N}^+$), m/z 58.066 ($\text{C}_3\text{H}_8\text{N}^+$), m/z 86.099 ($\text{C}_5\text{H}_{12}\text{N}^+$), and m/z 100.113 ($\text{C}_6\text{H}_{14}\text{N}^+$). Higher mass oxidized fragments included m/z 191.084 ($\text{C}_6\text{H}_{11}\text{N}_2\text{O}_5^+$). The thesis offers no further interpretation of the results, but it is clear that extensive processing had taken place in the aerosol phase.

Present studies. Six diethylamine photo-oxidation experiments were carried out – four under high-NO_x conditions during the spring campaign 2011, and two under low-NO_x conditions during the summer campaign 2011. Table 3.4 summarises the ion signals above 1% of the diethylamine ion signal loss detected by PTR-TOF-MS during the photo-oxidation experiments; the 6 largest ion signals are highlighted in boldface type in the table. All experiments are to some extent affected by “wall impurities” from previous experiments. Figure 3.20 illustrates the data from the 2011.03.28 morning experiment; five ion signals (m/z 46.0655, 42.0344, 44.0498, 58.0660 and 60.0456) that vary in intensity during the experiments and originate in ethylamine and ethylamine photo-oxidation products have been excluded from the figure.

The major ion signals observed are m/z 74.0958 ($\text{C}_4\text{H}_{12}\text{N}^+$, protonated diethylamine), m/z 72.0802 ($\text{C}_4\text{H}_{10}\text{N}^+$, protonated ethylethanamine), m/z 45.0347 ($\text{C}_2\text{H}_5\text{O}^+$, protonated acetaldehyde), m/z 119.0791 ($\text{C}_4\text{H}_{11}\text{N}_2\text{O}_2^+$, protonated *N*-nitro diethylamine), m/z 31.0185 (CH_3O^+ , protonated formaldehyde) and m/z 88.0765 ($\text{C}_4\text{H}_{10}\text{NO}^+$, protonated *N*-ethyl acetamide). In addition, the m/z 103.0871 ($\text{C}_4\text{H}_{11}\text{N}_2\text{O}^+$, protonated *N*-nitroso diethylamine) ion signal is highlighted in Figure 3.20. In the low-NO_x experiments the m/z 103.0871 and 119.0791 – the nitrosamine and nitramine signals – are, naturally, much smaller than in the example shown.

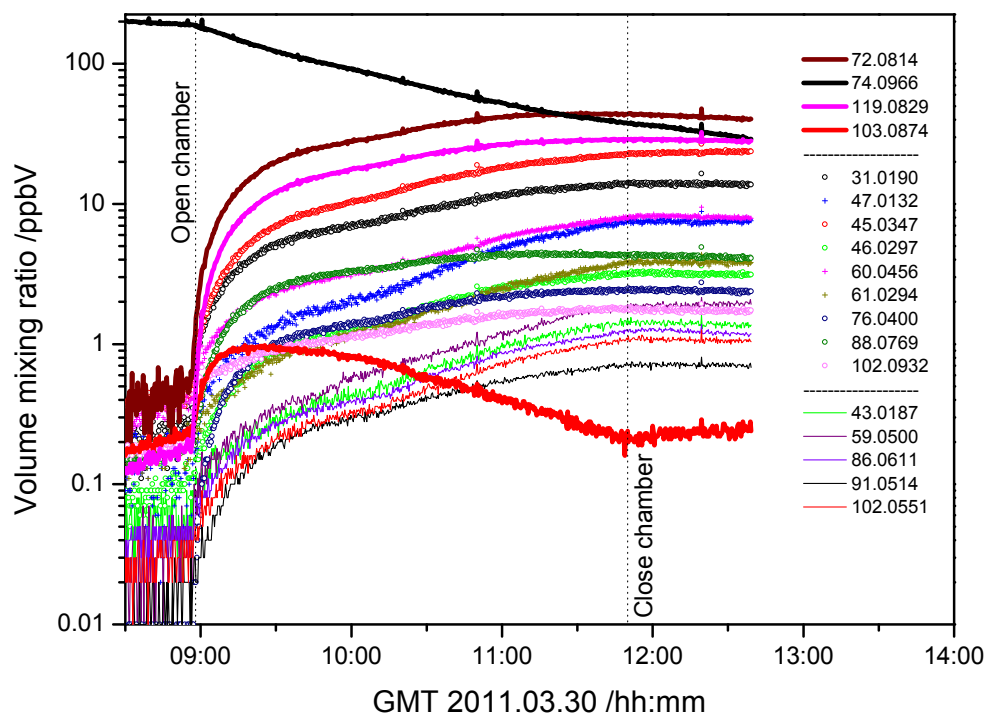


Figure 3.20. Observed ion signals and ion precursor volume mixing ratios during the diethylamine photo-oxidation experiment in the morning of 2011.03.28.

Table 3.4. Major ion signals observed in the $(\text{CH}_3\text{CH}_2)_2\text{NH}$ photo-oxidation experiments.

High-NOx		Low-NOx		Ion sum formula	Ion precursor and comments
2011.03.28 morning	2011.03.28 afternoon	2011.03.29	2011.03.30		
			2011.06.01		
			2011.06.01		
				CH_3O^+	CH_2O
				$\text{C}_2\text{H}_4\text{N}^+$	CH_3CN , from $\text{CH}_3\text{CH}_2\text{NH}_2$
				$\text{C}_2\text{H}_3\text{O}^+$	Fragment ion
				$\text{C}_2\text{H}_6\text{N}^+$	$\text{CH}_3\text{CH}=\text{NH}$, from $\text{CH}_3\text{CH}_2\text{NH}_2$
				$\text{C}_2\text{H}_5\text{O}^+$	CH_3CHO
				CH_4NO^+	NH_2CHO
				$\text{C}_2\text{H}_8\text{N}^+$	$\text{CH}_3\text{CH}_2\text{NH}_2$, Impurity
				CH_3O_2^+	HCOOH , from CH_2O
				$\text{C}_3\text{H}_8\text{N}^+$	$\text{CH}_2=\text{NCH}_2\text{CH}_3$, from $\text{CH}_3\text{CH}_2\text{NH}_2?$
				$\text{C}_3\text{H}_7\text{O}^+$	$\text{CH}_3\text{C}(\text{O})\text{CH}_3$, Impurity
				$\text{C}_2\text{H}_6\text{NO}^+$	$\text{NH}_2\text{C}(\text{O})\text{CH}_3$, $\text{NH}_2\text{CH}_2\text{CHO}$
				$\text{C}_2\text{H}_5\text{O}_2^+$	CH_3COOH
				$\text{C}_4\text{H}_{10}\text{N}^+$	$\text{CH}_3\text{CH}_2\text{N}=\text{CHCH}_3$
				$\text{C}_4\text{H}_{12}\text{N}^+$	$(\text{CH}_3\text{CH}_2)_2\text{NH}$
				$\text{C}_2\text{H}_6\text{NO}_2^+$	$\text{CH}_3\text{CH}_2\text{NO}_2$
				$\text{C}_4\text{H}_8\text{NO}^+$	$\text{CH}_3\text{C}(\text{O})\text{N}=\text{CHCH}_3?$
				$\text{C}_4\text{H}_{10}\text{NO}^+$	$\text{CH}_3\text{CH}_2\text{NHC}(\text{O})\text{CH}_3$
				$\text{C}_2\text{H}_7\text{N}_2\text{O}_2^+$	$\text{CH}_3\text{CH}_2\text{NHNO}_2$, from $\text{CH}_3\text{CH}_2\text{NH}_2$
				$\text{C}_4\text{H}_8\text{NO}_2^+$	$\text{CH}_3\text{C}(\text{O})\text{NHC}(\text{O})\text{CH}_3$
				$\text{C}_5\text{H}_{12}\text{NO}^+$	$(\text{CH}_3\text{CH}_2)_2\text{NCHO}?$
				$\text{C}_4\text{H}_{11}\text{N}_2\text{O}^+$	$(\text{CH}_3\text{CH}_2)_2\text{NNO}$
				$\text{C}_4\text{H}_{11}\text{N}_2\text{O}_2^+$	$(\text{CH}_3\text{CH}_2)_2\text{NNO}_2$

A group of 5 ion signals grow slowly with time of experiment: m/z 43.0187 ($C_2H_3O^+$, fragment ion from compounds like PAN and acetic acid), 59.0500 ($C_3H_7O^+$, protonated acetone), 86.0611 ($C_4H_8NO^+$, $CH_3C(O)N=CHCH_3?$), 91.0514 ($C_2H_7N_2O_2^+$, protonated *N*-nitro ethylamine from ethylamine impurity) and 102.0932 ($C_5H_{12}NO^+$, *N,N*-diethyl formamide?). The latter compound contains more carbon atoms than the parent amine and must either result from triethylamine desorbing from the chamber walls or from a condensation reaction. In any case, the amount formed of this compound was small. The ethylamine impurity was significant in the first diethylamine experiments and decreased in the following experiments; as mentioned above, ethylamine originates from wall exchange.

The amount of aerosol formed in the experiment on 2011.03.30 is presented in Figure 3.21; the aerosol composition is primarily diethylammonium nitrate and the estimated uncertainty in the aerosol mass is $\pm 30\%$. AMS analyses of the aerosol composition in the diethylamine photo-oxidation experiments suggests that the total aerosol mass yield can amount to as much as 15% of which the organic fraction accounts for around half (see ANNEX D, page 146). A first estimate of the amount of diethylamine removed from the gas phase by nitric acid salt formation is therefore 7-8%.

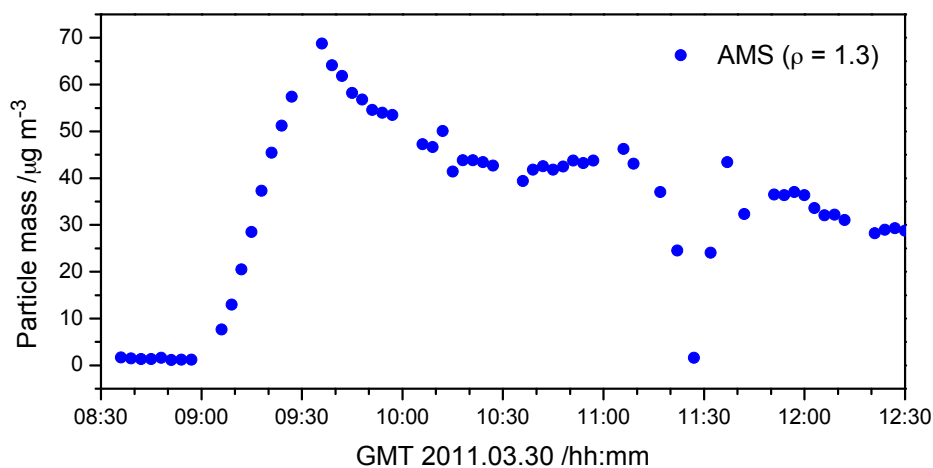
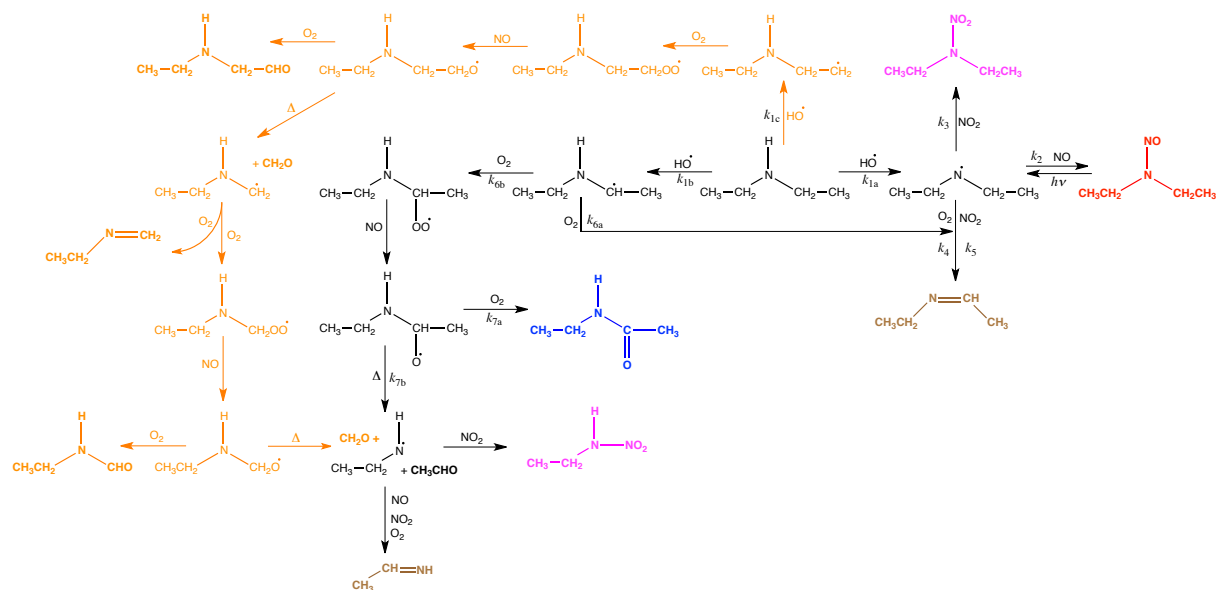


Figure 3.21. Particle mass as determined by AMS during the diethylamine photo-oxidation experiment on 2011.03.30. The irregular profile from 11:10 to 11:50 is due to thermogram measurements.

3.3.1 Branching ratios in the photo-oxidation of diethylamine

The initial H-abstraction by OH radicals may take place at three sites in diethylamine (>N-H, -CH₂- and -CH₃), of which the methyl groups are expected to be the least reactive. The diethylamine gas phase photo-oxidation is expected to follow the routes indicated in Scheme 3.3



Scheme 3.3. Theoretical atmospheric photo-oxidation scheme for diethylamine. The orange coloured route is expected to be of less importance.

The predicted major products resulting from H-abstraction from the CH₃-groups include CH₃CH₂NHCH₂CHO (2-(ethylamino) acetaldehyde), CH₂O (formaldehyde), CH₂=NCH₂CH₃ (ethyl methanimine) and CH₃CH₂NHCHO (*N*-ethyl formamide). Of these, *N*-ethyl formamide and ethyl methanimine are unique markers of this route. 2-(Ethylamino) acetaldehyde is an isomer of *N*-ethyl acetamide (CH₃C(O)NHCH₂CH₃) and these compounds cannot be distinguished by PTR-MS. However, there are no indications of 2-(ethylamino) acetaldehyde in DNPH cartridges collected during the diethylamine photo-oxidation experiments. Ethylamine photo-oxidation experiments were carried out prior to diethylamine experiments, and ethylamine was present as an impurity in all diethylamine experiments. Ethyl methanimine is a condensation product in ethylamine photo-oxidation experiments, and the amounts of ethylamine impurity and ethyl methanimine formed in the 6 experiments both decrease through the series of diethylamine experiments. This suggests that ethyl methanimine primarily originates from ethylamine condensation reactions and not as a result of hydrogen abstraction from the methyl groups in diethylamine.

It is concluded that H-abstraction from the CH₃-groups is a minor route in the OH-initiated photo-oxidation of diethylamine. Considering that there are two additional branching steps to the only unique marker of the route, *N*-ethyl formamide, a conservative upper limit to the branching ratio will be $k_{1c}/k_1 < 0.1$.

As mentioned above, the diethylamine photo-oxidation experiments always included ethylamine as an impurity from wall exchange. Excluding compounds that can be related to ethylamine photo-oxidation in the experiments results in a gas phase carbon balance of 60-80% and a nitrogen balance of 55-75% based upon the PTR-TOF MS results. The missing 20-40% in the gas phase mass balance is then accounted for by aerosol formation, Figure 3.21. The left-hand side of Figure 3.22 shows the diethylamine loss and the growth of the two major products, ethyl ethanimine and *N*-nitro diethylamine. The right-hand side of Figure 3.22 illustrates carbon and nitrogen balance in the ethylamine photo-oxidation experiment in the morning of 2011.03.29. The figure demonstrates that substantial secondary chemistry is taking place during the experiment.

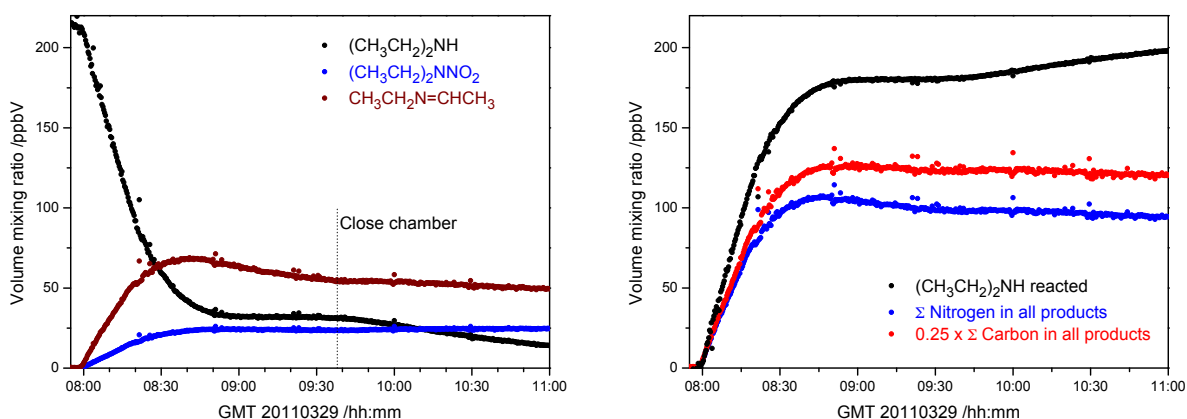


Figure 3.22. (Left): Selected ion signals and ion precursor volume mixing ratios during the diethylamine photo-oxidation experiment in the morning of 2011.03.29. (Right): Ethylamine loss curve (\bullet), carbon accounting curve (\bullet), nitrogen accounting curve (\bullet).

In the analysis of the diethylamine photo-oxidation experiments the following assumptions have been made:

1. H-abstraction from the CH_3 -groups can be neglected.
This assumption does not influence the derived branching ratio k_{1a}/k_1 .
2. Branching ratios and relative photolysis rate from the N-nitroso diethylamine photolysis study (section 4.7) $k_2/k_3 = 0.7$, $k_4/k_3 = 0$, $k_5/k_3 = 11.2 \times 10^{-7}$, and $j_{\text{Nitrosamine}}/j_{\text{NO}_2} = 0.30$.
These assumptions will influence the derived branching ratio k_{1a}/k_1 . The assumptions will, however, not influence the validity of extrapolating the laboratory results to ambient conditions (the parameters constitute a self consistent set).
3. $k_{\text{DEA}+\text{OH}} = 7.4 \times 10^{-11} \text{ cm}^3 \text{ molecule}^{-1} \text{ s}^{-1}$ at 298 K (see section 2.1), $k_{\text{DEANO}_2+\text{OH}} = 4.6 \times 10^{-12} \text{ cm}^3 \text{ molecule}^{-1} \text{ s}^{-1}$ at 298 K (see section 2.2), $k_{\text{DEANO}+\text{OH}} = 3.5 \times 10^{-12}$, and $k_{\text{imine}+\text{OH}} = 2 \times 10^{-11} \text{ cm}^3 \text{ molecule}^{-1} \text{ s}^{-1}$ at 298 K (see section 4).
These assumptions have very little impact (< 1%) on the derived branching ratio k_{1a}/k_1 . The assumptions will, however, affect determination of the subsequent branching ratios.
5. Mass balance is obtained by introducing a continuous 8% loss of diethylamine to aerosol (see ANNEX D, page 146) in addition to that caused by dilution and wall loss. The remaining organic aerosol constituents are assumed to stem from compounds other than N-nitro ethylamine.
These assumptions will influence the derived branching ratio k_{1a}/k_1 . Should the amount of diethylamine lost to aerosol be 20 instead of 8%, the derived branching will increase from 0.6 to 0.75. Further, should 10% of the N-nitro diethylamine that is formed in the photo-oxidation experiments be transferred to the aerosol, the determined initial branching ratio would be 10% too low. It is noted that N-nitro diethylamine has not been detected in the aerosol.

Under the assumptions given above, the N-H:C-H branching ratio in the initial hydrogen abstraction reaction by OH radicals, k_{1a}/k_{1b} is essentially determined by the N-nitro diethylamine time profiles. The branching k_{6a}/k_6 is then determined by the ethyl ethanimine time profiles, and k_{7a}/k_7 is then adjusted to fit the N-ethyl acetamide time profiles. A best-balanced fit of the data from the 4 high-NO_x and 2 low-NO_x diethylamine photo-oxidation experiments was obtained for $k_{1a}/k_1 = 0.6 \pm 0.1$, $k_{6a}/k_6 = 0.6 \pm 0.1$ and $k_{7a}/k_7 = 0.2 \pm 0.1$. The observed and modelled time profiles are illustrated in Figure 3.23 through Figure 3.28.

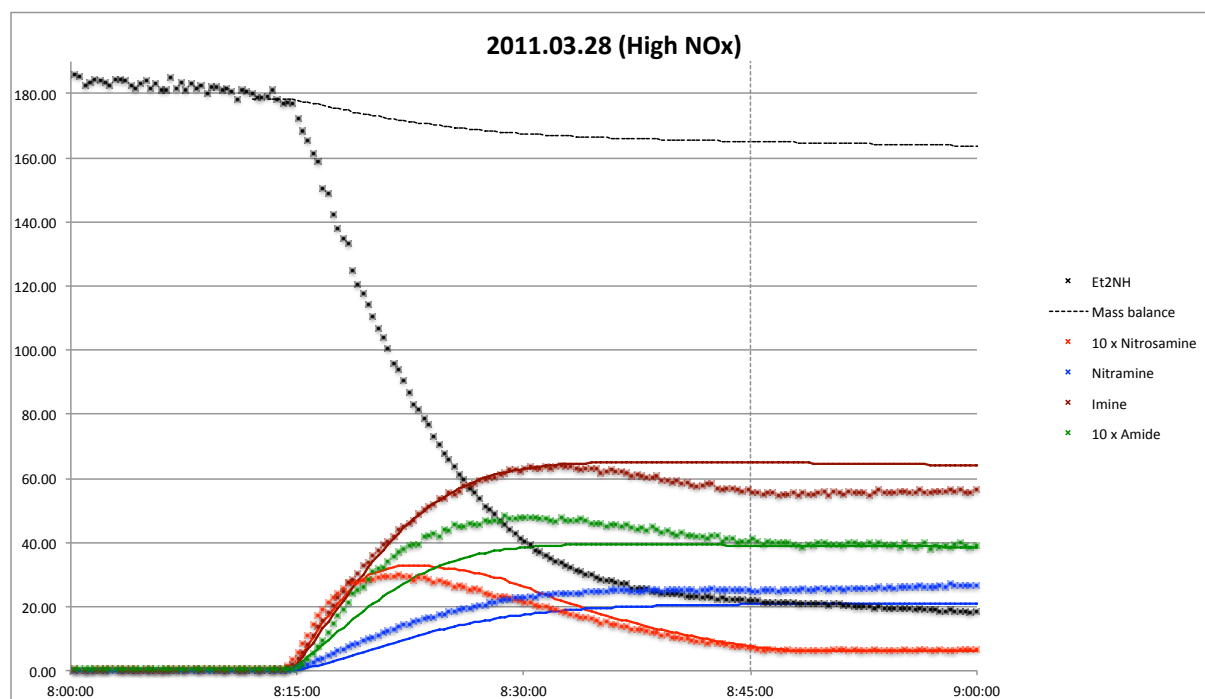


Figure 3.23. Observed and modelled diethylamine, *N*-nitro diethylamine, *N*-nitroso diethylamine, *N*-ethyl ethanimine and *N*-ethyl acetamide mixing ratios during the high-NO_x diethylamine photo-oxidation experiment on the morning of 2011.03.28.

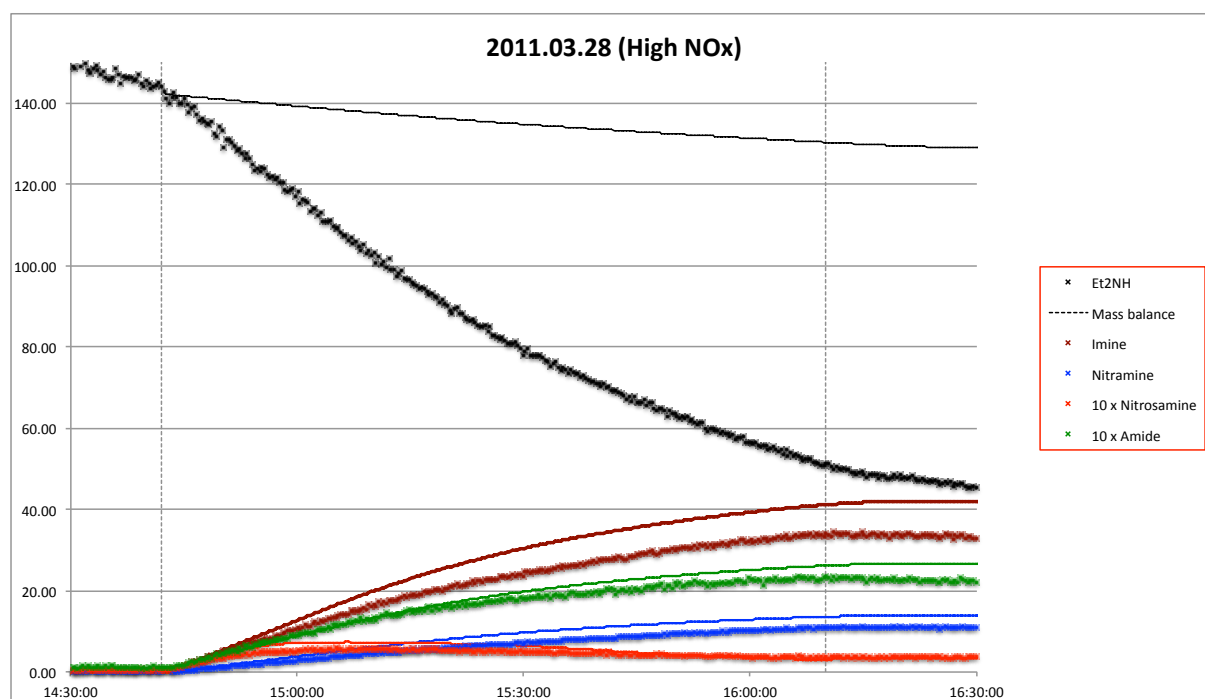


Figure 3.24. Observed and modelled diethylamine, *N*-nitro diethylamine, *N*-nitroso diethylamine, *N*-ethyl ethanimine and *N*-ethyl acetamide mixing ratios during the high-NO_x diethylamine photo-oxidation experiment on the afternoon of 2011.03.28.

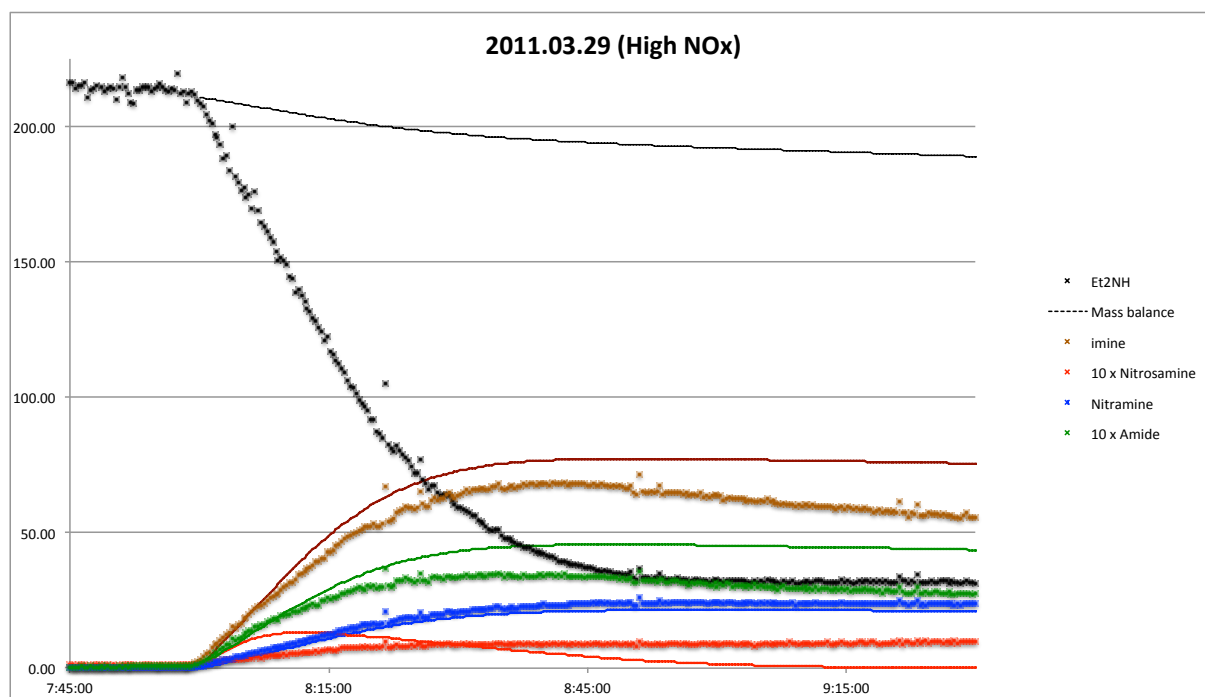


Figure 3.25. Observed and modelled diethylamine, *N*-nitro diethylamine, *N*-nitroso diethylamine, *N*-ethyl ethanimine and *N*-ethyl acetamide mixing ratios during the high-NO_x diethylamine photo-oxidation experiment on 2011.03.29.

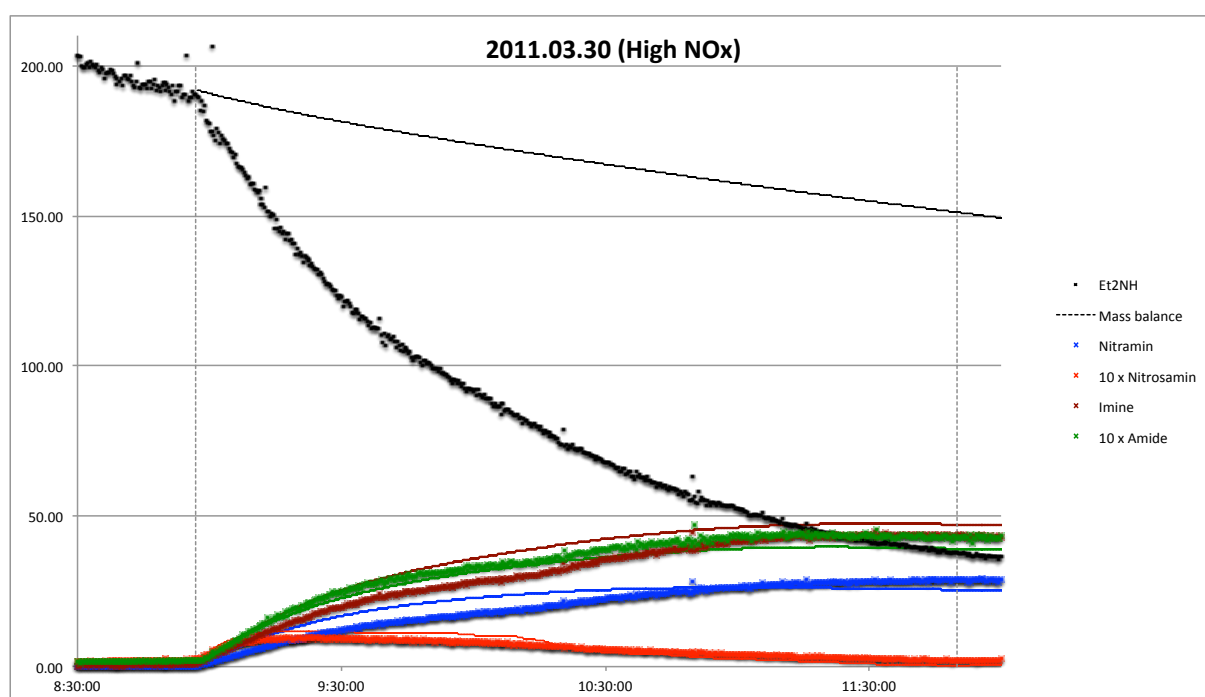


Figure 3.26. Observed and modelled diethylamine, *N*-nitro diethylamine, *N*-nitroso diethylamine, *N*-ethyl ethanimine and *N*-ethyl acetamide mixing ratios during the high-NO_x diethylamine photo-oxidation experiment on 2011.03.30.

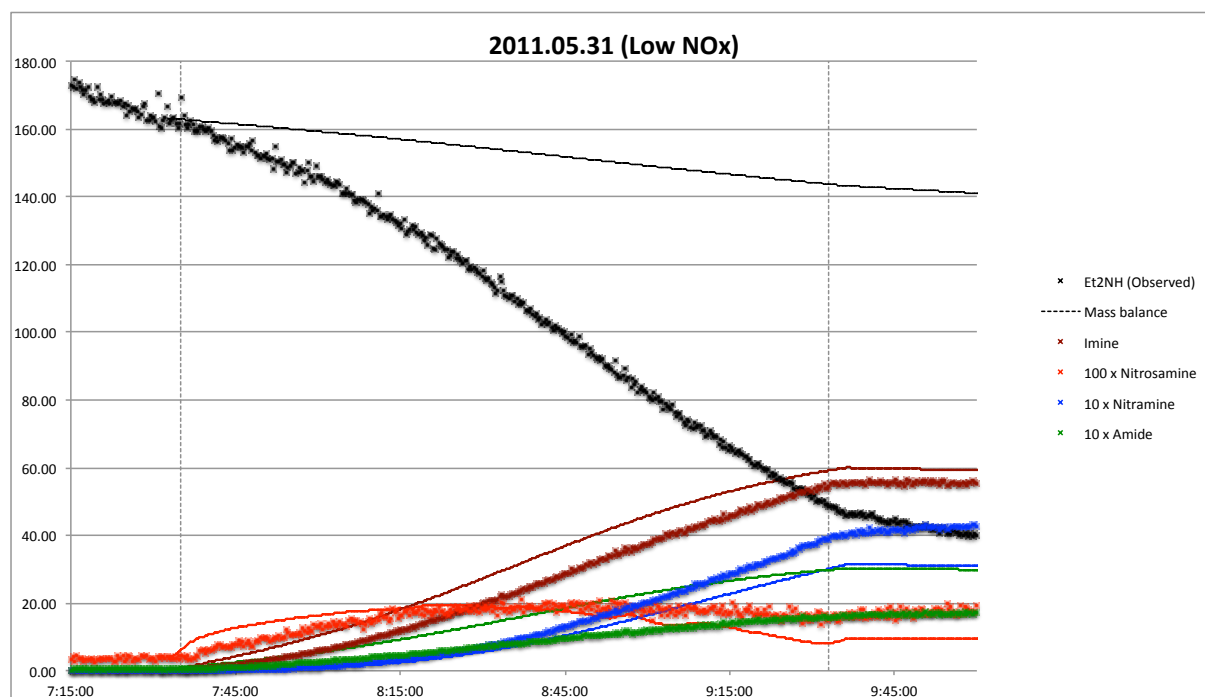


Figure 3.27. Observed and modelled diethylamine, *N*-nitro diethylamine, *N*-nitroso diethylamine, *N*-ethyl ethanimine and *N*-ethyl acetamide mixing ratios during the low-NO_x diethylamine photo-oxidation experiment on 2011.05.31.

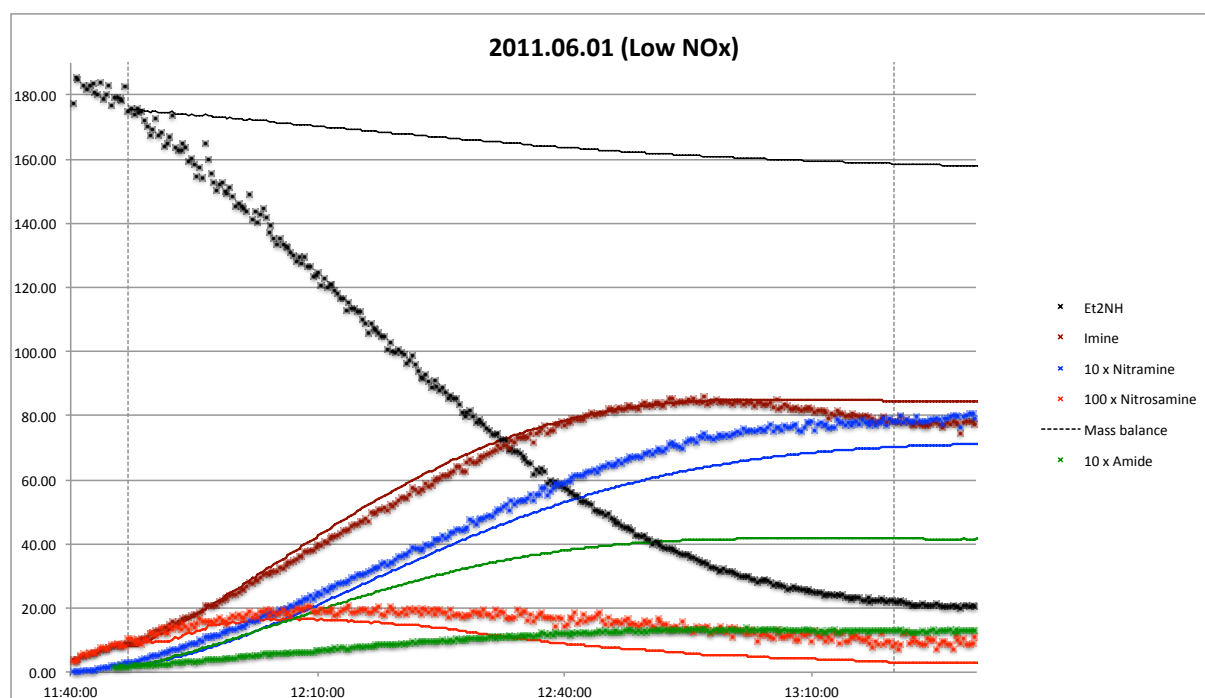


Figure 3.28. Observed and modelled diethylamine, *N*-nitro diethylamine, *N*-nitroso diethylamine, *N*-ethyl ethanimine and *N*-ethyl acetamide mixing ratios during the low-NO_x diethylamine photo-oxidation experiment on 2011.06.01.

3.3.2 NO₃ radical chemistry

The diethylamine photo-oxidation experiments on 2011.05.31 showed continued radical activity after the chamber canopy was closed. This radical activity is illustrated in Figure 3.29 showing selected ion signals; there is a slight increase in the m/z 119.0829 signal (protonated *N*-nitro diethylamine) and a pronounced increase in the m/z 45.0347 signal (protonated acetaldehyde).

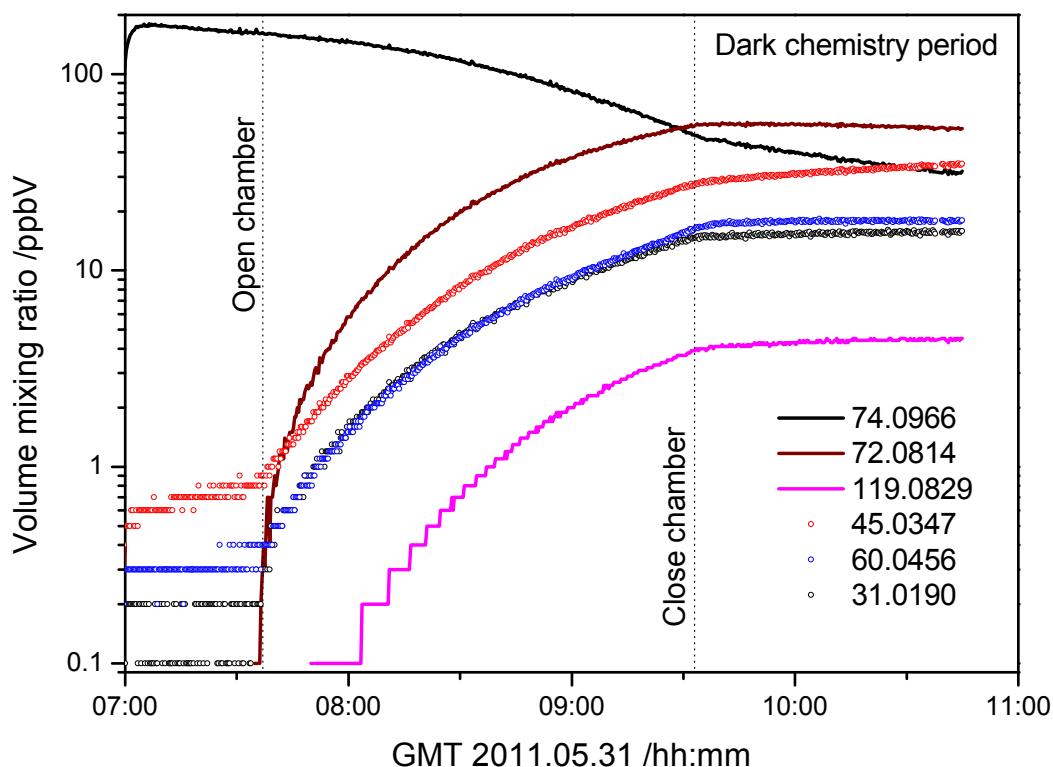
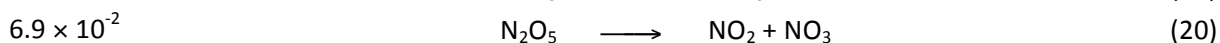
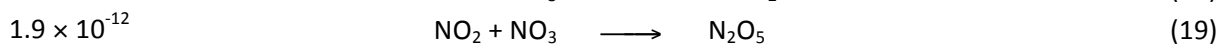
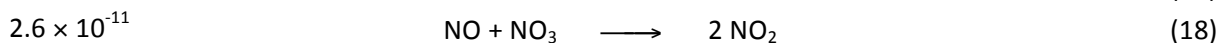
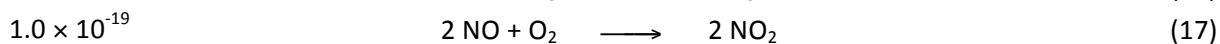
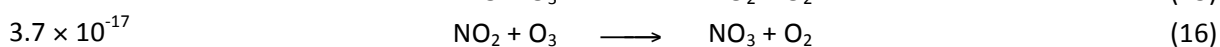
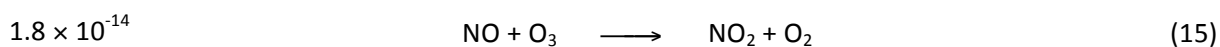


Figure 3.29. Selected ion signals and ion precursor volume mixing ratios during the ethylamine photo-oxidation experiment on 2011.05.31.

During sunlight conditions NO₃ radicals photolyze quickly ($\text{NO}_3 \xrightarrow{h\nu} \text{NO} + \text{O}_2$), and the NO₃ radical concentration never reaches significant levels. Under dark conditions (chamber canopy closed) NO₃ radical concentration will build up and the concentration can be calculated from the following reactions:



The rate coefficients given above stem from the MCM web site (<http://mcm.leeds.ac.uk/MCM/>). The NO, NO₂ and O₃ time profiles during the 2011.05.31 photo-oxidation experiment are given in Figure 3.30. Taking the NO, NO₂ and O₃ levels depicted in the figure, the NO₃ radical concentration is calculated to be 5.3×10^7 just after closing the chamber canopy and slowly decreasing to 3.2×10^7 at the end of experiment.

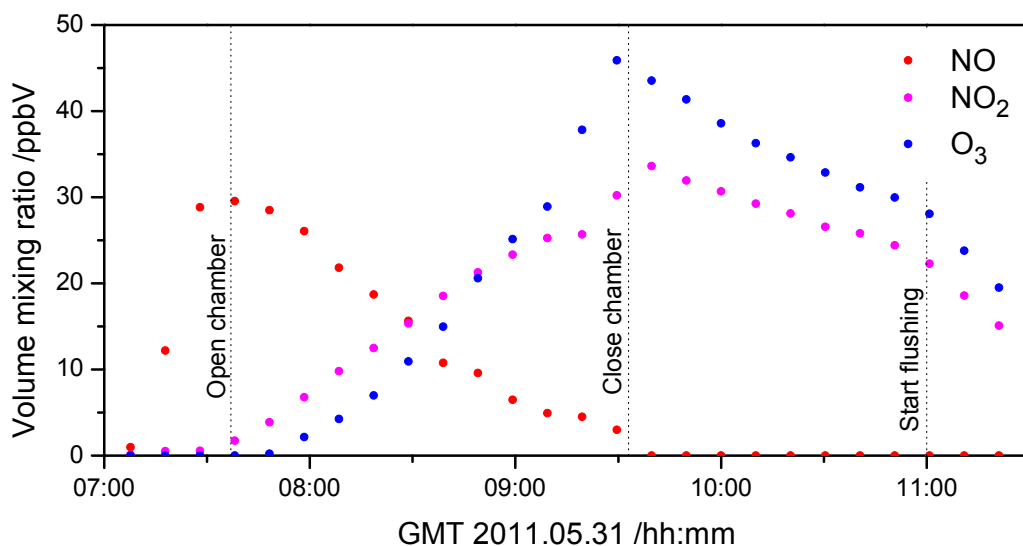
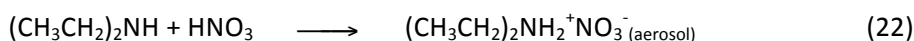


Figure 3.30. NOx and O₃ time profiles retrieved by FTIR spectroscopy during the diethylamine photo-oxidation experiment on 2011.05.31.

The following reactions will take place under dark conditions:



In addition to the chemical loss processes there is a dilution due to air replenishment compensating for sampling etc; the dilution coefficient was measured to be $9.0 \times 10^{-6} \text{ s}^{-1}$. Assuming that for every diethylamine reacting with NO₃ another diethylamine molecule reacts with the HNO₃ formed and thereby is transferred from the gas phase to the aerosol, it is possible to extract a rate coefficient for reaction of NO₃ radicals with diethylamine. Figure 3.31 shows the results of modelling the observed diethylamine time profile.

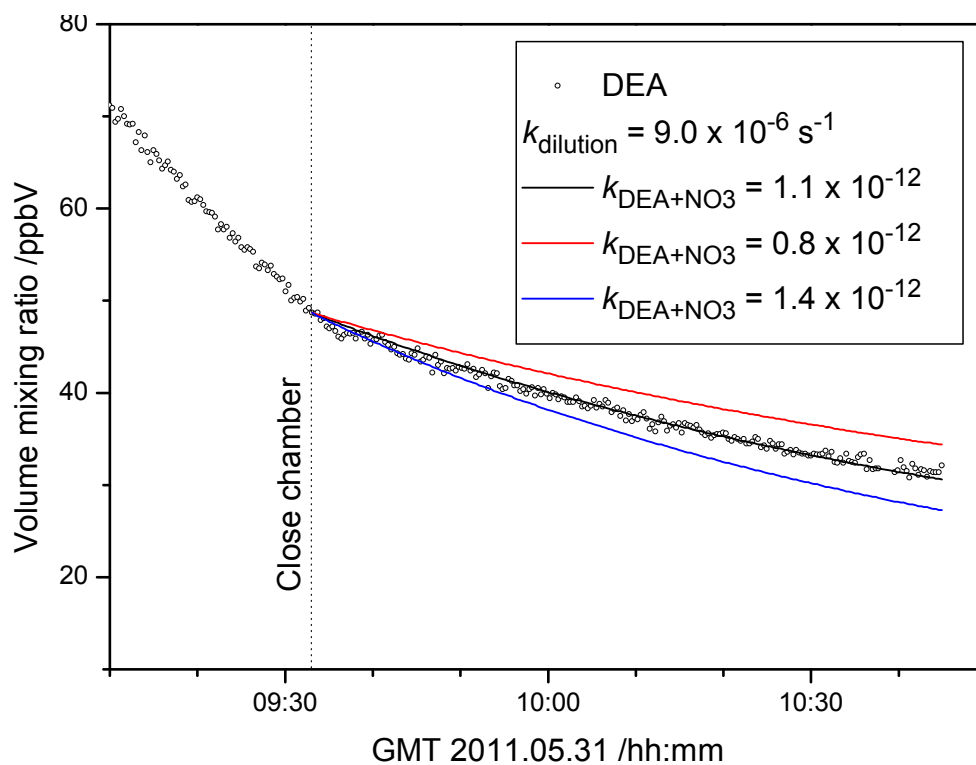


Figure 3.31. Observed and modelled diethylamine time profile during the dark chemistry experiment on 2011.05.31.

With a rate coefficient $k_{(\text{CH}_3\text{CH}_2)_2\text{NH}+\text{NO}_3} = (1.1 \pm 0.3) \times 10^{-12} \text{ cm}^3 \text{ molecule}^{-1} \text{ s}^{-1}$, the reaction is among the fastest NO_3 reactions with organics reported. There are no rate coefficients for the amine + NO_3 reaction in the open literature. However, unpublished results from kinetic studies of methylamine, dimethylamine and trimethylamine reaction with NO_3 radicals confirm that these reactions are very fast.⁵⁷

Assuming an average diurnal NO_3 radical concentration of $10^7 - 10^9 \text{ cm}^{-3}$, the lifetime of diethylamine with respect to reaction with NO_3 radicals will range from from $\tau_{\text{NO}_3} \approx 25$ hours to only 25 minutes. In polluted areas, the NO_3 radical may therefore constitute the major gas phase loss process.

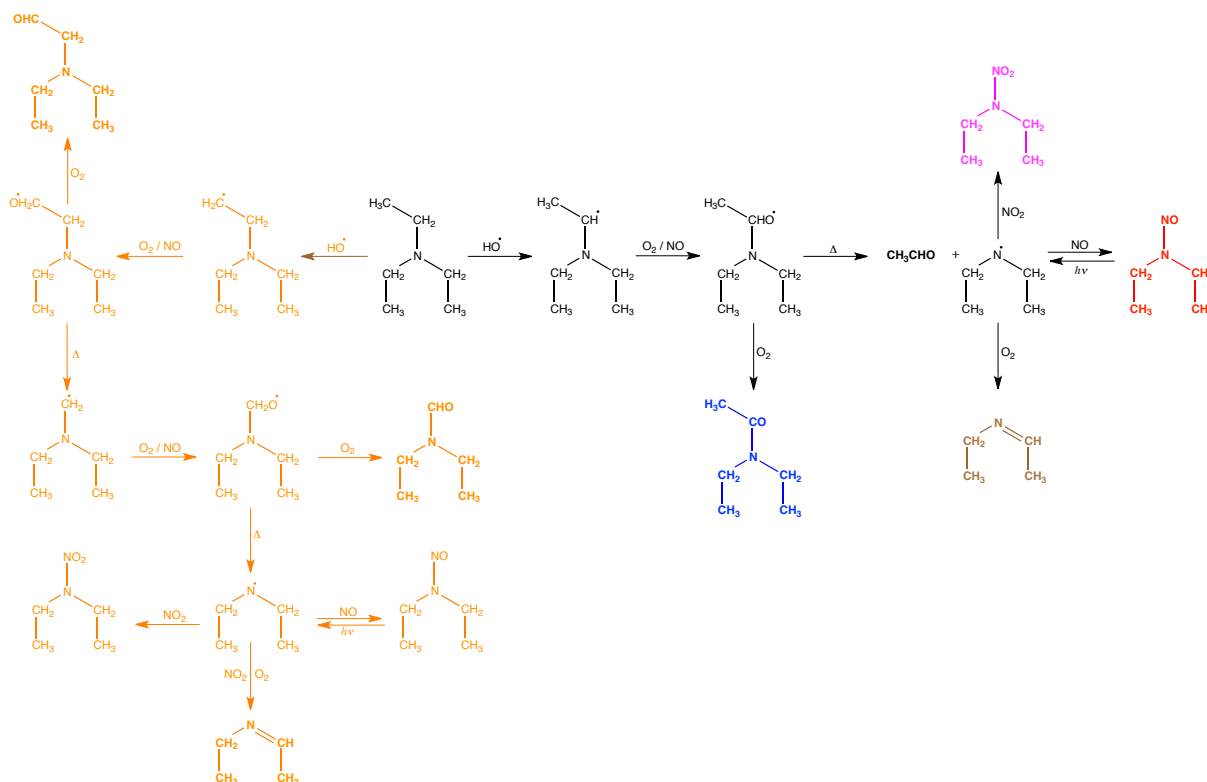
3.4 Triethylamine

Previous studies. Pitts *et al.*⁵⁰ carried out a study of the products formed when a mixture of 500 ppbV $(\text{CH}_3\text{CH}_2)_2\text{NH}$ + 80 ppbV NO + 160 ppbV NO_2 was subjected to natural sunlight conditions. They found the following molar product yields (taking into account the number of ethyl groups): 47% CH_3CHO (acetaldehyde), 5% $\text{CH}_3\text{CO}(\text{OO})\text{NO}_2$ (PAN), 1.8% $(\text{CH}_3\text{CH}_2)_2\text{NNO}$ (diethylnitrosamine), 7.4% $(\text{CH}_3\text{CH}_2)_2\text{NNO}_2$ (diethylnitramine), 8.6% $(\text{CH}_3\text{CH}_2)_2\text{NCHO}$ (diethylformamide), 0.6% $(\text{CH}_3\text{CH}_2)_2\text{NC}(\text{O})\text{CH}_3$ (diethylacetamide), 2.6% $\text{CH}_3\text{CH}_2\text{NC}(\text{O})\text{CH}_3$ (*N*-ethyl acetamide), 2.4% “unknown amide-like compound with $M=87$ ”, and trace amounts of $(\text{CH}_3\text{CO})_2\text{NH}$ (diacetamide) in the gas phase. In the course of the experiment up to 260 ppbV O_3 and $370 \mu\text{g m}^{-3}$ aerosol was registered. The aerosol formed contained ca. $8.7 \mu\text{g m}^{-3}$ CH_3CONH_2 (acetamide), $7.6 \mu\text{g m}^{-3}$ $(\text{CH}_3\text{CH}_2)_2\text{NOH}$ (diethylhydroxylamine) and otherwise essentially only nitrate. The mass balance reported was 59% for nitrogen and 69% for carbon. Pitts *et al.*⁵⁰ also reported a minor formation of $(\text{CH}_3\text{CH}_2)_2\text{NNO}$ under dark, humid conditions when triethylamine was mixed HONO, NO and NO_2 in air. Slagle *et al.*⁴⁵ employed photo-ionization mass spectrometry and identified C_2H_5 , $\text{C}_4\text{H}_{11}\text{NO}$, $\text{C}_6\text{H}_{13}\text{N}$ and $\text{C}_6\text{H}_{14}\text{N}$ as products in the $\text{O}(^3\text{P})$ reaction with triethylamine. The rate coefficient for O_3 reaction with triethylamine was reported to be $k_{\text{O}_3} = (8.2 \pm 1.0) \times 10^{-17} \text{ cm}^3 \text{ molecule}^{-1} \text{ s}^{-1}$ at 298 K.⁵⁴ Grosjean speculated on the atmospheric chemistry of triethylamine and outlined a simplified scheme for reaction with OH radicals.⁵⁵

Murphy *et al.*⁴⁷ reported a 5% mass yield of non-salt aerosol during ozonolysis experiments and an 8% mass yield of non-salt aerosol during photo-oxidation experiments with $(\text{CH}_3\text{CH}_2)_3\text{N}$. A particulate phase compound with molecular weight of triethylamine-*N*-oxide was identified that previously had been detected by Angelino *et al.*⁵⁸ Murphy *et al.*⁴⁷ also studied the stability of the nitrate aerosol forming from $(\text{CH}_3\text{CH}_2)_3\text{N}$ relative to the stability of ammonium nitrate aerosol. They concluded that the stability of triethylammonium nitrate is close to that of ammonium nitrate. Erupe *et al.*⁵⁹ investigated the secondary organic aerosol formation from reaction of triethylamine with nitrate radicals, produced in situ by adding NO to a mixture of triethylamine with excess O_3 under dark condition, and followed the gas phase VOCs by PTR-MS. Their interpretation of the major ion masses $[\text{MH}]^+$ were as follows: m/z 31, HCHO (formaldehyde); m/z 45, CH_3CHO (acetaldehyde); m/z 47, HCOOH (formic acid) and/or CH_3OH (methanol); m/z 59, $(\text{CH}_3)_2\text{CO}$ (acetone) and/or $\text{CH}_3\text{CH}_2\text{CHO}$ (propanal); m/z 60, $\text{CH}_3\text{CH}_2\text{NO}$ (nitrosoethane); m/z 61, CH_3COOH (acetic acid) and/or $\text{CH}_3\text{CH}_2\text{CH}_2\text{OH}$ (propanol); m/z 72, $\text{CH}_3\text{CH}_2\text{N}=\text{CHCH}_3$ (ethylidene-ethanamine); m/z 74, $\text{CH}_3\text{CH}_2\text{NHCHO}$ (ethyl formamide); m/z 76, $\text{CH}_3\text{CH}_2\text{NO}_2$ (nitroethane); m/z 102, $(\text{CH}_3\text{CH}_2)_3\text{N}$ (triethylamine); m/z 103, $(\text{CH}_3\text{CH}_2)_2\text{NNO}$ (diethylnitrosamine); m/z 116, $(\text{CH}_3\text{CH}_2)_2\text{NC}(\text{O})\text{CH}_3$ (diethylacetamide); m/z 119, $(\text{CH}_3\text{CH}_2)_2\text{NNO}_2$, (diethylnitramine).

Europe *et al.*⁵⁹ also reported ion peaks from the aerosol: low mass peaks include m/z 44.052 ($\text{C}_2\text{H}_6\text{N}^+$), m/z 58.065 ($\text{C}_3\text{H}_8\text{N}^+$), m/z 72.082 ($\text{C}_4\text{H}_{10}\text{N}^+$) and m/z 86.095 ($\text{C}_5\text{H}_{12}\text{N}^+$) that represent fragments from the amine backbone. Other ions detected are m/z 72.046 ($\text{C}_3\text{H}_6\text{NO}^+$), m/z 86.068 ($\text{C}_4\text{H}_8\text{NO}^+$), m/z 102.05 ($\text{C}_4\text{H}_8\text{NO}_2^+$) and m/z 146.07 ($\text{C}_6\text{H}_{12}\text{NO}_3^+$). In each of these cases, one, two, or three oxygen atoms have been added representing oxidized amine fragments. Apart from a short burst shortly after NO injection, nitrate salt formation was generally minimal.

Present studies. Four triethylamine photo-oxidation experiments were carried out – two under high-NOx conditions during the spring campaign 2011, and two under low-NOx conditions during the summer campaign 2011. In addition a triethylamine – ozone reaction experiment was carried out under dark conditions. Table 3.5 summarises the ion signals above 1% of the triethylamine ion signal loss detected by PTR-TOF-MS during the experiments, while Scheme 3.4 shows the expected main photo-oxidation routes of triethylamine. Figure 3.32 illustrates the data from the 2011.04.01 experiment. The time profiles of ion signals in the other experiments are very similar: 4 dominating ion signals, highlighted in boldface types in Table 3.5 and a suite of much weaker signals.



Scheme 3.4. Theoretical atmospheric photo-oxidation scheme for triethylamine. The orange coloured route is expected to be of minor importance.

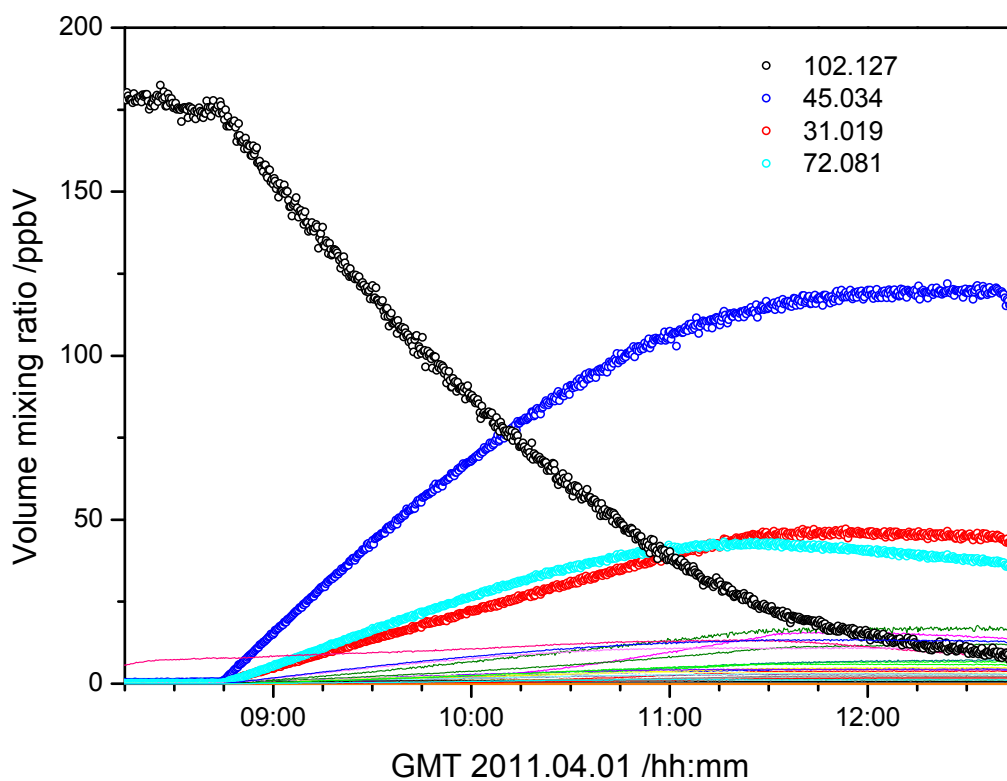
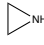


Figure 3.32. Observed ion signals and ion precursor volume mixing ratios during the triethylamine photo-oxidation experiment on 2011.04.01.

The most prominent product is m/z 45.0340 (protonated acetaldehyde), followed by m/z 31.0186 (protonated formaldehyde) and m/z 72.0814 (protonated ethyl ethanimine) – one of the expected

major products. The MH^+ ion signals of other expected major products such as *N*-nitro diethylamine (m/z 119.0831) and *N,N*-diethyl acetamide (m/z 116.0772) are much weaker. *N*-nitroso diethylamine is barely detected in the high-NO_x experiments and is not detected above the 0.1%-level of the triethylamine ion signal loss detected by PTR-TOF-MS during the low-NO_x experiments.

Table 3.5. Major ion signals observed in the $(CH_3CH_2)_3N$ photo-oxidation experiments.

High-NO _x		Low-NO _x		Ozonolysis		
2011.03.31	2011.04.01	2011.05.26	2011.05.30	2011.05.27	Ion sum formula	Ion precursor and comments
31.0186	31.0186	31.0186	31.0186	31.0186	CH₃O⁺	CH ₂ O
42.0349	42.0349	42.0349	42.0349	42.0349	C ₂ H ₄ N ⁺	CH ₃ CN
43.0186	43.0186	43.0186	43.0186	43.0186	C ₂ H ₃ O ⁺	Fragment ion
44.0502	44.0502	44.0502	44.0502	44.0502	C ₂ H ₆ N ⁺	 Aziridine ?
45.0340	45.0340	45.0340	45.0340	45.0340	C₂H₅O⁺	CH ₃ CHO
45.9928	45.9928	45.9928	45.9928		NO ₂ ⁺	Fragment ion
46.0308	46.0308	46.0308	46.0308	46.0308	CH ₄ NO ⁺	NH ₂ CHO
				46.0655	C ₂ H ₈ N ⁺	CH ₃ CH ₂ NH ₂ , (CH ₃) ₂ NH, impurity
47.0134	47.0134	47.0134	47.0134	47.0134	CH ₃ O ₂ ⁺	HCOOH, chamber artefact
58.0660	58.0660	58.0660	58.0660	58.0660	C ₃ H ₈ N ⁺	CH ₂ =NCH ₂ CH ₃
59.0498	59.0498	59.0498	59.0498	59.0498	C ₃ H ₇ O ⁺	CH ₃ C(O)CH ₃ , chamber artefact
60.0449	60.0449	60.0449	60.0449	60.0449	C ₂ H ₆ NO ⁺	CH ₃ C(O)NH ₂ ?
61.0292	61.0292	61.0292	61.0292	61.0292	C ₂ H ₅ O ₂ ⁺	CH ₃ COOH, chamber artefact
72.0814	72.0814	72.0814	72.0814	72.0814	C₄H₁₀N⁺	CH ₃ CH ₂ N=CHCH ₃
74.0233	74.0233	74.0233	74.0233	74.0233	C ₂ H ₄ NO ₂ ⁺	
74.0605	74.0605	74.0605	74.0605	74.0605	C ₃ H ₈ NO ⁺	CH ₃ CH ₂ NHCHO
74.0970	74.0970	74.0970	74.0970	74.0970	C ₄ H ₁₂ N ⁺	CH ₃ CH ₂ N=CHCH ₂
76.0406	76.0406	76.0406	76.0406	76.0406	C ₂ H ₆ NO ₂ ⁺	CH ₃ CH ₂ NO ₂
86.0606	86.0606	86.0606	86.0606	86.0606	C ₄ H ₈ NO ⁺	CH ₂ C(O)N=CHCH ₃
88.0395	88.0395	88.0395	88.0395	88.0395	C ₃ H ₆ NO ₂ ⁺	
88.0768	88.0768	88.0768	88.0768	88.0768	C ₄ H ₁₀ NO ⁺	CH ₃ CH ₂ NHC(O)CH ₃
91.0507	91.0507	91.0507	91.0507		C ₂ H ₇ N ₂ O ₂ ⁺	CH ₃ CH ₂ NHNO ₂
		102.0550	102.0550		C ₄ H ₈ NO ₂ ⁺	CH ₃ C(O)N(OH)CH=CH ₂ ?
102.0922	102.0922				C ₅ H ₁₂ NO ⁺	(CH ₃ CH ₂)NCHO ?
102.1265	102.1265	102.1265	102.1265	102.1265	C₆H₁₆N⁺	(CH ₃ CH ₂) ₃ N, parent amine
103.0866	103.0866				C ₄ H ₁₁ N ₂ O ⁺	(CH ₃ CH ₂) ₂ NNO
104.0727	104.0727	104.0727	104.0727	104.0727	C ₄ H ₁₀ NO ₂ ⁺	CH ₃ CH ₂ N(OH)CH ₂ CHO ?
116.0722	116.0722	116.0722	116.0722		C ₅ H ₁₀ NO ₂ ⁺	CH ₃ CH ₂ N(CHO)C(O)CH ₃ ?
		116.1045	116.1045	116.1045	C ₆ H ₁₄ NO ⁺	(CH ₃ CH ₂) ₂ NC(O)CH ₃
119.0831	119.0831	119.0831	119.0831		C ₄ H ₁₁ N ₂ O ₂ ⁺	(CH ₃ CH ₂) ₂ NNO ₂
132.1001	132.1001	132.1001	132.1001	132.1001	C ₆ H ₁₄ NO ₂ ⁺	

It is highly significant that the amount of *N*-nitro diethylamine formed in the high-NO_x photo-oxidation experiments with triethylamine is incongruent to the amounts of acetaldehyde and ethyl ethanimine formed since all three species in some way are linked to the $(CH_3CH_2)_2NCHCH_3$ radical. It is also highly significant that *N,N*-diethyl acetamide yield is very small in all experiments. A

comparison with the product distribution in the high NO_x diethylamine photo-oxidation experiments (Section 3.3) suggests that triethylamine photo-oxidation either differs significantly from the expected scheme or that the dominant triethylamine gas phase loss may not be due to OH radical chemistry. In this context it should be noted that the observed products of the ozone reaction with triethylamine to a large part are exactly the same as those of the OH-initiated photo-oxidation.

3.4.1 O₃ chemistry

The O₃ reaction with triethylamine is fast ($k_{O_3} = (8.2 \pm 1.0) \times 10^{-17} \text{ cm}^3 \text{ molecule}^{-1} \text{ s}^{-1}$ at 298 K⁵⁴), and since O₃ always builds up during the amine photo-oxidation experiments O₃ may contribute significantly to triethylamine gas phase loss. Figure 3.33 shows the ion signals detected in the ozonolysis experiment on 2011.05.27 in which the starting volume mixing ratio of O₃ was around 250 ppbV. The most dominant product is acetaldehyde – around 2 molecules of acetaldehyde are formed for every triethylamine reacted. The second most abundant product is ethyl ethanimine; the third is formaldehyde.

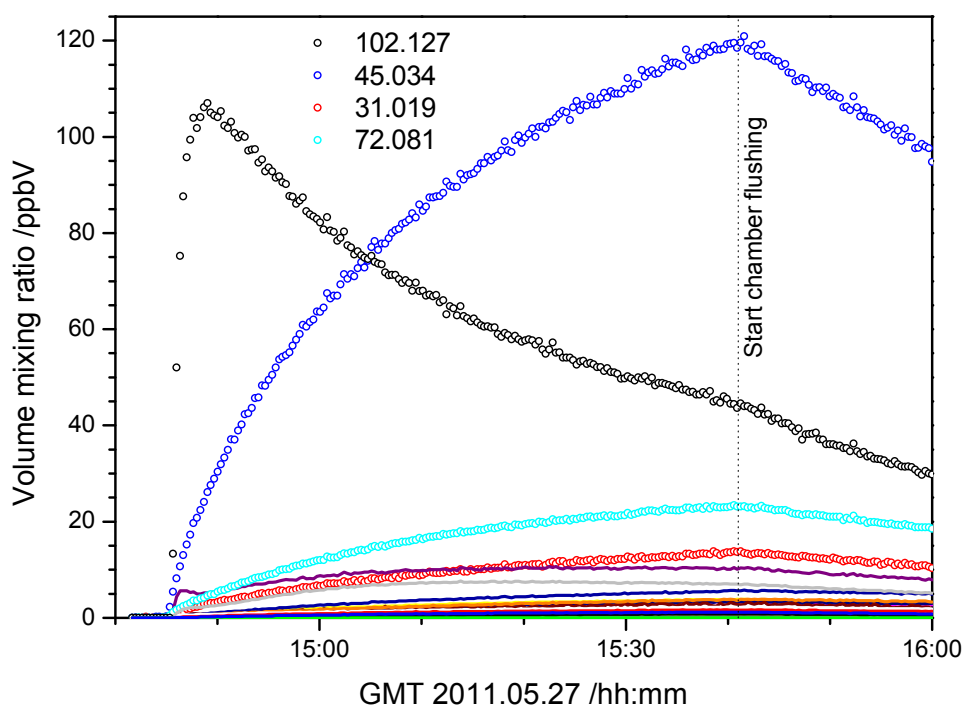


Figure 3.33. Observed ion signals and ion precursor volume mixing ratios during the triethylamine photo-oxidation experiment on 2011.05.27.

It is possible to derive the rate coefficient for O₃ reaction with triethylamine from an analysis of the triethylamine and O₃ time profiles:

$$\frac{d[\text{TEA}]}{dt} = -k_{O_3+\text{TEA}} \cdot [\text{TEA}] \cdot [\text{O}_3] \Rightarrow k_{O_3+\text{TEA}} = \frac{-d[\text{TEA}]}{[\text{TEA}] \cdot [\text{O}_3] \cdot dt}$$

The results of combining numerical differentiation of PTR-TOS-MS data for triethylamine (TEA) with O₃ data (FTIR) are displayed in Figure 3.34; the derived rate coefficient for O₃ reaction with

triethylamine is $k_{\text{O}_3+\text{TEA}} = (6.4 \pm 1.4) \times 10^{-17} \text{ cm}^3 \text{ molecule}^{-1} \text{ s}^{-1}$, which compares well to the literature value, see above.[#]

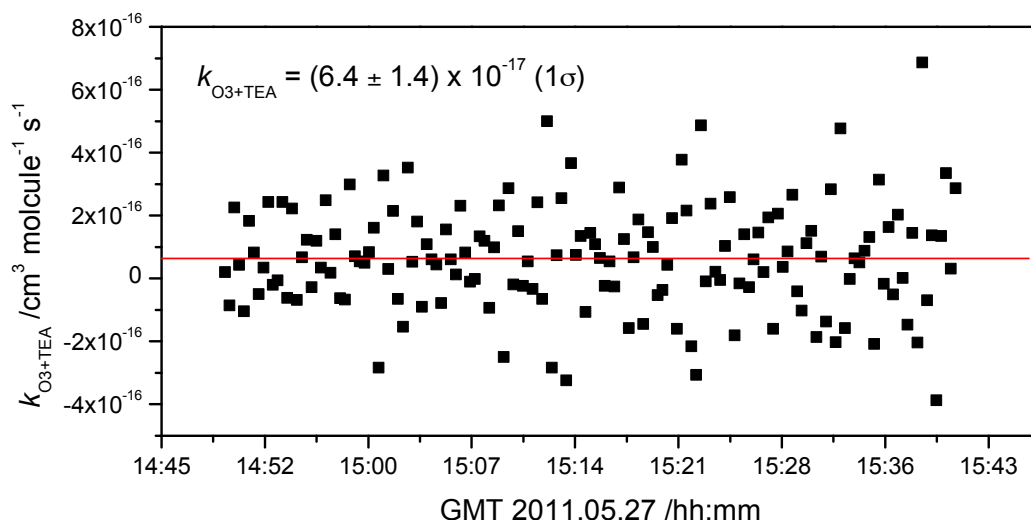
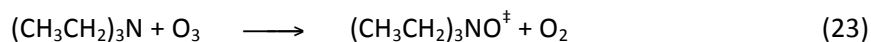


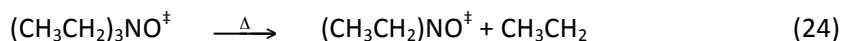
Figure 3.34. Scatter-plot of $k_{\text{O}_3+\text{TEA}}$ derived from numerical differentiation of PTR-TOF-MS data for triethylamine (TEA) and FTIR data for O_3 volume mixing ratios during the experiment on 2011.05.27.

The first conclusion to be drawn is that the triethylamine gas phase loss observed in the 2011.05.27 experiment is essentially due to reaction with O_3 .

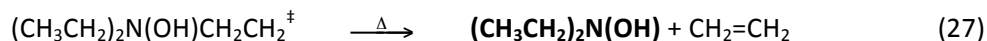
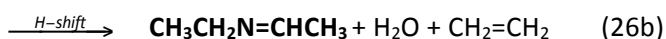
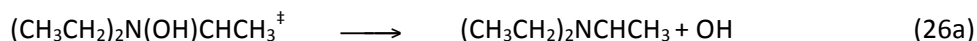
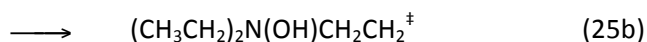
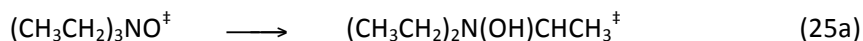
Tuazon *et al.*⁵¹ studied product formation in the O_3 reaction with triethylamine and explained the products observed by a mechanism in which the initial step is the formation of an energy-rich *N*-oxide, similar to the mechanism outlined by Slagle *et al.*⁴⁵ for the reaction of $\text{O}(^3\text{P})$ atoms with alkylamines. For triethylamine the reaction sequence is expected to be:



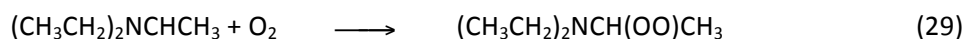
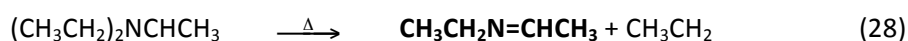
The excited triethylamine *N*-oxide may decompose via N-C scission; the CH_3CH_2 radical loss leading to acetaldehyde formation:



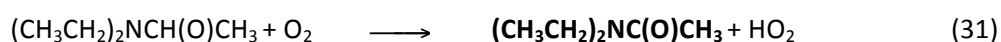
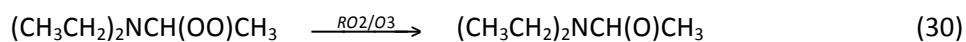
or it can undergo H-atom migration to the oxygen atom:



The alkyl radical formed in (26a) may either decompose or react with O_2 :



[#] An alternative way of deriving the rate coefficient is to fit the time profiles by polynomials and to differentiate the analytical expression for [TEA] – the same result is obtained.



The second conclusion to be drawn is that the mechanism suggested for $\text{O}(^3\text{P})$ reaction with amines⁴⁵ also explains the main products observed in the triethylamine ozonolysis experiment.

Ozone builds up in all the triethylamine photo-oxidation experiments (see Supplementary Information, *ADA-2011: Protocols and monitor data*). In the 2011.03.31 experiment O_3 increased from 20 to 70 ppbV during the experiment; in the 2011.04.01 experiment O_3 increased from 10 to 40 ppbV; in the 2011.05.26 experiment O_3 increased from 5 to 40 ppbV; in the 2011.5.30 experiment O_3 increased from 5 to 70 ppbV. Figure 3.35 shows the triethylamine time profile and the modelled accumulated triethylamine gas phase loss due to reaction with O_3 and OH during the high-NO_x photo-oxidation experiment on 2011.03.31. The corresponding data from the low-NO_x triethylamine photo-oxidation experiment on 2011.05.26 is shown in Figure 3.36.

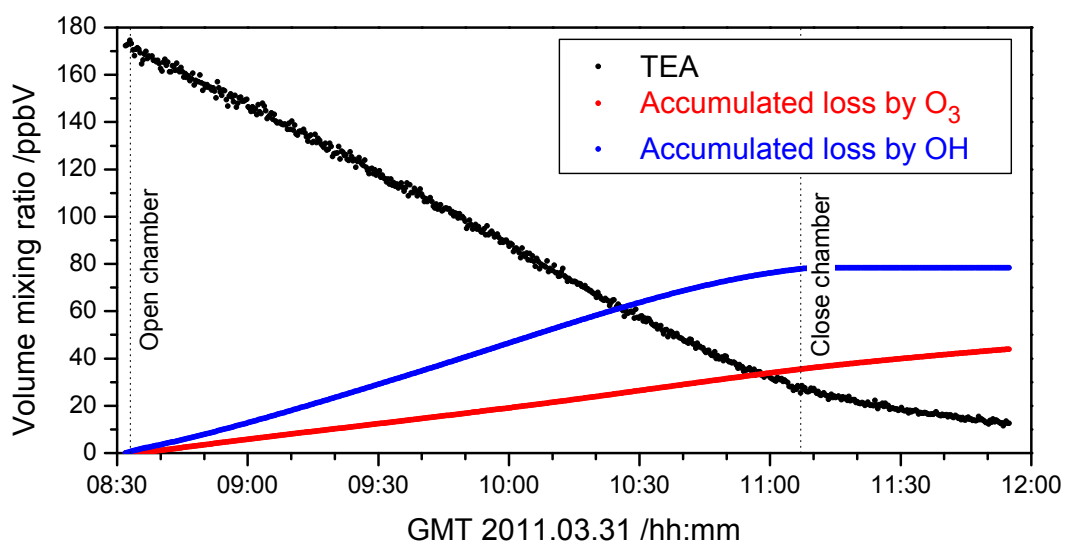


Figure 3.35. Time-profile of triethylamine (TEA) and accumulated triethylamine gas phase loss due to reaction with O_3 and OH radicals during the high-NO_x photo-oxidation experiment on 2011.03.31.

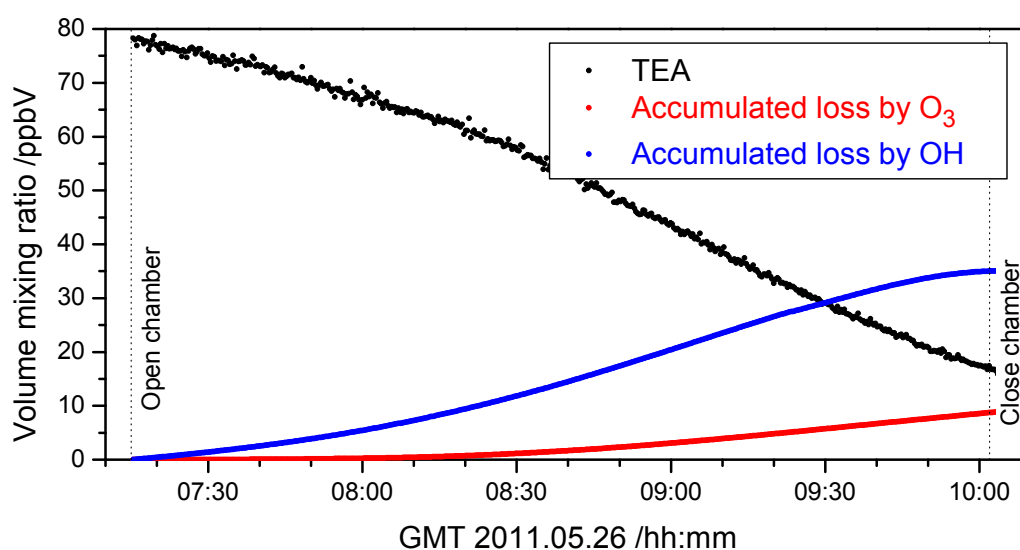


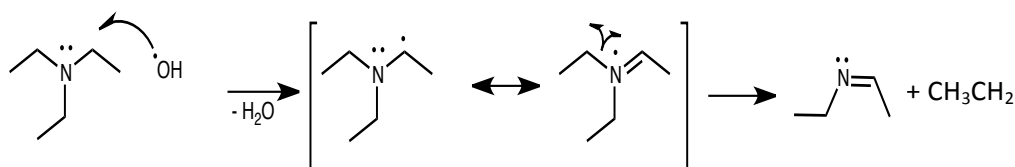
Figure 3.36. Time-profile of triethylamine (TEA) and accumulated triethylamine gas phase loss due to reaction with O_3 and OH radicals during the low-NO_x photo-oxidation experiment on 2011.05.26.

It can be seen that after a 15 minutes induction period of the high-NO_x experiment on 2011.03.31, the O₃ reaction with triethylamine accounts for around 30% of the gas phase removal throughout the rest of experiment. In the low NO_x experiment on 2011.05.26 the accumulated triethylamine gas phase removal by O₃ is 5% after the first hour and around 20% at the end of the experiment.

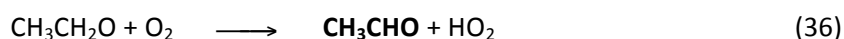
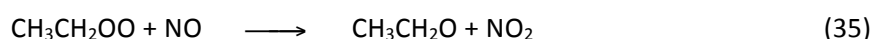
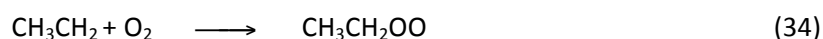
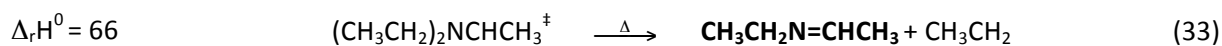
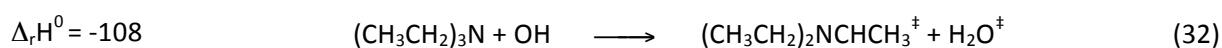
The third conclusion to be drawn is that ozone reaction cannot be neglected in analyses of the triethylamine chamber photo-oxidation experiments.

3.4.2 OH chemistry

Even allowing for the competing O₃ reaction with triethylamine during the OH photo-oxidation experiments, it is obvious from Figure 3.32 that the theoretical scheme for OH initiated photo-oxidation of triethylamine, Scheme 3.4, cannot explain the observed product distribution. In particular, there must clearly exist another route leading to acetaldehyde without simultaneous formation of the (CH₃CH₂)₂N radical – far too little (CH₃CH₂)₂NNO and (CH₃CH₂)₂NNO₂ is observed in the experiments. The route must also bypass formation of the (CH₃CH₂)₂NCH(O)CH₃ radical as this will lead to *N,N*-diethyl acetamide, which is only observed in traces. Following the mechanism for O(³P) atom reaction with alkylamines, proposed by Slagle *et al.*,⁴⁵ it is suggested that unimolecular dissociation of the (CH₃CH₂)₂NCHCH₃ radical leading to ethyl ethanimine and the ethyl radical may be the additional route:



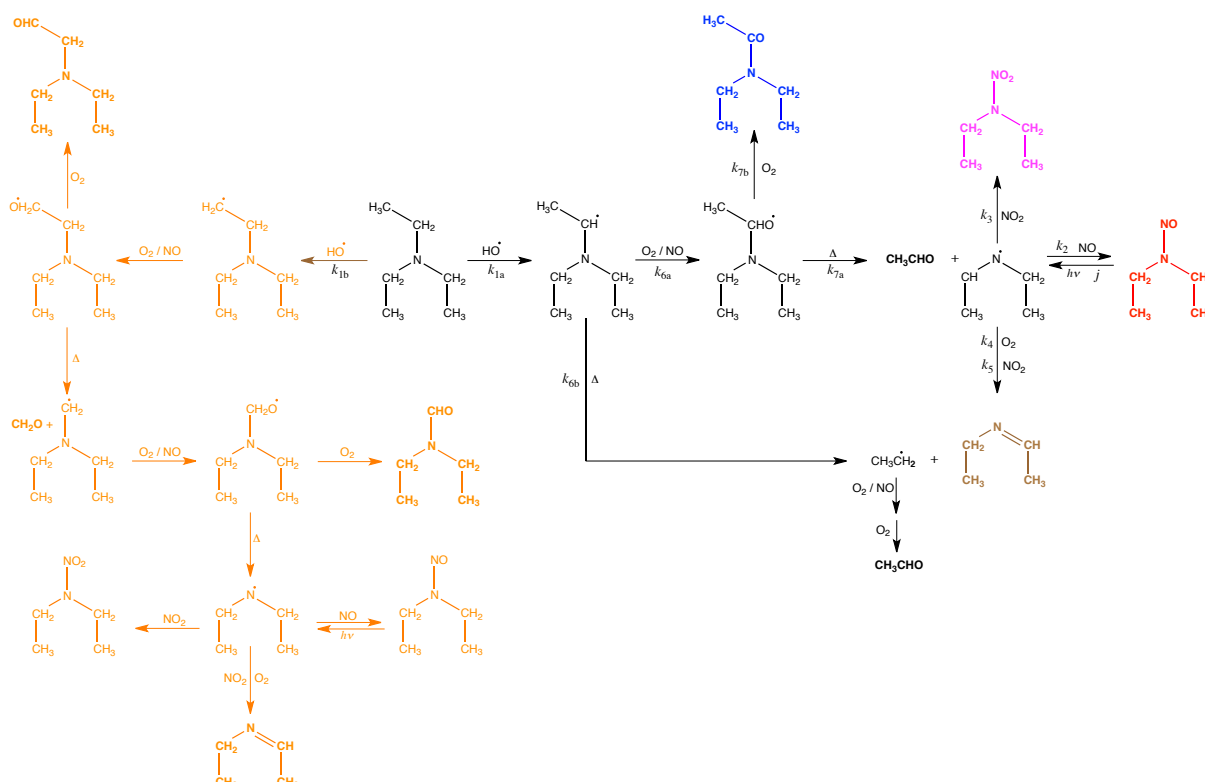
The unimolecular dissociation of the (CH₃CH₂)₂NCHCH₃ radical is endothermic by 66 kJ mol⁻¹ (result from G3-calculations³⁸), and is only expected to be important if sufficient internal energy is available. The initial hydrogen abstraction is exothermic by 108 kJ mol⁻¹ and, assuming equipartitioning of the reaction enthalpy, there is ample energy available to the dissociation:



The above sequence will result in a 1:1 ratio of acetaldehyde and ethyl ethanimine. The same is almost also the case for the route via the (CH₃CH₂)₂NCH(O)CH₃ radical. The experimental acetaldehyde to ethyl ethanimine ratio is near 3:1 in the 2011.04.01 experiment; the additional acetaldehyde is explained by O₃-triethylamine chemistry.

It should be noted that the ADA-2010 project reported minor, unexplained features in the product distribution in similar triethylamine photo-oxidation experiments.⁶

A revised triethylamine photo-oxidation scheme is presented in Scheme 3.5



Scheme 3.5. Updated theoretical atmospheric photo-oxidation scheme for triethylamine. The orange coloured route is expected to be of minor importance.

3.4.3 Branching ratios in the photo-oxidation of triethylamine

Ethylamine and diethylamine photo-oxidation experiments were carried out prior to the triethylamine experiments, and unfortunately both compounds were present as impurities in all triethylamine experiments. The photo-oxidations of ethylamine and diethylamine are relatively well-understood (sections 3.2 and 3.3) and taken into account in the analyses.

The initial H-abstraction by OH radicals may take place at two sites in triethylamine ($-\text{CH}_2-$ and $-\text{CH}_3$), of which the methyl groups are expected to be the least reactive. The predicted major products resulting from H-abstraction from the CH_3 -groups, Scheme 3.5, include $(\text{CH}_3\text{CH}_2)_2\text{NCH}_2\text{CHO}$ (2-(diethylamino) acetaldehyde), $(\text{CH}_3\text{CH}_2)_2\text{NCHO}$ (*N,N*-diethyl formamide), $\text{CH}_2=\text{NCH}_2\text{CH}_3$ (ethyl ethanimine), $(\text{CH}_3\text{CH}_2)_2\text{NNO}$ (*N*-nitroso diethylamine) and $(\text{CH}_3\text{CH}_2)_2\text{NNO}_2$ (*N*-nitro diethylamine); only *N,N*-diethyl formamide is a unique marker of this route. 2-(Diethylamino) acetaldehyde is an isomer of *N,N*-diethyl acetamide ($(\text{CH}_3\text{CH}_2)_2\text{NC}(\text{O})\text{CH}_3$) and these compounds cannot be distinguished by PTR-MS. There were no indications of 2-(diethylamino) acetaldehyde) in DNPH cartridges collected during the triethylamine photo-oxidation experiments. There were, however, observations of ions at m/z 102.0922 ($\text{C}_5\text{H}_{12}\text{NO}^+$, interpreted as protonated of *N,N*-diethyl formamide) with around 5% yield in the high- NO_x triethylamine photo-oxidation experiments. The m/z 102.0922 ion signal was not detected above 1% yield in the low- NO_x experiments.

In the analysis of the triethylamine photo-oxidation experiments the following assumptions have been made, Scheme 3.5:

- H-abstraction from the CH_3 -groups can be neglected.
This assumption influences the branching ratio k_{6a}/k_{6r} , but not the validity of extrapolating the laboratory results to ambient conditions.
- Branching ratios and relative photolysis rate from the *N*-nitroso diethylamine photolysis study (section 4.7) $k_2/k_3 = 0.7$, $k_4/k_3 = 0$, $k_5/k_3 = 11.2 \times 10^{-7}$, and $j_{\text{Nitrosamine}}/j_{\text{NO}_2} = 0.30$.

These assumptions will influence the derived branching ratio k_{6a}/k_6 . The assumptions will, however, not influence the validity of extrapolating the laboratory results to ambient conditions (the parameters constitute a self consistent set).

3. $k_{\text{TEA}+\text{OH}} = 7.7 \times 10^{-11} \text{ cm}^3 \text{ molecule}^{-1} \text{ s}^{-1}$ at 298 K (see section 2.1), $k_{\text{DEANO}_2+\text{OH}} = 4.6 \times 10^{-12} \text{ cm}^3 \text{ molecule}^{-1} \text{ s}^{-1}$ at 298 K (see section 2.2), $k_{\text{DEANO}+\text{OH}} = 3.5 \times 10^{-12}$, and $k_{\text{Imine}+\text{OH}} = 2 \times 10^{-11} \text{ cm}^3 \text{ molecule}^{-1} \text{ s}^{-1}$ at 298 K (see section 4).

These assumptions have very little impact (< 1%) on the derived branching ratio k_{6a}/k_6 .

4. Mass balance is obtained by introducing a continuous 7% loss of triethylamine to aerosol (see ANNEX D, page 146) in addition to that caused by dilution and wall loss. The remaining organic aerosol constituents are assumed to stem from other compounds than *N*-nitro ethylamine.

These assumptions will influence the derived branching ratio k_{6a}/k_6 . Should the amount of triethylamine lost to aerosol be 3 times larger (21 instead of 7%), the derived branching will increase by 14%. Further, should 10% of the *N*-nitro diethylamine that is formed in the photo-oxidation experiments be transferred to the aerosol, the determined initial branching ratio would be 10% too low. It is noted that *N*-nitro diethylamine has not been detected in the aerosol.

The *N,N*-diethyl acetamide yield is close to 0 and k_{7a}/k_7 is therefore close to 1. Under the assumptions given above, the branching in the $(\text{CH}_3\text{CH}_2)_2\text{NCHCH}_3$ radical dissociation versus O_2 reaction, k_{6a}/k_6 , is then determined from the *N*-nitro diethylamine time profiles, and k_{7a}/k_7 is then adjusted to fit the *N,N*-diethyl acetamide time profiles. A best-balanced fit of the data from the 2 high-NO_x and 2 low-NO_x triethylamine photo-oxidation experiments was obtained for $k_{6a}/k_6 = 0.35 \pm 0.05$, and $k_{7a}/k_7 = 0.99 \pm 0.01$. The observed and modelled time profiles are illustrated in Figure 3.37 through Figure 3.40.

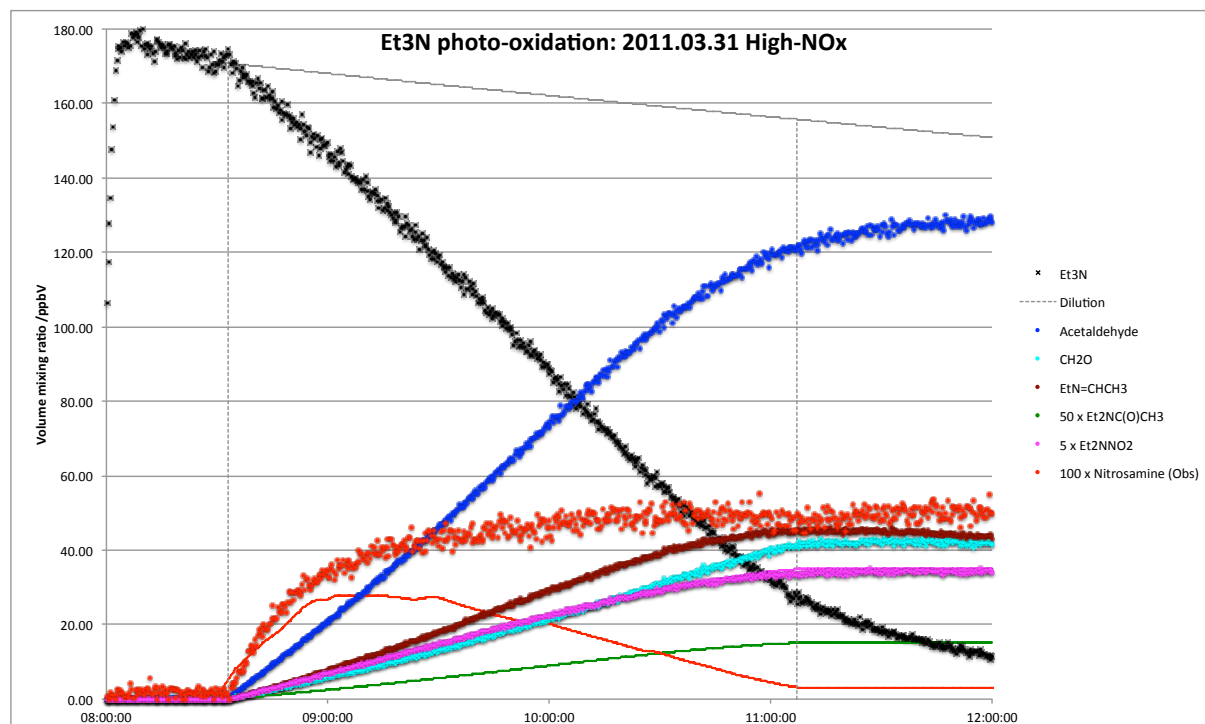


Figure 3.37. Selected ion signals and ion precursor volume mixing ratios during the triethylamine photo-oxidation experiment on 2011.03.31. The full curves represent model results/predictions.

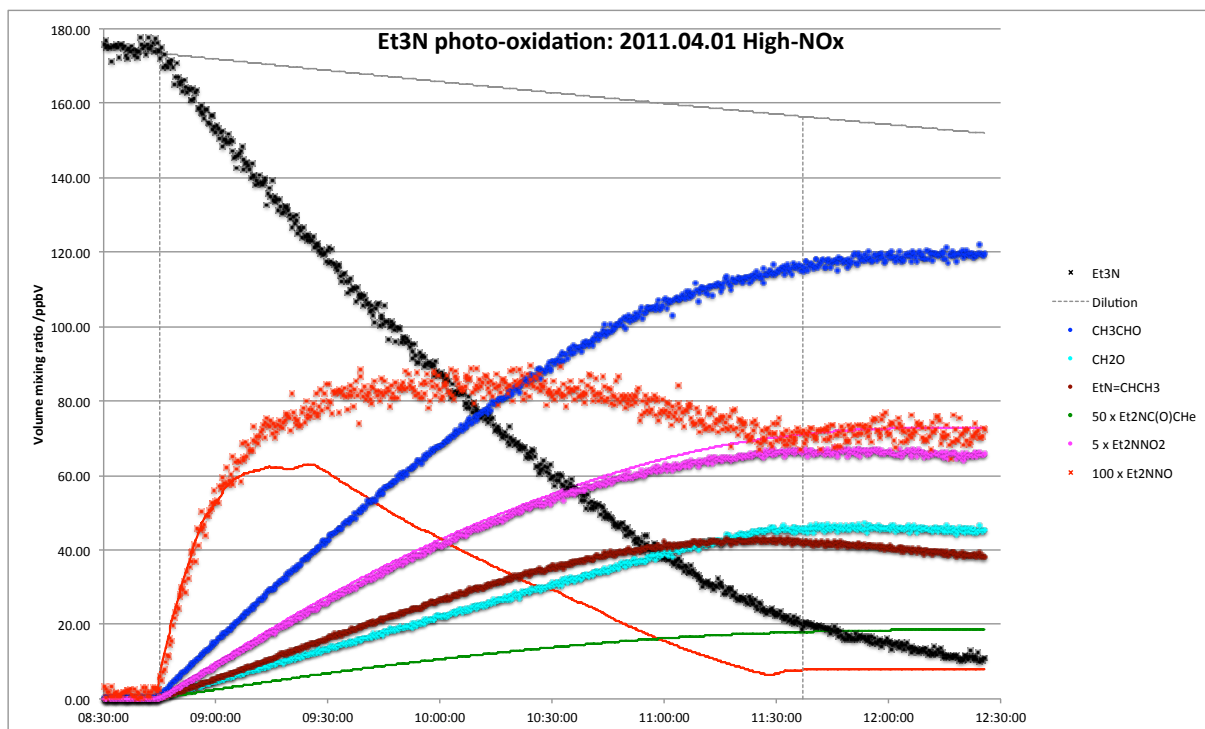


Figure 3.38. Selected ion signals and ion precursor volume mixing ratios during the triethylamine photo-oxidation experiment on 2011.04.01. The full curves represent model results/predictions.

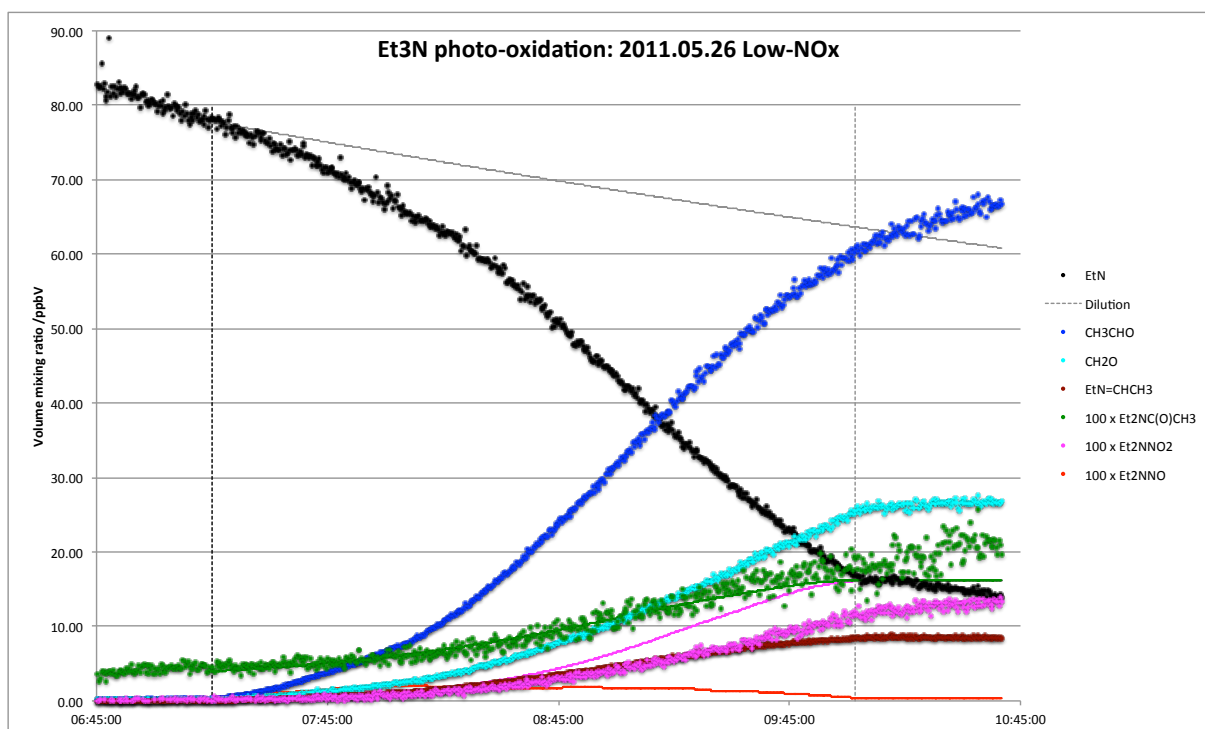


Figure 3.39. Selected ion signals and ion precursor volume mixing ratios during the triethylamine photo-oxidation experiment on 2011.05.26. The full curves represent model results/predictions.

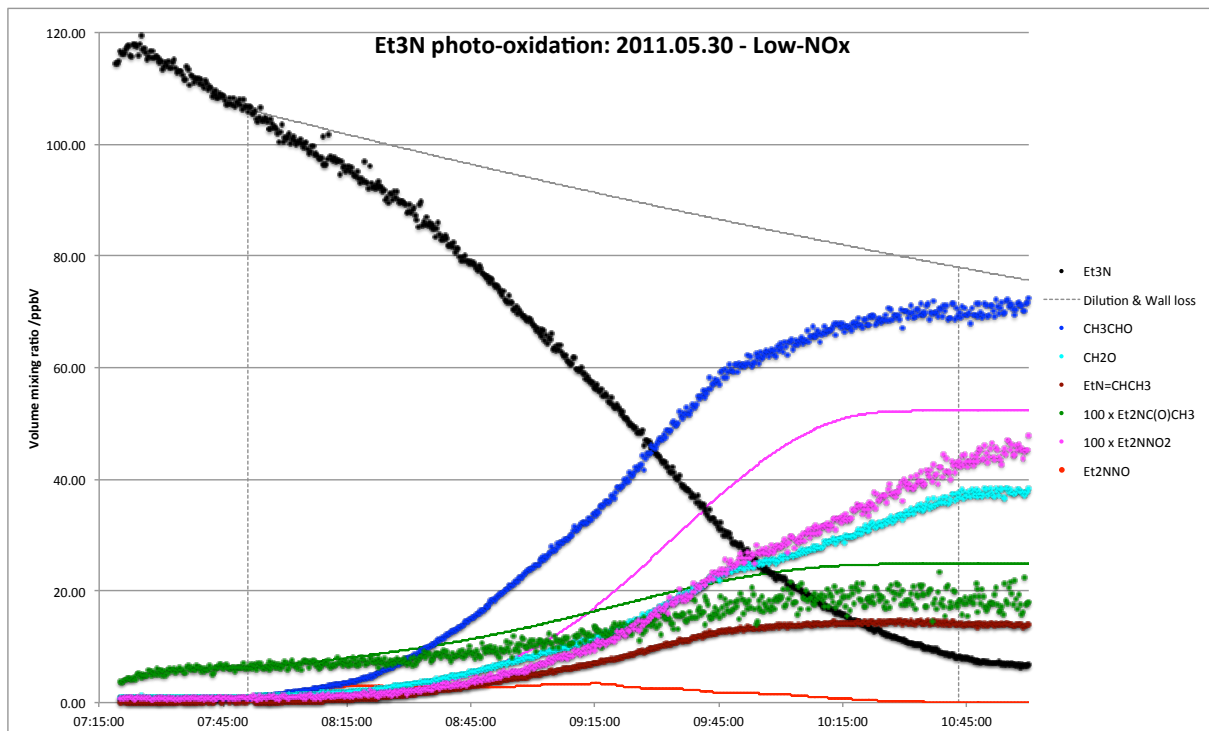


Figure 3.40. Selected ion signals and ion precursor volume mixing ratios during the triethylamine photo-oxidation experiment on 2011.05.30. The full curves represent model results/predictions.

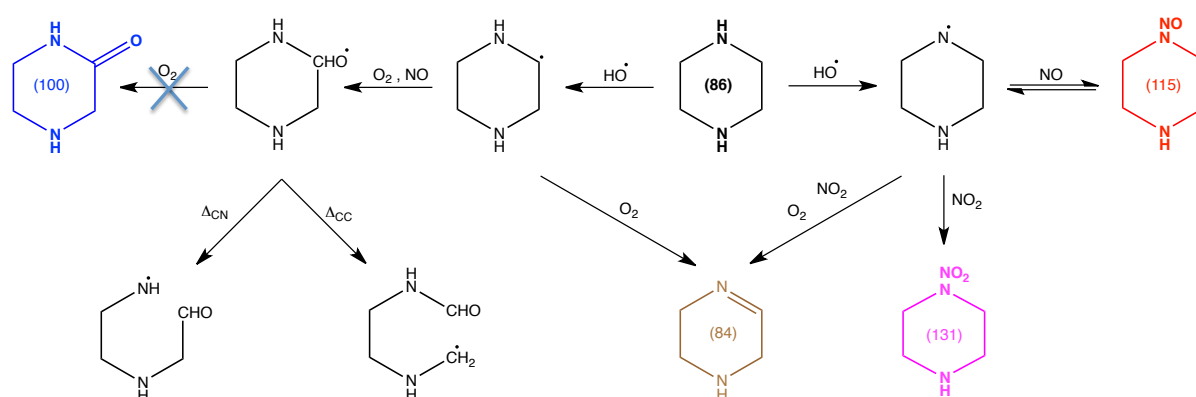
3.5 Piperazine

Previous studies. There are no experimental data available for the atmospheric gas phase photo-oxidation of piperazine. The only publicly available information relevant to the atmospheric photo-oxidation of piperazine stems from the theoretical work reported by Bråthen *et al.*⁶⁰

Present studies. Seven piperazine photo-oxidation studies have been carried out – three in 2010 (2010.03.04, 2010.07.21 and 2010.07.22) and four in 2011 (2011.04.05, 2011.04.06, and two on 2011.06.09). Piperazine is a difficult compound to study in smog chambers; it has a very high surface affinity, and the 2010 experiments are of inferior quality compared to the 2011 experiments due to the conditions of the Teflon dome (the Teflon dome was replaced late 2010). The 2010 data are not included in the present report. One experiment was carried out under low-NO_x conditions (ca. 20 ppbV NO_x) – the other three under high-NO_x conditions (≥ 50 ppbV NO_x). IPN-d6 was added as additional OH precursor in one experiment. Table 3.6 summarises the ion signals observed in the four experiments; the ion signals have been converted from normalized counts to volume mixing ratios without correcting for specific molecular dipole moments and polarizabilities and not considering fragment ion formation; the reported mixing ratios are therefore purely indicative

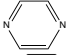
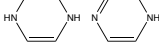
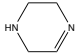
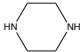
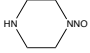
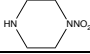
In summary, the experiments indicate that piperazine will have a short atmospheric lifetime. The rate coefficient for OH radical reaction with piperidine, which has only one amino group, is $7.4 \times 10^{-11} \text{ cm}^3 \text{ molecule}^{-1} \text{ s}^{-1}$ (see section 2.1, page 15), and the rate coefficient for OH reaction with piperazine is expected to be larger than $10^{-10} \text{ cm}^3 \text{ molecule}^{-1} \text{ s}^{-1}$. Concerning product formation, three of the four expected primary products in the OH-initiated photo-oxidation of piperazine have been observed in the present experiments, Scheme 3.6. The fourth, 2-piperazinone, is a well-known, stable compound, but apparently ring opening and imine formation are such efficient processes that the compound is not formed in detectable amounts. The results obtained are only qualitative:

- It has not been possible to derive an estimate of the branching ratio in the initial OH reaction with piperazine.
- It has not been possible to derive the subsequent atmospheric fate of the primary products and of the radicals formed upon ring opening.
- The experiments show that the primary products – the piperazine imine (1,2,3,6-tetrahydro pyrazine), the nitrosamine and the nitramine – are all short-lived with lifetimes of around 30 minutes in the EUPHORE reactor.
- The sum formulae of other products detected in the experiments rule out any significant formation of smaller alkyl nitramines in the atmospheric photo-oxidation of piperazine.



Scheme 3.6. Initial steps in the atmospheric photo-oxidation of piperazine. The nominal masses of the compounds are indicated in parentheses.

Table 3.6. Major ion signals observed in piperazine photo-oxidation experiments.

m/z	Ion sum formula	Ion precursor and comments
18.0343	NH ₄ ⁺	NH ₃
31.0189	CH ₃ O ⁺	CH ₂ O
45.0345	C ₂ H ₅ O ⁺	CH ₃ CHO
46.0301	CH ₄ NO ⁺	NH ₂ CHO
46.0656	C ₂ H ₈ N ⁺	CH ₃ CH ₂ NH ₂ or (CH ₃) ₂ NH. Wall desorption
47.0139	CH ₃ O ₂ ⁺	HCOOH
60.0447	C ₂ H ₆ NO ⁺	
69.0447	C ₃ H ₅ N ₂ ⁺	
72.0835	C ₄ H ₁₀ N ⁺	
74.0243	C ₂ H ₄ NO ₂ ⁺	
74.0981	C ₄ H ₁₂ N ⁺	(CH ₃ CH ₂) ₂ NH. Wall desorption
81.0462	C ₄ H ₅ N ₂ ⁺	
83.0604	C ₄ H ₇ N ₂ ⁺	
85.0756	C ₄ H ₉ N ₂ ⁺	From piperazine ^a and 
86.0846	C ₄ H ₁₀ N ₂ ⁺	
87.0900	C ₄ H ₁₁ N ₂ ⁺	
99.0561	C ₄ H ₇ N ₂ O ⁺	
99.0923	C ₅ H ₁₁ N ₂ ⁺	
115.0862	C ₅ H ₁₁ N ₂ O ⁺	
116.0787	C ₄ H ₁₀ N ₃ O ⁺	
119.0855	C ₄ H ₁₁ N ₂ O ₂ ⁺	
132.0750	C ₄ H ₁₀ N ₃ O ₂ ⁺	

^a C₄H₁₀N₂ + H₃O⁺ → C₄H₁₁N₂⁺ + H₂O; C₄H₁₁N₂⁺ → C₄H₉N₂⁺ + H₂

Piperazine was injected into the chamber in a stream of N₂ passing over a gently heated piperazine sample. Upon injection several ion signals increased. In the following, the detected ion signals in the piperazine experiments are separated according to their time evolution: (1) signals that appear upon injection of piperazine along with that of protonated piperazine, (2) signals that grow and decrease again during the photo-oxidation experiment (intermediate products), and (3) signals that grow steadily after opening the chamber canopy. Figure 3.41 includes the more prominent ion signals that increase during the injection in the high-NO_x experiment on 2011.04.05.

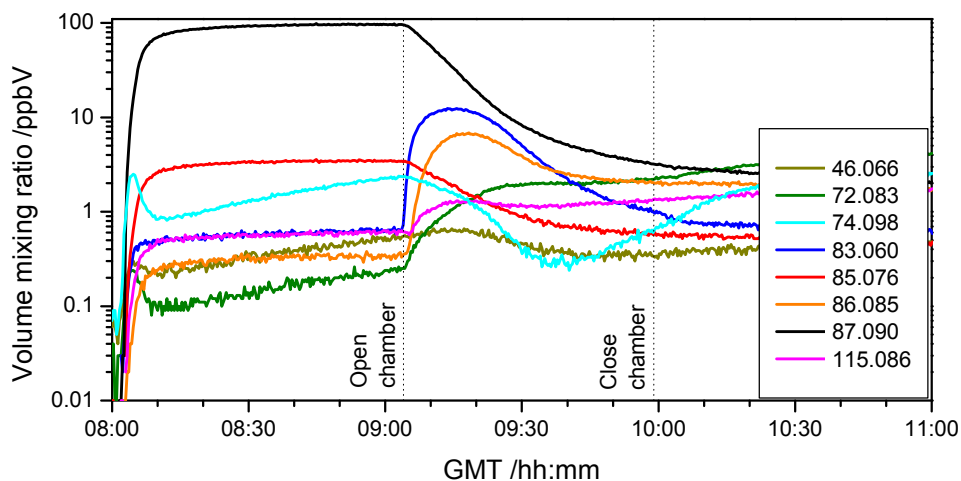


Figure 3.41. Selected ion signals appearing during piperazine injection and photo-oxidation. Data from 2011.04.05.

Three of the signals, m/z 46.066, 72.083 and 74.098, show time profiles that indicate they in part stem from molecules desorbing from the chamber surface as a result of piperazine being injected and subsequently adsorbed on the chamber walls. The time profiles of the m/z 46.066 and 74.098 ion signals show that the ion precursors are not related to piperazine photo-oxidation, and they are assigned to respectively ethylamine/dimethylamine and diethylamine studied in previous experiments. The m/z 85.076 ion signal ($C_4H_9N_2^+$) is apparently almost perfectly correlated to the ion signal of protonated piperazine (m/z 87.090, $C_4H_{11}N_2^+$), in contrast to the m/z 72.083, 83.060, 86.085 and 115.086 that also grow during piperazine photo-oxidation. These ion signals can therefore, in principle, originate in several isomeric species or be fragments from other species.

A closer inspection of the m/z 85.076 ion signal shows that it does not only stem from dehydrogenation of protonated piperazine, but that there is an additional component, Figure 3.42, which tentatively is interpreted in terms of the piperazine imine, 1,2,3,6-tetrahydro pyrazine. Similar residual signals are observed in the other three experiments.

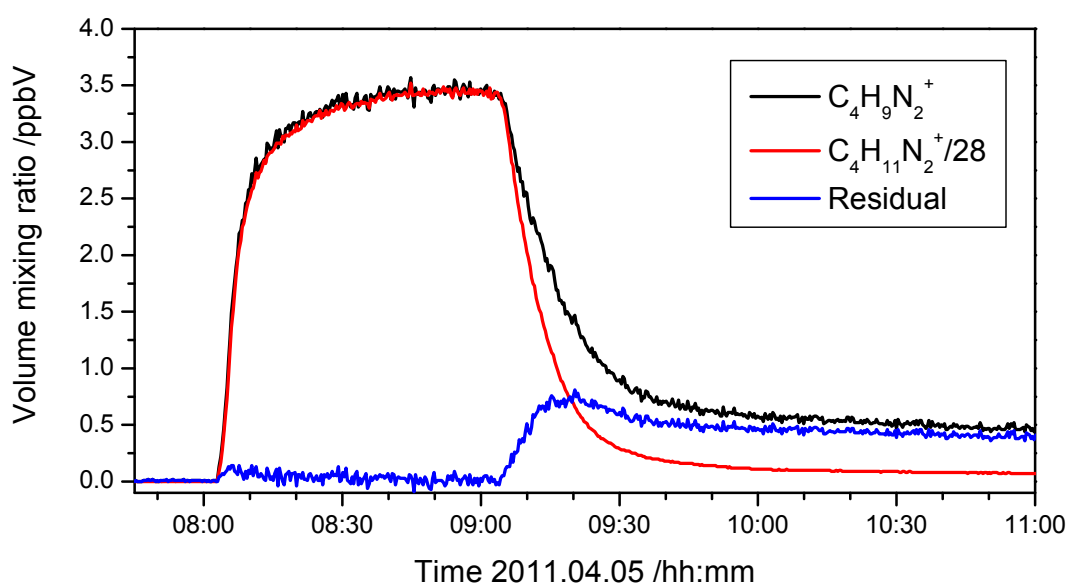


Figure 3.42. The m/z 85.076 and scaled 87.090 ion signals appearing during injection of piperazine, and the residual signal emerging upon photo-oxidation, attributed to piperazine imine, 1,2,3,6-tetrahydro pyrazine. Data from 2011.04.05.

The ion signals from intermediate products in the 2011.04.05 photo-oxidation experiment are shown in Figure 3.43, and include m/z 116.0836, 132.0772 attributed to *N*-nitroso piperazine and *N*-nitro piperazine, respectively. The figure shows that both compounds are formed and removed from the gas phase within only 30 minutes during the experiment. It is expected that the nitrosamine will have a short photolysis lifetime. But that the atmospheric lifetime of the nitramine is so short indicates that the second amino group in these compounds retains a very high reactivity.

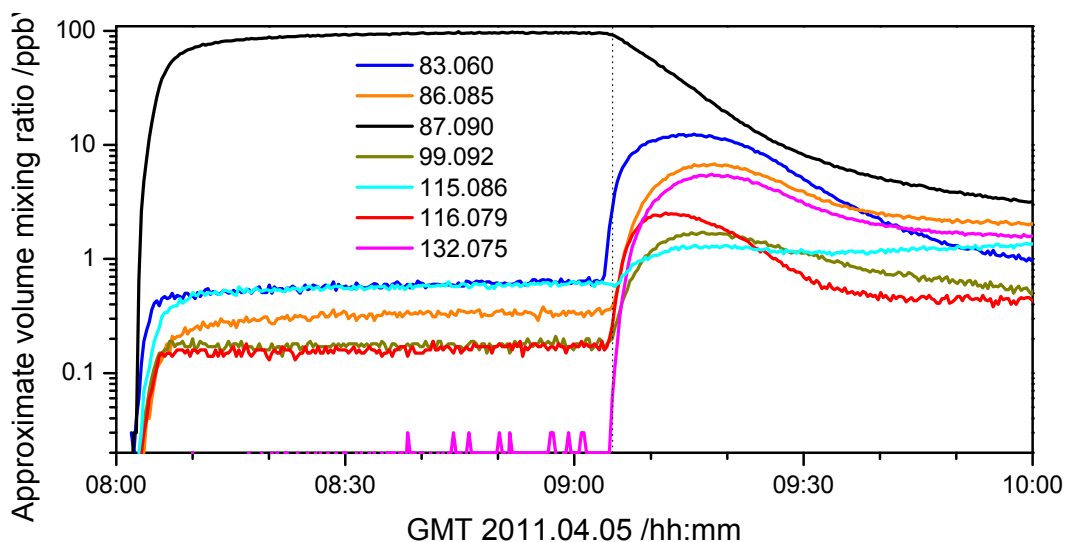
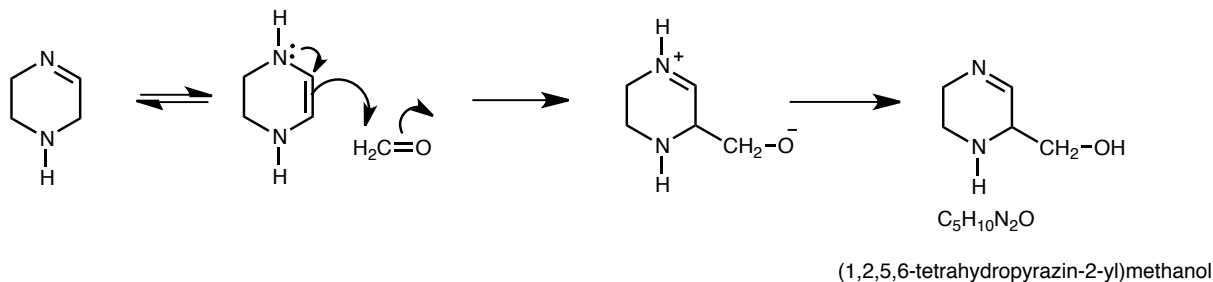


Figure 3.43. Ion signals growing in and decreasing fast again during piperazine photo-oxidation. Data from 2011.04.05.

It should be noted that two of the signals in the group of intermediate products have more carbon atoms than piperazine itself: m/z 99.092 ($C_5H_{11}N_2^+$) and 115.086 ($C_5H_{11}N_2O^+$). The corresponding neutral molecules of both ions must originate from (heterogeneous?) condensation reactions. The m/z 115.086 ion may originate from the condensation between the piperazine imine and formaldehyde as shown in Scheme 3.7.



Scheme 3.7. Proposed condensation reaction between 1,2,3,6-tetrahydro pyrazine and CH_2O .

Figure 3.44 shows the ion signals that essentially only grow after opening the chamber canopy and piperazine photo-oxidation setting in. For the sake of clarity, the ion masses below and above m/z 75 have been divided into two panels. The m/z 69.045 ion signal ($C_3H_5N_2^+$) is the only one having a clearly different time-profile, suggesting it being a secondary product. On the other hand it is not likely that the m/z 60.0447 ($C_2H_6NO^+$), 72.0835 ($C_4H_{10}N_2^+$), 74.0243 ($C_2H_4NO_2^+$), 86.0846 ($C_4H_{10}N_2^+$), 99.0561 ($C_4H_7N_2O^+$) and 119.0855 ($C_4H_{11}N_2O_2^+$) all stem from primary products. A more detailed analysis of these signals goes beyond the time frame of this project.

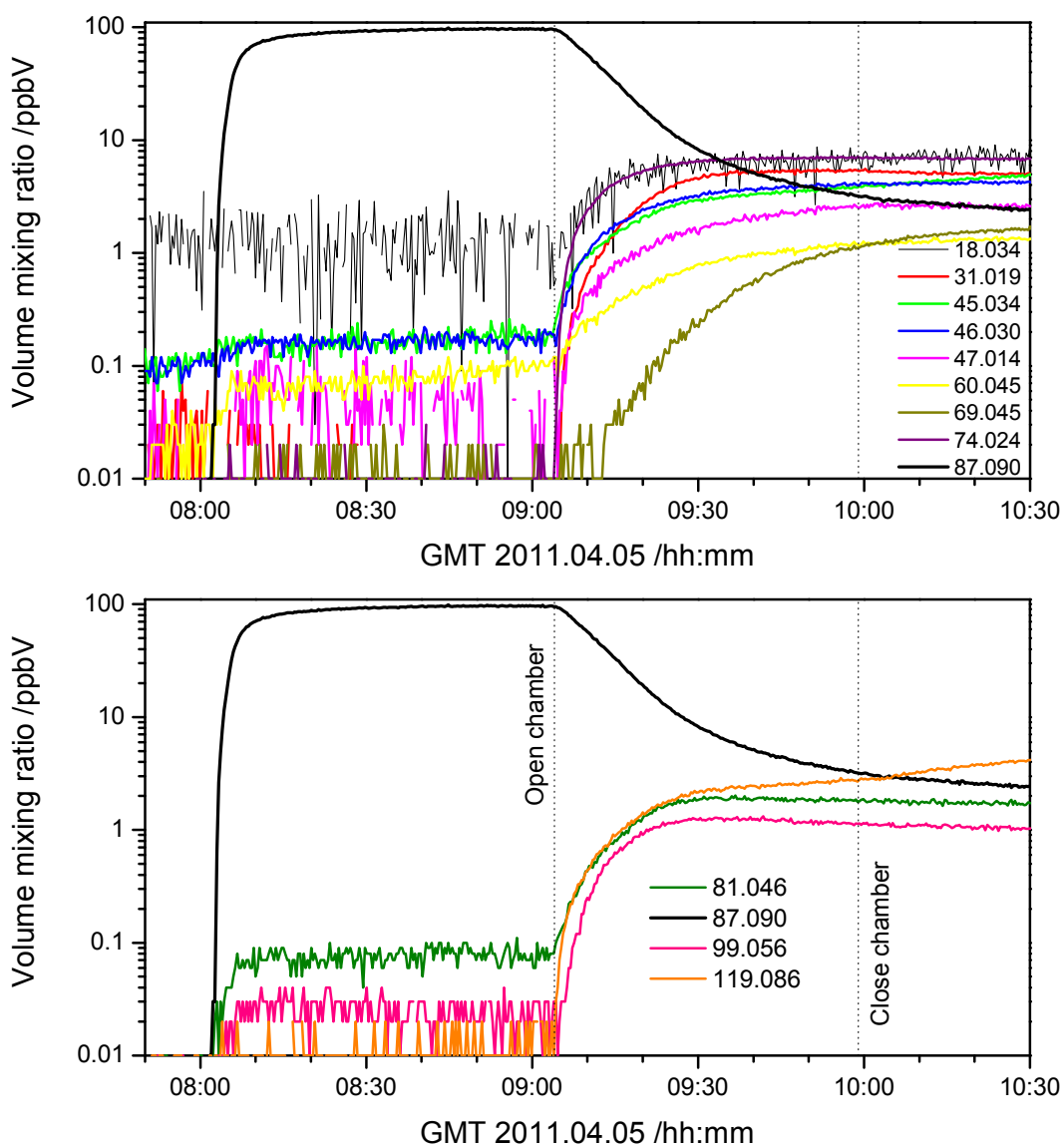


Figure 3.44. Ion signals growing in during the piperazine photo-oxidation experiment on 2010.07.21.

The present piperazine experiments are hampered by wall adsorption/desorption and particle formation, and the data are insufficient to allow an unambiguous determine the neutral molecules corresponding to the detected ion signals. However, it can be noted that none of the molecular formulae can be related to alkyl nitramines.

3.6 Amides

Previous studies. There are four kinetic studies of OH radical reactions with amides. Koch *et al.*⁶¹ investigated 4 amides (*N*-methyl acetamide, *N,N*-dimethyl acetamide, *N*-methyl propylamide and *N,N*-dimethyl propylamide) with the aim of testing/extending a commonly used structure-activity relationship²⁶ for prediction of OH rate constants. The reactions were found to show *negative* Arrhenius temperature dependencies and to conflict with the SAR predictions. Solignac *et al.*⁶² studied the OH (and Cl) reaction kinetics of 3 amides (*N*-methyl formamide, *N,N*-dimethyl formamide and *N,N*-dimethyl acetamide); the results support that the reactivity of amides deviate from SAR predictions. Aschmann and Atkinson⁶³ studied the reactions of 1-methyl-2-pyrrolidone at 296 K and proposed a scheme for the reactions. Finally, Barnes *et al.*⁶⁴ studied the OH reaction kinetics of *N*-methyl acetamide, and the Cl atom kinetics of formamide and *N*-methyl acetamide. In addition there are two kinetic studies of NO₃ radical reaction with amides. Aschmann and Atkinson⁶³ studied the reactions of 1-methyl-2-pyrrolidone at 296 K; Dib and Chakir⁶⁵ studied the temperature dependence of the NO₃ rate coefficient of reaction with 4 amides (*N,N*-dimethyl formamide, *N,N*-dimethyl acetamide, *N,N*-dimethyl propylamide and 1-methyl-2-pyrrolidone).

There are two reports in the open literature of products in the reactions between OH radicals and amides. Aschmann and Atkinson⁶³ report the formation of *N*-methyl succinimide and 1-formyl-2-pyrrolidinone from the OH reaction with 1-methyl-2-pyrrolidinone and essentially only 1-formyl-2-pyrrolidinone from the NO₃ reaction. In addition, the ADA-2010 project has reported both product distributions and branching ratios. Table 3.7 summarizes the products reported in amide photo-oxidation experiments by Barnes *et al.*⁶⁴ and Nielsen *et al.*⁶

Table 3.7. Products of atmospheric amide photo-oxidation.

Amide	Barnes <i>et al.</i> ⁶⁴	Nielsen <i>et al.</i> ⁶
NH ₂ CHO	HNCO	HNCO
CH ₃ NHCHO	HN(CHO) ₂ , CH ₃ NCO, CH ₃ NHC(O)OONO ₂	CH ₃ NCO, HN(CHO) ₂ , CH ₃ NHNO ₂ , CH ₂ O
(CH ₃) ₂ NCHO	CH ₃ N(CHO) ₂ , (CH ₃) ₂ NC(O)OONO ₂	CH ₃ NCO, CH ₂ O, CH ₃ N(CHO) ₂ , CH ₃ N=CH ₂ , (CH ₃) ₂ NNO ₂
NH ₂ C(O)CH ₃	HNCO	
CH ₃ NHC(O)CH ₃	CH ₃ C(O)NHCHO, CH ₃ NCO	
(CH ₃) ₂ NC(O)CH ₃	CH ₃ C(O)N(CH ₃)CHO	

3.6.1 *N*-ethylacetamide

Table 3.8 lists the ion signals observed during the *N*-ethylacetamide photo-oxidation experiment. Only ions with a yield > 1% (ncps/ncps) are reported. Figure 3.45 displays the time evolution of protonated *N*-ethylacetamide (calculated exact *m/z* 88.07569) and the ions reported in Table 3.8.

A detailed analysis (based on different relative ion abundances observed in replicate experiments with different instrumental settings: *E/N* = 88 Td and *E/N* = 52 Td) indicates that the *m/z* 46.0311 and *m/z* 60.0440 ions are fragment ions of the *m/z* 88.0366 and *m/z* 102.0542 ions, respectively. Absolute quantification has not been attempted.

Table 3.8. Measured m/z of ion signals observed during the *N*-ethylacetamide photo-oxidation experiment. The table includes the calculated exact m/z , the assigned ion sum formula, the suggested neutral precursors and comments. Only ions with a yield > 1% (ncps/ncps) are reported.

measured m/z	calculated m/z	Ion sum formula	Neutral precursor	Comments
31.0187	31.01784	CH_3O^+	formaldehyde	
45.0349	45.03349	$\text{C}_2\text{H}_5\text{O}^+$	acetaldehyde	
46.0311	46.02874	CH_4NO^+		fragment ion from 88.0366
60.0440	60.04439	$\text{C}_2\text{H}_6\text{NO}^+$		fragment ion from 102.0542
88.0366	88.03931	$\text{C}_3\text{H}_6\text{NO}_2^+$	<i>N</i> -formylacetamide	
102.0542	102.05496	$\text{C}_4\text{H}_8\text{NO}_2^+$	<i>N</i> -acetylacetamide, <i>N</i> -(2-oxoethyl)acetamide	isomers

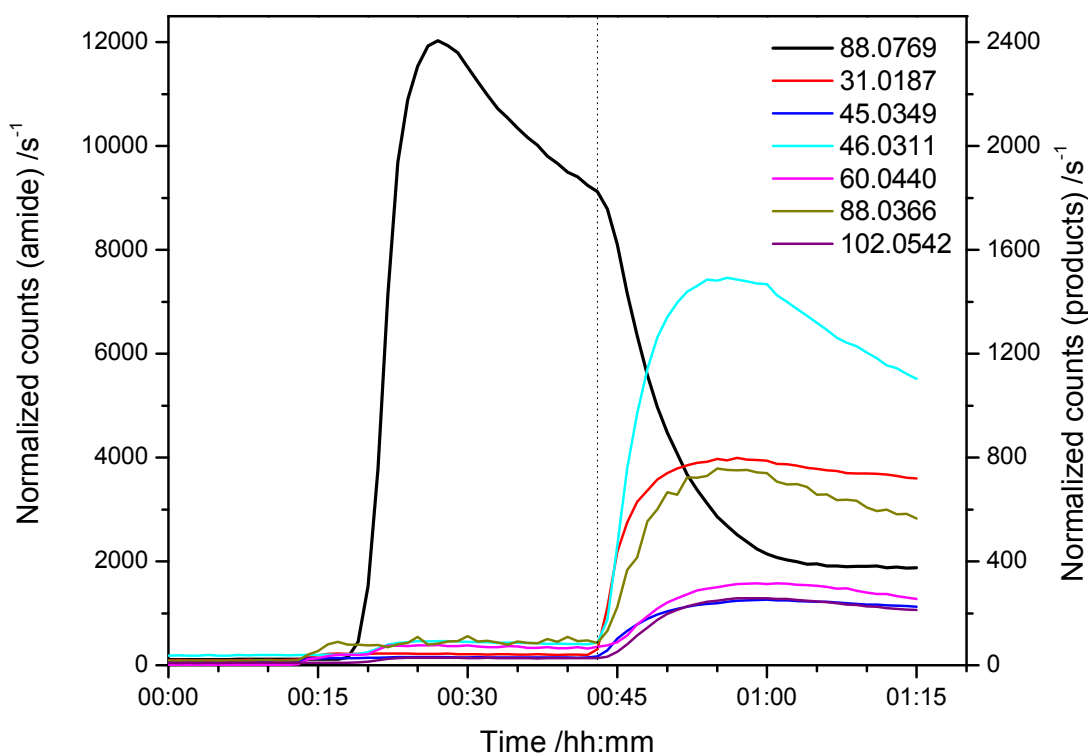
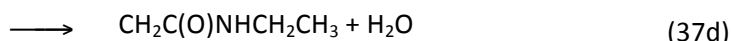
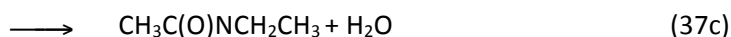
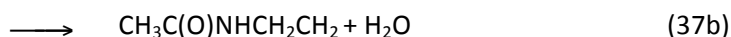
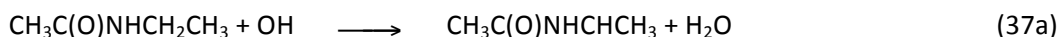
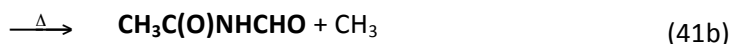
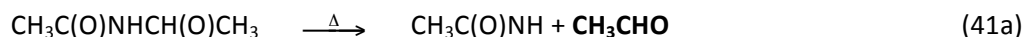
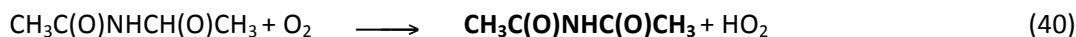
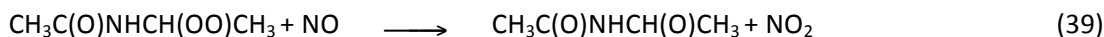
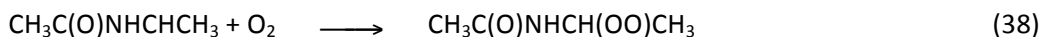


Figure 3.45. Time evolution of protonated *N*-ethyl acetamide (left y-axis, in ncps) and of ion signals generated by *N*-ethyl acetamide photo-oxidation products (right y-axis, in ncps)

OH radicals are expected to preferably attack the CH_2 site of *N*-ethylacetamide, which results in the formation of *N*-acetylacetamide and/or *N*-formylacetamide plus formaldehyde; H-abstraction from CH_3 of the ethyl group is expected to be less important. However, this hydrogen abstraction will result in *N*-(2-oxoethyl)acetamide (an isomer of *N*-acetylacetamide) and/or *N*-formylacetamide plus formaldehyde. Given that two reaction channels produce identical m/z signals, it is not possible to quantify their relative contribution.

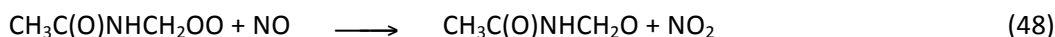
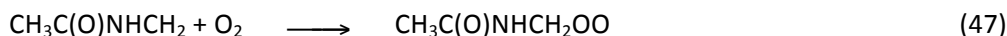
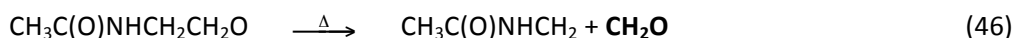
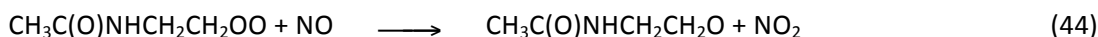
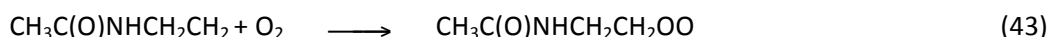


Expected products from OH attack at the N atom, reaction (37c), and the CH_3 site of the acetyl group, reaction (37d), were below 1% yield, and these routes are not considered further here.



The methyl radicals formed in reactions (41b) and (42) will then result in formaldehyde, CH_2O .

The route initiated by H-abstraction from the CH_3 in the ethyl group is expected to proceed as follows:



3.6.2 *N,N*-diethylacetamide

Table 3.9 lists the ion signals observed during the *N,N*-diethylacetamide photo-oxidation experiment. Only products with a yield > 1% (ncps/ncps) are reported. Figure 3.46 displays the time evolution of protonated *N,N*-diethylacetamide (calculated exact m/z 116.09442) and the ions reported in Table 3.9.

Table 3.9. Measured m/z of ion signals observed during the *N,N*-diethylacetamide photo-oxidation experiment. The table includes the calculated exact m/z , the assigned ion sum formula, the suggested neutral precursors and comments. Only ions with a yield > 1% (ncps/ncps) are reported.

measured m/z	calculated m/z	ion sum formula	neutral precursor	comment
31.0189	31.01784	CH_3O^+	formaldehyde	
45.0352	45.03349	$\text{C}_2\text{H}_5\text{O}^+$	acetaldehyde	
74.0653	74.06004	$\text{C}_3\text{H}_8\text{NO}^+$		fragment ion from 116.071
77.0251	77.02332	$\text{C}_2\text{H}_5\text{O}_3^+$	peroxyacetyl nitrate (PAN)	secondary product
88.0791	88.07569	$\text{C}_4\text{H}_{10}\text{NO}^+$		fragment ion from 130.0862
114.0916	114.09134	$\text{C}_6\text{H}_{12}\text{NO}^+$		
116.0711	116.07061	$\text{C}_5\text{H}_{10}\text{NO}_2^+$	<i>N</i> -ethyl- <i>N</i> -formylacetamide	
130.0862	130.08626	$\text{C}_6\text{H}_{12}\text{NO}_2^+$	<i>N</i> -acetyl- <i>N</i> -ethylacetamide <i>N</i> -ethyl- <i>N</i> -(2-oxoethyl)acetamide	isomers
193.0384	193.04552	$\text{C}_5\text{H}_9\text{N}_2\text{O}_6^+$	<i>N</i> -ethyl- <i>N</i> -[(nitroperoxy) carbonyl]acetamide	secondary product

A detailed analysis (based on different relative ion abundances observed in replicate experiments with different instrumental settings: $E/N = 88$ Td and $E/N = 52$ Td) indicates that m/z 74.060 and m/z 88.076 ions are fragment ions of the m/z 116.0711 and m/z 130.0862 ions, respectively.

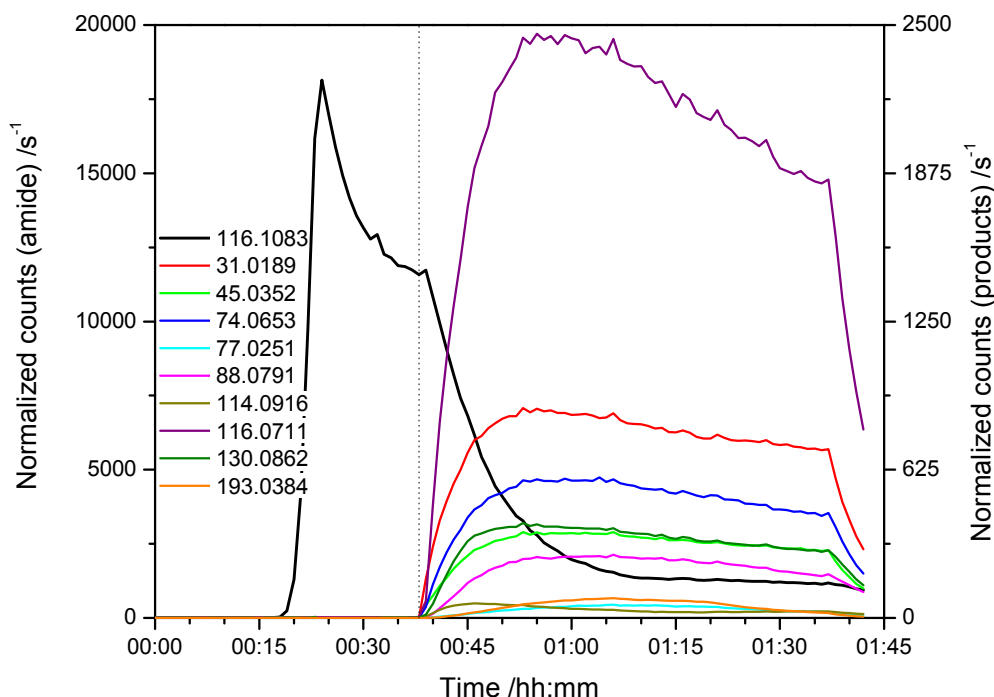
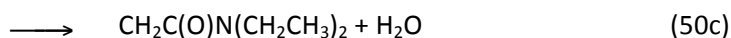
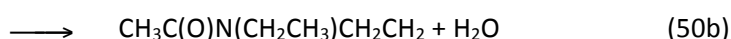
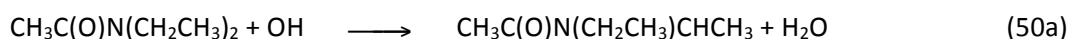
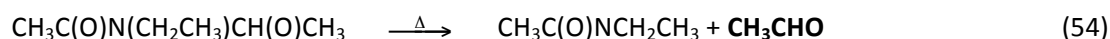
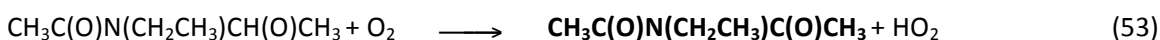
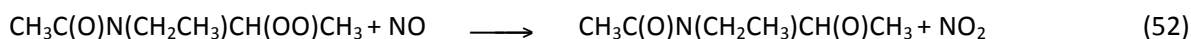
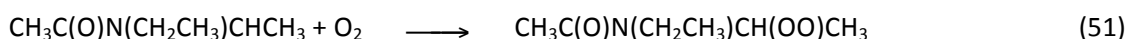


Figure 3.46. Time evolution of protonated *N,N*-diethylacetamide (left y-axis, in ncps) and of ion signals generated by *N,N*-diethylacetamide photo-oxidation products (right y-axis, logarithmic scale in ncps). At $t = 40$ min a large amount of NO was added to the chamber which resulted in a decrease of PAN-type compounds.

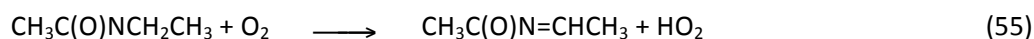
OH radicals are expected to preferably attack the CH_2 sites of *N,N*-diethylacetamide, which results in the formation of *N*-acetyl-*N*-ethylacetamide and/or *N*-ethyl-*N*-formylacetamide, plus formaldehyde. Hydrogen atom abstraction from the CH_3 sites of the ethyl groups is expected to produce *N*-ethyl-*N*-(2-oxoethyl)acetamide (an isomer of *N*-acetyl-*N*-ethylacetamide) and/or *N*-ethyl-*N*-formylacetamide plus formaldehyde. Given that two reaction channels produce identical m/z signals, it is not possible to quantify their relative contribution.



Expected products from OH attack at the CH_3 site of the acetyl group were below 1% yield. Peroxyacetyl nitrate (PAN) and *N*-ethyl-*N*-[(nitroperoxy)carbonyl]acetamide are secondary products formed in the photo-oxidation of acetaldehyde and *N*-ethyl-*N*-formylacetamide, respectively.



The *N*-ethyl acetamido radical formed in reaction x may undergo H-abstraction by O_2 giving y or dissociate to Z and ethyl radicals that will result in acetaldehyde.

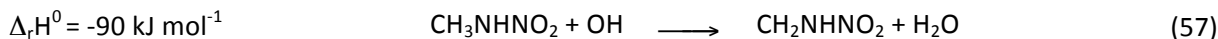


3.7 Nitramines

There are no reports in the open literature on products formed in the atmospheric photo-oxidation of nitramines. The ADA-2010 project⁶ initiated studies on product formation in the atmospheric photo-oxidation of *N*-nitro methylamine and *N*-nitro dimethylamine. These studies have been extended by additional experiments in the Oslo chamber, and new results are included here.

3.7.1 *N*-nitro methylamine

The reaction of CH_3NHNO_2 with OH radicals (and Cl atoms) may in principle proceed via hydrogen abstraction from either the $-\text{CH}_3$ group or the $>\text{NH}$ group:



Under the conditions in the Oslo chamber reaction (57) is expected to proceed via the alkyl dioxy radical and the alkoxy radical to form *N*-nitro formamide, CHONHNO_2 , or directly via hydrogen abstraction by O_2 to give *N*-nitro methanimine, $\text{CH}_2=\text{NNO}_2$, in analogy to the atmospheric reactions of the CH_2NH_2 and CH_3NH radicals.⁶ Similarly, the CH_3NNO_2 radical is expected to lead to the *N*-nitro methanimine. Both of these compounds are likely to have much shorter lifetimes than their parent precursor, which may explain why only weak bands attributable to these organics were observed in the OH photo-oxidation experiments.

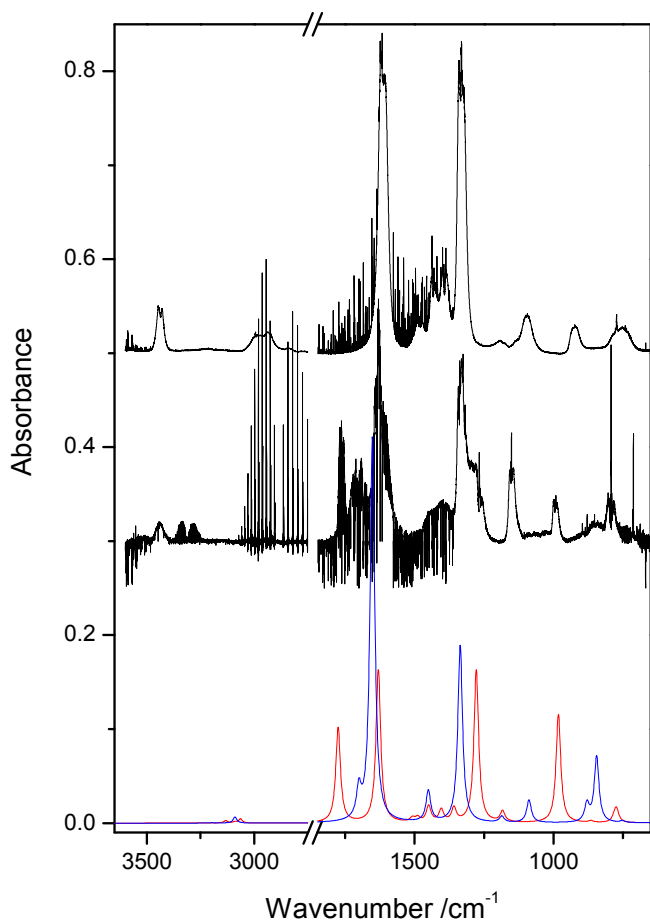


Figure 3.47. Infrared absorption spectra from Cl atom reaction with *N*-nitro methylamine. (A) Spectrum of *N*-nitro methylamine. (B) Spectrum recorded after 5 min of reaction. (C) Predicted spectra of CHONHNO_2 (red curve) and $\text{CH}_2=\text{NNO}_2$ (blue curve).

The FTIR spectra from OH initiated photo-oxidation experiments with CH_3NHNO_2 are congested and only show indications of nitro-containing products. Oxidation experiments with Cl atoms, however, revealed clear spectral features of the NHNO_2 moiety, Figure 3.47.

The N-H stretching mode is blue-shifted by 5 cm^{-1} , the two NO_2 stretching bands are shifted from 1611 and 1331 cm^{-1} in CH_3NHNO_2 to 1631 and 1286 cm^{-1} in the product, and a carbonyl-stretching band appears at 1763 cm^{-1} . These spectral features are consistent with *N*-nitro formamide, CHONHNO_2 , as a major product in the photo-oxidation of *N*-nitro methylamine. Quantum chemistry calculations on the B3LYP/aug-cc-pVTZ level support this assignment; the $-\text{NO}_2$ vibrational wavenumbers in CH_3NHNO_2 and CHONHNO_2 are predicted at $1635/1347$ and $1659/1356 \text{ cm}^{-1}$, respectively. The other possible product, $\text{CH}_2=\text{NNO}_2$, cannot be unambiguously identified from the spectra, see Figure 3.47.

3.7.2 *N*-nitro dimethylamine

The FTIR spectra from the OH initiated photo-oxidation of $(\text{CH}_3)_2\text{NNO}_2$ show bands typical of the nitro group. The reaction of $(\text{CH}_3)_2\text{NNO}_2$ with OH radicals is expected to proceed via hydrogen abstraction from the $-\text{CH}_3$ group eventually leading to *N*-nitro-*N*-methyl formamide, $\text{CHON}(\text{CH}_3)\text{NO}_2$. Photo-oxidation experiments with Cl atoms confirm the spectral features that are attributed to *N*-methyl-*N*-nitro formamide, Figure 3.48.

3.7.3 *N*-nitro ethylamine

The ethylnitramine + OH reaction is relatively slow which complicates the analysis and interpretation of the obtained product study data. With one exception, the ion signals observed are not unambiguously related to ethylnitramine photo-oxidation but rather to the oxidation of 2-propylnitrite that was used as OH precursor, Table 3.10 and Figure 3.49. It should be noted, however, that acetaldehyde and related compounds might be products of the ethylnitramine photo-oxidation.

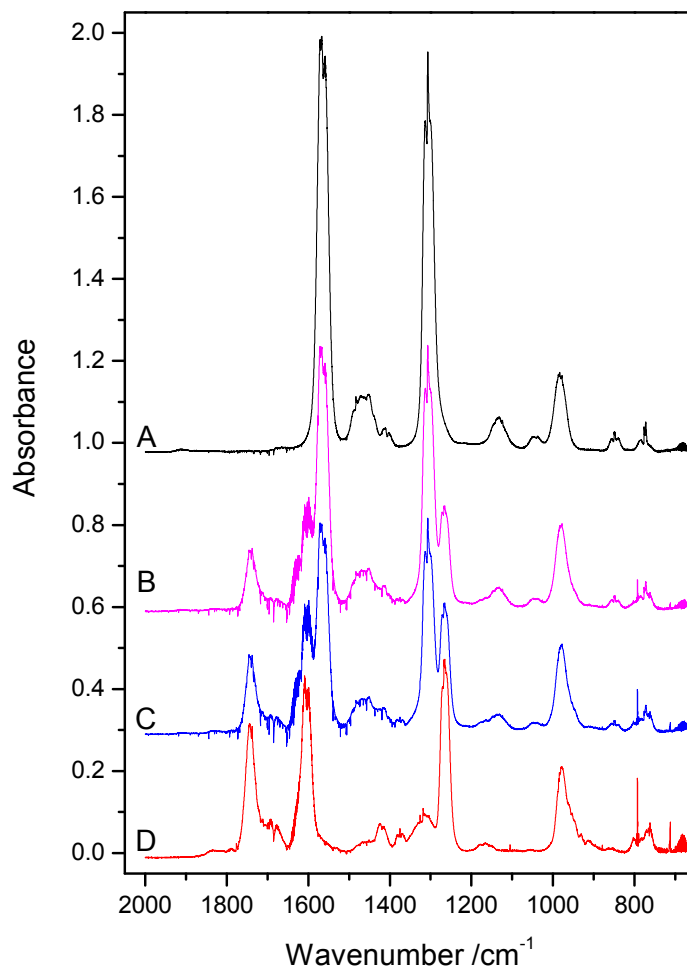


Figure 3.48. Infrared absorption spectra from Cl atom reaction with *N*-nitro dimethylamine. (A) Spectrum of *N*-nitro dimethylamine. (B)-(D) Spectra recorded after 5, 10, and 15 min of reaction.

Table 3.10. Measured m/z of ion signals observed during the ethylnitramine photo-oxidation experiment. The table includes the calculated exact m/z , the assigned ion sum formula, the suggested neutral precursors and comments. Only ions with a yield $> 1\%$ (ncps/ncps) are reported.

m/z (high E/N)	m/z (low E/N)	Artefacts ^a	Ion sum formula	Neutral precursor
31.0190	31.0185	x	CH_3O^+	formaldehyde
42.0341	42.0354		$\text{C}_2\text{H}_4\text{N}^+$	acetonitrile
	43.0194	x	$\text{C}_2\text{H}_3\text{O}^+$	acetic acid (fragment)
45.0353	45.0353	x	$\text{C}_2\text{H}_5\text{O}^+$	acetaldehyde
45.9936	45.9934	xx	NO_2^+	nitric acid
47.0148		xx	CH_3O_2^+	formic acid
59.0491	59.0499	xx	$\text{C}_3\text{H}_7\text{O}^+$	acetone
60.0546	60.0538	xx	$^{13}\text{C}_3\text{H}_7\text{O}^+$	^{13}C -acetone
61.0327	61.0320	x	$\text{C}_2\text{H}_5\text{O}_2^+$	acetic acid
	63.0444	x	$\text{C}_2\text{H}_7\text{O}_2^+$	acetaldehyde (hydrate)
	77.0267	x	$\text{C}_2\text{H}_5\text{O}_3^+$	peroxyacetyl nitrate
77.0564	77.0575	xx	$\text{C}_3\text{H}_9\text{O}_2^+$	acetone (hydrate)

^a (x), ethylnitramine/2-propyl nitrate experiments produced higher levels than experiments with only 2-propyl nitrate. (xx), ethylnitramine/2-propyl nitrate experiments produced similar levels as experiments with only 2-propyl nitrate.

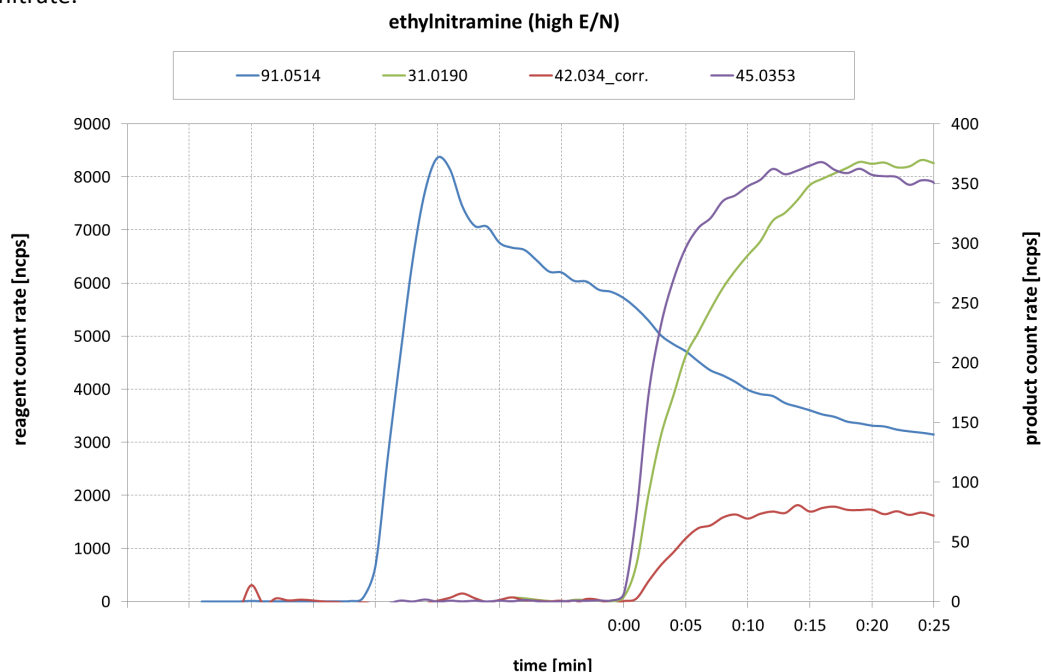
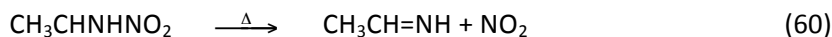
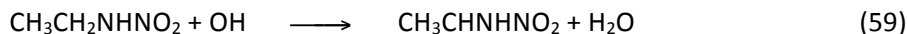


Figure 3.49. Time evolution of protonated ethylnitramine (left y-axis, in ncps) and of ion signals generated by ethylnitramine photo-oxidation products (right y-axis, in ncps).

The m/z 42.0341 (42.0354) corresponds to the ion sum formula $C_2H_4N^+$ that most likely stems from acetonitrile. This suggests a reaction mechanism in which H-abstraction from the CH_2 -group takes place followed by $RNH-NO_2$ scission:



The reactions of ethanimine are described in section 3.2 (page 36), and the main products are expected to be CH_3CN and $CH_3C(O)NH_2$. The mechanism is currently under study by quantum chemistry methods.

3.7.4 *N*-nitro diethylamine

The diethylnitramine + OH reaction is slow which complicates the analysis and interpretation of the obtained product study data. With two exceptions, the ion signals observed are not unambiguously related to diethylnitramine photo-oxidation but rather to the oxidation of 2-propylnitrite that was used as OH precursor, Table 3.11 and Figure 3.50. It should be noted, however, that acetaldehyde and related compounds might be products of the diethylnitramine photo-oxidation.

The m/z 42.0350 (42.0356) corresponds to the ion sum formula $C_2H_4N^+$ that most likely stem from acetonitrile. The m/z 72.0831 (72.0841) corresponds to the ion $C_4H_{10}N^+$, which most likely stem from *N*-ethyl ethanimine, $CH_3CH_2N=CHCH_3$. This suggests a reaction mechanism in which $RR'N-NO_2$ scission takes place. The mechanism is currently under study by quantum chemistry methods.

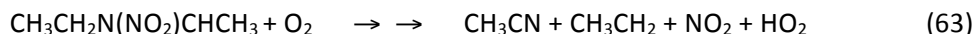
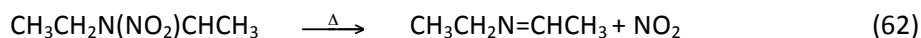
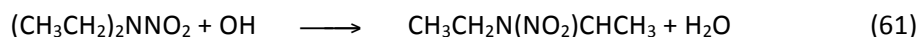


Table 3.11. Measured m/z of ion signals observed during the diethylnitramine photo-oxidation experiment. The table includes the calculated exact m/z , the assigned ion sum formula, the suggested neutral precursors and comments. Only ions with a yield > 1% (ncps/ncps) are reported.

m/z (high E/N)	m/z (low E/N)	Artefacts ^a	Ion sum formula	Neutral precursor
31.0187	31.0186	x	CH_3O^+	formaldehyde
42.0350	42.0356		$\text{C}_2\text{H}_4\text{N}^+$	acetonitrile
43.0190		xx	$\text{C}_2\text{H}_3\text{O}^+$	acetic acid (fragment)
45.0349	45.0355	x	$\text{C}_2\text{H}_5\text{O}^+$	acetaldehyde
45.9931		xx	NO_2^+	nitric acid
47.0137		xx	CH_3O_2^+	formic acid
59.0490		xx	$\text{C}_3\text{H}_7\text{O}^+$	acetone
60.0543		xx	$^{13}\text{C}_3\text{H}_7\text{O}^+$	^{13}C -acetone
61.0326		x	$\text{C}_2\text{H}_5\text{O}_2^+$	acetic acid
72.0831	72.0841		$\text{C}_4\text{H}_{10}\text{N}^+$	N-ethylethanamine
77.0559		xx	$\text{C}_3\text{H}_9\text{O}_2^+$	acetone (hydrate)

^a (x), diethylnitramine/2-propyl nitrate experiments produced higher levels than experiments with only 2-propyl nitrate. (xx), diethylnitramine/2-propyl nitrate experiments produced similar levels as experiments with only 2-propyl nitrate.

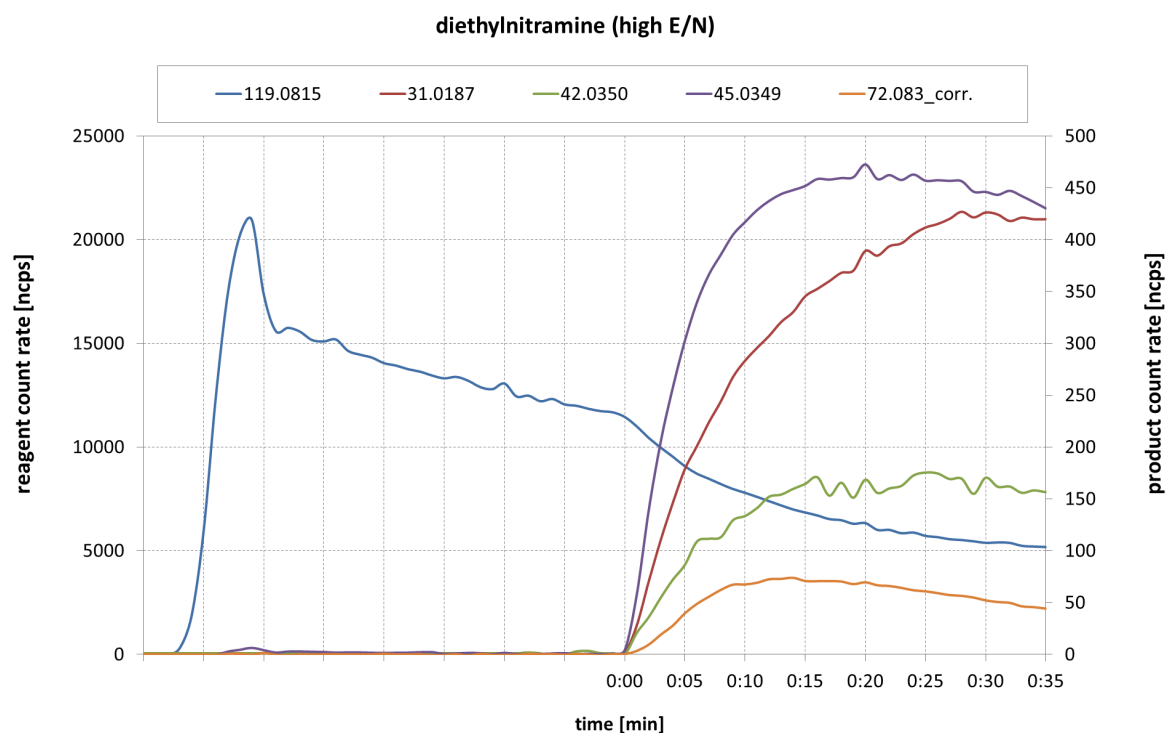


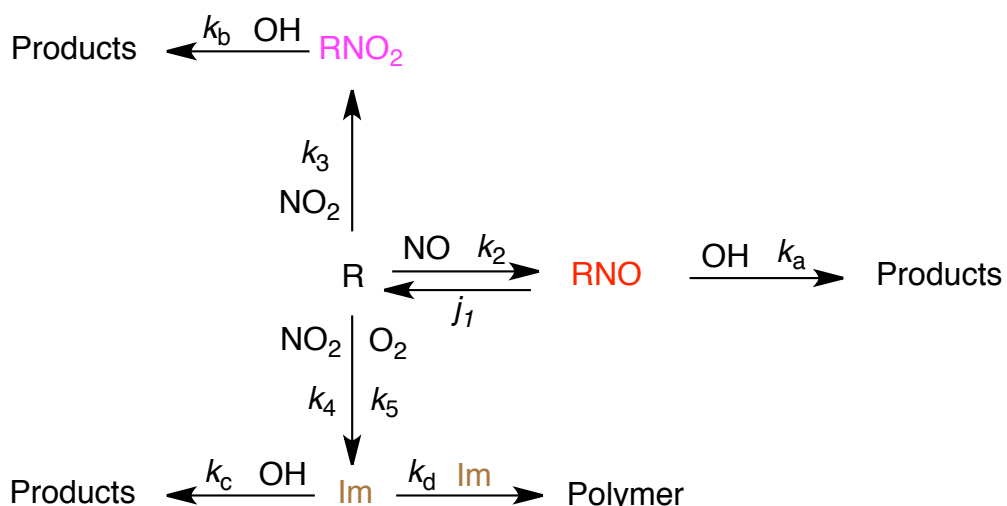
Figure 3.50. Time evolution of protonated diethylnitramine (left y-axis, in ncps) and of ion signals generated by diethylnitramine photo-oxidation products (right y-axis, in ncps).

4. Results from nitrosamine photolysis experiments

22 nitrosamine photolysis experiments with *N*-nitroso dimethylamine (NDMA, Me₂NNO), *N*-nitroso diethylamine (NDEA, Et₂NNO), *N*-nitroso morpholine (NMOR), *N*-nitroso piperazine (NPZ), *N*-nitroso piperidine (NPIP) and *N*-nitroso pyrazine (NPYR) were carried out during July 2010, and the periods March-April 2011 and May-June 2011. The experiments were generally carried out as an “extra experiment” during the late afternoons after a photo-oxidation experiment if time allowed sufficient cleaning of the chamber. In addition, a relative photolysis rate experiment with *N*-nitroso pyrrolidine, *N*-nitroso piperidine and *N*-nitroso morpholine was carried out. Four *N*-nitroso dimethylamine photolysis experiments, reported by the ADA-2010 project,⁶ were re-analysed in combination with new *N*-nitroso dimethylamine photolysis data.

The experiment protocols and monitor data from the experiments are collected as Supplementary Information in: *ADA-2011: Protocols and monitor data*. This information can be downloaded from the ADA-project web portal: <http://www.mn.uio.no/ada>

Scheme 4.1 summarises the processes occurring during nitrosamine photolysis: the nitrosamine dissociates to give a dialkylamino radical that then reacts with O₂, NO₂ or NO to give the corresponding imine, nitramine or nitrosamine. OH radicals are inevitably generated during the photolysis experiments (see section 4.2), and the reactions of these are included in the chemistry model:



Scheme 4.1. Reaction scheme for chemical processes occurring during a nitrosamine photolysis experiment.

In general, it is difficult to fit the observed imine concentration profiles employing a chemistry model in which reaction with OH radicals is the only gas phase imine removal process. High mixing ratios of imines are correlated to particle formation. An additional rate coefficient, k_d , was therefore included as variable in the fitting procedure – the intention being that the rate limiting step in an imine polymerization process could be mimicked by a second order “imine + imine” reaction. The inclusion of such a polymerization reaction improved the agreement between observed and calculated curvature of the imine time profile(s).

The rate coefficients for OH reaction with nitrosamines and nitramines were estimated from the Kwok-Atkinson SAR for OH reactions with organics,²⁹ see section 2.2.2, page 26. The rate coefficients for the OH reactions with imines were tentatively assumed to be equal to those of the corresponding alkenes.

For each nitrosamine all experimental data were analysed jointly employing an iterative, non-linear least-squares method based on a numerical model of reaction Scheme 4.1 (for description of the model see section 4.5, page 86). The experimental data sets consist of synchronized data:

- NO_x-data from monitors and FTIR (see section 4.3, page 85, and ANNEX A, page 122)
- Actinic flux data (see section 4.4 on page 86, and ANNEX B, page 130)
- PTR-TOF-MS data for the volume mixing ratios of the nitrosamines, nitramines and imines
- OH radical concentrations derived from PTR-TOF-MS data for the volume mixing ratios of cyclohexanone (see section 4.2, page 83) and FTIR data for the volume mixing ratios of cyclohexane.

The results from analyses of the experiments are collected in Table 4.1, which also includes information on the number of experiments and the number of observations included in the analyses, and the root mean square deviation of the fit, *rms*. Details on the data analyses are found in sections 4.2 through 4.11.

Table 4.1. Parameters describing nitrosamine photolysis.

	Me ₂ NNO	Et ₂ NNO	NMOR	NPZ	NPIP	NPYR
$j_{rel} = j_1/j_{NO_2}$	0.340 ± 0.010 ^a (0.53, ³² 0.25 ⁶)	0.299 ± 0.007	0.340 ± 0.008	0.34 ± 0.04	0.309 ± 0.003	0.353 ± 0.003
k_2/k_3	0.67 ± 0.09 (0.26, ³⁹ 0.75 ⁶)	0.70 ^b	0.576 ± 0.035	0.3 ^b	0.5 ^b	0.5 ^b
k_4/k_3	0.20 ± 0.03 (0.22 ± 0.06, ³⁹ 0.10 ⁶)	0.0 ^b	0.63 ± 0.4	0.3 ^b	0.049 ± 0.015	0.5 ^b
$k_5/k_3/10^{-7}$	1.70 ± 0.16 (3.90 ± 0.28, ³⁹ 3.0 ⁶)	11.20 ± 0.25	0.115 ± 0.030	1.0 ^b	0.345 ± 0.022	60 ^b
$k_a/10^{-11}$	0.25 ^b	0.35 ^b	2.32		2.56 ^b	1.55 ^b
$k_b/10^{-11}$	0.35 ^b	0.46 ^b	2.45		2.57 ^b	1.67 ^b
$k_c/10^{-11}$	0.1 ^b	2.0 ^b	11.7		5.6 ^b	6.4 ^b
$k_d/10^{-7}$	3.2 ± 0.7	58 ± 3	6.0		109 ± 14	1.0 ^b
N_{exp}/N_{Obs}	7 / 1888	7 / 3249	6 / 1822		3 / 1738	2 / 289
<i>rms</i> /ppbv	10.0	6.4	5.8		3.5	1.0

^a 3σ statistical errors from least-squares fit of data. ^b Constrained.

It can be seen from Table 4.1 that the photolysis rates of the nitrosamines studied in the ADA project all fall in the range 0.30–0.35 times that of NO₂. For Me₂NNO, Et₂NNO and NMOR the branching ratios of the NO, NO₂ and O₂ reactions with the amino radicals (k_2/k_3 , k_4/k_3 and k_5/k_3) are relatively well determined. For NPZ, NPIP and NPYR the experimental data are insufficient to determine all branching ratios. However, it can be seen that there are significant differences, which can be related to the structures of the individual compounds. This will not be discussed in further detail here.

4.1 Interpretation of photolysis results

The photolysis rate coefficient of a compound *M*, j_M , depends on the absorption cross-section, $\sigma_M(\lambda)$, the actinic flux, $F(\lambda)$, and the quantum yield to photo-dissociation, $\Phi(\lambda)$, where λ is the radiation wavelength:

$$j_M = \int \sigma_M(\lambda) \cdot F(\lambda) \cdot \Phi_M(\lambda) \cdot d\lambda \quad (I)$$

For NO₂ the quantum yield is close to 1 up to 400 nm while absorption in the long wavelength part of the absorption band is non-dissociative, $\Phi_{NO_2}^{dissociation}(\lambda > 420 \text{ nm}) = 0$. Figure 4.1 shows the recommended UV absorption cross-section of NO₂ including the quantum efficiency convoluted cross section, $\Phi(\lambda) \cdot \sigma(\lambda)$.⁶⁶ Figure 4.1 also includes parts of the UV absorption cross-section of *N*-nitroso dimethylamine (NDMA) for comparison.⁶ It can be seen that the NDMA UV-A/B absorption band essentially is overlapped by the quantum efficiency convoluted NO₂ band.

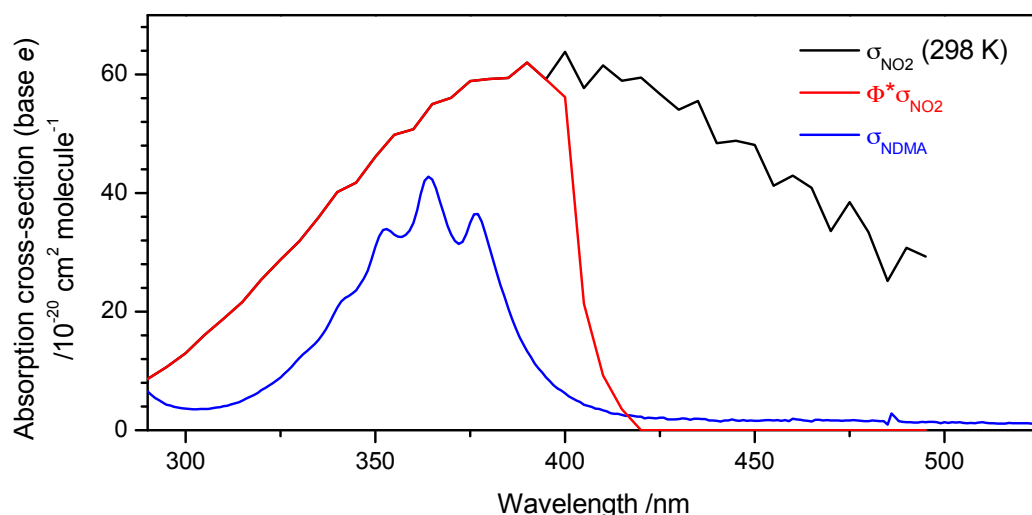


Figure 4.1. Absorption cross-sections of NO_2 and *N*-nitroso dimethylamine in the UV-A (400-315 nm) and UV-B (315-280 nm) regions of the actinic spectrum.

Assuming a unity quantum yield to photo-dissociation over the whole nitrosamine absorption band results in the relative photolysis rate coefficient, $j_{\text{NDMA}}/j_{\text{NO}_2}$, shown in Figure 4.2; the actinic flux data are taken from the ADA-2010 NDMA photolysis experiments.⁶ The relative, theoretical photolysis rate is essentially constant throughout the experiment: $j_{\text{NDMA}} : j_{\text{NO}_2} \approx 0.56$ (for a unity quantum yield to photo-dissociation of NDMA over the whole absorption band). One may therefore, to a very good approximation, scale the NDMA photolysis to that of NO_2 . This is very convenient since j_{NO_2} is one of the photolysis rates that are always needed in atmospheric chemistry modelling.

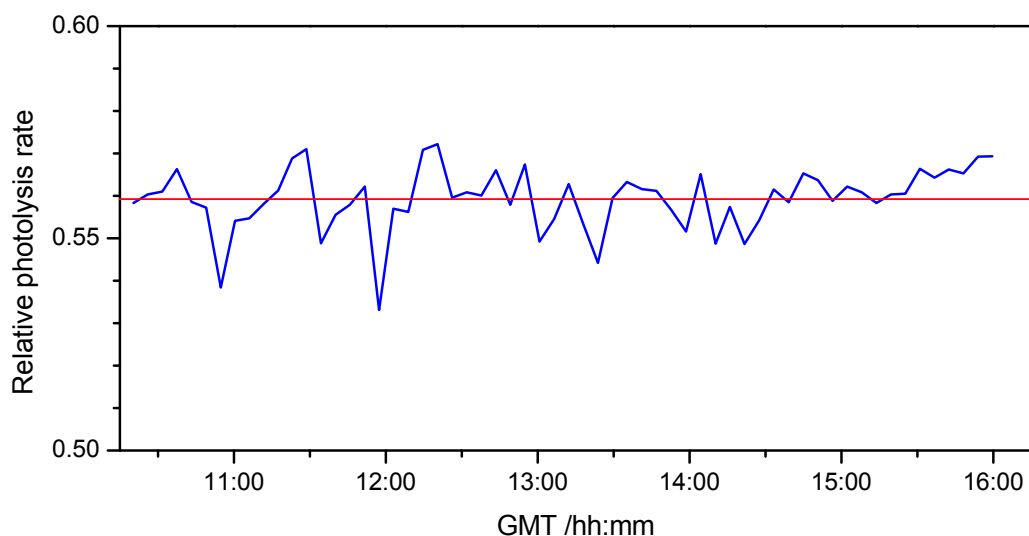


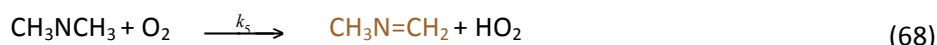
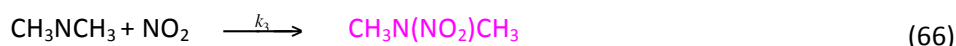
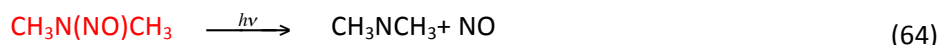
Figure 4.2. Calculated photolysis rate of *N*-nitroso dimethylamine relative to that of NO_2 assuming a quantum yield of unity to photo-dissociation of *N*-nitroso dimethylamine in the region 300-400 nm.

The absorption cross-section of NDMA is believed to be accurate within $\pm 5\%$.⁶ Since the electronic transition ($\pi^* \leftarrow n$) is located to the $>\text{N}-\text{NO}$ chromophore, the transition moment is expected to be the same for all compounds studied. With a quantum efficiency to photo-dissociation of 1 over the whole absorption band the relative photolysis rate of NDMA should in theory be 0.56 ± 0.03 , *c.f.* Figure 4.2. This is clearly not the case; all nitrosamines have j_{rel} in the range 0.30–0.35. The discrepancy could be caused by a systematic error in measuring the actinic flux. Hence, extra care was taken to ensure correct and accurate actinic flux measurements. This is documented in ANNEX B, and the j_{NO_2} values derived are believed to be accurate within $\pm 10\%$. Since the ratio $j_{\text{rel}}(\text{Observed})$ to

j_{rel} (Theoretical) is in the region 0.53 to 0.63 it is to be concluded that the effective quantum yield to nitrosamine photo-dissociation is not unity as was reported for NDMA photolysis under low pressure conditions at 363.5 nm by Geiger *et al.*^{67,68}

4.2 Retrieval of OH radical concentration during photolysis of nitrosamines

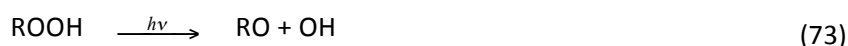
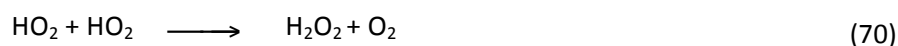
In addition to the amino radical reactions with O₂, NO and NO₂, the nitrosamine, nitramine and imine will react with OH radicals that are invariably formed in the reactions following nitrosamine photolysis. Taking dimethylamine as example:



HONO, formed in reaction (4), readily undergoes photolysis under the same actinic radiation conditions as the nitrosamines do:



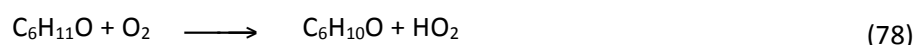
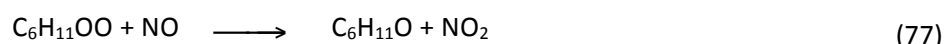
HO₂ radicals, formed in reaction (5), may react with other dioxy radicals and form hydrogen peroxide and/or peroxy alcohols, which will slowly undergo photolysis under the experimental conditions of the present experiments:



HO₂ radicals may also react with NO and form OH radicals directly:



It is difficult to monitor OH radicals directly. The OH radical can, however, be monitored indirectly by adding a tracer that reacts with OH radicals with a well-known rate coefficient. Cyclohexane is commonly used as OH quencher, the major route being:



At first sight, the OH reaction with cyclohexane will just regenerate OH radicals via another HO₂ radical, see above. However, the formation of dioxy compounds and nitric acid in reaction (17) will quench the OH re-cycling fast.



Cyclohexanone, formed in reaction (78), may also react with OH radicals; the rate coefficients for OH reaction with cyclohexane and cyclohexanone are, in units of $10^{-12} \text{ cm}^3 \text{ molecule}^{-1} \text{ s}^{-1}$, respectively 6.97^{69} and 6.39^{70} at 298 K.

The cyclohexane concentration is quantified by FTIR, and the OH radical concentration can then be determined from an analysis of the cyclohexanone formation rate; the differential rate law for cyclohexanone production is:

$$\frac{d[\text{C}_6\text{H}_{10}\text{O}]}{dt} = k_{\text{OH}+\text{C}_6\text{H}_{12}} \cdot [\text{C}_6\text{H}_{12}] \cdot [\text{OH}] - k_{\text{OH}+\text{C}_6\text{H}_{10}\text{O}} \cdot [\text{C}_6\text{H}_{10}\text{O}] \cdot [\text{OH}]$$

which can be solved numerically to give the OH concentration:

$$[\text{OH}]_{i+1} = \frac{\Delta[\text{C}_6\text{H}_{10}\text{O}]_i}{\Delta t \cdot \left(k_{\text{OH}+\text{C}_6\text{H}_{12}} \cdot [\text{C}_6\text{H}_{12}]_i - k_{\text{OH}+\text{C}_6\text{H}_{10}\text{O}} \cdot [\text{C}_6\text{H}_{10}\text{O}]_i \right)}$$

Since the cyclohexanone yield in the OH reaction with cyclohexane is not unity but only 0.321 ± 0.035 ,⁷¹ the OH concentration calculated in the above expression should be multiplied by 3. Figure 4.3 shows the cyclohexanone concentration as retrieved by PTR-TOF-MS during the diethyl-nitrosamine photolysis experiment on March 29, 2011. The cyclohexane mixing ratio in this experiment was around 2 ppmV as retrieved by FTIR spectroscopy (not shown). Figure 4.4 shows the derived OH radical concentration as a function of time in the experiment.

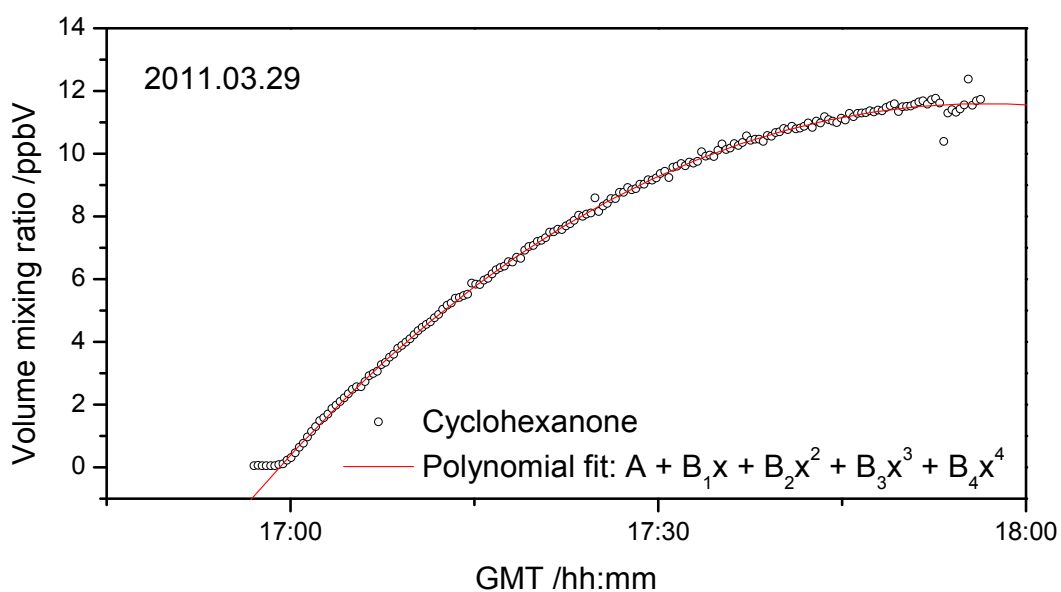


Figure 4.3. Example of polynomial fitting of cyclohexanone volume mixing data obtained during the *N*-nitroso diethylamine photolysis experiment on 2011.03.29.

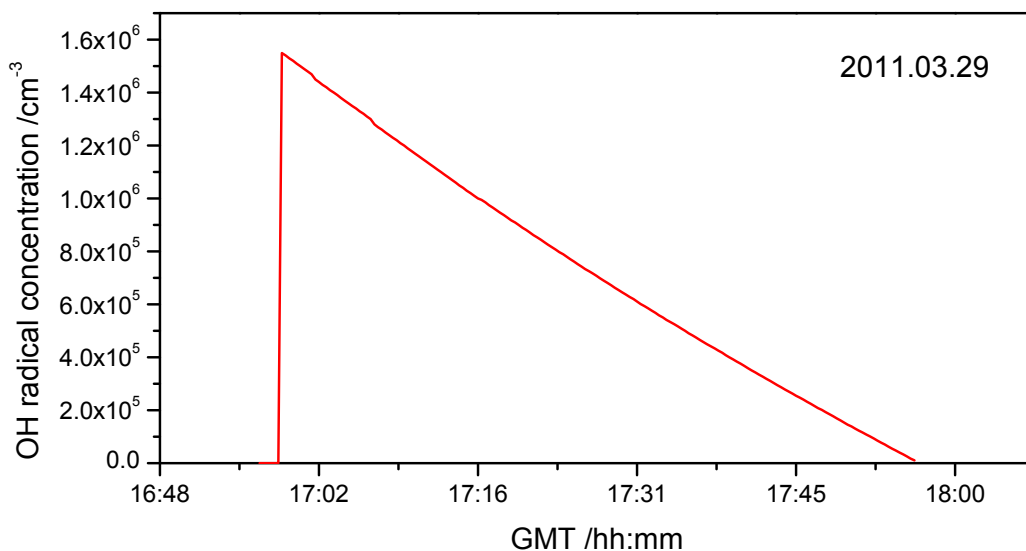


Figure 4.4. Example of the OH radical concentration during the *N*-nitroso diethylamine photolysis experiment on March 29, 2011.

4.3 Retrieval of NO_x from FTIR spectra

High-resolution, long-path Fourier-Transform infrared spectroscopy (FTIR) is a very powerful tool to determine trace gas concentrations. There are two basic problems: time-resolution and interference. Interference problems are not limited to FTIR; nitrosamines give rise to severe interference problems in most NO_x-monitors based on photolytic or catalytic NO₂-to-NO conversion due to conversion of the nitrosamine to NO (see also ANNEX A “Monitor calibration and data analysis”). In contrast, the interference problem in high-resolution infrared spectra is not severe for small molecules like NO and NO₂.

Figure 4.5 and Figure 4.6 illustrate how volume mixing ratios of NO and NO₂ were derived from the analyses of the 1898.5 – 1914.0 and 1590.0 – 1614.0 cm⁻¹ regions, respectively, of the infrared spectra (optical path-length 553.5 m, pressure 1 atm, spectral resolution 0.25 cm⁻¹, 10 min time resolution). The estimated accuracy of the retrieval method is, depending upon the water content, around ±5% (detection limit ca. 5 ppbV) for NO and NO₂.

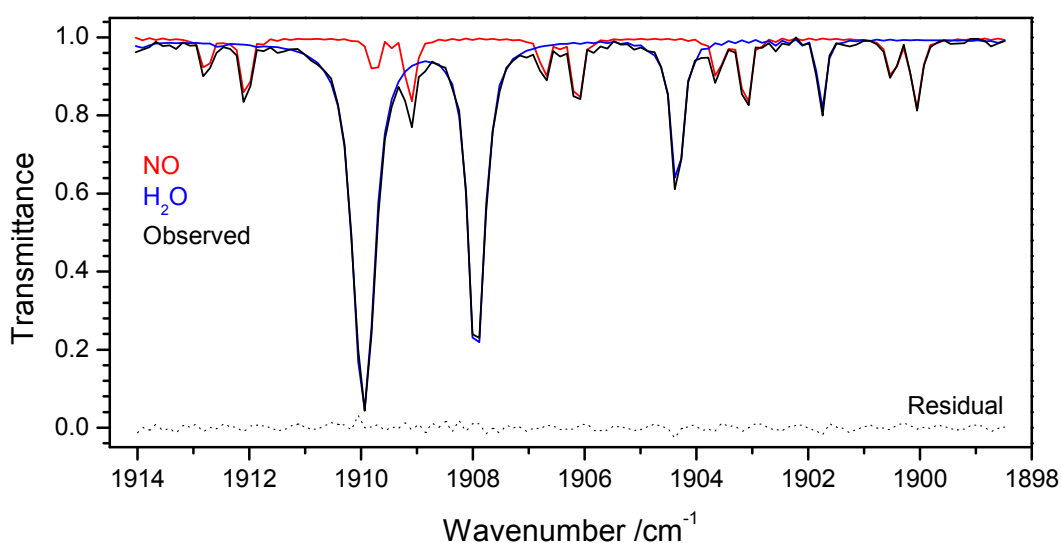


Figure 4.5. Example of NO volume mixing ratio retrieval from an infrared spectrum obtained during the *N*-nitroso diethylamine photolysis experiment on 2011.03.29. NO = 365 ± 13 ppbV.

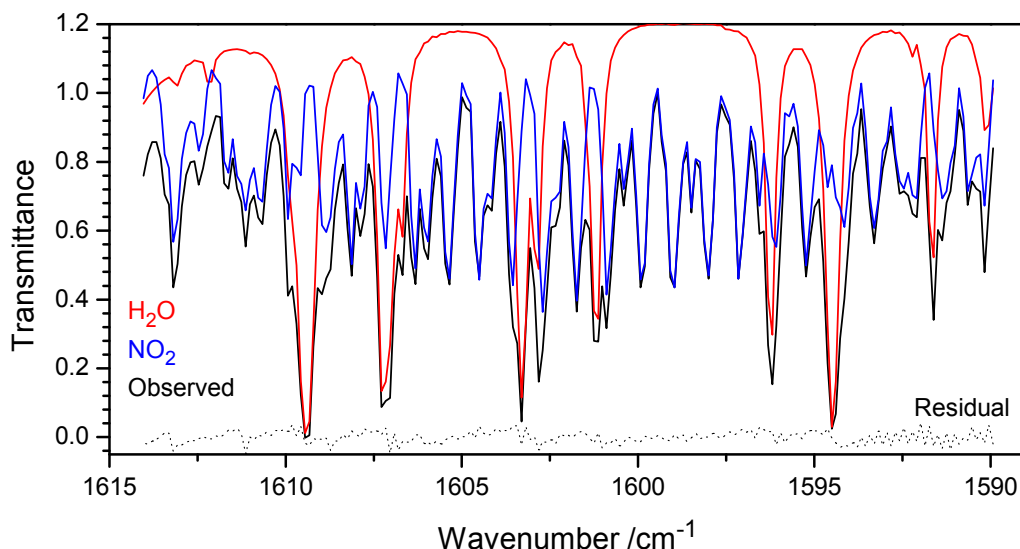


Figure 4.6. Example of NO_2 volume mixing ratio retrieval from an infrared spectrum obtained during the *N*-nitroso diethylamine photolysis experiment on 2011.03.29. $\text{NO}_2 = 305 \pm 13$ ppbV.

4.4 Actinic flux data – j_{NO_2}

Three instruments measured the actinic flux simultaneously: a filter radiometer, a Bentham spectrometer and a vendor calibrated JAZ spectrometer. The filter radiometer data are included in the Supporting Information *ADA-2011: Protocols and monitor data*. An inter-comparison between the instruments has been performed j_{NO_2} Filter Radiometer data have been corrected accordingly. The NO_2 -photolysis frequency calibration is documented in ANNEX B, page 130.

4.5 Numerical model of the EUPHORE photolysis experiments

In the nitrosamine photolysis experiments the nitrosamine is added to the chamber along with NO , NO_2 (and cyclohexane as OH scavenger). At time $t = 0$ the chamber canopy is opened and the photolysis starts.

In addition to the photolysis and subsequent chemical reactions, there is also a first order loss of all compounds due to air replenishment compensating for air drawn from the chamber by instruments and other sampling. This loss is characterized by rate constant, k_{loss} , that is determined by monitoring an inert tracer, SF_6 , by FTIR. Assuming that no additional reactions are taking place, the time evolution of the nitrosamine, nitramine and imine is described by the following set of differential rate equations:

$$\begin{aligned} \frac{d[\text{RNO}]}{dt} &= -j_1 \cdot [\text{RNO}] + k_2 \cdot [\text{R}] \cdot [\text{NO}] - k_{\text{loss}} \cdot [\text{RNO}] - k_a \cdot [\text{RNO}] \cdot [\text{OH}] \\ &= -\phi \cdot j_{\text{NO}_2} \cdot [\text{RNO}] + k_2 \cdot [\text{R}] \cdot [\text{NO}] - k_{\text{loss}} \cdot [\text{RNO}] - k_a \cdot [\text{RNO}] \cdot [\text{OH}] \end{aligned}$$

$$\frac{d[\text{RNO}_2]}{dt} = k_3 \cdot [\text{R}] \cdot [\text{NO}_2] - k_{\text{loss}} \cdot [\text{RNO}_2] - k_b \cdot [\text{RNO}_2] \cdot [\text{OH}]$$

$$\frac{d[\text{IM}]}{dt} = k_4 \cdot [\text{R}] \cdot [\text{NO}_2] + k_5 \cdot [\text{R}] \cdot [\text{O}_2] - k_{\text{loss}} \cdot [\text{IM}] - k_c \cdot [\text{IM}] \cdot [\text{OH}]$$

in which the relative photolysis rate, $j_{\text{rel}} = j_1/j_{\text{NO}_2}$, has been introduced.

The amino radical, R, has a very short lifetime and its concentration will be very small at all times. The contribution from k_{loss} ($\approx 10^{-5} \text{ s}^{-1}$) to the amino radical concentration is orders of magnitude smaller than the other amino radical loss terms. Employing the steady-state approximation gives:

$$\frac{d[\text{R}]}{dt} = \phi \cdot j_{\text{NO}_2} \cdot [\text{RNO}] - k_2 \cdot [\text{R}] \cdot [\text{NO}] - k_3 \cdot [\text{R}] \cdot [\text{NO}_2] - k_4 \cdot [\text{R}] \cdot [\text{NO}_2] - k_5 \cdot [\text{R}] \cdot [\text{O}_2] \approx 0$$

From which one derives the steady-state value:

$$[\text{R}]_{\text{ss}} = \frac{\phi \cdot j_{\text{NO}_2} \cdot [\text{RNO}]}{k_2 \cdot [\text{NO}] + (k_3 + k_4) \cdot [\text{NO}_2] + k_5 \cdot [\text{O}_2]}$$

The differential rate equations can be solved numerically. At time $t = 0$ we have: $[\text{RNO}] = [\text{RNO}]_0$, and ideally $[\text{RNO}_2]_0 = [\text{IM}]_0 = 0$. At time t_{i+1} we then have:

$$[\text{RNO}]_{i+1} = [\text{RNO}]_i \cdot \left(1 - k_{\text{loss}} \cdot \Delta_i - k_a \cdot [\text{OH}]_i\right) - \left(\phi \cdot j_{\text{NO}_2,i} \cdot [\text{RNO}]_i - k_2 \cdot [\text{R}]_i \cdot [\text{NO}]_i\right) \cdot \Delta_i$$

$$[\text{RNO}_2]_{i+1} = [\text{RNO}_2]_i \cdot \left(1 - k_{\text{loss}} \cdot \Delta_i - k_b \cdot [\text{OH}]_i\right) + k_3 \cdot [\text{R}]_i \cdot [\text{NO}_2]_i \cdot \Delta_i$$

$$[\text{IM}]_{i+1} = [\text{IM}]_i \cdot \left(1 - k_{\text{loss}} \cdot \Delta_i - k_c \cdot [\text{OH}]_i\right) + \left(k_4 \cdot [\text{NO}_2]_i + k_5 \cdot [\text{O}_2]_i\right) \cdot [\text{R}]_i \cdot \Delta_i$$

$$[\text{R}]_{i+1} = \frac{\phi \cdot j_{\text{NO}_2,i} \cdot [\text{RNO}]_i}{k_2 \cdot [\text{NO}]_i + (k_3 + k_4) \cdot [\text{NO}_2]_i + k_5 \cdot [\text{O}_2]_i} = \frac{\phi \cdot j_{\text{NO}_2,i} \cdot [\text{RNO}]_i}{Q_i}$$

in which we have introduced $Q_i = k_2 \cdot [\text{NO}]_i + (k_3 + k_4) \cdot [\text{NO}_2]_i + k_5 \cdot [\text{O}_2]_i$ and $\Delta_i = t_{i+1} - t_i$. Substituting $[\text{R}]$ with the steady-state expression results in:

$$[\text{RNO}]_{i+1} = [\text{RNO}]_i \cdot \left(1 - k_{\text{loss}} \cdot \Delta_i - k_a \cdot [\text{OH}]_i\right) - \phi \cdot j_{\text{NO}_2,i} \cdot [\text{RNO}]_i \cdot \left(1 - [\text{NO}]_i \cdot \frac{k_2}{Q_i}\right) \cdot \Delta_i$$

$$[\text{RNO}_2]_{i+1} = [\text{RNO}_2]_i \cdot \left(1 - k_{\text{loss}} \cdot \Delta_i - k_b \cdot [\text{OH}]_i\right) + \phi \cdot j_{\text{NO}_2,i} \cdot [\text{RNO}]_i \cdot [\text{NO}_2]_i \cdot \Delta_i \cdot \frac{k_3}{Q_i}$$

$$[\text{IM}]_{i+1} = [\text{IM}]_i \cdot \left(1 - k_{\text{loss}} \cdot \Delta_i - k_c \cdot [\text{OH}]_i\right) + \phi \cdot j_{\text{NO}_2,i} \cdot [\text{RNO}]_i \cdot \Delta_i \cdot \left([\text{NO}_2]_i \cdot \frac{k_4}{Q_i} + [\text{O}_2]_i \cdot \frac{k_5}{Q_i}\right)$$

The parameters j_{rel} , k_2 , k_3 , k_4 , k_5 , k_a , k_b and k_c may then be extracted from a non-linear least squares procedure by fitting the observed data. However, k_2 - k_5 are correlated – they always appear with Q_i as denominator, and Q_i is a linear combination of k_2 - k_5 . It is therefore only possible to determine ratios of the rate coefficients from the photolysis experiments, *i.e.* k_2/k_3 , k_4/k_3 and k_5/k_3 . This is not a “real” problem since the important matter is the branching of the amino radical reactions with NO, NO₂ and O₂, and the branching is determined by the same ratios.

4.6 N-Nitroso dimethylamine gas phase photolysis

Previous studies. *N*-nitroso dimethylamine (NDMA) is the only nitrosamine for which literature data on the gas phase photolysis kinetics is available. The gas phase photolysis of *N*-nitroso dimethylamine (NDMA) was studied by Bamford,⁷² Lindley *et al.*,³⁹ Geiger *et al.*,⁶⁷ Geiger and Huber,⁶⁸ Tuazon *et al.*³² and by ADA-2010.⁶ Tuazon *et al.*³² employed black-lamps as irradiation source and determined the photolysis rate of NDMA relative to that of NO₂ to be $j_{\text{NDMA}}/j_{\text{NO}_2} = 0.53 \pm 0.03$ while ADA-2010 experiments using natural sunlight indicated a lower relative rate of $j_{\text{NDMA}}/j_{\text{NO}_2} = 0.26 \pm 0.03$.⁶ Geiger *et al.*^{67,68} report a quantum yield to photo-dissociation of NDMA following $S_1(n\pi^*) \leftarrow S_0$ excitation at 363.5 nm to be 1.03 ± 0.10 .

The NDMA photolysis experiments by Tuazon *et al.*³² were carried out in the presence of excess O₃ (~4 ppm NDMA and ~12 ppm O₃). They found 33% CH₃NO₂, 38% HCHO and 2% CO in addition to 65% (CH₃)₂NNO₂ and accounted for ~100% of the carbon and ~95% of the nitrogen. Lindley *et al.*³⁹ studied the gas phase reactions of the (CH₃)₂N radical following photolysis of NDMA with O₂, NO and NO₂, and reported relative rates (2σ statistical errors) $k_5/k_2 = (1.48 \pm 0.07) \times 10^{-6}$, $k_5/k_3 = (3.90 \pm 0.28) \times 10^{-7}$ and $k_4/k_3 = 0.22 \pm 0.06$. Normalizing to k_3 , the branching ratios in the amino radical reactions with O₂, NO and NO₂ (Scheme 4.1) are therefore $k_2/k_3 = 0.264 \pm 0.023$, $k_5/k_3 = (3.90 \pm 0.28) \times 10^{-7}$ and $k_4/k_3 = 0.22 \pm 0.06$. The ADA-2011 results for the branching ratios were 0.75, 3.0×10^{-7} and 0.10, with estimated ±15% uncertainties.⁶

Lazarou *et al.*⁷³ studied the reactions of the (CH₃)₂N radical with NO and NO₂ by the Very Low Pressure Reactor (VLPR) technique and reported absolute rates of reactions $k_2 = (8.53 \pm 1.42) \times 10^{-14}$ and $k_3 + k_4 = (9.08 \pm 1.36) \times 10^{-13} \text{ cm}^3 \text{ molecule}^{-1} \text{ s}^{-1}$ at 300 K.

Present studies. Seven *N*-nitroso dimethylamine (NDMA) photolysis experiments have been analysed; four experiment data sets stem from the ADA-2010 project,⁶ and three new data sets were obtained during the ADA-2011 campaigns. The experimental protocols and monitor data are included in the Supporting Information: ADA-2011: *Protocols and monitor data*.

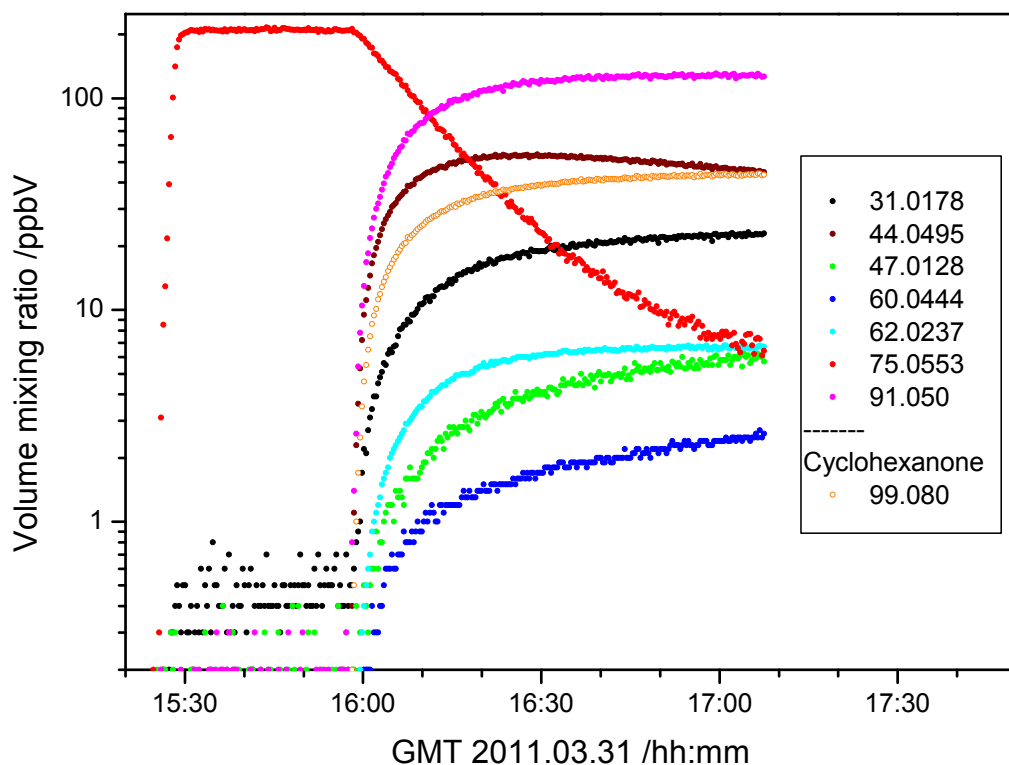
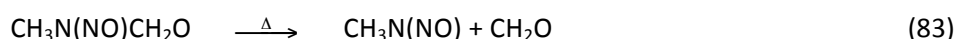
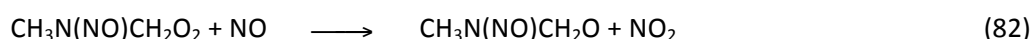
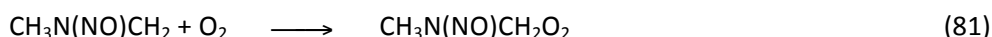
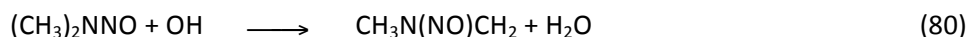


Figure 4.7. Volume mixing ratios of the major chemical components (MH⁺ ions) during the *N*-nitroso dimethylamine photolysis experiment on 2011.05.26.

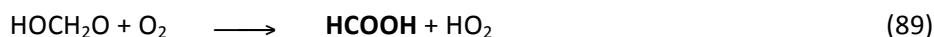
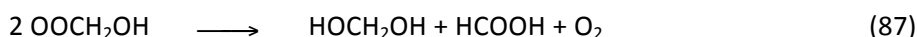
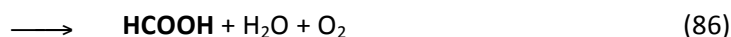
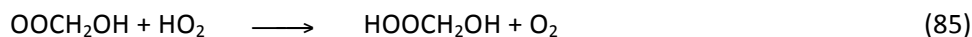
The observed ion signals above 1% of the *N*-nitroso dimethylamine signal loss in the seven experiments are collected in Table 4.2 (fragment ions, ¹³C-containing ions, instrument-intrinsic ions, and ions arising from side reactions were omitted from this list). Figure 4.7 shows the time evolution of the major ion signals in the 2011.03.31 experiment.

The two ion signals (*m/z* 31.0178 and 47.0128, parent molecules: CH₂O and HCOOH) show time evolutions similar to that of *N*-nitro dimethylamine, *m/z* 91.0492. Both formaldehyde and formic acid are “normal”, well known chamber artefacts. However, in the present experiments the signals are larger than normal chamber artefacts. Formaldehyde may, in part, originate from the OH radical reaction with NDMA:

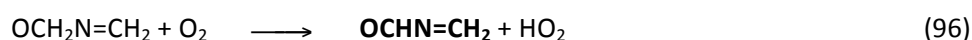
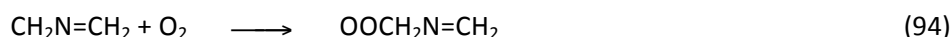
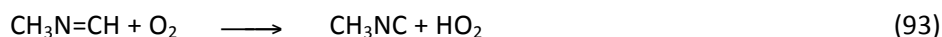
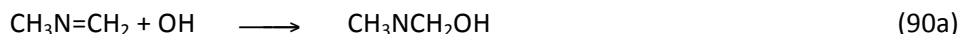


and analogous OH radical reactions with *N*-nitro dimethylamine. Formaldehyde may also stem from OH radical reaction with the primary product *N*-methyl methanimine, see eq. (68).

HO₂ radicals are always formed in photo-oxidation reactions, and formic acid is formed in the gas-phase reaction between formaldehyde and HO₂ radicals. The first step is a reversible reaction with HO₂ radicals to form a formaldehyde adduct:⁷⁴⁻⁸⁰



The two small signals at *m/z* 60.0449 and 62.0237, corresponding to ion sum formulas C₂H₆NO⁺ and C₂H₅O₂⁺, respectively, had a slightly different time profile, and are most likely products from OH radical reactions with the very reactive *N*-methyl methanimine. The ion signal *m/z* 58.0290, observed in amounts larger than 1% of the *N*-nitroso dimethylamine signal loss in only one experiment, is tentatively attributed to a product of the OH radical reaction with *N*-methyl methanimine, CH₂=NCHO:



Nitromethane, CH₃NO₂, is a minor product in every NDMA photolysis experiment; the yield being in the range (1-2%). Tuazon *et al.*³² reported a very different product distribution in their NDMA

photolysis experiment with 33% CH₃NO₂. As the major difference between the present and photolysis experiments and that of Tuazon *et al.* is the amount of ozone being present, it is suggested that nitromethane originates from a reaction between the (CH₃)₂N radical and ozone. A study of O₃ gas phase reactions with amines shows that the amount of nitromethane formed from (CH₃)₃N increases with O₃ concentration,⁵¹ indicating a mechanism involving the nitroxide radical, (CH₃)₂NO. Dialkyl nitroxides are known to react with O₃ in solution to yield nitroalkanes,⁸¹ and one may expect that a similar oxidation can take place in the gas phase:

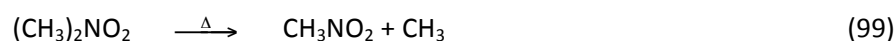
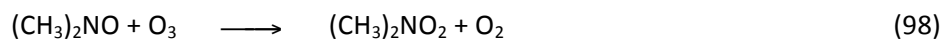
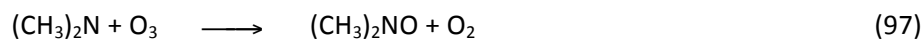


Table 4.2. Ions observed in *N*-nitroso dimethylamine photolysis experiments.

2010.03.23	2010.07.01	2010.07.02 am	2010.07.02 pm	2011.03.30	2011.03.31	2010.04.06	Ion sum formula	Ion precursor	Comments
31.0179	31.0182	31.0186	31.0184	31.0178	31.0178	31.0178	CH ₃ O ⁺	CH ₂ O	
44.0496	44.0497	44.0502	44.0499	44.0495	44.0495	44.0495	C ₂ H ₆ N ⁺	CH ₃ N=CH ₂	
	46.0292						C ₂ H ₈ N ⁺	(CH ₃) ₂ NH	
		47.0143	47.0143	47.0128	47.0128	47.0128	CH ₃ O ₂ ⁺	HCOOH	From CH ₂ O
	58.0290						C ₂ H ₄ NO ⁺	CH ₂ =NCHO?	From CH ₃ N=CH ₂
	60.0449			60.0444	60.0444	60.0444	C ₂ H ₆ NO ⁺	CH ₃ NHCHO	From CH ₃ N=CH ₂
62.0239	62.0240	62.0244	62.0241	62.0237	62.0237	62.0237	C ₂ H ₅ O ₂ ⁺	CH ₃ NO ₂	
75.054	75.0522	75.0538	75.0537	75.0553	75.0533	75.0533	C ₂ H ₅ N ₂ O ₂ ⁺	(CH ₃) ₂ NNO	
91.0492	91.0500	91.0495	91.048	91.050	91.050	91.050	C ₂ H ₇ N ₂ O ₂ ⁺	(CH ₃) ₂ NNO ₂	

The relative photolysis rate (j_{rel}) and relative rate coefficients (k_2/k_3 , k_4/k_3 and k_5/k_3) derived from a least squares analysis of the photolysis data from the seven experiments are included in Table 4.1 (page 81). The rate coefficients for OH reaction with *N*-nitroso dimethylamine and *N*-nitro dimethylamine were constrained to their experimental values in the analysis (2.5×10^{-12} and 3.5×10^{-12} cm³ molecule⁻¹ s⁻¹, respectively). The rate coefficient for OH reaction with the imine, CH₃N=CH₂, was, as mentioned above, at first assumed to be equal to that of propene, 2.9×10^{-11} cm³ molecule⁻¹ s⁻¹.³¹ Attempts to refine k_c led to a negative rate coefficient, and k_c was subsequently constrained to 0.1×10^{-11} cm³ molecule⁻¹ s⁻¹.

The initial data analyses showed that the nitrosamine and nitramine time profiles could be reasonably reproduced, but that the imine data showed systematic deviations that could not be accounted for by OH radical reaction alone. An additional parameter describing imine loss, k_d , was therefore included in the fitting procedure – the intention being that the rate limiting step in an imine polymerization process could be mimicked by a second order “imine + imine” reaction. The inclusion of this polymerization reaction reduced the *rms* considerably and improved the agreement between observed and calculated curvature of the imine time profile(s), Figure 4.8. It can be seen that data from 2010 were less well reproduced. This is linked to problems with the determination of NO₂ in these experiments and will be dealt with at a later time.

Table 4.3 summarizes the amounts of nitrosamine, nitramine and imine that were removed from the gas phase either by reaction with OH radicals or by “polymerization”. It can be seen that only a few

per cent of the initial *N*-nitroso dimethylamine was removed by reaction with OH radicals during the photolysis process.

Table 4.3. Initial volume mixing ratio of *N*-nitroso dimethylamine and the loss of *N*-nitroso dimethylamine, *N*-nitro dimethylamine and *N*-methyl methanimine (/ppbV) due to reaction with OH radicals and polymerization in the *N*-nitroso dimethylamine photolysis experiments.

Experiment	Initial	Nitrosamine	Nitramine	Imine	Imine polymerization
20100323.34221	242.0	3.0	1.0	0.3	32.3
20100701.61191	117.5	0.8	0.1	0.0	5.7
20100702.39042	236.5	3.0	1.3	0.2	13.5
20100702.62494	312.5	2.8	2.5	0.3	10.2
20110330.60614	217.5	0.7	0.1	0.0	0.0
20110331.57009	211.0	5.1	4.3	0.6	3.9
20110406.56426	261.5	6.2	4.5	1.6	13.9

The derived parameters are, to some degree, correlated, Table 4.4. The largest correlation coefficient, -0.87, is between k_4/k_3 and k_5/k_3 . In general, the parameters are well determined.

Table 4.4. Correlation matrix for the parameters derived from analysis of the *N*-nitroso dimethylamine photolysis data.

	j_{rel}	k_2/k_3	k_4/k_3	k_5/k_3	k_d
j_{rel}	1.000				
k_2/k_3	0.652	1.000			
k_4/k_3	0.110	0.018	1.000		
k_5/k_3	-0.111	-0.018	-0.870	1.000	
k_d	0.105	0.059	-0.068	0.301	1.000

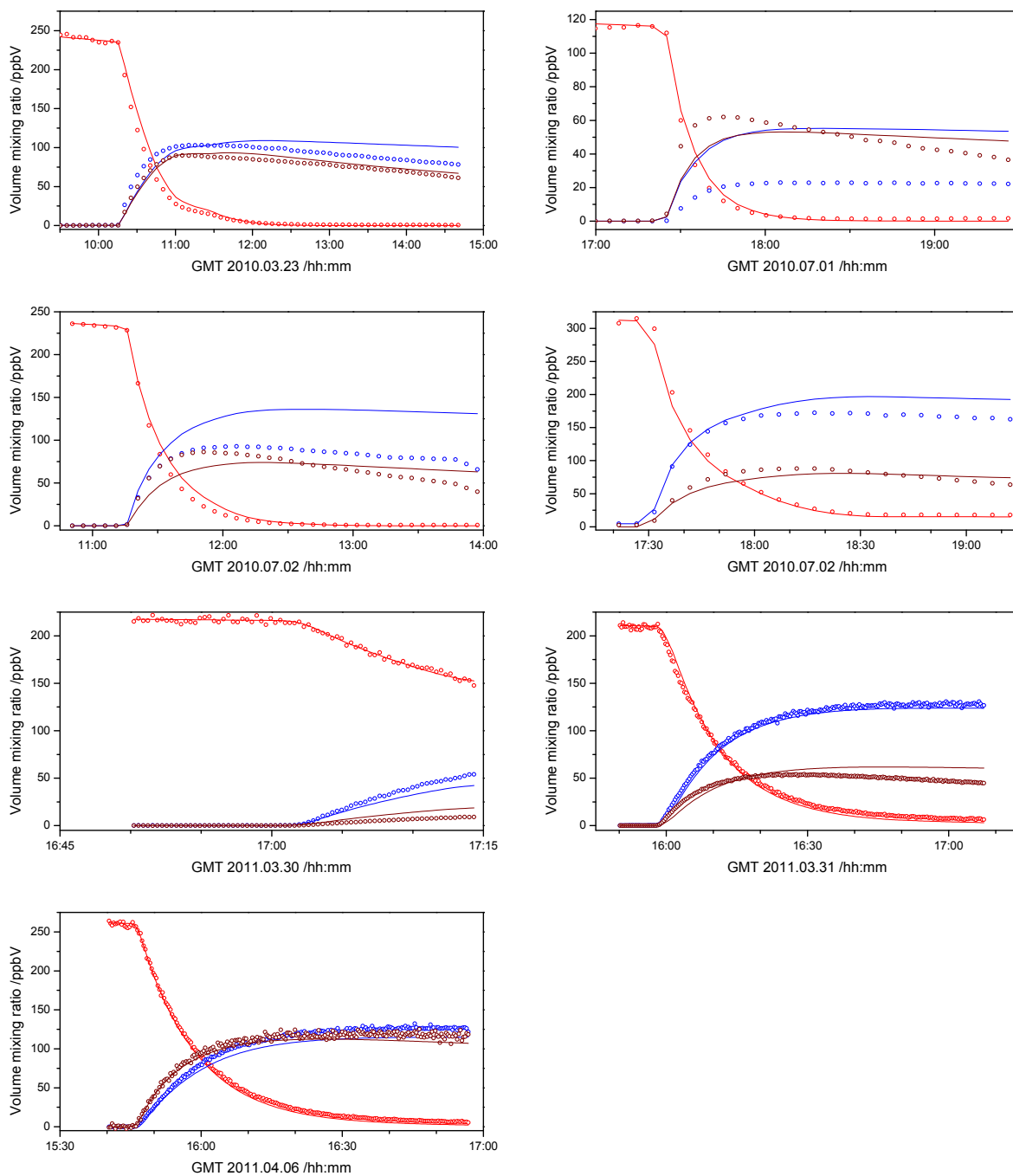


Figure 4.8. Observed and calculated mixing ratios of *N*-nitroso dimethylamine, *N*-nitro dimethylamine and *N*-methyl methanimine during *N*-nitroso dimethylamine photolysis experiments.

4.7 *N*-Nitroso diethylamine gas phase photolysis

Seven *N*-nitroso diethylamine photolysis experiments have been carried out – three in July 2010 and four during the 2011 campaigns. The experimental protocols and monitor data are included in the Supporting Information: *ADA-2011: Protocols and monitor data*.

The observed ion signals above 1% of the *N*-nitroso diethylamine (NDEA) signal loss in the seven experiments are collected in Table 4.5. Only signals with a count-rate yield > 1% relative to the signal decrease observed for *N*-nitroso diethylamine are included in the Table. Fragment ions, ¹³C-containing ions, instrument-intrinsic ions, and ions arising from side reactions were omitted here.

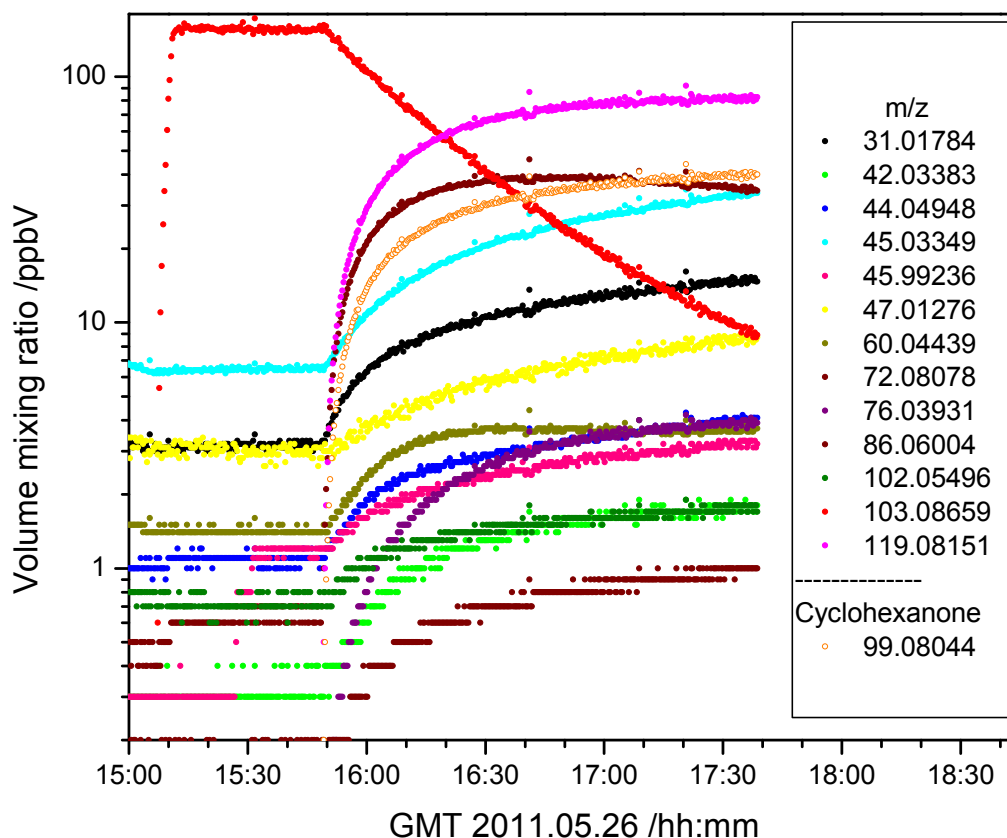
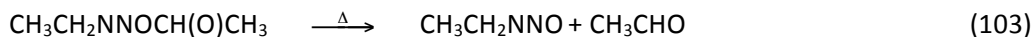
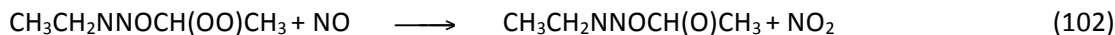
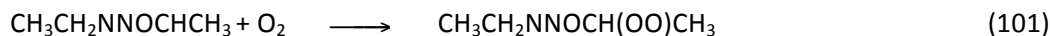


Figure 4.9. Observed ion signals and ion precursor volume mixing ratios during the *N*-nitroso diethylamine photolysis experiment on 2011.05.26.

Table 4.5. Ions observed in *N*-nitroso diethylamine photolysis experiments.

2010.07.09	2010.05.15	2010.07.21	2011.03.29	2011.01.04	2011.05.26	2011.05.30	Ion sum formula	Ion precursor	Comments
			31.01784	31.01784	31.01784	31.01784	CH ₃ O ⁺	CH ₂ O	
42.0338	42.0343	42.0344	42.03383	42.03383	42.03383	42.03383	C ₂ H ₄ N ⁺	CH ₃ CN	
44.0493	44.0501	44.0502	44.04948	44.04948	44.04948	44.04948	C ₂ H ₆ N ⁺	CH ₃ N=CH ₂	
45.0336	45.0341	45.0342	45.03349	45.03349	45.03349	45.03349	C ₂ H ₅ O ⁺	CH ₃ CHO	Chamber artefact
			47.01276	47.01276	47.01276		CH ₃ O ₂ ⁺	HCOOH	Chamber artefact
60.0442	60.0449	60.0450	60.04439	60.04439	60.04439	60.04439	C ₂ H ₆ NO ⁺		
72.0809	72.0814	72.0813	72.08078	72.08078	72.08078	72.08078	C ₄ H ₁₀ N ⁺	CH ₃ CH ₂ N=CHCH ₃	
			76.03931	76.03931	76.03931	76.03931	C ₂ H ₆ NO ₂ ⁺		
86.0599	86.0609	86.0608	86.06004	86.06004	86.06004	86.06004	C ₄ H ₈ NO ⁺	CH ₃ C(O)N=CHCH ₃	From photo-oxidation of CH ₃ CH ₂ N=CHCH ₃
			102.05496	102.05496	102.05496	102.05496	C ₄ H ₈ NO ₂ ⁺	?	
103.0839	103.0845	103.0849	103.08659	103.08659	103.08659	103.08659	C ₄ H ₁₁ N ₂ O ⁺	(CH ₃ CH ₂) ₂ NNO	
119.0810	119.0816	119.0816	119.08151	119.08151	119.08151	119.08151	C ₄ H ₁₁ N ₂ O ₂ ⁺	(CH ₃ CH ₂) ₂ NNO ₂	

The three ion signals (m/z 31.0178, 45.0445 and 47.0128, parent molecules: CH_2O and CH_3CHO and HCOOH) are “normal”, well known chamber artefacts. However, also in these experiments the signals from these species were larger than normal chamber artefacts. Acetaldehyde may, in part, originate from the OH radical reaction with NDEA:



and analogous OH radical reactions with *N*-nitro dimethylamine. Formaldehyde may in part stem from OH radical reaction with acetaldehyde, and the HCOOH formation from CH_2O was already addressed in Section 4.6.

Table 4.6. Initial volume mixing ratio of *N*-nitroso diethylamine and the loss of *N*-nitroso diethylamine, *N*-nitro diethylamine and *N*-ethyl methylamine (/ppbV) due to reaction with OH radicals and polymerization in the *N*-nitroso diethylamine photolysis experiments.

Experiment	Initial	Nitrosamine	Nitramine	Imine	Imine polymerization
20100709.57278	160.4	1.4	0.5	5.7	66.3
20100715.60541	152.7	1.6	0.5	4.5	57.9
20100721.56070	145.6	1.3	0.4	5.3	74.0
20110329.61022	201.7	1.2	0.4	1.1	15.3
20110401.57075	190.6	2.8	1.8	7.2	53.6
20110526.54721	155.4	2.5	1.5	4.0	31.9
20110530.57606	161.4	0.7	0.0	0.8	57.0

The derived parameters are, to some degree, correlated, Table 4.7; the largest correlation coefficient, 0.80, is between j_{rel} and k_2/k_3 , and the best-fit values are $k_2/k_3 = 0.97$ and $j_{\text{rel}} = 0.31$. The minimum on the response function of the fit (the root-mean-square deviation, *rms*) is rather shallow, Figure 4.10, which makes data balancing an issue.

Table 4.7. Correlation matrix for the parameters derived from analysis of the *N*-nitroso dimethylamine photolysis data.

	j_{rel}	k_2/k_3	k_5/k_3	k_d
j_{rel}	1.000			
k_2/k_3	0.808	1.000		
k_5/k_3	0.119	0.085	1.000	
k_d	0.120	0.075	0.351	1.000

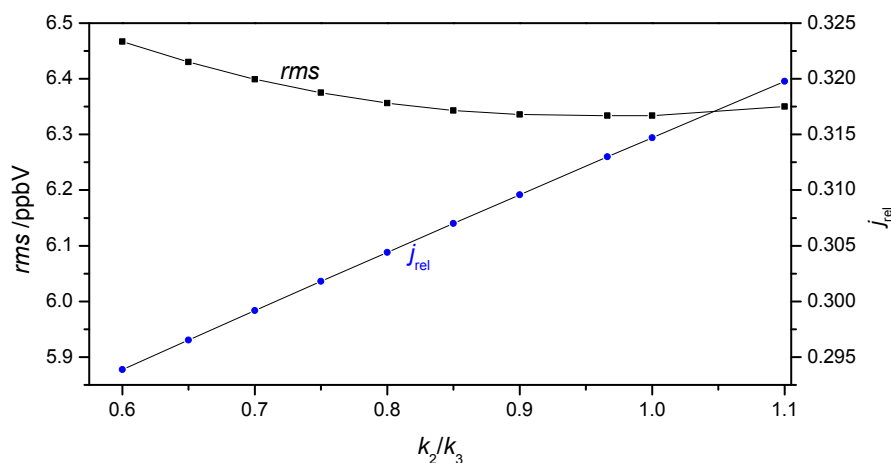


Figure 4.10. Illustration of the correlation between k_2/k_3 and j_{rel} in the least squares fit of data from 7 *N*-nitroso diethylamine photolysis experiments.

The diethylamine photo-oxidation experiments (section 3.3.1, page 28) suggest that k_2/k_3 cannot be as large as 0.97, but that a value in the range 0.6 to 0.7 will be in better agreement with the observed nitrosamine time-profiles in the photo-oxidation experiments. Ultimately, the nitrosamine photolysis experiments and the amine photo-oxidation experiments should be analysed jointly by a least-squares method. However, this is outside the scope of the present work, and k_2/k_3 was therefore constrained to 0.7 in the final analysis.

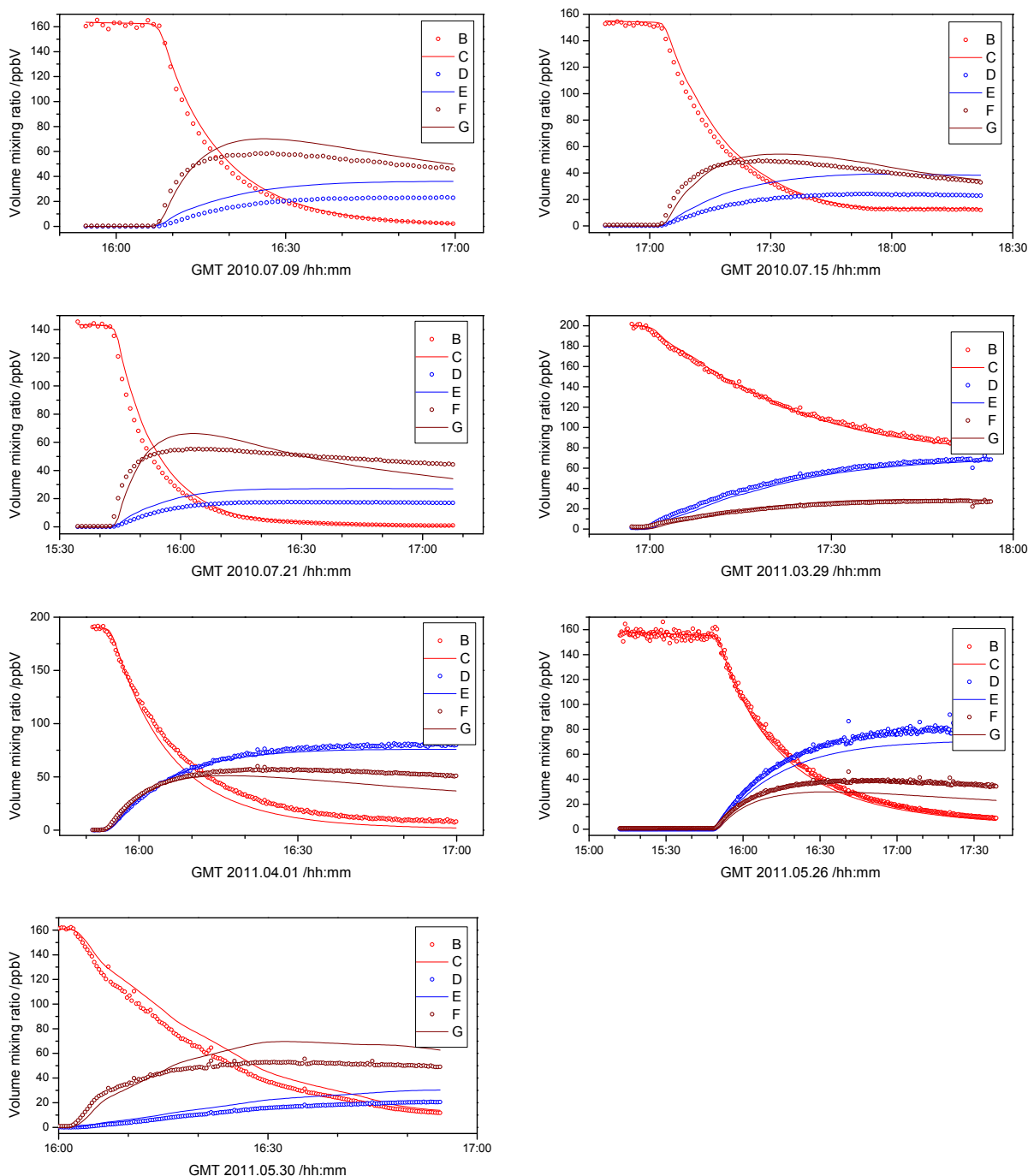


Figure 4.11. Observed (circles) and calculated (full curves) mixing ratios of *N*-nitroso diethylamine (○), *N*-nitro diethylamine (○) and *N*-ethyl ethanimine (○) during *N*-nitroso diethylamine photolysis experiments.

4.8 *N*-Nitroso morpholine gas phase photolysis

Six *N*-nitroso morpholine photolysis experiments have been carried out, three in July 2010 and three during the 2011 campaigns. The experimental protocols and monitor data are included in the Supporting Information: *ADA-2011: Protocols and monitor data*.

The observed ion signals above 1% of the *N*-nitroso morpholine signal loss in the six experiments are collected in Table 4.8, while Figure 4.12 shows the time evolution of the ion signals observed in the experiment on 2011.06.02. Only signals with a count-rate yield > 1% relative to the signal decrease observed for *N*-nitroso dimethylamine are included in the Table. Fragment ions, ¹³C-containing ions, instrument-intrinsic ions, and ions arising from side reactions were omitted here.

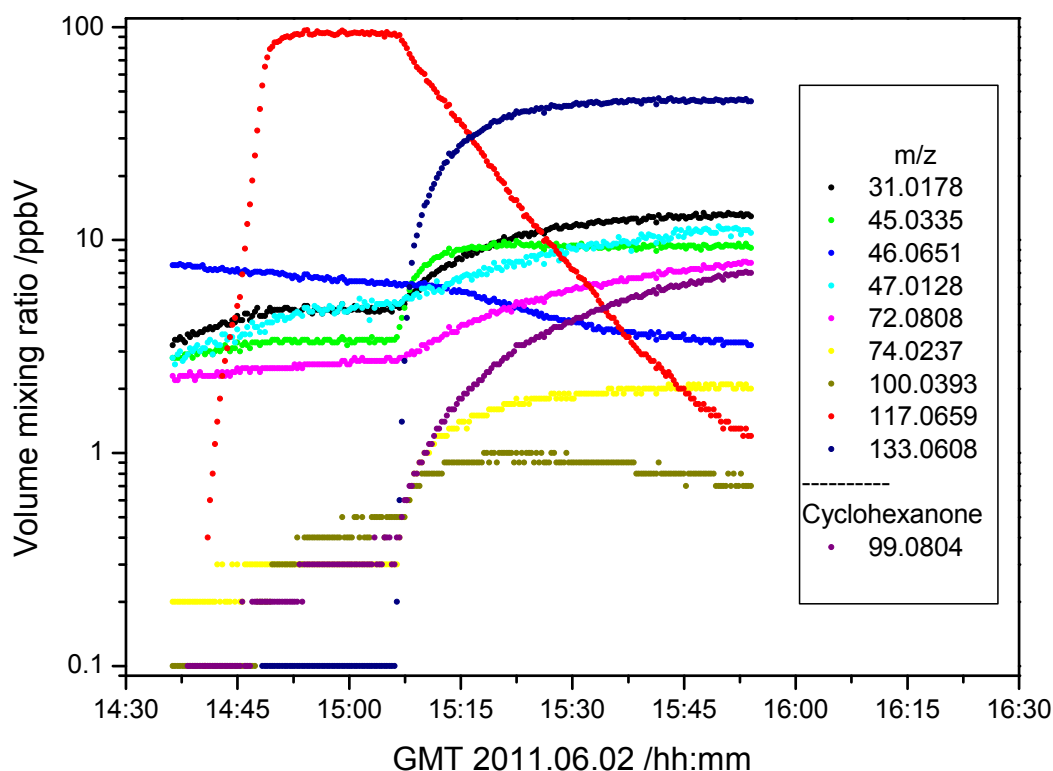
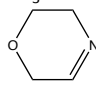
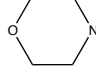
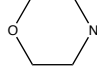


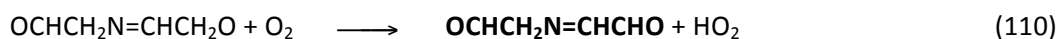
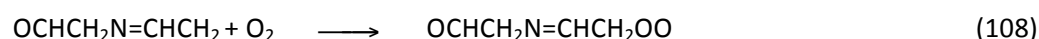
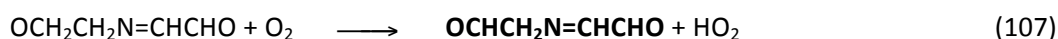
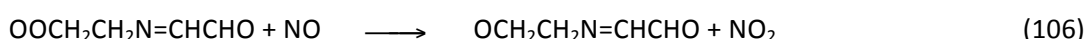
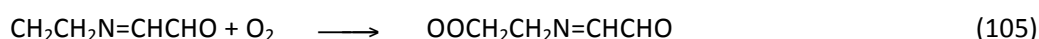
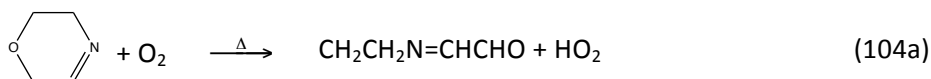
Figure 4.12. Observed ion signals and ion precursor volume mixing ratios during the *N*-nitroso morpholine photolysis experiment on 2011.06.02.

Table 4.8. Ions observed in *N*-nitroso morpholine photolysis experiments.

Ion m/z	Ion m/z	Ion m/z	Ion m/z	Ion m/z	Ion m/z	Ion sum formula	Ion precursor	Comments
07.07.10	08.07.10	21.07.10	21.03.11	31.05.11	02.06.11			
31.0178	31.0178	31.0178	31.0178	31.0178	31.0178	CH ₃ O ⁺	CH ₂ O	
45.0335	45.0335	45.0335	45.0335	45.0335	45.0335	C ₂ H ₅ O ⁺	CH ₃ CHO	Chamber artefact
46.02874	46.02874	46.02874				CH ₄ NO ⁺	NH ₂ CHO	
					46.0651	C ₂ H ₈ N ⁺	(CH ₃) ₂ NH	Impurity
47.0128	47.0128	47.0128	47.0128	47.0128	47.0128	CH ₃ O ₂ ⁺	HCOOH	Chamber artefact
					72.0808	C ₄ H ₁₀ N ⁺		Et-N=CHCH ₃ ?
74.0237	74.0237	74.0237	74.0237	74.0237	74.0237	C ₂ H ₄ NO ₂ ⁺		
						CH ₅ N ₂ O ₂ ⁺	CH ₃ NHNO ₂	
86.06004	86.06004	86.06004				C ₄ H ₈ NO ⁺		
100.0393	100.0393	100.0393	100.0393	100.0393	100.0393	C ₄ H ₆ NO ₂ ⁺	OCHCH ₂ N=CHCHO	Ring opening ?
117.0659	117.0659	117.0659	117.0659	117.0659	117.0659	C ₄ H ₉ N ₂ O ₂ ⁺		<i>N</i> -nitroso morpholine
133.0608	133.0608	133.0608	133.0608	133.0608	133.0608	C ₄ H ₉ N ₂ O ₃ ⁺		<i>N</i> -nitro morpholine

It is somewhat surprising that the four most abundant products of the *N*-nitroso morpholine photolysis were m/z 133.0608, 31.0178, 47.0128 and 45.0335 originating in *N*-nitro morpholine, formaldehyde, formic acid and acetaldehyde, respectively. The expected imine, 3,6-dihydro-2H-1,4-oxazine, was only observed in very small amounts, and not even in all photolysis experiments. It can be seen from Figure 4.12 that the mass balance was not good.

It is tentatively suggested that the imine formed in the O_2 reaction with the 4-morpholinyl radical is unstable (the compound has never been isolated), and that it will react with O_2 under ring-opening that eventually leads to a dicarbonyl compound, $C_4H_5NO_2$:



This reaction sequence can explain the ion signal m/z 100.0393 ($C_4H_6NO_2^+$) that was observed in every photolysis experiment. Moreover, $\text{OCHCH}_2\text{N}=\text{CHCHO}$ enters keto-enol equilibrium with $\text{HOCH}=\text{CHN}=\text{CHCHO}$ (2-[(2-hydroxyethenyl)imino]-acetaldehyde) and is expected to be extremely reactive. Its formation can therefore also explain the lack of mass balance in the experiments.

Table 4.9. Initial volume mixing ratio of *N*-nitroso dimethylamine and the loss of *N*-nitroso morpholine, *N*-nitro morpholine and 3,6-dihydro-2H-1,4-oxazine (/ppbV) due to reaction with OH radicals and polymerization in the *N*-nitroso morpholine photolysis experiments.

Experiment	Initial	Nitrosamine	Nitramine	Imine	Imine Polymerization
20100707.53631	48.0	0.7	1.5	5.7	0.1
20100708.58319	171.7	3.2	2.6	8.7	0.8
20100713.59628	161.4	2.7	2.6	8.5	0.7
20110321.62581	135.6	3.9	0.2	1.1	0.1
20110531.54602	103.2	2.1	2.3	6.9	0.4
20110602.53823	94.5	1.1	1.4	5.9	0.3

Table 4.10. Correlation matrix for the parameters derived from analysis of the *N*-nitroso dimethylamine photolysis data.

	j_{rel}	k_2/k_3	k_4/k_3	k_5/k_3
j_{rel}	1.000			
k_2/k_3	0.795	1.000		
k_4/k_3	0.021	-0.029	1.000	
k_5/k_3	0.100	0.102	-0.850	1.000

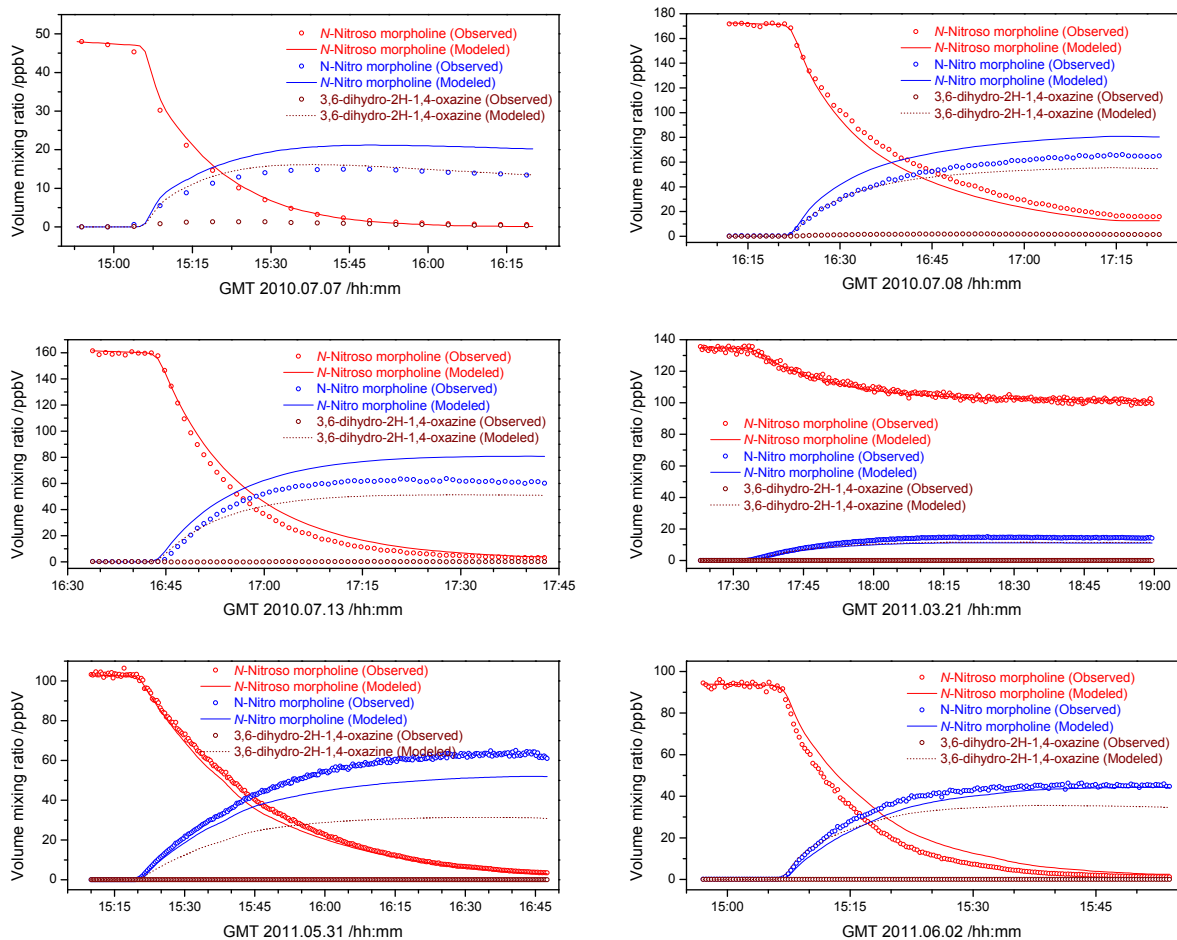


Figure 4.13. Observed and calculated mixing ratio of *N*-nitroso morpholine, *N*-nitro morpholine and 3,6-dihydro-2H-1,4-oxazine during *N*-nitroso morpholine photolysis experiments.

4.9 *N*-Nitroso piperazine gas phase photolysis

Three *N*-nitroso piperazine photolysis experiments have been carried out. The first experiment failed due to problems getting the sample into the chamber, the next two were successfully carried out in July 2010 employing a different inlet system. The experimental protocols and monitor data are included in the Supporting Information: *ADA-2011: Protocols and monitor data*.

Figure 4.14 shows the major PTR-TOF-MS ion signals observed during the photolysis experiment on 2010.03.23. It can be seen that there was a substantial loss of *N*-nitroso piperazine to the chamber walls prior to opening the canopy. However, there was a clear change in the loss rate upon opening the chamber. It can also be seen that essentially all other ion signals that can be attributed to *N*-nitroso piperazine increased as the *N*-nitroso piperazine sample was introduced to the chamber; the only clear exception being *m/z* 132.0774 (protonated *N*-nitro piperazine).

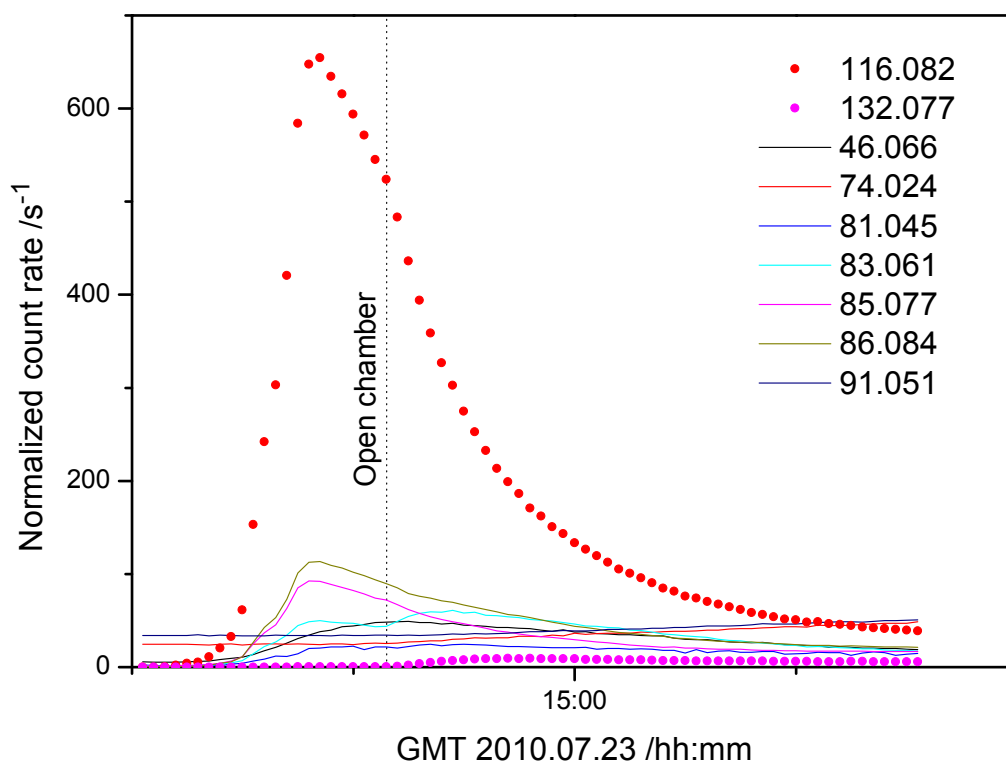


Figure 4.14. Observed ion signals during the *N*-nitroso piperazine photolysis experiment on 2010.07.23.

The expected major product (the imine), 1,2,3,4-tetrahydro pyrazine, was not unambiguously detected; the *m/z* 85.077 ion (protonated 1,2,3,4-tetrahydro pyrazine ?) was already detected during the injection of *N*-nitroso piperazine and this signal correlated perfectly with the *N*-nitroso piperazine ion signal. The same was true for the *m/z* 86.084 ($C_4H_{10}N_2^+$), 83.061 ($C_4H_7N_2^+$) and 81.045 ($C_4H_5N_2^+$) ion signals. The only ion signal, in addition to that of *N*-nitro piperazine, which showed a clear increase when the photolysis set in was *m/z* 83.061 ($C_4H_7N_2^+$). It is clear from the observation of *N*-nitro piperazine that the lifetime/stability of the alkylamino radical, formed in the photolysis of the nitrosamine, is sufficient for nitramine formation. One would therefore also expect the imine to be formed. The ion trio *m/z* 85.077, 83.061 and 81.045 was also observed by PTR-TOF-MS in other piperazine experiments (see Section 3.5, page 67), and it is tentatively suggested that H_2 -elimination is taking place from piperazine, tetrahydro pyrazine, and dihydro pyrazine upon gas phase protonation.

The available data are insufficient to determine the relative rate coefficients k_2/k_3 , k_4/k_3 and k_5/k_3 , and only a relative photolysis rate, j_{rel} , was derived from a least squares analysis of the data from the two experiments; the result is included in Table 4.1 (page 81).

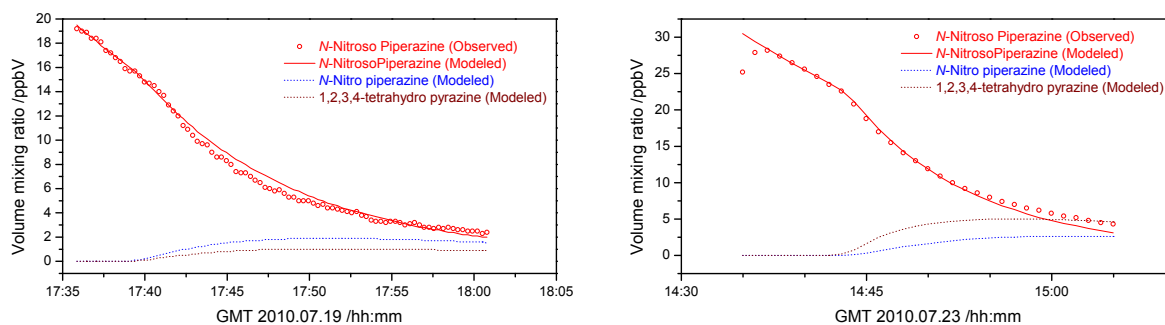


Figure 4.15. Observed and calculated mixing ratio of *N*-nitroso piperazine, 1,2,3,4-tetrahydro pyrazine and *N*-nitro piperazine during *N*-nitroso piperazine photolysis experiments.

4.10 *N*-Nitroso piperidine gas phase photolysis

Two photolysis experiments with *N*-Nitroso piperidine have been carried out. In addition, data from a relative-rate photolysis experiment (see Section 4.12) was included in the analysis. The experimental protocols and monitor data are included in the Supporting Information: *ADA-2011: Protocols and monitor data*. The prime motivation behind the photolysis study *N*-Nitroso piperidine was its structural relationship to the two target compounds *N*-nitroso piperazine and *N*-nitroso morpholine, Figure 4.16.

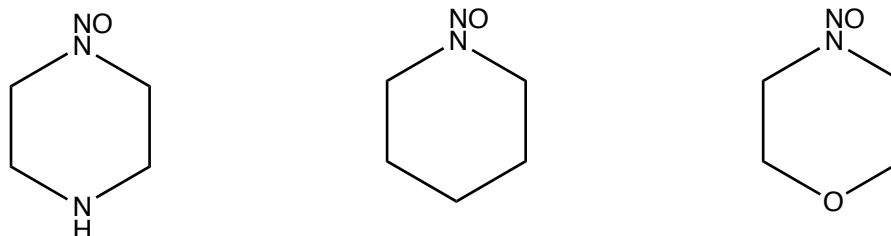


Figure 4.16. Structures of *N*-nitroso piperazine (left), *N*-nitroso piperidine (centre), and *N*-nitroso morpholine (right).

In two of the experiments the PTR-MS signal of cyclohexane was interfering with the signal of the piperidine imine (2,3,4,5-tetrahydro pyrimidine). The imine signal was therefore not included in the analysis. The parameters j_{rel} and k_2/k_3 correlated and the available data do not allow a simultaneous determination of both. Figure 4.17 compares observations and model results for $k_2/k_3 = 0.5$; the derived parameters are included in Table 4.1.

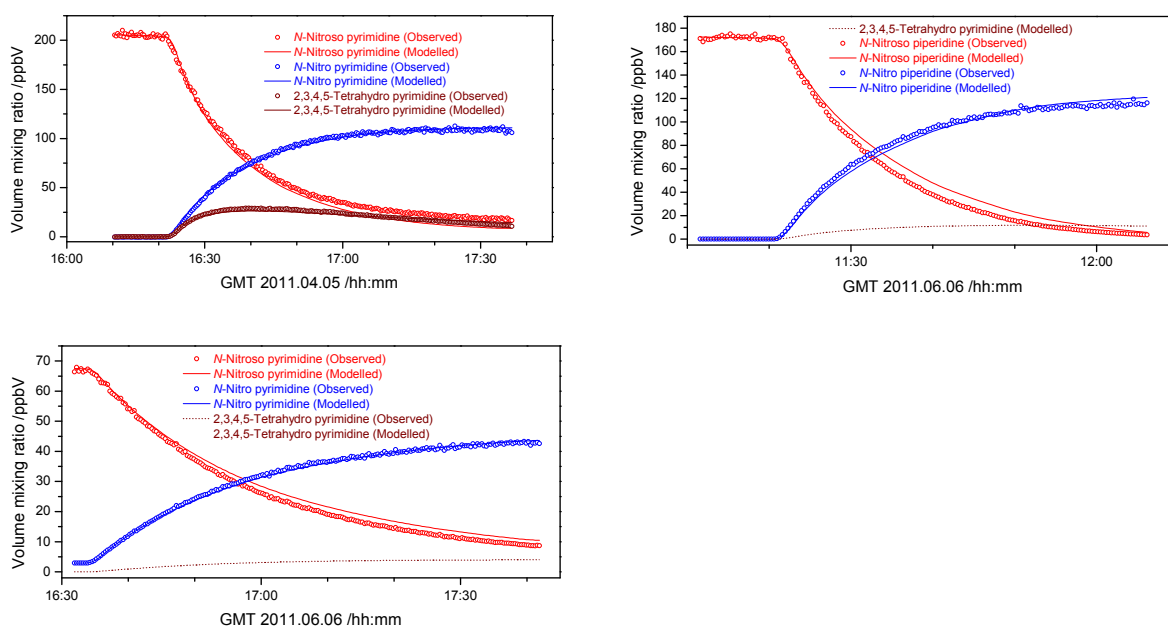


Figure 4.17. Observed and calculated mixing ratio of *N*-nitroso pyrrolidine, *N*-nitro pyrrolidine and 2,3,4,5-tetrahydro pyrimidine during *N*-nitroso pyrrolidine photolysis experiments.

The simulation shows that around 10% of the nitrosamine loss during the experiment was due to reaction with OH-radicals, Table 4.11. Similarly, OH radicals remove around 10% of the nitramine formed again. The imine formation was small in all experiments, but the time profile of the 20110405.58225 experiment clearly shows that there was a substantial imine loss during the experiment, which can either be modelled employing an unreasonably large rate coefficient for the

OH reaction or by introducing a polymerization reaction. The results listed in Table 4.1 and Table 4.11 stem from a fit in which a polymerization reaction was included in the analysis.

Table 4.11. Amount (/ppbV) of nitrosamine, nitramine and imine removed by OH radicals or by polymerization in the *N*-nitroso piperidine photolysis experiments.

Experiment	Initial	Nitrosamine	Nitramine	Imine	Imine polymerization
20110405.58225	204	20.5	12.6	8.2	20.3
20110606.40295	170	12.4	11.0	2.7	3.0
20110606.59514	66	5.2	3.1	0.6	0.4

It was mentioned above that the parameters j_{rel} and k_2/k_3 are correlated and the available data do not allow a simultaneous determination of both. Figure 4.18 illustrates the results from a series of simulations in which the parameter k_2/k_3 was varied between 0.3 and 0.9; there is a shallow minimum in the *rms* deviation for $k_2/k_3 = 0.5$. It can be seen that essentially only j_{rel} and k_4/k_3 are sensitive to variation in k_2/k_3 .

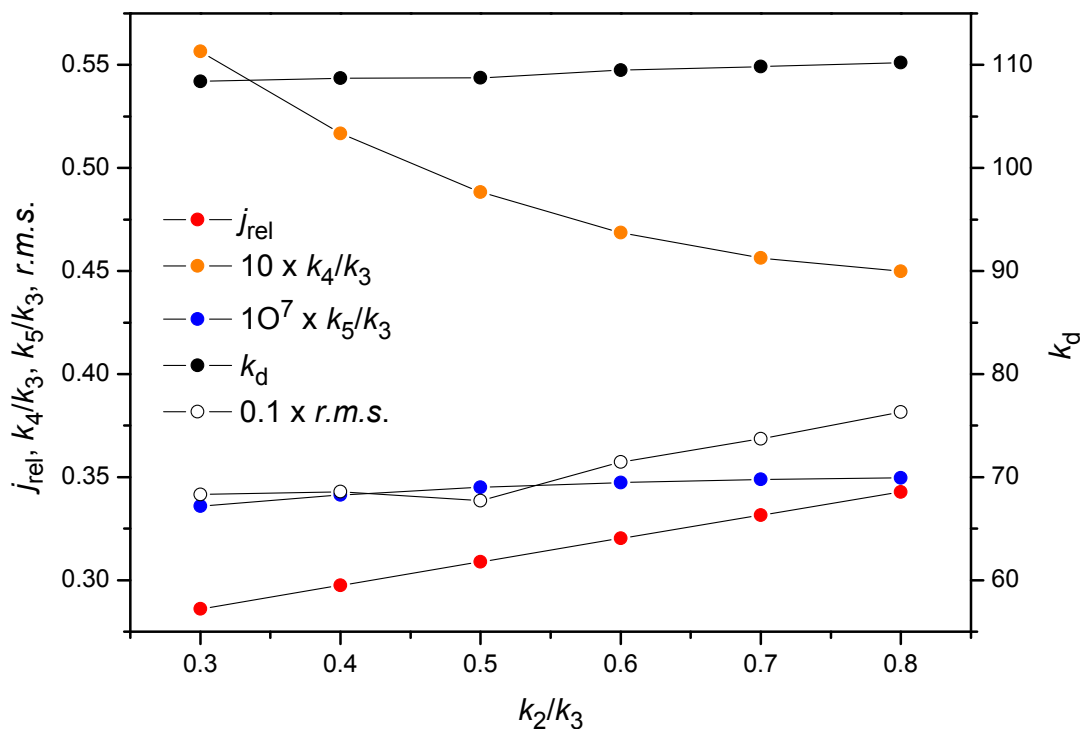


Figure 4.18. Variation in parameters derived by least-squares analysis of data from *N*-nitroso pyrrolidine photolysis experiments as a function of k_2/k_3 .

The correlation matrix of the LSQ-fitting is presented in Table 4.12, from which it can be seen that also k_5/k_3 and k_d are somewhat correlated. Obviously, additional experiments are needed to determine the parameters unambiguously and care should be taken not to over interpret the results.

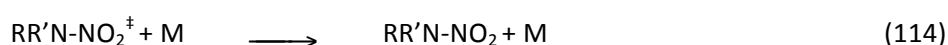
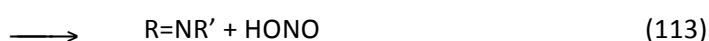
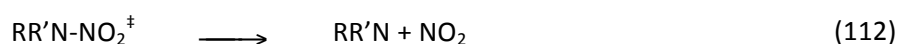
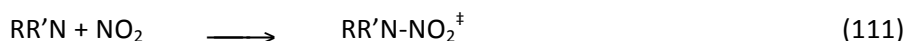
Table 4.12. Correlation matrix for the parameters derived in analysis of the *N*-nitroso piperidine photolysis data.

	j_{rel}	k_4/k_3	k_5/k_3	k_d
j_{rel}	1.000			
k_4/k_3	0.212	1.000		
k_5/k_3	0.006	-0.823	1.000	
k_d	0.168	0.054	0.159	1.000

4.11 *N*-Nitroso pyrrolidine gas phase photolysis

A single *N*-nitroso pyrrolidine photolysis experiment was carried out in the afternoon on 2011.04.07. In addition, data from a relative-rate photolysis experiment (see Section 4.12) was included in the analysis. The experimental protocol and monitor data are included in the Supporting Information: *ADA-2011: Protocols and monitor data*.

The NO_x-conditions in the *N*-nitroso pyrrolidine and *N*-nitroso piperidine experiments were almost identical, but the product distribution was very different. Photolysis of *N*-nitroso piperidine (6-member ring) gave primarily the nitramine, while photolysis of the more rigid *N*-nitroso pyrrolidine (5-membered ring) gives primarily the imine (3,4-dihydro-2H-pyrrole). This is in accordance with nitramine formation being highly exothermic and the principles of internal redistribution of energy:



The experimental data were insufficient to allow the determination of all the parameters describing the photolysis process and the subsequent reactions. A systematic variation of the parameters k_2/k_3 and k_4/k_3 showed that the data were insensitive to these parameters and they were therefore constrained to a value of 0.5. A least-squares analysis of the nitrosamine and imine data gave $j_{\text{rel}} = 0.390 \pm 0.009$ and $k_5/k_3 = (165 \pm 150) \times 10^{-5}$. The imine data force an overestimation of j_{rel} in the least-squares fit, and a much-improved agreement between observed and modelled time-profiles of the nitrosamine data was obtained when only the nitrosamine data were fitted. Figure 4.19 compares observations and model results, while Table 4.13 shows the amounts of nitrosamine, nitramine and imine that were lost during the experiments due to reaction with OH-radicals – around 5% of the nitrosamine loss was caused by reaction with OH radicals. The model parameters are included in Table 4.1.

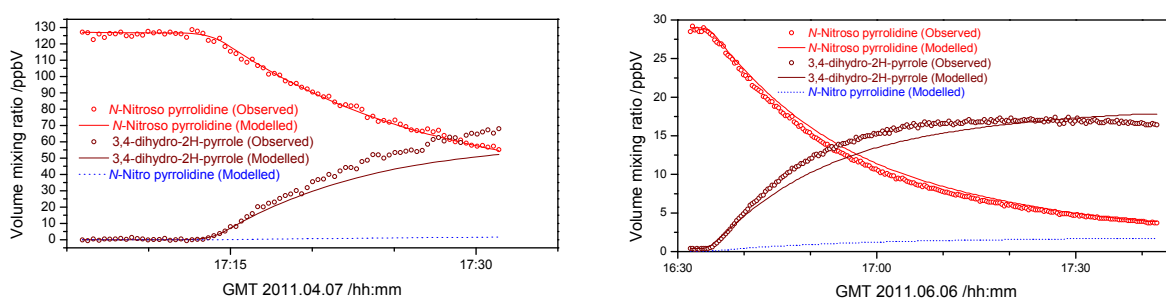


Figure 4.19. Observed and calculated mixing ratio of *N*-nitroso pyrrolidine, 3,4-dihydro-2H-pyrrole and *N*-nitro pyrrolidine during the photolysis experiments on 2011.04.07 and 2011.06.06.

Table 4.13. Amount (/ppbV) of nitrosamine, nitramine and imine removed by OH radicals or by polymerization in the *N*-nitroso pyrrolidine photolysis experiments.

Experiment	Initial	Nitrosamine	Nitramine	Imine	Imine polymerization
20110407.61557	121	6.7	0.1	10.0	0.1
20110606.40295	28	1.3	0.1	3.2	0.1

4.12 Nitrosamine relative photolysis rate experiment

A relative photolysis rate experiment was carried out with *N*-nitroso pyrrolidine, *N*-nitroso piperidine and *N*-nitroso morpholine. The initial NO₂-level was around 150 ppbV to reduce the back-reaction of the amino radicals with NO reforming the nitrosamines; cyclohexane was added to quench OH radical activity (~2 ppmV). Figure 4.20 shows the NO_x-level during the photolysis experiment, while Figure 4.21 shows the PTR-TOF-MS signals of the 3 nitrosamines as a function of time.

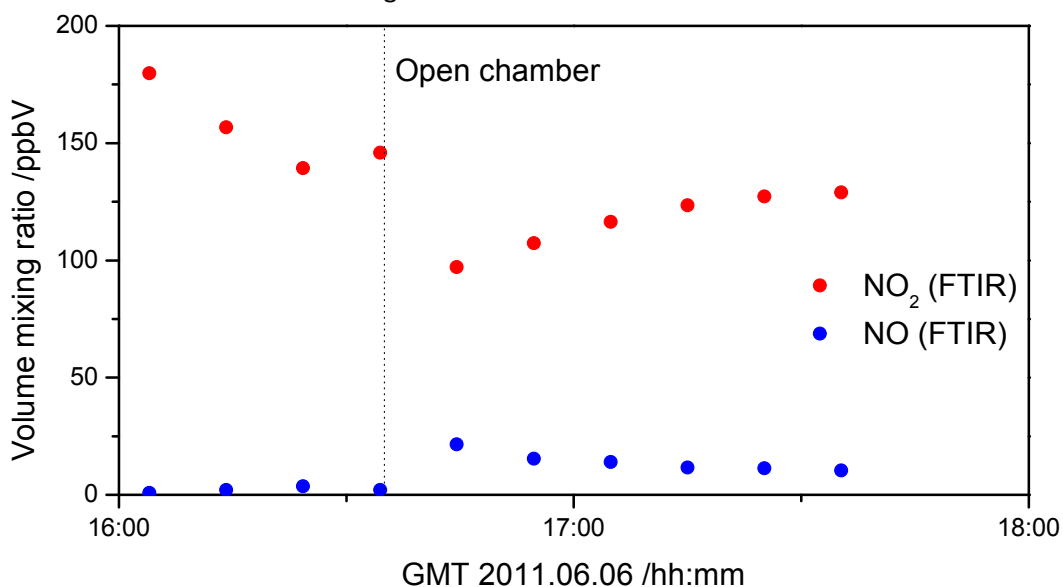


Figure 4.20. NO and NO₂ levels during the relative photolysis rate experiment on 2011.06.06.

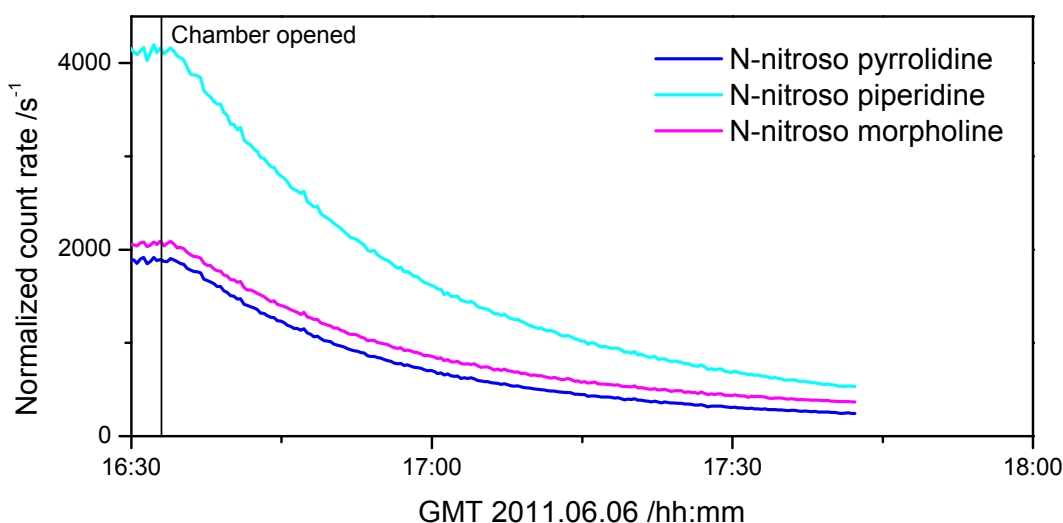


Figure 4.21. PTR-TOF-MS ion signals (ncps) observed during the *N*-nitroso pyrrolidine, *N*-nitroso piperidine and *N*-nitroso morpholine photolysis experiment on 2011.06.11.

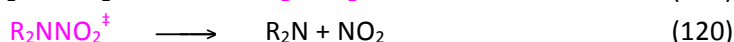
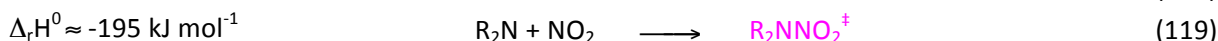
Assuming that the following photolysis processes were of the type, $A \rightarrow B \rightarrow \text{Products}$, the mixing ratios of the 3 nitrosamines should all follow exponential decay:

$$\frac{d[\text{RNO}_x]}{dt} = -j_x \cdot [\text{RNO}_x] + k_{2,x} \cdot [\text{R}] \cdot [\text{NO}]$$

Assuming $j_x \cdot [\text{RNO}_x] \gg k_{2,x} \cdot [\text{R}] \cdot [\text{NO}]$ a plot of the data in the form of $\ln\{[\text{Nitrosamine Y}]_0 / [\text{Nitrosamine Y}]_t\}$ versus $\ln\{[\text{Nitrosamine X}]_0 / [\text{Nitrosamine X}]_t\}$ should consequently follow a straight

line with the slope j_N/j_X . The data included in Figure 4.21 are plotted in this form in Figure 4.22. The figure illustrates that at longer radiation times, there is a systematic deviation. Taking only the first 50 data points of the experiment, the slope of the *N*-nitroso piperidine curve is 0.91 while that of *N*-nitroso morpholine is 0.87. There are no absolute UV absorption cross-sections available for the three compounds. There is, however, no reason to expect any significant differences in the gas phase UV absorption cross-sections of the nitrosamine $S_1(n\pi^*) \leftarrow S_0$ band in these three molecules.

The nitrosamine photolysis process and the (relevant) subsequent reactions are:



The $\text{R}_2\text{N}-\text{NO}$ bond enthalpy is around -185 kJ mol^{-1} (from G3 calculations³⁸) and the threshold excitation energy is around 380 nm ($\approx 315 \text{ kJ mol}^{-1}$). There is therefore more than sufficient energy available to homolytic dissociation on the ground state surface. Further, the S_1 surface possesses a dissociative character.⁸² It is suggested that the small differences in apparent photolysis rates primarily are due to differences in the dissipation of excess energy in the nitrosamines and nitramines: pyrrolidine is a strained 5-membered ring, piperidine and morpholine are both unstrained 6-membered rings with larger densities of vibrational states.

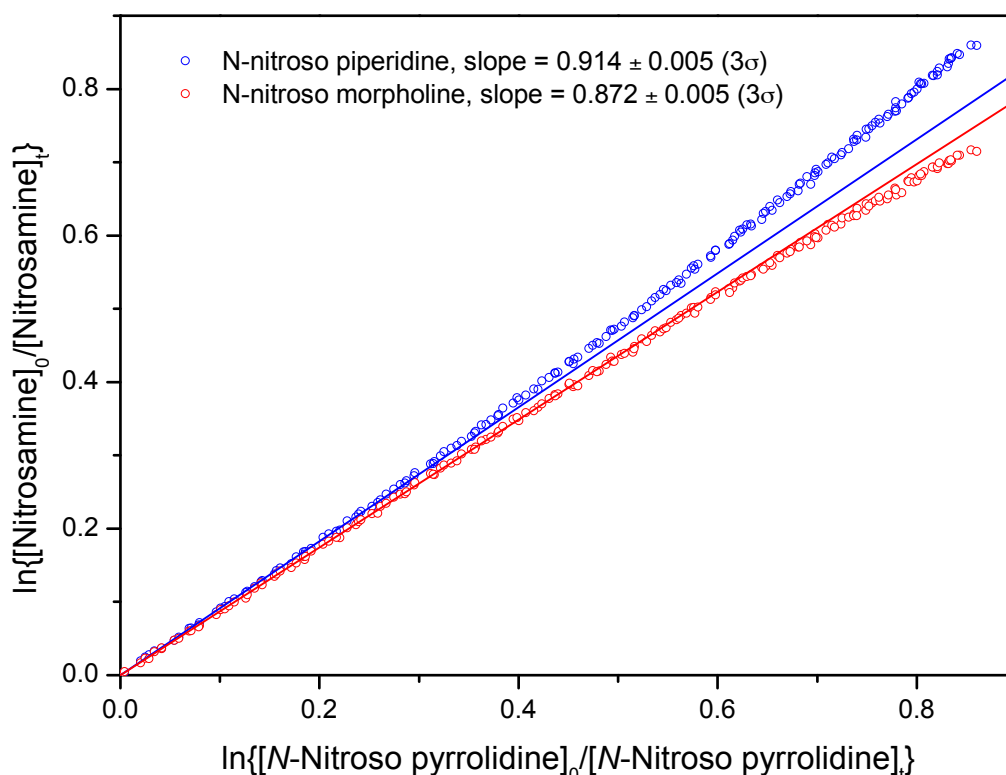


Figure 4.22. Plot of $\ln\{[N\text{-nitroso piperidine}]_0/[N\text{-nitroso piperidine}]_t\}$ and $\ln\{[N\text{-nitroso morpholine}]_0/[N\text{-nitroso morpholine}]_t\}$ versus $\ln\{[N\text{-nitroso pyrrolidine}]_0/[N\text{-nitroso pyrrolidine}]_t\}$ during photolysis.

5. Results from aerosol formation studies

The aerosol generated upon OH radical initiated photo-oxidation of ethylamine, diethylamine, triethylamine and piperazine was studied using both on-line and off-line techniques. Aerosol formation was investigated under both high and low NO_x mixing ratios and under dry conditions. Table 5.1 summarizes the major features of the particles formed. Aerosol yields varied from 6 to 64% depending on both the NO_x concentration and the type of amine. Under high NO_x more HNO₃ is formed in the gas phase which readily reacts with the amine forming the corresponding aminium salt. Aminium nitrate salt represented by far the major aerosol constituent during photo-oxidation of ethylamine and diethylamine. Triethylamine degradation was very different and independent of the NO_x conditions, the aerosol mass was dominated by secondary organic products and the ratio organic/nitrate increased with time.

Volatility of the aerosol was investigated using a VTDMA (volatility tandem differential mobility analyser). Under high NO_x conditions the particles formed from piperazine were the least volatile ones, followed by triethylamine and ethylamine. For low NO_x experiments triethylamine and piperazine produced the least volatile particles followed by diethylamine and ethylamine. In general, particles formed under low NO_x are less volatile than the corresponding aerosol formed under high NO_x conditions, where the contribution of the primary aminium salt is more important. Generally, ageing of particles produced a less volatile aerosol with time. Volatility was highly sensitive with respect to small changes in chemical composition during ageing. Even a small fraction of oxygenated species or higher molecular weight compounds were able to drastically change the volatility of EA and DEA.

In an emission plume, salt formation from amines will necessarily compete with NH₃. The process will depend on the available ammonia concentration and the possibility of atmospheric transformation of the amine salt by ammonia exchange. The ammonia exchange was evaluated for the ethylamine under low NO_x conditions (2011.06.03) where as much as 35 ppbV of ammonia was produced, and even when ethylamine and ammonia were present at similar concentrations, only trace levels of ammonium (0.7 mg/m³) were observed in the aerosol. Nevertheless in a plume, the concentration of ammonia will most probably be 10 to 100 times larger than those of the amines and exchange cannot be neglected.

Once the primary aminium salt has been formed in the plume, the aerosol could partly evaporate upon dilution. The fresh aerosol is semi-volatile for the first few hours. Dilution tests suggested that the aerosol formed from piperazine and -triethylamine was not affected by dilution while the aerosol formed from ethylamine and diethylamine did partly evaporate. The evaporated amines could further react with available radicals such as OH yielding lower volatility products that may be able to partition back into the condensed phase. The amine oxidation products have a high probability to be basic and take part in secondary salt formation. This additional condensation of secondary organic compounds could possibly shield the primary salt core of the particle from further exchange, at least for a limited amount of time.⁴⁷

The experiments performed at EUPHORE have shown that ageing is an important process; it will reduce the volatility of the particles and increase their atmospheric lifetime. Recent publications report that amines released to the atmosphere can also take part in new particle formation and increase both nucleation and growth rates.⁸³⁻⁸⁵ The photo-oxidation studies of amines were performed in a dry atmosphere, while in a typical plume the partial pressure of water will be much higher. It is expected that water will play a crucial role in enhancing aerosol formation and changing solubility of oxidants and amine precursors in the aerosol phase.

5.1 General

During the ADA campaigns performed at EUPHORE facility in Valencia 2011 aerosol concentrations, composition and thermal properties have been measured using several on-line instruments. A SMPS (Scanning Mobility Particle Sizer), a TEOM (Tapered Element Oscillating Monitor), a C-TOF-AMS (Compact Time of Flight Aerosol Mass Spectrometer) and a VTDMA (Volatility Tandem Differential Mobility Analyser) were used to follow aerosol formation and ageing. In addition, filter samples were collected at the end of the experiment for off-line analysis using a qTOF-MS (Quadrupole Time-of-Flight Mass Spectrometry). In this section the general features of aerosol formation from the investigated amines are described followed by a more detailed description of ethylamine (EA) as an example. Information regarding the other amines is found in ANNEX D.

Table 5.1 presents a summary of the major features of the aerosols monitored during ADA campaign 2011. We selected two experiments for each amine, one at high and one at low NO_x conditions as representative examples. For each condition we evaluated the yields, the ratio of nitrate in the primary aminium salt vs. total nitrate, the organic vs. nitrate fraction and a few key compounds identified among the reaction products. The ageing and the thermal properties are illustrated by the volume fraction remaining (VFR).

Table 5.1. Summary of important chemical and physical parameters of the aerosol derived during the ADA campaign 2011 for EA, DEA, TEA and Piperazine under high and low NO_x conditions. One experiment was selected for each condition as being representative.

	Aerosol yield (total/organic)	Nitrate primary salt/total nitrate (%)	Ratio nitrate vs organic	Selected compounds	Volatility, VFR _{323K} (fresh/aged)	Dissociation constant, K _p , for the Nitrate salt. (Pa ²)
EA (2011-06-03, low NO _x)	0.3/0.11	80-100	1.0-1.4	C ₆ H ₁₂ N, C ₆ H ₁₁ N ₂ , N-ethylethaninimium, N-methylethaninimium	0.75/0.90	2.83 x 10 ⁻⁸
EA (high NO _x 2011-03-25) afternoon	0.64/0.21	80-100	1.0-1.4	nitroethyl-amine N-ethylethaninimne, N-methylethanimine	0.63/0.82	2.83 x 10 ⁻⁸
DEA (2011-05-31, low NO _x)	0.13/0.07	80-100	0.7-0.9	C ₄ H ₁₁ N, C ₆ H ₁₄ N ₂ . ethanimine	0.64/0.91	7.01 x 10 ⁻⁹
DEA (2011-03-30, high NO _x)	0.25/0.12	90-100	0.9-1.1	nitroethyl-amine, ethanimine	n.a.	7.01 x 10 ⁻⁹
TEA (high-NO _x 2011-03-31)	0.09/0.07	32-45	0.53-1.0	Methylformamide nitroethyl-amine	0.80/0.91	9.39 x 10 ⁻⁸
TEA (low-NO _x 2011-05-30)	0.29 ^c	30-45	0.15-0.3	C ₃ H ₆ NO, C ₅ H ₁₀ NO ₂	0.65/0.95	9.39 x 10 ⁻⁸
Piperazine (low-NO _x 2011-06-09) morning	n.a ^d	49-71 ^b	0.2-0.35	C ₄ H ₇ N ₂ O, C ₄ H ₈ N ₃ O	0.95/0.95	n. a.
Piperazine (high-NO _x 2011-04-06)	n.a ^d	40-70 ^b	0.5-0.85	C ₄ H ₈ N ₂ , C ₄ H ₈ N ₃ O, C ₆ H ₁₁ N ₂ O	0.95/0.95	n. a.

^a K_p, for NH₄NO₃ 4.48 x 10⁻⁸ Pa², Refs. ^{47,86}. ^b Low NO_x formed mainly mono-nitrate piperazine aminium salt, while under high NO_x dinitrate piperazine aminium salt is formed. ^c Calculated using total mass loading of the SMPS (d=1.3g/cm³). ^d Piperazine quantitative values in the gas phase are not available yet.

The aerosol yield is a quantitative measure of the conversion of the amine from the gas to the particulate phase. The mass aerosol yield can be defined as the mass of the aerosol formed divided by the mass of the precursor consumed in the gas phase. During the ADA campaign both the total aerosol yield (which takes into account both nitrate and organic mass contribution to the aerosol mass) and the organic aerosol yield (which takes into account only the organic present in the condensed phase) has been calculated.

The volume fraction remaining (VFR) varies between 0 (everything evaporates) and 1 (nothing evaporates). A low value (25%) implies a volatile aerosol while a high value (75%) indicates a semi

volatile aerosol. The aging is illustrated by giving the VFR for the fresh and aged aerosol. We also included the solid/gas equilibrium dissociation constant of the primary nitrate salt (K_p) that reflects the potential for NH_3 -displacement, i.e. if the aminium nitrate salt in presence of gaseous NH_3 is prone to be converted into NH_4NO_3 while the amine is transferred back into the gas phase. The K_p values provided should be compared to the literature K_p value of NH_4NO_3 , that is $4.48 \times 10^{-8} \text{ Pa}^2$.⁸⁶ Unfortunately, the uncertainties of these numbers are large but will provide a general idea about this possibility. The magnitude of any displacement will also depend on the concentrations of the amine and NH_3 in an air mass with limited HNO_3 concentrations.

Figure 5.1 depicts the major processes for aerosol formation and ageing during the photo-oxidation experiments of amines. The most important pathway is represented by primary salt formation (path 1) at least for primary and secondary aliphatic amines. Path 2 involves the oxidation of the parent amine with subsequent aerosol formation via secondary salt (2b) or direct partitioning of the oxidation products (2a). The aerosol is then subjected to ageing via heterogeneous processes such as HNO_3 uptake, O_3 and OH surface reaction (path 3) or by condensed phase processes within an aerosol particle or cloud droplet (path 4). The importance of each process is reflected in the chemical composition and physical properties and how these change with time as described below.

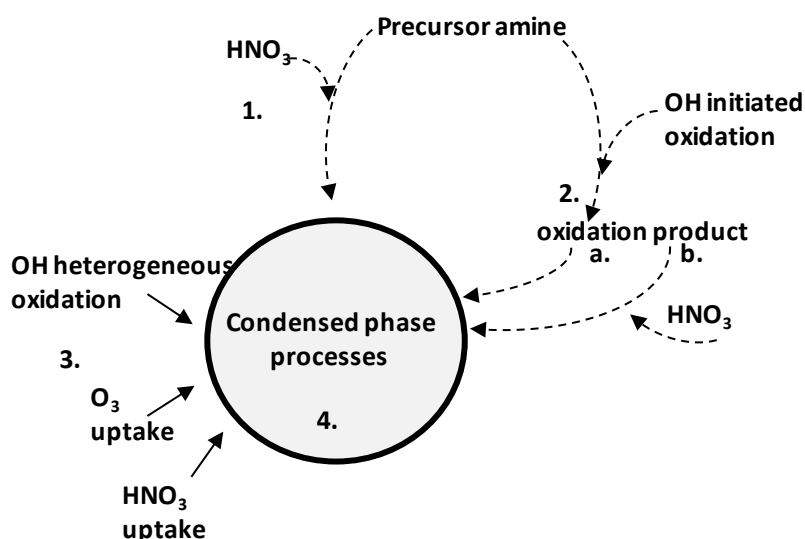
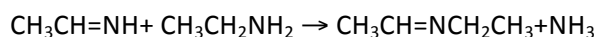
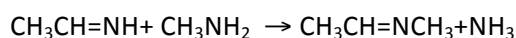


Figure 5.1. Aerosol forming and ageing processes: 1. Formation of the primary aminium salt. Path 2a and 2b: oxidation of the amine followed by partitioning of the product or formation of a secondary salt. 3. Reactive uptake of HNO_3 , O_3 or OH-radicals on the pre-existing particle. 4. Condensed phase processes e.g. aqueous chemistry or formation of oligomers. The dotted black arrows denote aerosol forming reactions and processes. The solid black arrows: ageing processes.

5.1.1 Composition

The contribution of the primary nitrate (path 1) to the total nitrate yield was determined and is presented in Table 5.1 (column 2). As can be seen in Table 5.1, the EA and DEA experiments (both at the high and low NO_x conditions) show little variability in terms of composition. The total aerosol is dominated by the primary aminium nitrate salt of ethylamine and diethylamine. It is evident that some condensation reactions do occur during the EA and DEA experiments and the following products are observed both in the gas phase and in the aerosol (as salt probably):



For EA and DEA very few fragments associated with oxygenated species have been detected and they represent a minor fraction of the total aerosol mass. The photo-oxidative degradation of

triethylamine seems to be very different and both at low and high NO_x conditions the aerosol mass is dominated by secondary organic products, both the oxygenated fragments increase with time and the organic fraction increases with time (for more details about TEA see ANNEX D, page 146). Analysis of formamides, nitramines and nitrosamines (by GC-MS) in samples from March 2011 showed minimal concentrations in the aerosol phase compared to the gas phase, which was also expected (aerosol data are listed in ANNEX D).

5.1.2 Thermal properties and ageing of particles

For the fresh aerosol produced in the ADA 2011 campaign the volatility of mono-, di- and triethylamine and piperazine aerosols, formed under low and high NO_x photo-oxidation conditions were compared (Table 5.1). Under high NO_x conditions the particles formed from piperazine were the least volatile ones, followed by triethylamine and ethylamine. For low NO_x experiments triethylamine produced the least volatile particles followed by diethylamine and ethylamine, due to the formation of secondary organic products that have lower volatility. In general, particles formed under low NO_x were less volatile than the corresponding aerosol formed under high NO_x conditions, when the contribution of the primary aminium salt is more important.

Generally, ageing of particles produced a less volatile aerosol with time. Ageing also increased the organic fraction of the aerosol. The ageing effect on the physical and chemical properties was more pronounced in some of the experiments (EA, DEA, TEA low NO_x conditions and EA high NO_x conditions). Aerosol particles formed during the high NO_x TEA experiment showed smaller, but still significant ageing effects, while none of the piperazine experiments, disregarding the NO_x conditions, did show any significant ageing with time.

The formation of the less volatile aerosol particles under low NO_x conditions is believed to take place through reaction path 2 in Figure 5.1. *i.e.* oxidation of the parent amine and partitioning of the oxidation product into the aerosol phase or, if an alkaline compound is formed, in the oxidation reaction, formation of a secondary salt via the reaction of the oxidation product with HNO₃ to form a secondary salt product. The processes denoted 3 and 4 are thought to be responsible for the change in aerosol properties with time during the experiments, *i.e.* ageing. The results from the experiments performed using DEA, TEA and piperazine are only briefly described here, for a more extensive description see ANNEX D. An extended description of the EA low NO_x experiment is presented in the following section. It should be noted that in all experiments done at EUPHORE the relative humidity was considerably lower than typical atmospheric conditions, which could influence the results in several ways *e.g.* by changing the relative importance of the reaction pathways shown in Figure 5.1; most probably enhancing the rates of pathways 3 and 4.

5.2 Photo-oxidation of ethylamine under low NO_x conditions (03.06.2011)

Figure 5.2 depicts the evolution of the ethylamine, ozone, NO₂ and aerosol loading (total, organic and nitrate) during the experiment. EA and low NO_x were injected at 7:19 into the chamber; the canopy was opened at 7:49 and closed at 10:13. A maximum aerosol mass loading of approximately 65 μg/m³ was detected by the SMPS at 10:21, nearly 2½ h after the canopy was opened. Both 70 and 30 eV electron impact ionization energy data were analysed but for clarity only the 30 eV values are presented in Figure 5.2. The aerosol was composed of nitrate (blue), organic (green) and traces of water (light blue). The SMPS mass loadings were calculated using the number of particles and the derived effective density ($\rho = 1.3 \text{ g cm}^{-3}$) and are shown in red (line with squares). A discrepancy of about 12% between SMPS data and AMS at 30 eV was observed in this experiment. These discrepancies are important when the aerosol is not anymore the primary salt, since we did not have a valuable quantitative calibration for the reaction products.

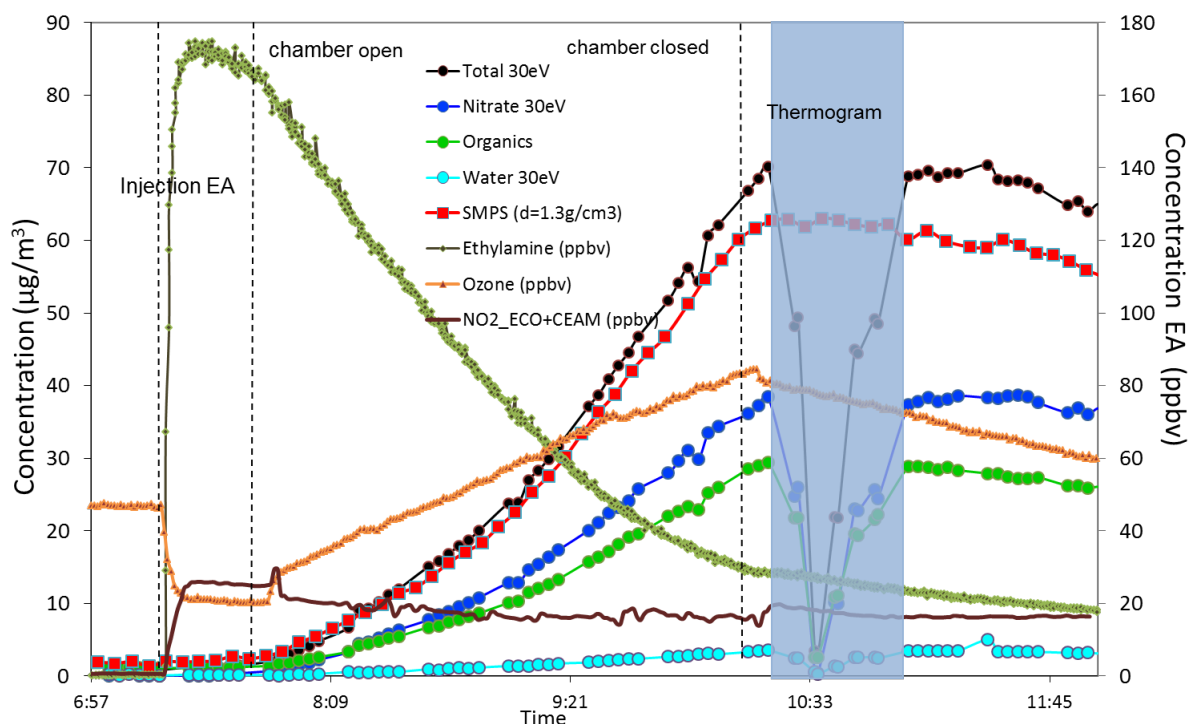


Figure 5.2. Temporal evolution of Ethylamine (green olive), ozone (orange), NO_2 (brown) concentrations and aerosol mass monitored by the SMPS (red squares) and AMS during the 2011.06.03 low NO_x experiment. AMS data: total aerosol (black dots), nitrate (blue dots), organic (green dots) and organic-water (light blue).

5.2.1 Aerosol Yield

Aerosol yield was calculated using PTR-MS gas phase values of the ethylamine and the aerosol loading given by the AMS. Figure 5.3 shows the yield as function of the time until the maximum aerosol yield was reached (at 10:21).

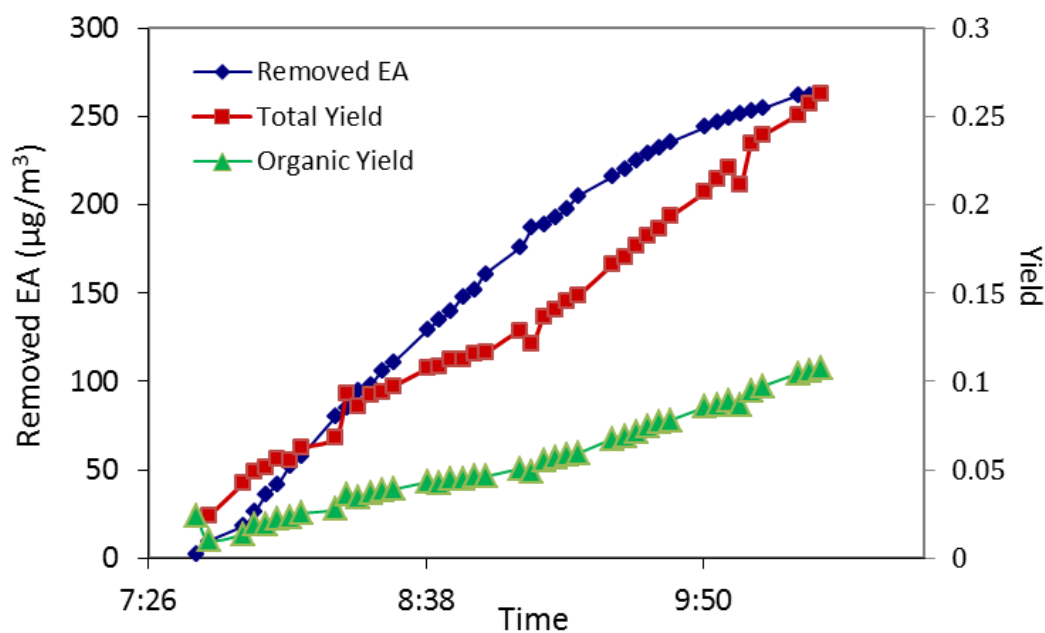


Figure 5.3. Mass yields (total and organic yield) calculated towards the removed EA from the gas phase.

The gas-to-particle conversion phase is driven by several processes (see Figure 5.1): in the case of the ethylamine photo-oxidation the acid-base reaction (path 1) is the most important process for aerosol formation and the primary aminium salt is by far the major product. The process is driven by protonation of the ethylamine by the HNO_3 available in the chamber and indirectly by NO_2 as HNO_3 precursor. The organic yield is calculated from the organic aerosol mass vs. the removed ethylamine mass from the chamber. The total yield considers the total mass of the aerosol and is also normalized to the mass of ethylamine converted, i.e. it does not account for NO_2 loss as the precursor to nitrate, which is a significant contributor to total aerosol mass.

5.2.2 Aerosol composition

The more significant fragments associated with primary aminium nitrate salt were CH_2N^+ (m/z 28.018), CH_4N^+ (m/z 30.034), $\text{C}_2\text{H}_3\text{N}^+$ (m/z 41.029), $\text{C}_2\text{H}_6\text{N}^+$ (m/z 44.049) and $\text{C}_2\text{H}_7\text{N}^+$ (m/z 45.061). The full list of the identified ion sum formulas is listed in Table 5.2. Some of the reaction products, however, give rise to the same fragment ions as the primary amine (CH_4N^+ , $\text{C}_2\text{H}_3\text{N}^+$ and $\text{C}_2\text{H}_6\text{N}^+$). Using reference spectra of synthesized DEANO_3 it was possible to discriminate the nitrate contribution to the primary amine salt and to the reaction products (Figure 5.4). The index “a” indicates the fraction of the fragment arising from the EANO_3 .

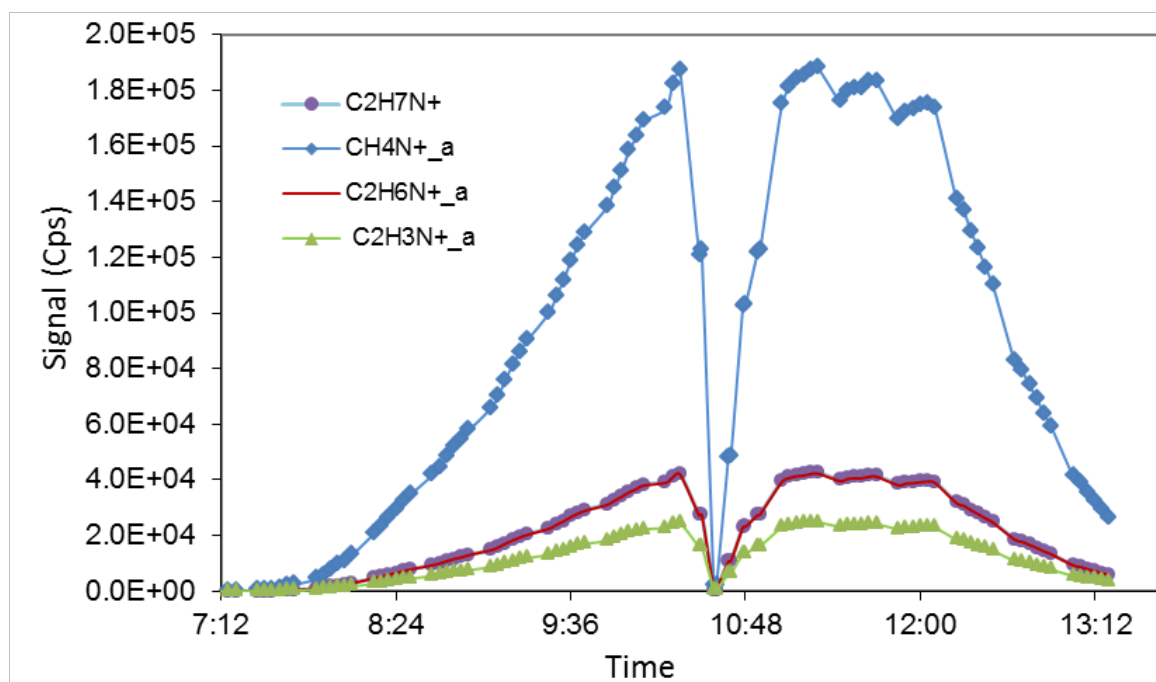


Figure 5.4. Major identified fragments associated with the organic fraction of the ethylaminium nitrate salt.

The reference mass spectrum of the EANO_3 salt is shown in Figure 5.5 together with a mass spectrum from the photo-oxidation experiment of EA under high- NO_x conditions. It is clearly seen that the fragments identified in the EANO_3 salt reference are also the major spectral features of the aerosol during the experiment. Using the most pronounced fragments identified in the ethylaminium nitrate reference (Figure 5.5 top panel) and using their ratio with respect to the nitrate signal in the EANO_3 reference it was possible to derive the amount of nitrate associated with the primary salt during the EA experiments (e.g. Figure 5.6). In the experiment shown in Figure 5.6 all nitrate is in the form of pure EANO_3 until around 9:30, when the EANO_3 contribution to the total nitrate decreases to around 80%.

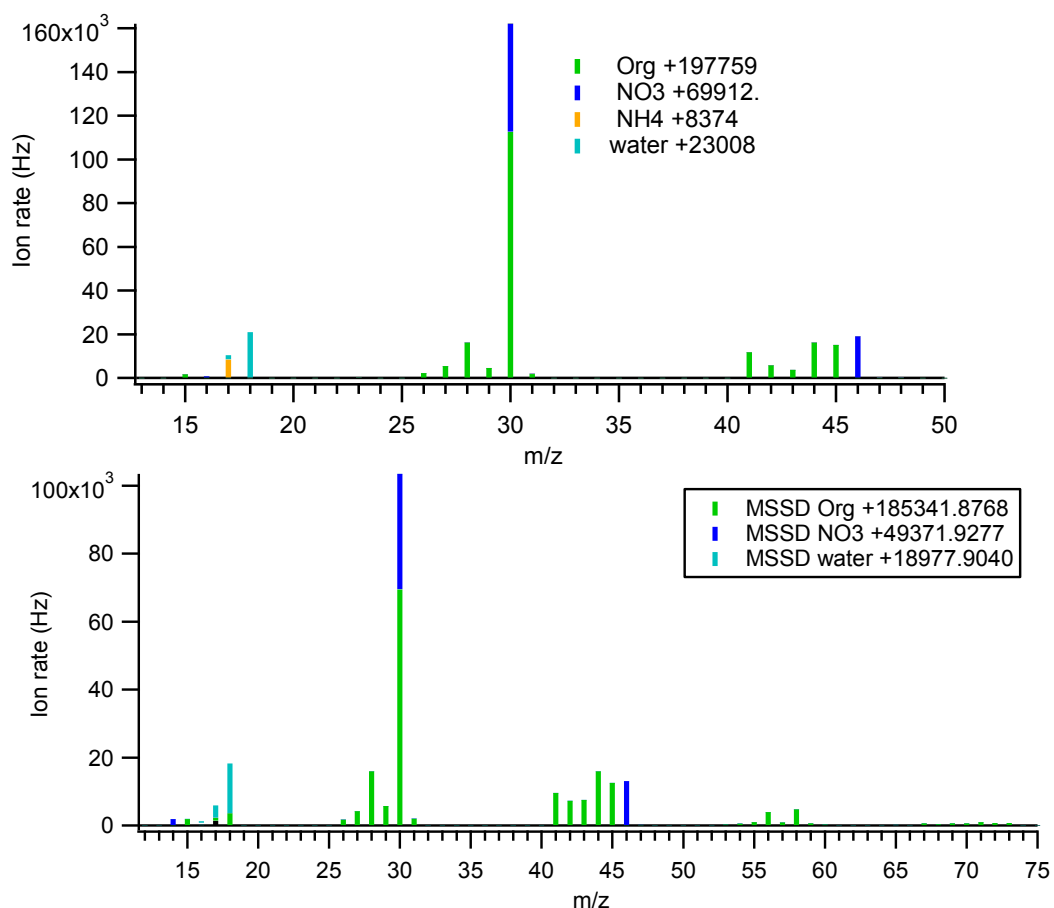


Figure 5.5. AMS spectra acquired at 30eV of the EANO₃ reference (top panel) and the aerosol during the photo-oxidation of EA of the 2011/06/03 at 10h06 (bottom panel).

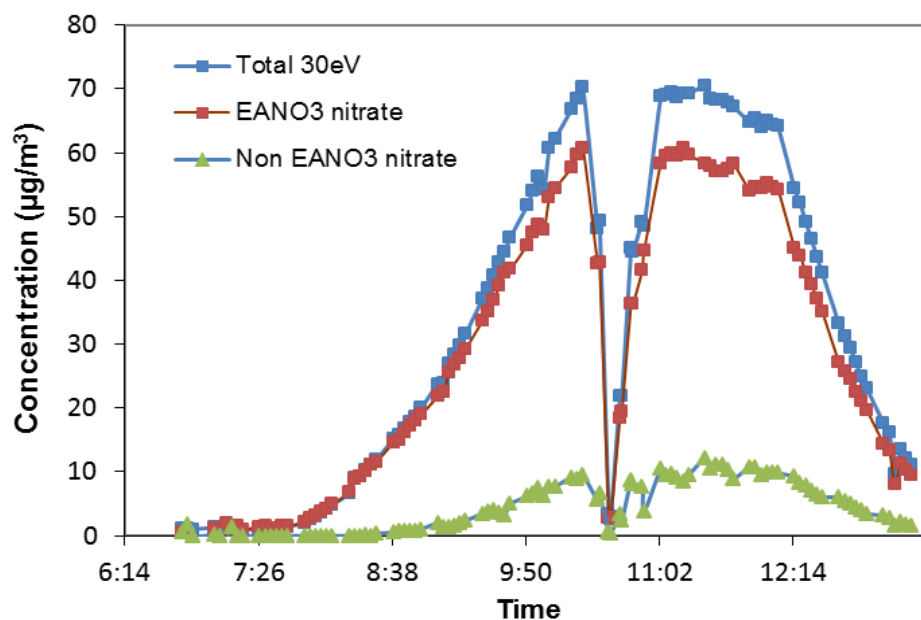


Figure 5.6. Measured total nitrate (blue line) and nitrate associated to the ethylammonium salt (brown line), the remaining nitrate is associated with the non-EA organic fraction.

Figure 5.7 shows the other organic fragments detected that do not belong to the primary salt ethylammonium nitrate, during the photo-oxidation of EA. As we can see, two family of fragments are observed: one group of fragments at higher m/z than the primary amine, probably *N*-ethyl methan-

imine and *N*-methyl methanimine) resulting from condensation reactions (see Table 5.2), and another group at lower m/z , such as $C_2H_3O^+$ and CO_2^+ , which were attributed to the photo-oxidation process.

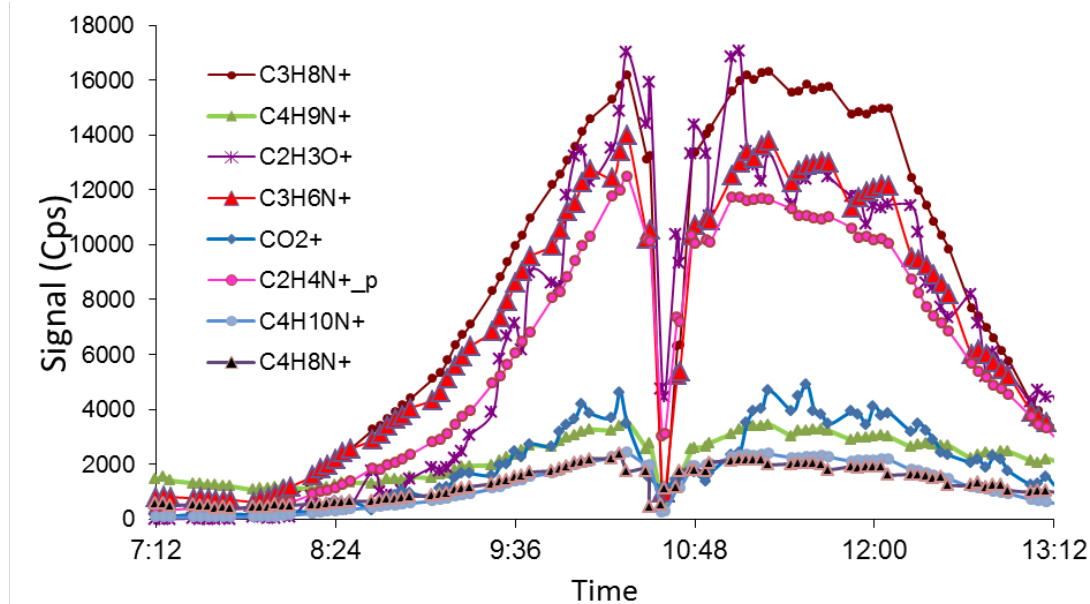


Figure 5.7. Most abundant fragments associated to the non-ethylammonium organic fraction.

Table 5.2 and Table 5.3 list major ion signals and compounds detected in the aerosol phase during photo-oxidation of ethylamine at low NO_x conditions. Generally the online system (AMS, Table 5.2) detects smaller ion fragments compared to the offline analysis (qTOF-MS, Table 5.3), because of differences in ionization energy and mass detection. The results showed fragments of ethylamine in the aerosol as well as its oxidation products. In addition, larger molecules and fragments from condensation reactions and heterogeneous processes were observed.

Table 5.2. Major ion signals observed in the particle phase during the photo-oxidation of the ethylamine May 2011 (at 30eV by on-line AMS data).

Ion sum formula	2011.06.02 Low NO_x	2011.06.03 Low NO_x	Comments
CH_2N^+ *			Mainly reaction product
CH_3N^+	29.029	29.030	Mainly reaction product
NO^+	29.997	29.997	Nitrate
CH_4N^+	30.034	30.034	Ethylamine + product
$C_2H_3N^+$	41.029	41.029	Ethylamine + product
$C_2H_4N^+$	42.035	42.034	Ethylamine + product
$C_2H_3O^+$	43.018	43.018	Oxidation product
CO_2^+	43.992	43.992	Minor oxidation product
$C_2H_4O^+$	44.025	44.025	Oxidation product
$C_2H_6N^+$	44.049	44.049	Ethylamine
$C_2H_7N^+$	45.060	45.061	Ethylamine
NO_2^+	45.993	45.993	Nitrate
$C_3H_6N^+$	56.054	56.054	<i>N</i> -methyl ethanimine [#]
$C_3H_8N^+$	58.055	58.055	<i>N</i> -methyl ethanimine [#]
$C_4H_8N^+$	70.067	70.067	<i>N</i> -ethyl ethanimine [#]
$C_4H_{10}N^+$	72.089	72.089	<i>N</i> -ethyl ethanimine [#]

* $CH_3CH=NH + CH_3NH_2 \rightarrow CH_3CH=NCH_3 + NH_3$; $CH_3CH=NH + CH_3CH_2NH_2 \rightarrow CH_3CH=NCH_2CH_3 + NH_3$
[#] Contribution calculated by subtracting the contribution of N_2^+ from the air, its exact m/z cannot be determined.

Table 5.3. Major compounds detected in ethylamine photo-oxidation by off-line qTOF-MS analysis.

2011.06.02 low NO _x m/z+ corr	2011.06.03 low NO _x m/z+ corr	Compound molecular mass	Suggested molecular formula	Suggested molecular mass
85.12	85.12	84.11	-	
97.12		96.11	-	
	99.10	98.10	C ₆ H ₁₂ N	98.10
107.11		106.10	-	-
	107.13	106.12	-	
111.14	111.14	110.13	-	
112.11	112.11	111.10	C ₆ H ₁₁ N ₂	111.09
125.14		124.13	-	
127.05		126.04	C ₅ H ₆ N ₂ O ₂	126.04

5.2.3 Thermal properties and ageing

In the VTDMA system, an increase in volume fraction remaining indicates that the particles are becoming less volatile i.e. less mass is evaporating when the temperature is increased. In a similar way as for DEA (low-NO_x), during TEA (low and high-NO_x) experiments a decrease in volatility i.e. an increase in VFR was observed with time in the EA experiment. This “ageing” was observed under both low and high NO_x conditions.

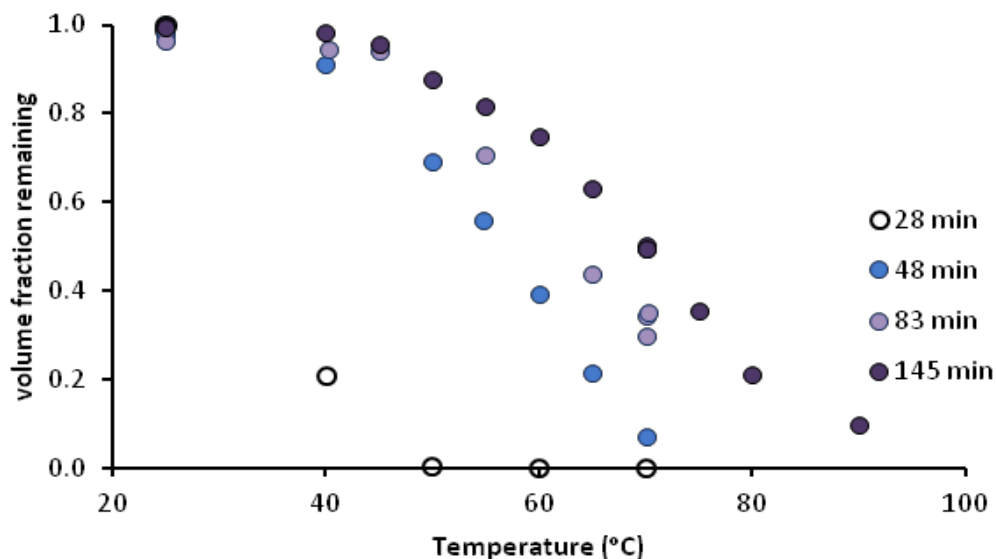


Figure 5.8. The volume fraction remaining at selected temperatures for EA particles in a low-NO_x experiment (2011-06-03), samples were collected at four times after the opening of the canopy.

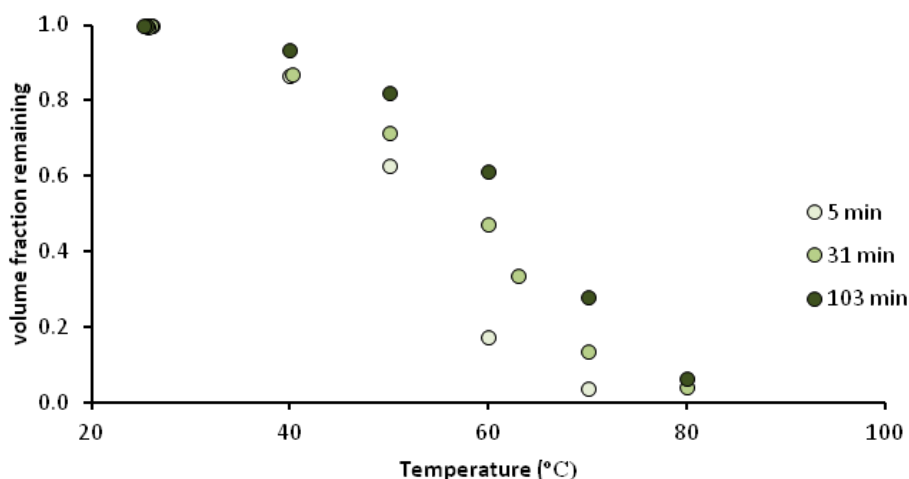


Figure 5.9. The volume fraction remaining (VFR) at selected temperatures for EA particles in a high- NO_x experiment (2011-03-25), samples were collected at three times after the opening of the canopy.

In both the experiments illustrated in Figure 5.8 and Figure 5.9 the volume fraction remaining increases significantly with time. This behaviour apparently contradicts the results from the aerosol analysis, which state that the large majority of the aerosol is EANO_3 . However, as shown in Figure 5.5, Figure 5.6 and in Table 5.3, oxygenated fragments and some reaction products with higher molecular weight than EA were observed to increase with time. Figure 5.10 shows the thermogram of a selected ensemble of ion fragments, which are compared to the major ion signal of the amine ($\text{C}_2\text{H}_7\text{N}^+$). The thermogram indicates a reduced volatility for the ion signal assigned to CO_2^+ , $\text{C}_2\text{H}_3\text{O}^+$ and $\text{C}_4\text{H}_9\text{N}^+$ and even if they represent a small fraction of the total aerosol their presence seems to radically change the aerosol volatility.

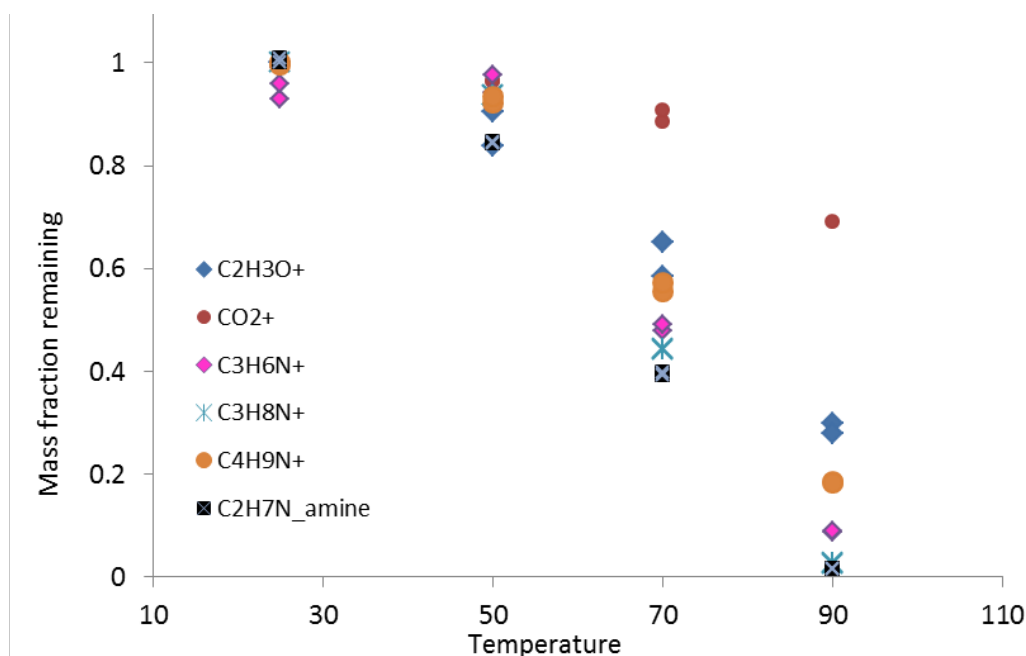


Figure 5.10. The mass fraction remaining (MFR) at selected temperatures for EA particles in a low- NO_x experiment (2011.06.03). The AMS thermogram was taken between 10:29 and 10:54.

These findings are in line with earlier observations done with the VTDMA. It is clear that even small changes in the chemical composition of aerosol can have a strong effect on the evaporation rate i.e. the volatility. Organic compounds that condense on the surface of the salt aerosol could possibly slow down the evaporation rate and make the particles less volatile. Oxidized organic compounds

can in some cases act as surfactants. This would concentrate them on the surface of the particle possibly shielding the more volatile aerosol constituents. The experiments were performed at low RH and it is possible that the initially formed aminium nitrate particles were solid or at least highly viscous, even in this case the organic matter formed later in the experiment would end up on the surface of the particles.

5.2.4 Atmospheric implications

The amines examined in this work are well known and have been identified in ambient aerosol samples in many different environments, *e.g.* rural, urban and marine.^{85,87-90} The processes shown in Figure 5.1 might also occur in the atmosphere but some will be more or less important compared to in the studied experiments. Generally, a polluted atmosphere contains acidic gas phase species such as H₂SO₄, HCl and HNO₃ that may react with the amines. When the amines are released into the atmosphere, particles will predominantly be formed via salt formation as described in Figure 5.1, path 1.

In a plume, salt formation from amines will necessarily compete with NH₃. The process will depend on the available ammonia concentration and the possibility of atmospheric transformation of the amine salt by ammonia exchange. The exchange of the amine with ammonia is believed to take place with amines having dissociation constants for the primary aminium nitrate (K_p) equal to or larger than that for ammonium nitrate ($4.48 \times 10^{-7} \text{ Pa}^2$),⁴⁷ see Table 5.1. Among the compounds studied in this work the lowest K_p value was found for the DEA-nitrate.⁸⁶ The ammonia exchange could be evaluated for the photo-oxidation of ethylamine under low NO_x conditions (2011.06.03) where as much as 35 ppbv of ammonia were produced, and even when ethylamine and ammonia were present at similar concentrations, only trace levels of ammonium ($0.7 \mu\text{g m}^{-3}$) were observed in the aerosol (see ANNEX D for more information). In a plume emitted into the real atmosphere, the concentration of ammonia will most probably be 10 to 100 times larger than those of amines and exchange cannot be neglected even for aminium salts with lower K_p than ammonium nitrate.

Once the primary aminium salt has been formed through an acid-base reaction, the aerosol could partly evaporate upon dilution. The fresh aerosol is semi-volatile for the first few hours. The primary amine salt contribution (path 1) will then decrease while the oxidation products (2a) and secondary amine salt (2b) fractions will increase. The volatility of the aerosol was also studied in some dilution experiments (during flushing with clean air of the EUPHORE chamber): Aerosol formed during photo-oxidative degradation of piperazine and TEA aerosol was not affected by this dilution while the aerosol formed during from EA and DEA did partly evaporate (more information in ANNEX D). The evaporated amines could subsequently react with available radicals such as OH yielding products with lower volatility that can partition into the condensed phase (2a) of the aerosol. The amine oxidation product has a high probability to also be basic and take part in secondary salt formation (2b). This additional condensation of secondary organic compounds could possibly shield the primary salt core of the particle from further exchange, at least for a limited amount of time⁴⁷. Water may play a crucial role, generally enhancing aerosol formation. We do expect the same will occur during photo-oxidation of amines.

The experiments described herein have shown that ageing is an important process; it will reduce the volatility of the particles and increase their atmospheric lifetime. Recent publications report that amines released to the atmosphere can also take part in new particle formation and increase both nucleation and growth rates.^{83,85}

The additional processes shown in Figure 5.1 are surface and bulk phase reactions that will modify the aerosol properties. The ADA campaign investigated amine photo-oxidation in a dry atmosphere, while in a plume the partial pressure of water will be much higher. Water may play a crucial role, since high humidity will enhance aerosol formation and solubility of oxidants and amine precursors in the aerosol phase will also be affected.

6. Literature

1. Becker, K. H. *The European Photoreactor EUPHORE, Design and Technical Development of the European Photoreactor and First Experimental Results, Final Report of the EC-Project Contract EV5V-CT92-0059*; 1996.
2. Magneron, I.; Thevenet, R.; Mellouki, A.; Le Bras, G.; Moortgat, G. K.; Wirtz, K., A study of the photolysis and OH-initiated oxidation of acrolein and trans-crotonaldehyde. *J. Phys. Chem. A* **2002**, *106* (11), 2526-2537.
3. Volkamer, R.; Platt, U.; Wirtz, K., Primary and secondary glyoxal formation from aromatics: Experimental evidence for the bicycloalkyl-radical pathway from benzene, toluene, and p-xylene. *J. Phys. Chem. A* **2001**, *105* (33), 7865-7874.
4. Klotz, B.; Sorensen, S.; Barnes, I.; Becker, K. H.; Etkorn, T.; Volkamer, R.; Platt, U.; Wirtz, K.; Martin-Reviejo, M., Atmospheric oxidation of toluene in a large-volume outdoor photoreactor: In situ determination of ring-retaining product yields. *J. Phys. Chem. A* **1998**, *102* (50), 10289-10299.
5. Wenger, J. C.; Le Calve, S.; Sidebottom, H. W.; Wirtz, K.; Reviejo, M. M.; Franklin, J. A., Photolysis of Chloral under Atmospheric Conditions. *Environmental Science and Technology* **2004**, *38* (3), 831-837.
6. Nielsen, C. J.; D'Anna, B.; Karl, M.; Aursnes, M.; Boreave, A.; Bossi, R.; Bunkan, A. J. C.; Glasius, M.; Hansen, A.-M. K.; Hallquist, M.; Kristensen, K.; Mikoviny, T.; Maguta, M. M.; Müller, M.; Nguyen, Q.; Westerlund, J.; Salo, K.; Skov, H.; Stenstrøm, Y.; Wisthaler, A. *Summary Report: Photo-oxidation of Methylamine, Dimethylamine and Trimethylamine. Climit project no. 201604; NILU OR 2/2011; NILU: 2011.*
7. Jordan, A.; Haidacher, S.; Hanel, G.; Hartungen, E.; Mark, L.; Seehauser, H.; Schottkowsky, R.; Sulzer, P.; Mark, T. D., A high resolution and high sensitivity proton-transfer-reaction time-of-flight mass spectrometer (PTR-TOF-MS). *International Journal of Mass Spectrometry* **2009**, *286* (2-3), 122-128.
8. Müller, M.; Graus, M.; Ruuskanen, T. M.; Schnitzhofer, R.; Bamberger, I.; Kaser, L.; Titzmann, T.; H⁺rnagl, L.; Wohlfahrt, G.; Karl, T.; Hansel, A., First eddy covariance flux measurements by PTR-TOF. *Atmos. Meas. Tech.* **2010**, *3* (2), 387-395.
9. Müller, M.; George, C.; D'Anna, B., Enhanced spectral analysis of C-TOF Aerosol Mass Spectrometer data: Iterative residual analysis and cumulative peak fitting. *International Journal of Mass Spectrometry* **2011**, *306* (1), 1-8.
10. Jonsson, A. M.; Hallquist, M.; Saathoff, H., Volatility of secondary organic aerosols from the ozone initiated oxidation of alpha-pinene and limonene. *Journal of Aerosol Science* **2007**, *38*, 843-852.
11. Salo, K.; Jonsson, A. M.; Andersson, P. U.; Hallquist, M., Aerosol Volatility and Enthalpy of Sublimation of Carboxylic Acids. *J. Phys. Chem. A* **2010**, *114* (13), 4586-4594.
12. Kalberer, M.; Paulsen, D.; Sax, M.; Steinbacher, M.; Dommen, J.; Prevot, A. S. H.; Fisseha, R.; Weingartner, E.; Frankevich, V.; Zenobi, R.; Baltensperger, U., Identification of polymers as major components of atmospheric organic aerosols. *Science* **2004**, *303* (5664), 1659-1662.
13. Offenberg, J. H.; Kleindienst, T. E.; Jaoui, M.; Lewandowski, M.; Edney, E. O., Thermal properties of secondary organic aerosols. *Geophysical Research Letters* **2006**, *33* (3).
14. An, W. J.; Pathak, R. K.; Lee, B. H.; Pandis, S. N., Aerosol volatility measurement using an improved thermodenuder: Application to secondary organic aerosol. *Journal of Aerosol Science* **2007**, *38* (3), 305-314.
15. Drewnick, F.; Hings, S.; DeCarlo, P.; Jayne, J.; Gonin, M.; Fuhrer, K.; Weimer, S.; Jimenez, J.; Demerjian, K.; Borrmann, S.; Worsnop, D., A New Time-of-Flight Aerosol Mass Spectrometer (TOF-AMS) - Instrument Description and First Field Deployment. *Aerosol Science and Technology* **2005**, *39* (7), 637-658.
16. Rothman, L. S.; Gordon, I. E.; Barbe, A.; ChrisBenner, D.; Bernath, P. F.; Birk, M.; Boudon, V.; Brown, L. R.; Campargue, A.; Champion, J.-P.; Chance, K.; Coudert, L. H.; Danaj, V.; Devi, V. M.; Fally, S.; Flaud, J.-M.; Gamache, R. R.; Goldman, A.; Jacquemart, D.; Kleiner, I.; Lacombe, N.; Lafferty, W. J.; Mandin, J.-Y.; Massie, S. T.; Mikhailenko, S. N.; Miller, C. E.; Moazzen-Ahmadi, N.; Naumenko, O. V.; Nikitin, A. V.; Orphal, J.; Perevalov, V. I.; Perrin, A.; Predoi-Cross, A.; Rinsland, C. P.; Rotger, M.; Simeckova, M.; Smith, M. A. H.; Sung, K.; Tashkun, S. A.; Tennyson, J.; Toth, R. A.; Vandaele, A. C.; VanderAuwera, J., The HITRAN 2008 molecular spectroscopic database. *Journal of Quantitative Spectroscopy & Radiative Transfer* **2009**, *110*, 533-572.
17. Atkinson, R.; Perry, R. A.; Pitts, J. N., Jr., Rate constants for the reactions of the hydroxyl radical with dimethylamine, trimethylamine, and ethylamine over the temperature range 298-426 K. *Journal of Chemical Physics* **1978**, *68* (4), 1850-3.

18. Carl, S. A.; Crowley, J. N., Sequential two (blue) photon absorption by NO₂ in the presence of H₂ as a source of OH in pulsed photolysis kinetic studies: Rate constants for reaction of OH with CH₃NH₂, (CH₃)₂NH, (CH₃)₃N, and C₂H₅NH₂ at 295 K. *J. Phys. Chem. A* **1998**, *102* (42), 8131-8141.
19. Pedersen, S., Private communication. 2011.
20. Atkinson, R.; Perry, R. A.; Pitts, J. N., Jr., Rate constants for the reaction of the hydroxyl radical with methanethiol and methylamine over the temperature range 299-426 K. *Journal of Chemical Physics* **1977**, *66* (4), 1578-81.
21. Karl, M.; Dye, C.; Schmidbauer, N.; Wisthaler, A.; Mikoviny, T.; D'Anna, B.; Müller, M.; Borrás, E.; Clemente, E.; Muñoz, A.; Porras, R.; Ródenas, M.; Vázquez, M.; Brauers, T., Study of OH-initiated degradation of 2-aminoethanol. *Atmos. Chem. Phys.* **2012**, *12*, 1881-1901.
22. Gorse, R. A., Jr.; Lii, R. R.; Saunders, B. B., Hydroxyl radical reactivity with diethylhydroxylamine. *Science (Washington, DC, United States)* **1977**, *197* (4311), 1365-7.
23. Harris, G. W.; Pitts, J. N., Rates of Reaction of Hydroxyl Radicals with 2-(Dimethylamino)Ethanol and 2-Amino-2-Methyl-1-Propanol in the Gas-Phase at 300 + 2 K. *Environmental Science & Technology* **1983**, *17* (1), 50-51.
24. Anderson, L. G.; Stephens, R. D., Kinetics of the Reaction of Hydroxyl Radicals with 2-(Dimethylamino)Ethanol from 234-364 K. *International Journal of Chemical Kinetics* **1988**, *20* (2), 103-110.
25. Koch, R.; Kruger, H. U.; Elend, M.; Palm, W. U.; Zetzsch, C., Rate constants for the gas-phase reaction of OH with amines: tert-Butyl amine, 2,2,2-trifluoroethyl amine, and 1,4-diazabicyclo[2.2.2]octane. *International Journal of Chemical Kinetics* **1996**, *28* (11), 807-815.
26. Atkinson, R., Kinetics and Mechanisms of the Gas-Phase Reactions of the Hydroxyl Radical with Organic Compounds under Atmospheric Conditions. *Chemical Reviews* **1986**, *86* (1), 69-201.
27. Aschmann, S. M.; Long, W. D.; Atkinson, R., Temperature-dependent rate constants for the gas-phase reactions of OH radicals with 1,3,5-trimethylbenzene, triethyl phosphate, and a series of alkylphosphonates. *J. Phys. Chem. A* **2006**, *110* (23), 7393-7400.
28. Atkinson, R., A Structure-Activity Relationship for the Estimation of Rate Constants for the Gas-Phase Reactions of OH Radicals with Organic-Compounds. *International Journal of Chemical Kinetics* **1987**, *19* (9), 799-828.
29. Kwok, E. S. C.; Atkinson, R., Estimation of Hydroxyl Radical Reaction-Rate Constants for Gas-Phase Organic-Compounds Using a Structure-Reactivity Relationship - an Update. *Atmos. Environ.* **1995**, *29* (14), 1685-1695.
30. D'Anna, B.; Andresen, W.; Gefen, Z.; Nielsen, C. J., Kinetic study of OH and NO₃ radical reactions with 14 aliphatic aldehydes. *Physical Chemistry Chemical Physics* **2001**, *3* (15), 3057-3063.
31. Atkinson, R.; Baulch, D. L.; Cox, R. A.; Crowley, J. N.; Hampson, R. F.; Hynes, R. G.; Jenkin, M. E.; Rossi, M. J.; Troe, J., Evaluated kinetic and photochemical data for atmospheric chemistry: Volume II - gas phase reactions of organic species. *Atmospheric Chemistry and Physics* **2006**, *6*, 3625-4055.
32. Tuazon, E. C.; Carter, W. P. L.; Atkinson, R.; Winer, A. M.; Pitts, J. N., Atmospheric Reactions of N-Nitrosodimethylamine and Dimethylnitramine. *Environmental Science & Technology* **1984**, *18* (1), 49-54.
33. Picquet, B.; Heroux, S.; Chebbi, A.; Doussin, J. F.; Durand-Jolibois, R.; Monod, A.; Loirat, H.; Carlier, P., Kinetics of the reactions of OH radicals with some oxygenated volatile organic compounds under simulated atmospheric conditions. *International Journal of Chemical Kinetics* **1998**, *30* (11), 839-847.
34. Campbell, I. M.; Parkinson, P. E., Rate constants for reactions of hydroxyl radicals with ester vapors at 292 K. *Chemical Physics Letters* **1978**, *53* (2), 385-387.
35. Wallington, T. J.; Dagaut, P.; Liu, R. H.; Kurylo, M. J., The gas-phase reactions of hydroxyl radicals with a series of esters over the temperature-range 240-440 K. *International Journal of Chemical Kinetics* **1988**, *20* (2), 177-186.
36. El Boudali, A.; LeCalve, S.; LeBras, G.; Mellouki, A., Kinetic studies of OH reactions with a series of acetates. *Journal of Physical Chemistry* **1996**, *100* (30), 12364-12368.
37. Frisch, M. J.; Trucks, G. W.; Schlegel, H. B.; Scuseria, G. E.; Robb, M. A.; Cheeseman, J. R.; Montgomery, J., J. A.; Vreven, T.; Kudin, K. N.; Burant, J. C.; Millam, J. M.; Iyengar, S. S.; Tomasi, J.; Barone, V.; Mennucci, B.; Cossi, M.; Scalmani, G.; Rega, N.; Petersson, G. A.; Nakatsuji, H.; Hada, M.; Ehara, M.; Toyota, K.; Fukuda, R.; Hasegawa, J.; Ishida, M.; Nakajima, T.; Honda, Y.; Kitao, O.; Nakai, H.; Klene, M.; Li, X.; Knox, J. E.; Hratchian, H. P.; Cross, J. B.; Bakken, V.; Adamo, C.; Jaramillo, J.; Gomperts, R.; Stratmann, R. E.; Yazyev, O.; Austin, A. J.; Cammi, R.; Pomelli, C.; Ochterski, J. W.; Ayala, P. Y.; Morokuma, K.; Voth, G. A.; Salvador, P.; Dannenberg, J. J.; Zakrzewski, V. G.; Dapprich, S.; Daniels, A. D.; Strain, M. C.; Farkas, O.; Malick, D. K.; Rabuck, A. D.; Raghavachari, K.; Foresman, J. B.; Ortiz, J. V.; Cui, Q.; Baboul, A. G.; Clifford, S.; Cioslowski, J.; Stefanov, B. B.; Liu, G.; Liashenko, A.; Piskorz, P.; Komaromi, I.; Martin, R. L.; Fox, D. J.; Keith,

- T.; Al-Laham, M. A.; Peng, C. Y.; Nanayakkara, A.; Challacombe, M.; Gill, P. M. W.; Johnson, B.; Chen, W.; Wong, M. W.; Gonzalez, C.; Pople, J. A. *Gaussian 03, Revision C.02*, Gaussian, Inc., Wallingford CT: 2004.
38. Curtiss, L. A.; Raghavachari, K.; Redfern, P. C.; Rassolov, V.; Pople, J. A., Gaussian-3 (G3) theory for molecules containing first and second-row atoms. *Journal of Chemical Physics* **1998**, *109* (18), 7764-7776.
 39. Lindley, C. R. C.; Calvert, J. G.; Shaw, J. H., Rate Studies of the Reactions of the (CH₃)₂N Radical with O₂, NO, and NO₂. *Chemical Physics Letters* **1979**, *67* (1), 57-62.
 40. Wolke, R.; Knoth, O., Implicit-explicit Runge-Kutta methods applied to atmospheric chemistry-transport modelling. *Environmental Modelling & Software* **2000**, *15* (6-7), 711-719.
 41. Wolke, R.; Knoth, O.; Hellmuth, O.; Schroder, W.; Renner, E., *The parallel model system LM-MUSCAT for chemistry-transport simulations: Coupling scheme, parallelization and applications*. 2004; Vol. 13, p 363-369.
 42. Tønnesen, D. A., *Overvåking av luftkvalitet ved StatoilHydro Mongstad i perioden november 2006-oktober 2007*. Norsk institutt for luftforskning: Lillestrøm, 2008; p 68 s.
 43. Nielsen, C. J.; D'Anna, B.; Dye, C.; George, C.; Graus, M.; Hansel, A.; Karl, M.; King, S.; Musabila, M.; Müller, M.; Schmidbauer, N.; Stenstrøm, Y.; Wisthaler, A., *Atmospheric Degradation of Amines (ADA). Summary Report: Gas phase photo-oxidation of 2-aminoethanol (MEA)*. NILU: 2010.
 44. Atkinson, R.; Pitts, J. J. N., Kinetics of the reactions of O(³P) atoms with the amines CH₃NH₂, C₂H₅NH₂, (CH₃)₂NH, and (CH₃)₃N over the temperature range 298-440 K. *The Journal of Chemical Physics* **1978**, *68* (3), 911-915.
 45. Slagle, I. R.; Dudich, J. F.; Gutman, D., Identification of reactive routes in the reactions of oxygen atoms with methylamine, dimethylamine, trimethylamine, ethylamine, diethylamine, and triethylamine. *The Journal of Physical Chemistry* **1979**, *83* (24), 3065-3070.
 46. Galano, A.; Alvarez-Idaboy, J. R., Branching Ratios of Aliphatic Amines + OH Gas-Phase Reactions: A Variational Transition-State Theory Study. *Journal of Chemical Theory and Computation* **2008**, *4* (2), 322-327.
 47. Murphy, S. M.; Sorooshian, A.; Kroll, J. H.; Ng, N. L.; Chhabra, P.; Tong, C.; Surratt, J. D.; Knipping, E.; Flagan, R. C.; Seinfeld, J. H., Secondary aerosol formation from atmospheric reactions of aliphatic amines. *Atmospheric Chemistry and Physics* **2007**, *7* (9), 2313-2337.
 48. Layer, R. W., Chemistry of Imines. *Chemical Reviews* **1963**, *63* (5), 489-510.
 49. Mascavage, L. M.; Sonnet, P. E.; Dalton, D. R., On the surface-catalyzed reaction between the gases 2,2-dimethylpropanal and methanamine. Formation of active-site imines. *Journal of Organic Chemistry* **2006**, *71* (9), 3435-3443.
 50. Pitts, J. N.; Grosjean, D.; Vancauwenberghe, K.; Schmid, J. P.; Fitz, D. R., Photo-Oxidation of Aliphatic-Amines under Simulated Atmospheric Conditions - Formation of Nitrosamines, Nitramines, Amides, and Photo-Chemical Oxidant. *Environmental Science & Technology* **1978**, *12* (8), 946-953.
 51. Tuazon, E. C.; Atkinson, R.; Aschmann, S. M.; Arey, J., Kinetics and Products of the Gas-Phase Reactions of O₃ with Amines and Related-Compounds. *Research on Chemical Intermediates* **1994**, *20* (3-5), 303-320.
 52. Nielsen, C. J.; D'Anna, B.; Aursnes, M.; Boreave, A.; Bossi, R.; Dye, C.; Hallquist, M.; Karl, M.; Mikoviny, T.; Maguta, M. M.; Müller, M.; Skov, H.; Salo, K.; Stenstrøm, Y.; Wisthaler, A. *Atmospheric Degradation of Amines (ADA) Progress Report June 2010: Gas Phase Photo-Oxidation of Methylamine, Dimethylamine and Trimethylamine*; 2010.
 53. Nielsen, C. J.; D'Anna, B.; Dye, C.; Graus, M.; Karl, M.; King, S.; Maguto, M. M.; Muller, M.; Schmidbauer, N.; Stenstroem, Y.; Wisthaler, A.; Pedersen, S., Atmospheric chemistry of 2-aminoethanol (MEA). *Energy Procedia* **2011**, *4* (Copyright (C) 2012 American Chemical Society (ACS). All Rights Reserved.), 2245-2252.
 54. Gai, Y.-B.; Ge, M.-F.; Wang, W.-G., Rate Constants for the Gas Phase Reactions of Ozone with Diethylamine and Triethylamine. *Acta Phys.-Chim. Sin.* **2010**, *26* (7), 1768-1772.
 55. Grosjean, D., Atmospheric chemistry of toxic contaminants. 6. Nitrosamines: dialkyl nitrosamines and nitrosomorpholine. *Journal of the Air & Waste Management Association (1990-1992)* **1991**, *41* (3), 306-11.
 56. Price, D. J. Field and Smog Chamber Studies of Agricultural Emissions and Reaction Products. Utah State University, 2010.
 57. Cabañas Galan, B., (Universidad de Castilla-La Mancha, Spain), *To be published*. **2012**.
 58. Angelino, S.; Suess, D. T.; Prather, K. A., Formation of aerosol particles from reactions of secondary and tertiary alkylamines: Characterization by aerosol time-of-flight mass spectrometry. *Environmental Science & Technology* **2001**, *35* (15), 3130-3138.

59. Erupe, M. E.; Price, D. J.; Silva, P. J.; Malloy, Q. G. J.; Qi, L.; Warren, B.; Cocker lli, D. R., Secondary organic aerosol formation from reaction of tertiary amines with nitrate radical. *Atmos. Chem. Phys. Discuss.* **2008**, *8* (4), 16585-16608.
60. Bråthen, H. B.; Bunkan, A. J.; Bache-Andreassen, L.; Solimannejad, M.; Nielsen, C. J. *Final report on a theoretical study on the atmospheric degradation of selected amines*; 978-82-425-2046-3; NILU: 2008.
61. Koch, R.; Palm, W. U.; Zetzsch, C., First rate constants for reactions of OH radicals with amides. *International Journal of Chemical Kinetics* **1997**, *29* (2), 81-87.
62. Solignac, G.; Mellouki, A.; Le Bras, G.; Barnes, I.; Benter, T., Kinetics of the OH and Cl reactions with N-methylformamide, N,N-dimethylformamide and N,N-dimethylacetamide. *J. Photochem. Photobiol. A-Chem.* **2005**, *176* (1-3), 136-142.
63. Aschmann, S. M.; Atkinson, R., Atmospheric chemistry of 1-methyl-2-pyrrolidinone. *Atmos. Environ.* **1999**, *33* (4), 591-599.
64. Barnes, I.; Solignac, G.; Mellouki, A.; Becker, K., Aspects of the Atmospheric Chemistry of Amides. *ChemPhysChem* **2010**, *11* (18), 3844-3857.
65. El Dib, G.; Chakir, A., Temperature-dependence study of the gas-phase reactions of atmospheric NO₃ radicals with a series of amides. *Atmos. Environ.* **2007**, *41*, 5887-5896.
66. Atkinson, R.; Baulch, D. L.; Cox, R. A.; Crowley, J. N.; Hampson, R. F.; Hynes, R. G.; Jenkin, M. E.; Rossi, M. J.; Troe, J., Evaluated kinetic and photochemical data for atmospheric chemistry: Volume I - gas phase reactions of O(x), HO(x), NO(x) and SO(x) species. *Atmospheric Chemistry and Physics* **2004**, *4*, 1461-1738.
67. Geiger, G.; Stafast, H.; Bruehlmann, U.; Huber, J. R., Photodissociation of dimethylnitrosamine. *Chemical Physics Letters* **1981**, *79* (3), 521-524.
68. Geiger, G.; Huber, J. R., Photolysis of Dimethylnitrosamine in the Gas-Phase. *Helvetica Chimica Acta* **1981**, *64* (4), 989-995.
69. Atkinson, R., Kinetics of the gas-phase reactions of OH radicals with alkanes and cycloalkanes. *Atmospheric Chemistry and Physics* **2003**, *3*, 2233-2307.
70. Dagaut, P.; Wallington, T. J.; Liu, R. Z.; Kurylo, M. J., A kinetics investigation of the gas-phase reactions of OH radicals with cyclic-ketones and -diones - mechanistic insights. *Journal of Physical Chemistry* **1988**, *92* (15), 4375-4377.
71. Aschmann, S. M.; Chew, A. A.; Arey, J.; Atkinson, R., Products of the Gas-Phase Reaction of OH Radicals with Cyclohexane: Reactions of the Cyclohexoxy Radical. *The Journal of Physical Chemistry A* **1997**, *101* (43), 8042-8048.
72. Bamford, C. H., A study of the photolysis of organic nitrogen compounds - Part I Dimethyl- and diethyl-nitrosoamines. *Journal of the Chemical Society* **1939**, 12-17.
73. Lazarou, Y. G.; Kambanis, K. G.; Papagiannakopoulos, P., Gas-Phase Reactions of (CH₃)₂N Radicals with NO and NO₂. *Journal of Physical Chemistry* **1994**, *98* (8), 2110-2115.
74. Su, F.; Calvert, J. G.; Shaw, J. H., Mechanism of the photo-oxidation of gaseous formaldehyde. *Journal of Physical Chemistry* **1979**, *83* (25), 3185-3191.
75. Burrows, J. P.; Moortgat, G. K.; Tyndall, G. S.; Cox, R. A.; Jenkin, M. E.; Hayman, G. D.; Veyret, B., Kinetics and mechanism of the photooxidation of formaldehyde. 2. Molecular modulation studies. *Journal of Physical Chemistry* **1989**, *93* (6), 2375-2382.
76. Veyret, B.; Lesclaux, R.; Rayez, M. T.; Rayez, J. C.; Cox, R. A.; Moortgat, G. K., Kinetics and mechanism of the photooxidation of formaldehyde. 1. Flash-photolysis study. *Journal of Physical Chemistry* **1989**, *93* (6), 2368-2374.
77. Zabel, F.; Sahetchian, K. A.; Chachaty, C., Electron spin-resonance spectra of free-radicals formed during the gas-phase photooxidation of formaldehyde - thermal-stability of the HOCH₂OO radical. *Chemical Physics Letters* **1987**, *134* (5), 433-437.
78. Barnes, I.; Becker, K. H.; Fink, E. H.; Reimer, A.; Zabel, F.; Niki, H., FTIR spectroscopic study of the gas-phase reaction of HO₂ with H₂CO. *Chemical Physics Letters* **1985**, *115* (1), 1-8.
79. Su, F.; Calvert, J. G.; Shaw, J. H.; Niki, H.; Maker, P. D.; Savage, C. M.; Breitenbach, L. D., Spectroscopic and kinetic studies of a new metastable species in the photo-oxidation of gaseous formaldehyde. *Chemical Physics Letters* **1979**, *65* (2), 221-225.
80. Veyret, B.; Rayez, J. C.; Lesclaux, R., Mechanism of the photo-oxidation of formaldehyde studied by flash-photolysis of CH₂O-O₂ mixtures. *Journal of Physical Chemistry* **1982**, *86* (17), 3424-3430.
81. Bailey, P. S., *Ozonation in organic chemistry*. Academic Press: New York, 1978.
82. Pelaez, D.; Arenas, J. F.; Otero, J. C.; Soto, J., Dependence of N-nitrosodimethylamine photodecomposition on the irradiation wavelength: Excitation to the S-2 state as a doorway to the dimethylamine radical ground-state chemistry. *Journal of Organic Chemistry* **2007**, *72* (13), 4741-4749.

83. Kurtén, T.; Loukonen, V.; Vehkamäki, H.; Kulmala, M., Amines are likely to enhance neutral and ion-induced sulfuric acid-water nucleation in the atmosphere more effectively than ammonia. *Atmospheric Chemistry and Physics* **2008**, *8* (14), 4095-4103.
84. Loukonen, V.; Kurtén, T.; Ortega, I. K.; Vehkamäki, H.; Pádua, A. A. H.; Sellegri, K.; Kulmala, M., Enhancing effect of dimethylamine in sulfuric acid nucleation in the presence of water - a computational study. *Atmos. Chem. Phys.* **2010**, *10* (10), 4961-4974.
85. Smith, J. N.; Barsanti, K. C.; Friedli, H. R.; Ehn, M.; Kulmala, M.; Collins, D. R.; Scheckman, J. H.; Williams, B. J.; McMurry, P. H., Observations of ammonium salts in atmospheric nanoparticles and possible climatic implications. *Proceedings of the National Academy of Sciences of the United States of America* **2010**, *107* (15), 6634-6639.
86. Ge, X.; Wexler, A. S.; Clegg, S. L., Atmospheric amines - Part II. Thermodynamic properties and gas/particle partitioning. *Atmos. Environ.* **2011**, *45* (3), 561-577.
87. Bzdek, B. R.; Ridge, D. P.; Johnston, M. V., Amine exchange into ammonium bisulfate and ammonium nitrate nuclei. *Atmospheric Chemistry and Physics* **2010**, *10* (8), 3495-3503.
88. Facchini, M. C.; Decesari, S.; Rinaldi, M.; Carbone, C.; Finessi, E.; Mircea, M.; Fuzzi, S.; Moretti, F.; Tagliavini, E.; Ceburnis, D.; O'Dowd, C. D., Important Source of Marine Secondary Organic Aerosol from Biogenic Amines. *Environmental Science & Technology* **2008**, *42* (24), 9116-9121.
89. Rehbein, P. J. G.; Jeong, C.-H.; McGuire, M. L.; Yao, X.; Corbin, J. C.; Evans, G. J., Cloud and Fog Processing Enhanced Gas-to-Particle Partitioning of Trimethylamine. *Environmental Science & Technology* **2011**, *45* (10), 4346-4352.
90. VandenBoer, T. C.; Petroff, A.; Markovic, M. Z.; Murphy, J. G., Size distribution of alkyl amines in continental particulate matter and their online detection in the gas and particle phase. *Atmospheric Chemistry and Physics* **2011**, *11* (9), 4319-4332.
91. Kramp, F.; Paulson, S. E., On the Uncertainties in the Rate Coefficients for OH Reactions with Hydrocarbons, and the Rate Coefficients of the 1,3,5-Trimethylbenzene and m-Xylene Reactions with OH Radicals in the Gas Phase. *The Journal of Physical Chemistry A* **1998**, *102* (16), 2685-2690.
92. Becke, A. D., Density-functional thermochemistry. III. The role of exact exchange. *J. Chem. Phys.* **1993**, *98*, 5648-5652.
93. Lee, C.; Yang, W.; Parr, R. G., Development of the Colle-Salvetti correlation-energy formula into a functional of the energy density. *Phys. Rev. B* **1988**, *37*, 785-789.
94. Vosko, S. H.; Wilk, L.; Nusair, M., Accurate spin-dependent electron liquid correlation energies for local spin-density calculations - a critical analysis. *Canadian Journal of Physics* **1980**, *58* (8), 1200-1211.
95. Stephens, P. J.; Devlin, F. J.; Chabalowski, C. F.; Frisch, M. J., Ab-initio calculation of vibrational absorption and circular-dichroism spectra using density-functional force-fields. *Journal of Physical Chemistry* **1994**, *98* (45), 11623-11627.
96. Dunning, T. H., Jr., Gaussian basis sets for use in correlated molecular calculations. I. The atoms boron through neon and hydrogen. *J. Chem. Phys.* **1989**, *90* (2), 1007-23.
97. Fischer, E.; Botskor, I., The microwave spectrum of gauche-ethylamine. *Journal of Molecular Spectroscopy* **1984**, *104* (2), 226-247.
98. Ohnishi, Y.; Kozima, K., Microwave spectrum of cyclohexanone. *Bull. Chem. Soc. Jap.* **1968**, *41* (Copyright (C) 2011 American Chemical Society (ACS). All Rights Reserved.), 1323-5.

ANNEX

A. Monitor calibration and data analysis

Monica Vazquez-Moreno

Instituto Universitario CEAM-UMH, EUPHORE Laboratory

C. Charles R. Darwin 14, 46980 Parque Tecnológico, Paterna - Valencia - (Spain)

INSTRUMENT DESCRIPTIONS

During the ADA, NITROSAMINE and DARKCHEM experiments performed from March to June 2011, to measure ozone, CO and NO_x concentrations the following monitors were used:

- **O₃-Monitor Labs 9810-SN2028 (O₃, ppb):** with this monitor it is possible to on-line measure the ozone concentration in the chamber, its principle of operation is a nondispersive ultraviolet photometer, which alternatively switches a selective ozone scrubber in and out of the measuring stream, and computes the ratio of transmitted light. A mercury vapour lamp is used as light source (254 nm) and a solar blind vacuum photodiode is used as detector.
- **NO_x-ECO Physics -Alppt SN77326 (NO, NO₂ and NO_x, ppb):** this monitor measures the NO, NO₂ and NO_x (ppb) concentration directly from the chamber. It has two independent units; the analyzer CLD 770 Alppt and the photolytic converter PLC 760. The principle of operation of the CLD 770 Alppt analyzer is the gas phase chemiluminescent reaction of nitric oxide (NO) with ozone (O₃). On the other hand, the photolytic converter PLC 760 performs a selective conversion of NO₂ to NO through photodissociation with a xenon lamp.
- **NO_x-ECO Physics II (NO, NO₂ and NO_x, ppb):** this instrument is a newer version of the previous one and was installed by the University of Innsbruck for intercomparison.
- **NO_x-Dasibi 2108A (NO, NO₂ and NO_x, ppb):** the principle of operation of this monitor is also the chemiluminescence of the reaction of NO+O₃ but for the NO₂ into NO transformation a catalytic converter is used.
- **CO-TE48C SN62733-335 (CO, ppb):** this monitor is based on the principle that carbon monoxide absorbs infrared radiation at a wavelength of 4.6 microns. During operation sample enters through the sample bulkhead and flows through the optical bench. Radiation from an infrared source is generated and then passed through a gas filter alternating between CO and N₂. The detector signal is modulated by the alternation between the two gas filters, with the amplitude related to the concentration of CO in the sample cell.

CALIBRATION

Before the campaign all the instruments were calibrated using a **SABIO 4010 Gas Dilution Calibrator** which has a diluent mass flow controller and two source flow controllers with the following characteristics:

Diluent MFC: range 0 - 10 SLM, input pressure 20-35 psig. Brooks, model 5850E

Source MFC1: range 0 - 50 SCCM, input pressure 20-35 psig. Brooks, model 5850E

Source MFC2: range 0 - 200 SCCM, input pressure 20-35 psig. Brooks, model 5850E

The system has also solenoid valves for diluent, source and purge ports. The air connected to the diluent port is well filtered of particulates, dry and free of low level pollutants. For the pneumatic connections it is used teflon or stainless steel, specially for the ozone analyzer connections is used teflon. Furthermore, the Calibrator has an internal Ozone Generator, a UV absorption photometer, a Gas Phase Titration (GPT) reaction chamber made in Teflon and static mixers used to enhance homogeneous blending of diluent and source gases.

Ozone, NOx and CO calibration sequences are summarized in Tables 1, 2 and 3 respectively.

Sequence Name	O3
Sequence Type	Ozone
Diluent Gas	AIR
Source Gas	Internal Ozone Generatos
Primary Gas	-
Source MFC	Source 1
Minimum Instrument Flow	5 SLPM
Conditioning Period	0 minutes
Running Order	Ascending
Instrument Solenoid	1
Concentration (ppb)/ Duration (min)	0/30', 50/20', 60/20', 70/20', 80/20', 90/20', 100/20', 120/20', 150/20', 200/20', 250/20'
Total Duration	3h 50'

Table 1: Calibration Sequence Ozone Monitor Labs 9810

Sequence Name	NOx 12
Sequence Type	Gas Dilution
Diluent Gas	AIR
Source Gas	NO Standard 20 ppm
Primary Gas	NO
Source MFC	Source 2
Minimum Instrument Flow	5 SLPM
Conditioning Period	0 minutes
Running Order	Ascending
Instrument Solenoid	4
Concentration (ppb)/ Duration (min)	0/25', 10/20', 20/15', 30/15', 40/15', 50/15', 60/15', 80/15', 100/15', 120/15', 150/15'
Total Duration	3h 0'

Table 2: Calibration Sequence NOx-ECO Alppt77326 and NOx-Dasibi 2108A

Sequence Name	CO
Sequence Type	Gas Dilution
Diluent Gas	AIR
Source Gas	CO Standard 200 ppm
Primary Gas	CO
Source MFC	Source 2
Minimum Instrument Flow	5 SLPM
Conditioning Period	0 minutes
Running Order	Ascending
Instrument Solenoid	2
Concentration (ppb)/ Duration (min)	0/25', 200/15', 500/15', 700/15', 900/15', 1100/15', 1300/15', 1500/15', 1700/15', 1800/15', 1900/15'
Total Duration	2h 55'

Table 3: Calibration Sequence CO TE48C SN 62733-335

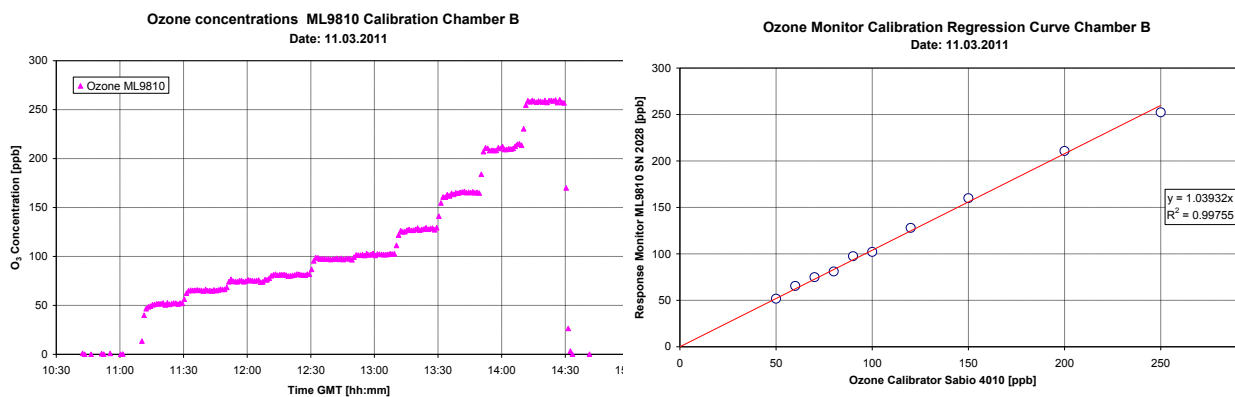


Figure 1: Ozone Monitor Labs 9810 Calibration results

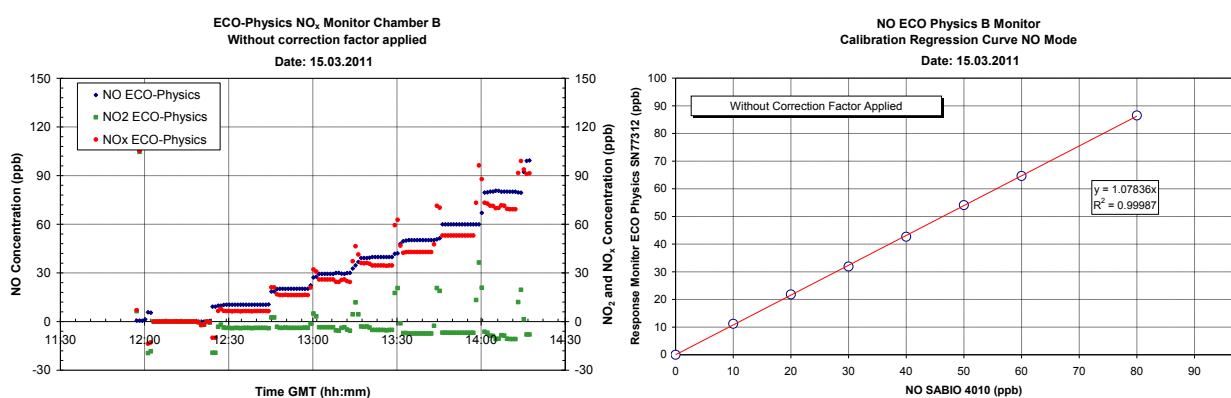


Figure 2: NOx-ECO ALpnt 77326 Calibration results

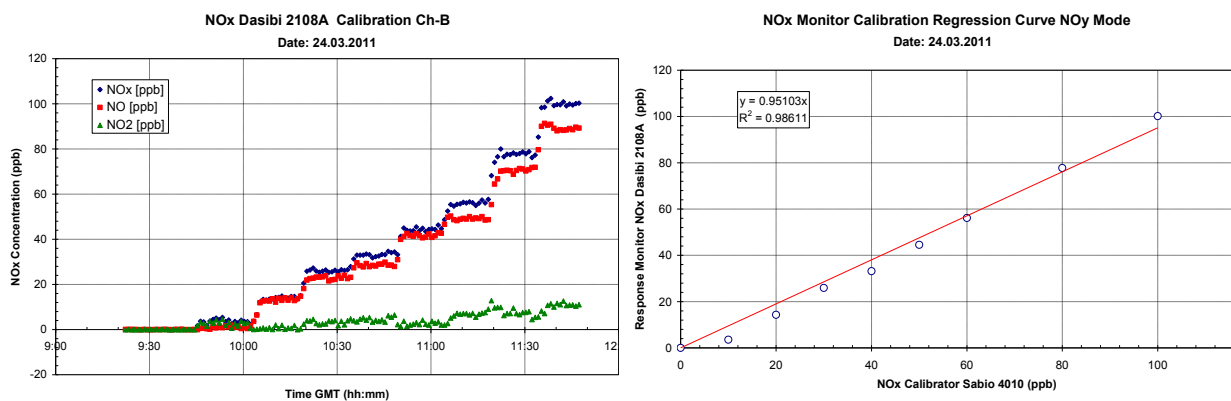


Figure 3: NOx-Dasibi 2108A Calibration results

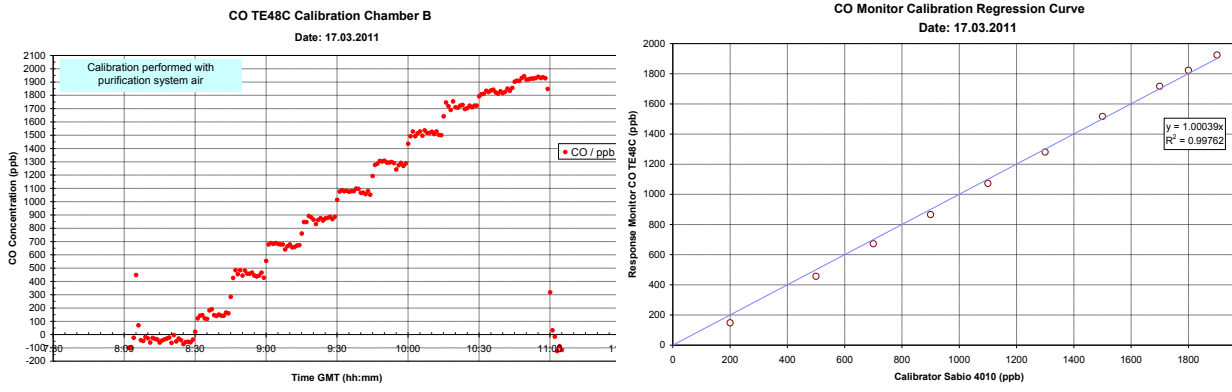


Figure 4: CO-TE48C Calibration results

NO_x INTERCALIBRATION

On 8/04/2011 several NO injections were performed in Chamber B and, afterwards, four steps of ozone additions with the objective of having different NO and NO₂ concentration levels for NO_x monitors inter-comparison with FTIR. The experimental protocol was the following:

06:00 FTIR Max=7.56, Min=-4.80, Gain=8
06:02 Stop chamber flushing
06:21 SF6 addition (5ml)
07:05 50 ML NO
07:10 50 ML NO addition
07:14 50 ML NO addition
07:31 50 ML NO addition
07:40 Chamber opened
08:00 Chamber closed
08:37 1 min. O3 added
09:30 1 min. O3 added
10:19 2 min. O3 added
11:03 2 min. O3 added
11:33 Chamber opened
13:34 Chamber closed

For NO determination a correction factor between NO-ECO Physics and FTIR was calculated. The results of this inter-comparison are shown in Figures

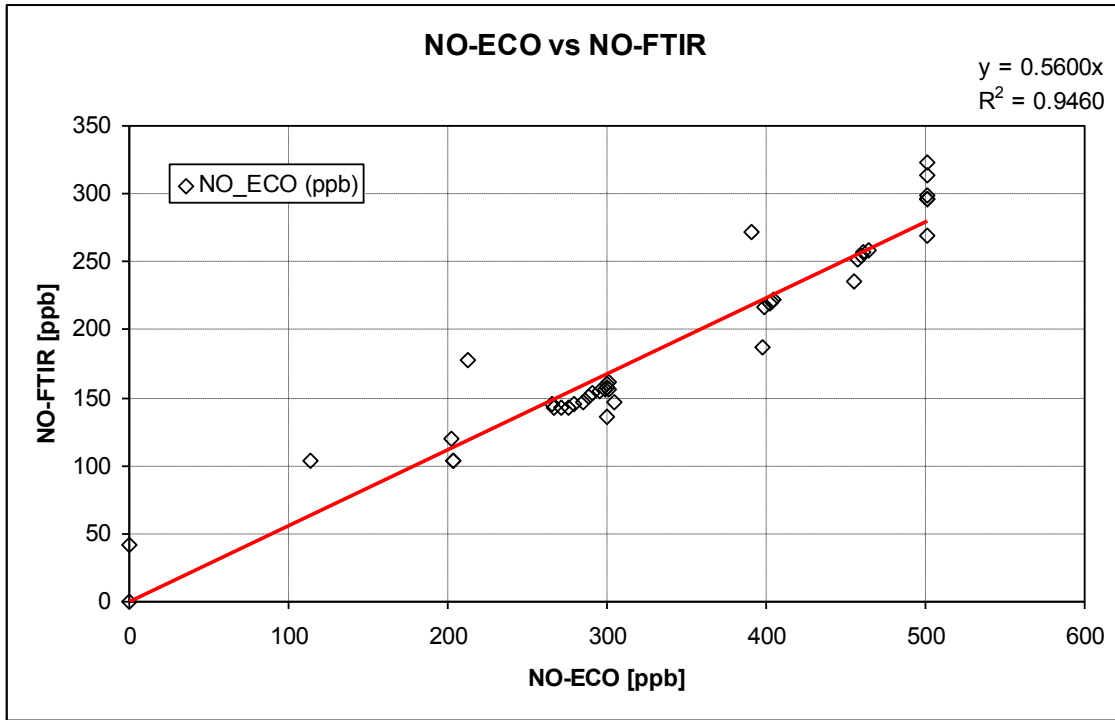


Figure 5: NO-ECO Alppt 77326 vs NO-FTIR Correction Factor

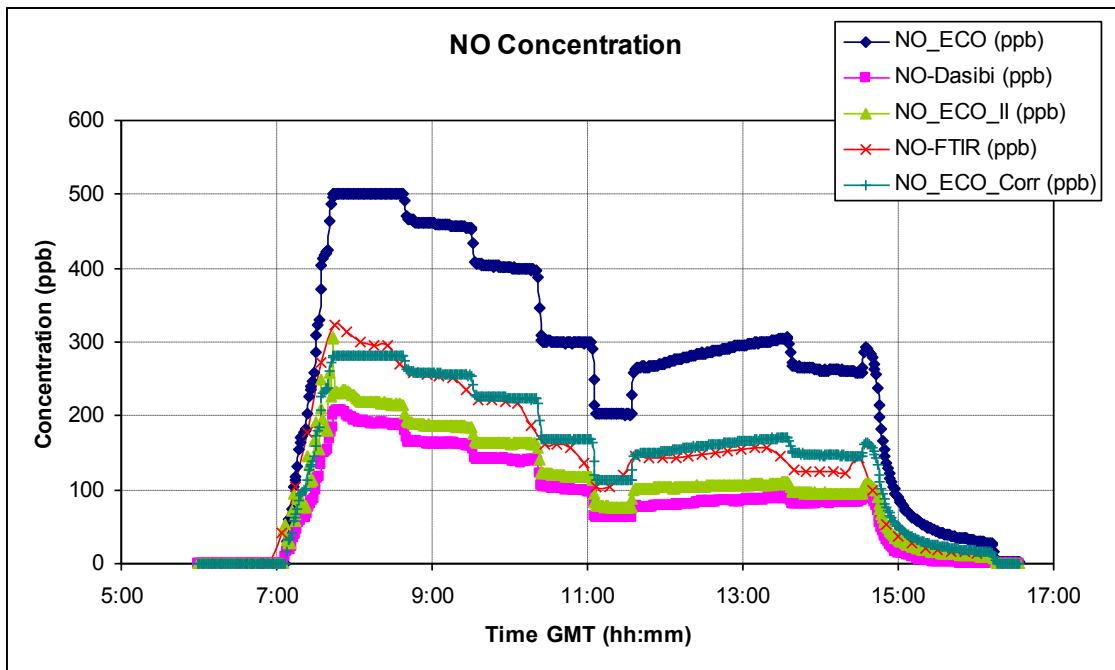


Figure 6: NO Concentration intercomparison

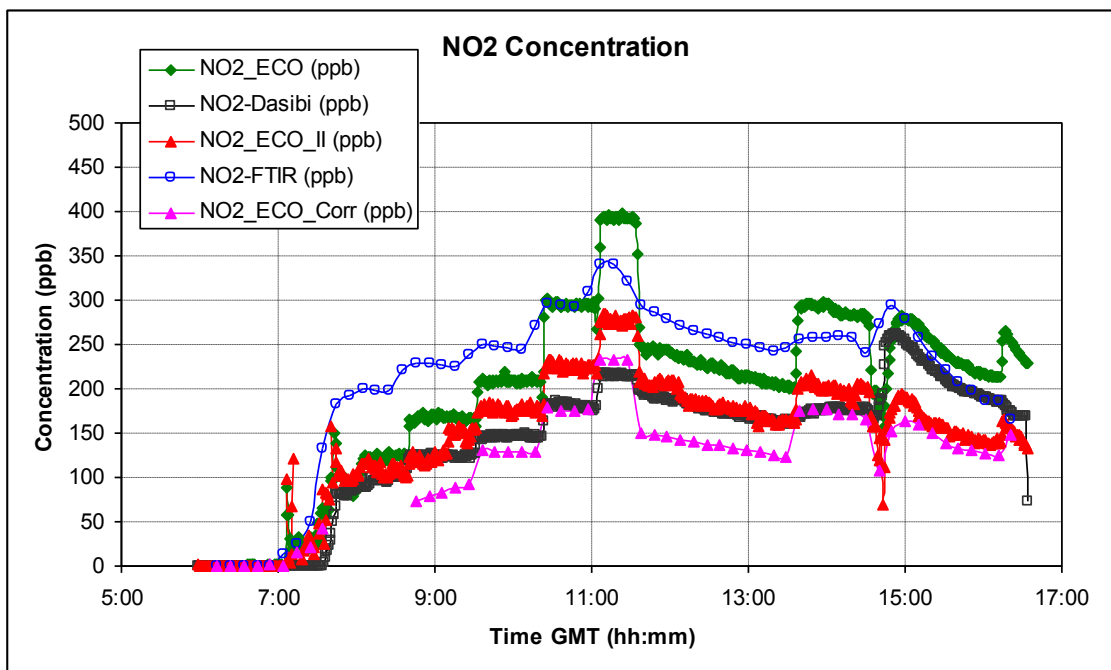


Figure 7: NO₂ Concentration intercomparison

DATA ANALYSIS

All monitors analog outputs are connected to a data logger and data are recorded with a one minute time resolution. The output voltage is transformed into ppb according to the range, monitor offset, calibration and correction factors.

B. NO₂ Photolysis frequency determination and inter-calibration

1. INSTRUMENTATION

During the ADA, NITROSAMINE and DARKCHEM experiments performed in EUPHORE Chamber B from March to June 2011, to obtain the NO₂ photolysis frequency (NO₂ → NO + O(³P)) three instruments with two channels each (Upward for global radiation and Downward for reflected from the chamber floor) were used (Figure 1).

1.1. Filter Radiometer (Meteorologie Consult GMBH, Glasshütten, Germany)

NO₂ photolysis frequency is measured using a filter radiometer installed inside the Teflon chamber and the output data is fed to a data processing computer.

Specifications:

Type: 4πsr J(NO₂) Filter Radiometer

Field of view: 2 x 180 degrees (4πsr)

Wavelength characteristics: Best fit to the photolysis frequency of the NO₂ molecule

Absolute calibration: Better than ±5% with respect to a chemical actinometer

Linearity: Better than 1% according to the detector characteristics

Output signal: 2 x 0-5 VDC for the two fields of view

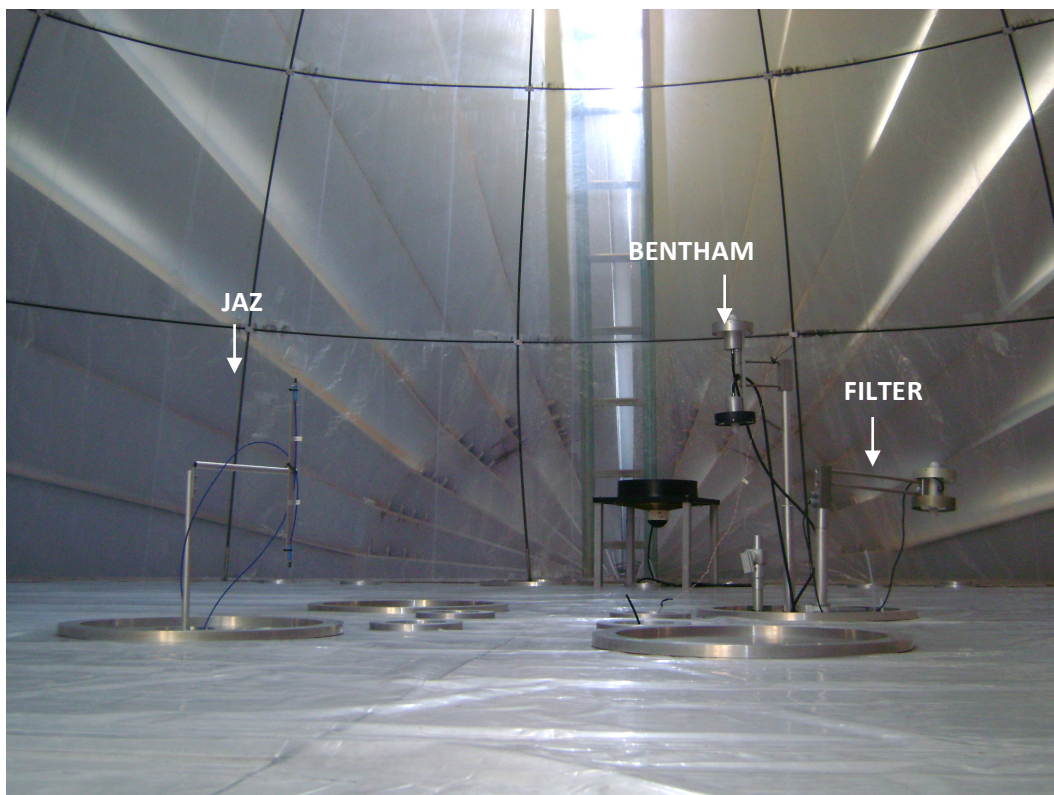


Figure 1: Filter Radiometer, Bentham and JAZ spectroradiometers located inside EUPHORE Chamber B

1.2. Bentham DTM300 Spectroradiometer (Bentham Instruments Ltd., Berkshire, United Kingdom)

This instrument measures directly the actinic flux inside the chamber thanks to its special designed measurement heads with a uniform sensitivity with respect to the incident angle of the solar light that are coupled through a quartz fibre bundle to the entrance optics of the monochromator. Two light beams, one for the direct light and the other for the reflected light, pass simultaneously but geometrical separated through the double monochromator. Independent detectors measure the light for both beams. The spectra is recorded every 4 min approximately in the range from 290 nm to 360 nm with a spectral resolution of 1 nm FWHM and step size of 1 nm and in the range from 360 nm to 510 nm with the same resolution but with a step size of 5 nm.

1.3. JAZ Spectroradiometer (Ocean Optics Inc., Florida, USA)

This system has two channels for direct and reflected by the floor spectral irradiance measurements in a bandwidth from 200 to 850 nm with a spectral resolution of 0.38 nm. Each channel has connected a five meters optical fiber with a CC3-UV Cosine corrector with spectralon diffusing material at the entrance that opens the field of view to 180°. The instrument was configured to obtain one spectrum per minute during the whole experiment.

Specifications:

Model:	JAZ-COMBO-2
Description:	Jaz System, 2 Spectrometer Channels with a DPU module
Grating:	600 Lines blazed at 400 nm
Bandwith:	200-850 nm
Options Installed:	ILX511b Detector, UV2/OFLV-4 Filter, L2 Lens, 25 µm slit

2. JAZ SPECTRORADIOMETER CALIBRATION

To calibrate the absolute spectral response of the JAZ spectroradiometer a DH2000-CAL (Ocean Optics Inc., Florida, USA) Deuterium Tungsten Halogen calibration standard UV-NIR light source was used as reference. Figure 2 shows the calibration reference data of the DH-2000 CAL light source using a CC3-UV Cosine Corrector at the fiber entrance.

The JAZ spectroradiometer was calibrated before the campaign. The spectral irradiance calibration factors obtained for each channel are illustrated in Figure 3.

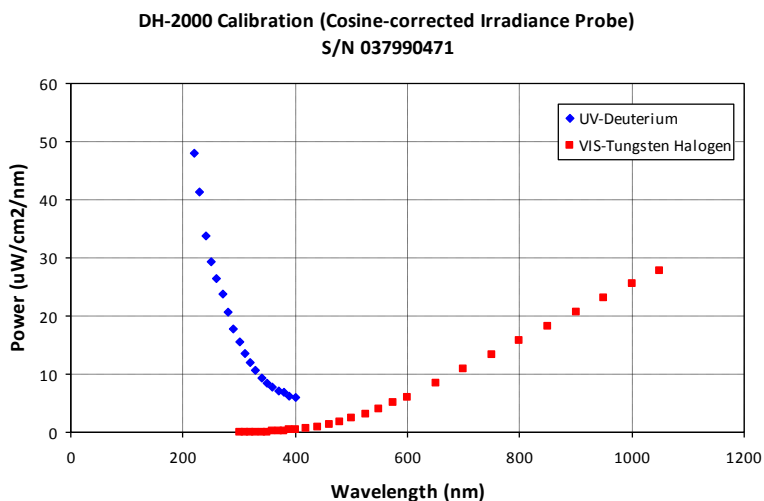


Figure 2: DH-2000 CAL calibration data light source with CC3-UV cosine corrector

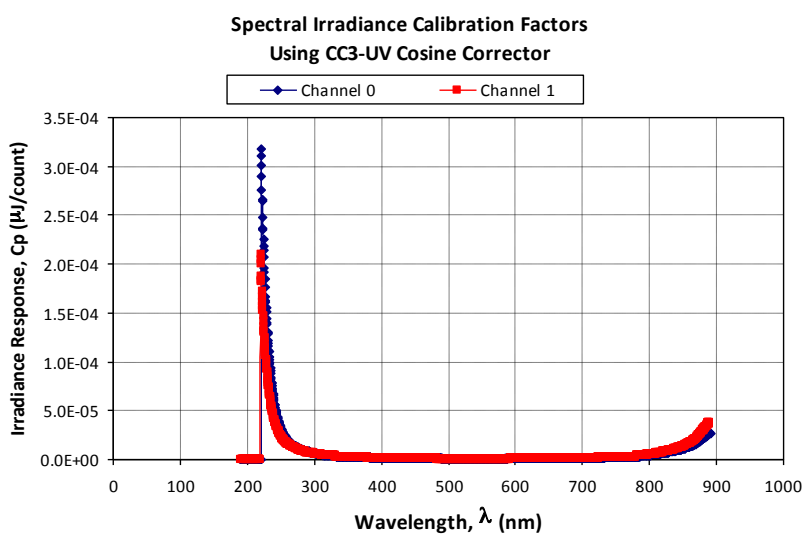


Figure 3: Spectral Irradiance calibration factors (C_p) for Channels 0 and 1

3. DATA ANALYSIS

3.1 Filter Radiometer

The analog output from this instrument is transformed into NO_2 photolysis frequencies according to Equations 1 and 2.

$$J(\text{NO}_2)_{\text{Filter-Up}} = \frac{(\text{RawSignal} - 0.023)}{1.54 \cdot 10^{-3}} \quad [\text{Eq. 1}]$$

$$J(NO_2)_{Filter-Down} = \frac{(RawSignal - 0.150)}{1.72 \cdot 10^{-3}} \text{ [Eq. 2]}$$

3.2 Bentham Spectroradiometer

From the recorded actinic flux data, the photolysis frequency for NO_2 is calculated using Equation 3 with the cross section and quantum yield values from DeMore et al., 1997 that are shown in Figure 4. The same methodology is used to obtain the photolysis frequencies from other compounds such as O_3 , HONO, H_2O_2 , HNO_3 , HCHO, carbonyl compounds, etc.

$$J(NO_2) = \int_{290}^{425} \sigma(\lambda) \cdot \phi(\lambda) \cdot F(\lambda) \cdot d\lambda \quad \text{[Eq. 3]}$$

where:

$\sigma(\lambda)$: absorption cross section

$\phi(\lambda)$: Quantum yield

$F(\lambda)$: actinic flux

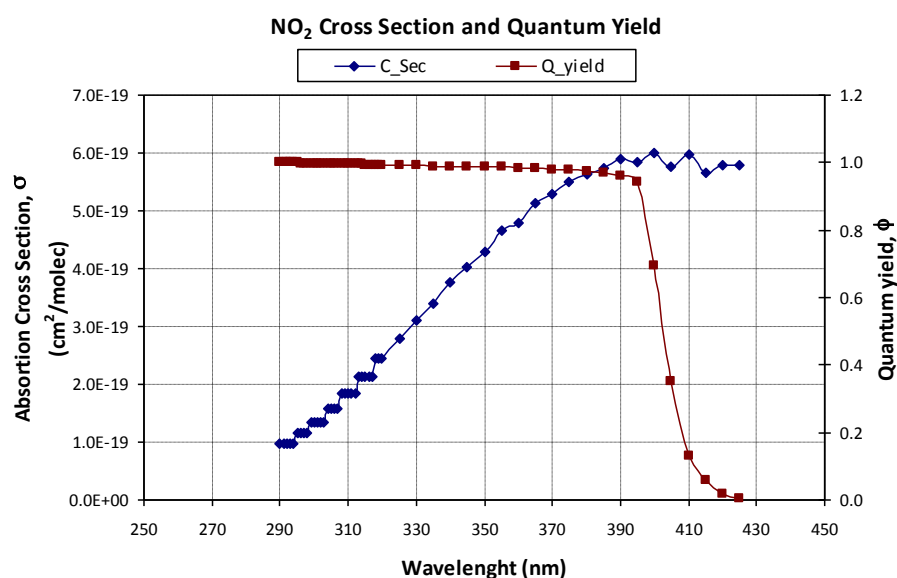


Figure 4: Absorption cross section and Quantum yields values used for NO_2 Photolysis Frequency calculation

3.3 JAZ Spectroradiometer

During the experiments the sample spectra are obtained in counts/nm, to transform these measurements into Absolute Irradiance Equation 4 is used.

$$I_p = \frac{(S_p - D_p)C_p}{(T \cdot A \cdot dL_p)} \quad \text{[Equation 4]}$$

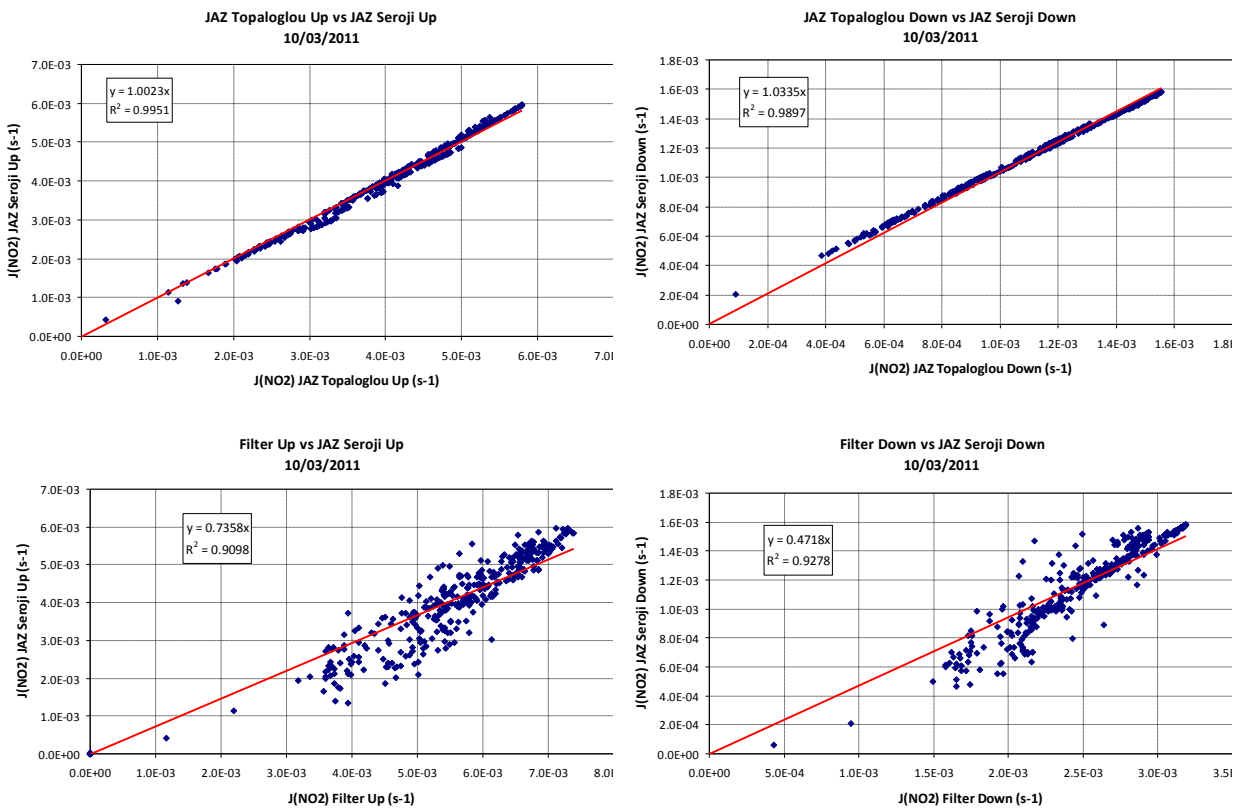
where the subscript P indicates a particular pixel of the detector and,

- S: sample spectrum (counts/nm)
- D: Dark spectrum (counts/nm)
- C: calibration factor obtained with the DH-2000 CAL light source (μJ/count)
- T: Integration time (seconds)
- A: collection area (cm²)
- dL: wavelength spread (nm)

From the irradiance measurements, NO₂ photolysis frequency is obtained following the methodologies published by Seroji et al., 2004 and Topaloglou et al., 2005.

4. j(NO₂) INTERCALIBRATION

An intercomparison of the three instruments was performed before the campaign on 10th March 2011. The J(NO₂) results obtained for each channel of all of the three instruments were correlated against the values obtained by the JAZ spectroradiometer using the Seroji method. The correlation results are represented in Figure 5.



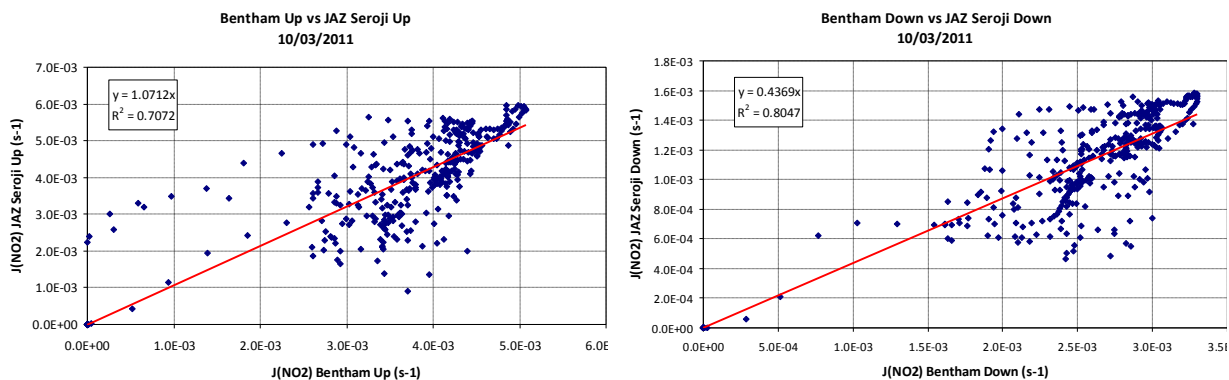
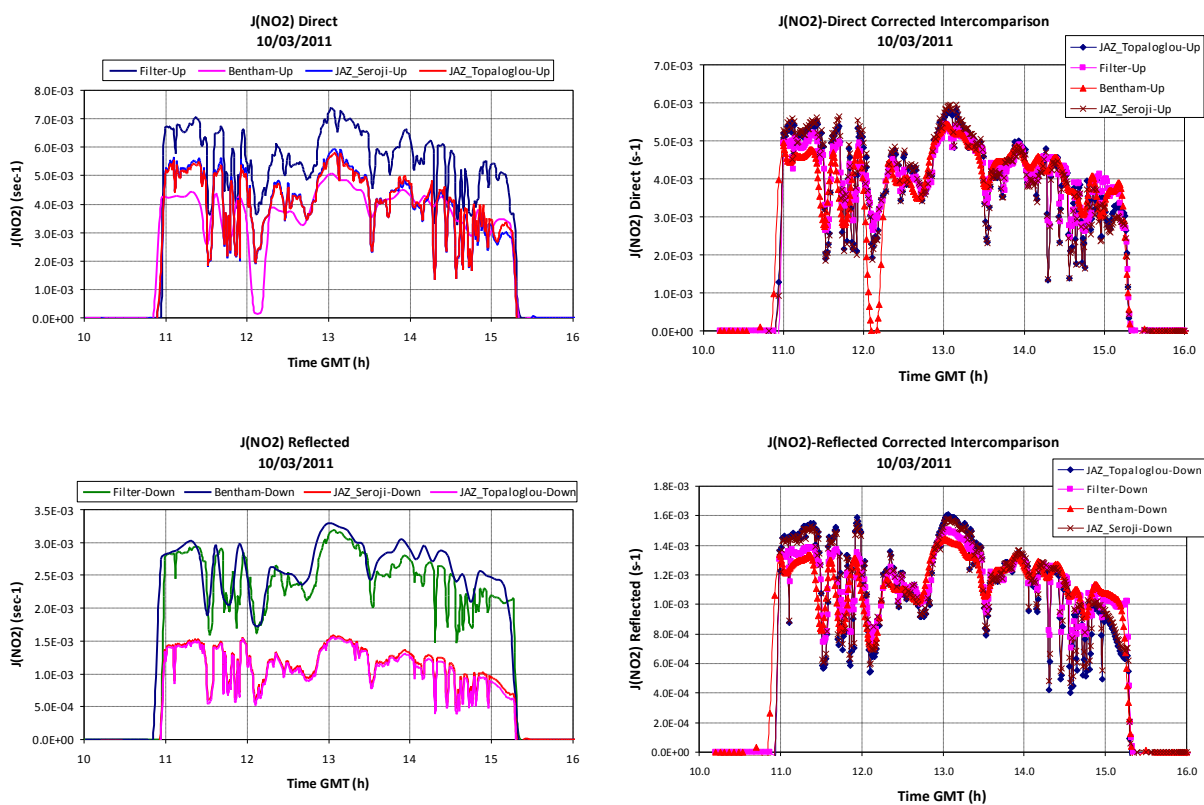


Figure 5: Correlation J(NO₂) results vs Seroji method

J(NO₂) values obtained with Filter radiometer and Bentham spectroradiometer are corrected by the correction factors obtained with the correlations shown in Figure 5. The original and corrected results appear in Figure 6.



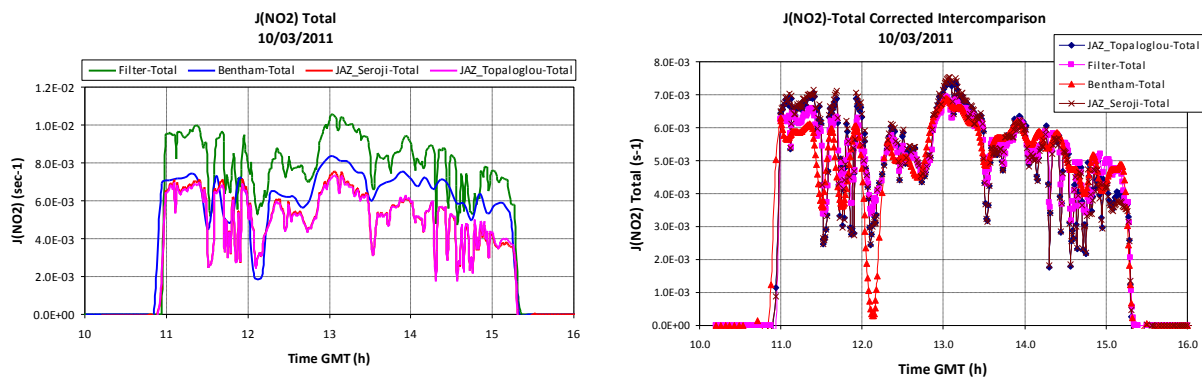


Figure 6: J(NO₂) Direct, Reflected and Total intercomparison corrected values

References

- DeMore W.B. et al. *Chemical kinetics and Photochemical data for use in stratospheric modelling*. Evaluation Number 12. JPL Publication 97-4. January 15, 1997
- Seroji A.R., Webb A.R., Coe H., Monks P.S., and Rickard A.R. *Derivation and Validation of photolysis rates of O₃, NO₂ and CH₂O from a GUV-541 radiometer*. Journal of Geophysical Research, Vol. 109, D21307, doi: 10.1029/2004JD004674. 2004
- Topaloglou C., Kazadzis S., Bais A.F., Blumthaler M., Schallhart B., and Balis D. *NO₂ and HCHO photolysis frequencies from irradiance measurement in Thessaloniki, Greece*. Atmos. Chem. Phys., 5, 1645-1653, 2005

C. Amine + OH Relative-Rate Experiments

Experiment #2. A relative-rate kinetics study of OH radical reactions with 4 amines ((CH₃)₂NH, (CH₃)₃N, (CH₃CH₂)₂NH and (CH₃CH₂)₃N) was carried out late in the afternoon of 2011.06.10. Tetrahydrofuran (THF) and 1,3,5-Trimethylbenzene (TMB) were used as reference compounds and IPN-d6 was injected as OH precursor. Figure C.1 shows the PTR-TOF-MS ion signals of the 6 compounds during the photo-oxidation experiment; the THF signal is rather noisy in this experiment.

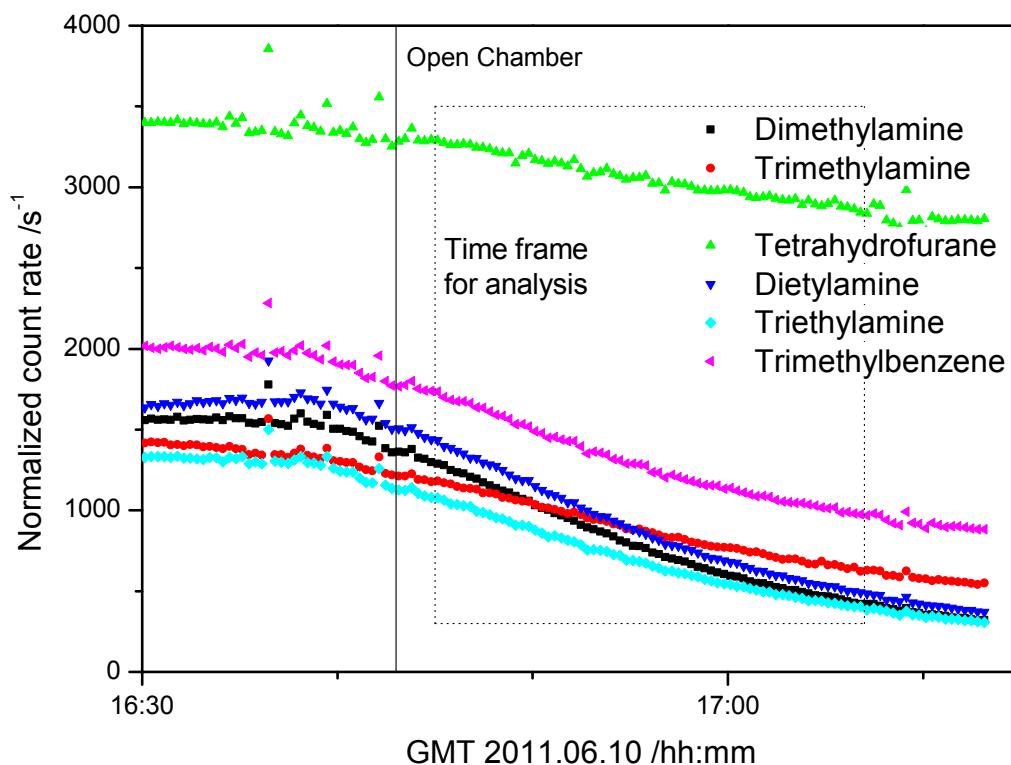


Figure C.1. The decays of (CH₃)₂NH, (CH₃)₃N, (CH₃CH₂)₂NH, (CH₃CH₂)₃N, tetrahydrofuran and 1,3,5-trimethylbenzene as a function of time in the presence OH radicals at 1013 hPa and 298 K.

The decays of (CH₃)₂NH (DMA), (CH₃)₃N (TMA), (CH₃CH₂)₂NH (DEA), (CH₃CH₂)₃N (TEA) and tetrahydrofuran in the presence of OH radicals during the time-span 16:45 to 17:13 are plotted as $\ln\{[\text{Substrate}]_0/[\text{Substrate}]_t\}$ vs. $\ln\{[\text{TMB}]_0/[\text{TMB}]_t\}$ in Figure C.2. It can be seen that there is an excellent correlation between the THF and TMB data throughout the experiment, $k_{\text{rel}} = 0.2444 \pm 0.0038$ (2σ). For the amines, however, there are systematic curvatures, which tentatively are ascribed to particle formation and addition amine uptake on these particles. The first third of the experiment is apparently not severely affected, and data from this part was subsequently used in the final analyses. The relative-rate plots, based on data from the smaller time span, are presented in Figure C.3 (DMA), Figure C.4 (TMA), Figure C.7 (DEA) and Figure C.8 (TEA). The results are included in Table 2.1, page 17.

The rate coefficients for OH reaction with the reference compound 1,3,5-trimethylbenzene (TMB) was reviewed by Kramp and Paulson,⁹¹ who also carried out relative rate studies of the OH reaction with TMB employing 10 different reference compounds and reported $k_{\text{OH}+\text{TMB}} = (5.73 \pm 0.53) \times 10^{-11} \text{ cm}^3 \text{ molecule}^{-1} \text{ s}^{-1}$ at 296 K. Aschmann and Atkinson later reported results from a temperature dependent study of the OH reaction with TMB and reported $k(T) = 4.40 \times 10^{-12} \exp(738(\pm 176)/T)$ for the temperature region 278-347 K and $k_{298} = (5.24 \pm 0.52) \times 10^{-12} \text{ cm}^3 \text{ molecule}^{-1} \text{ s}^{-1}$. The rate coefficient for OH reaction with tetrahydrofuran was reviewed by Atkinson;²⁶ the recommended value at 298 K is $k_{298} = (1.5 \pm 0.5) \times 10^{-11} \text{ cm}^3 \text{ molecule}^{-1} \text{ s}^{-1}$.

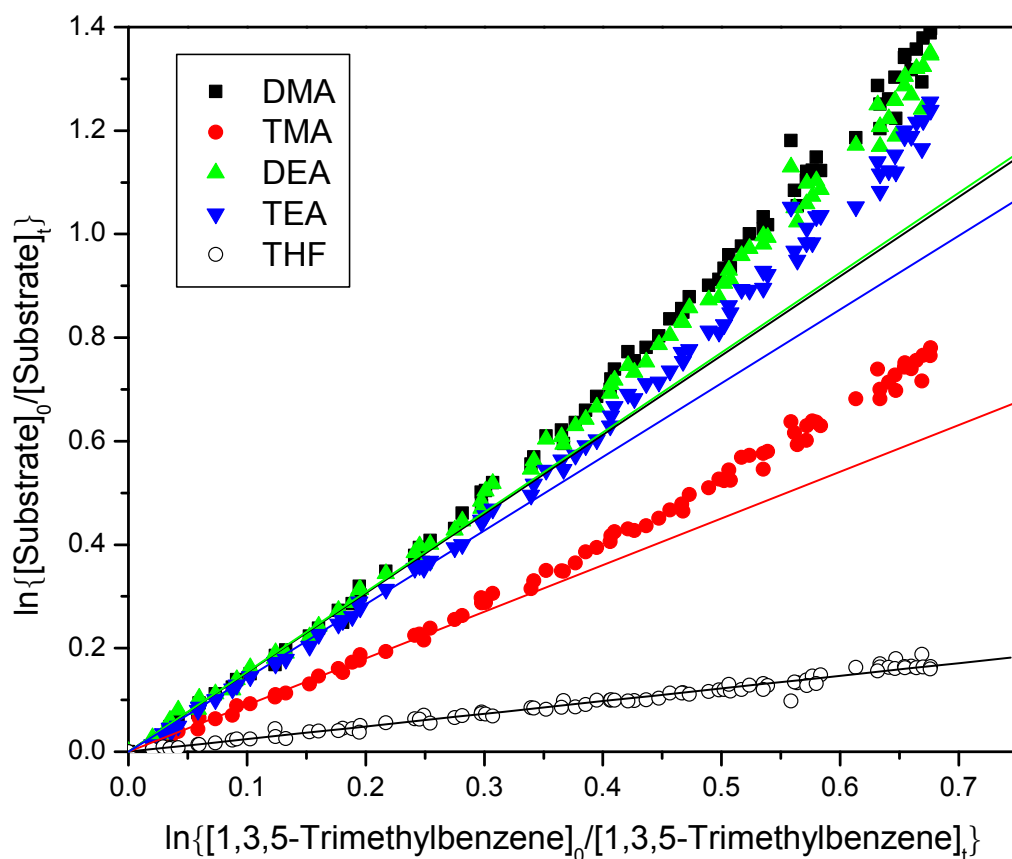


Figure C.2. Decays of $\text{CH}_3)_2\text{NH}$ (DMA), $(\text{CH}_3)_3\text{N}$ (TMA), $(\text{CH}_3\text{CH}_2)_2\text{NH}$ (DEA), $(\text{CH}_3\text{CH}_2)_3\text{N}$ (TEA), tetrahydrofuran and 1,3,5-trimethylbenzene (TMB) during reaction with OH radicals plotted in the form $\ln\{[\text{Substrate}]_0/[\text{Substrate}]_t\}$ vs. $\ln\{[\text{TMB}]_0/[\text{TMB}]_t\}$.

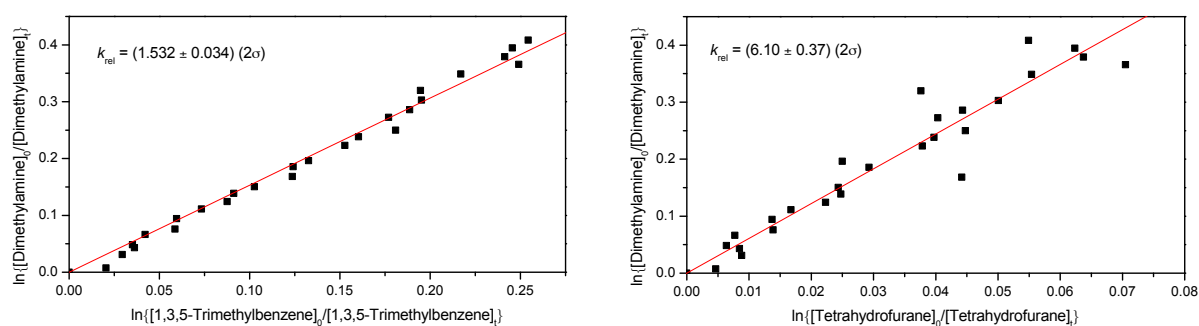


Figure C.3. Relative rate plots showing the decays of $(\text{CH}_3)_2\text{NH}$ versus 1,3,5-trimethylbenzene (left) and Tetrahydrofuran (right) during reactions with OH radicals at 1013 hPa and 298 K.

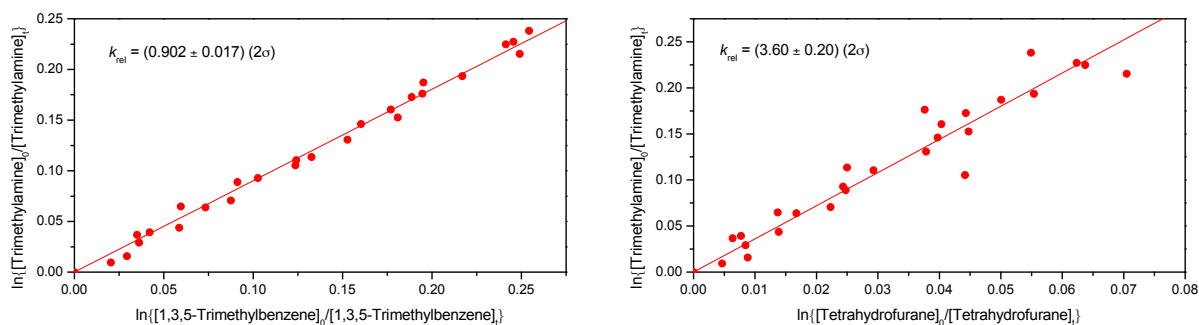


Figure C.4. Relative rate plots showing the decays of $(\text{CH}_3)_3\text{N}$ versus 1,3,5-trimethylbenzene (left) and Tetrahydrofuran (right) during reactions with OH radicals at 1013 hPa and 298 K.

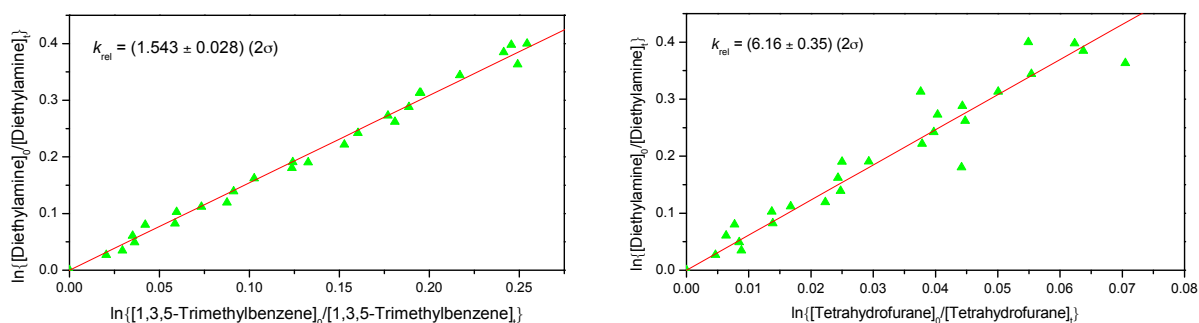


Figure C.5. Relative rate plots showing the decays of $(\text{CH}_3\text{CH}_2)_2\text{NH}$ versus 1,3,5-trimethylbenzene (left) and Tetrahydrofuran (right) during reactions with OH radicals at 1013 hPa and 298 K.

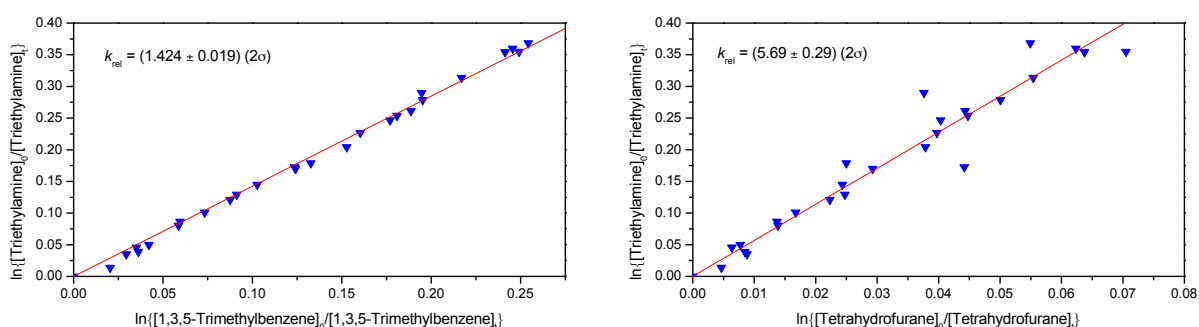


Figure C.6. Relative rate plots showing the decays of $(\text{CH}_3\text{CH}_2)_3\text{N}$ versus 1,3,5-trimethylbenzene (left) and Tetrahydrofuran (right) during reactions with OH radicals at 1013 hPa and 298 K.

Experiment #3. A relative A relative-rate kinetics study of OH radical reactions with 3 amines ($(\text{CH}_3)_2\text{NH}$ (DMA), $\text{CH}_3\text{NHCH}_2\text{CH}_2\text{CH}_3$ (MePrA) and piperidine (PIP)) was carried out between other experiments on 2011.06.08. Tetrahydrofuran (THF) and 1,3,5-Trimethylbenzene (TMB) were used as reference compounds and IPN-d6 was injected as OH precursor. Figure C.7 shows the PTR-TOF-MS ion signals of the 5 compounds during the photo-oxidation experiment.

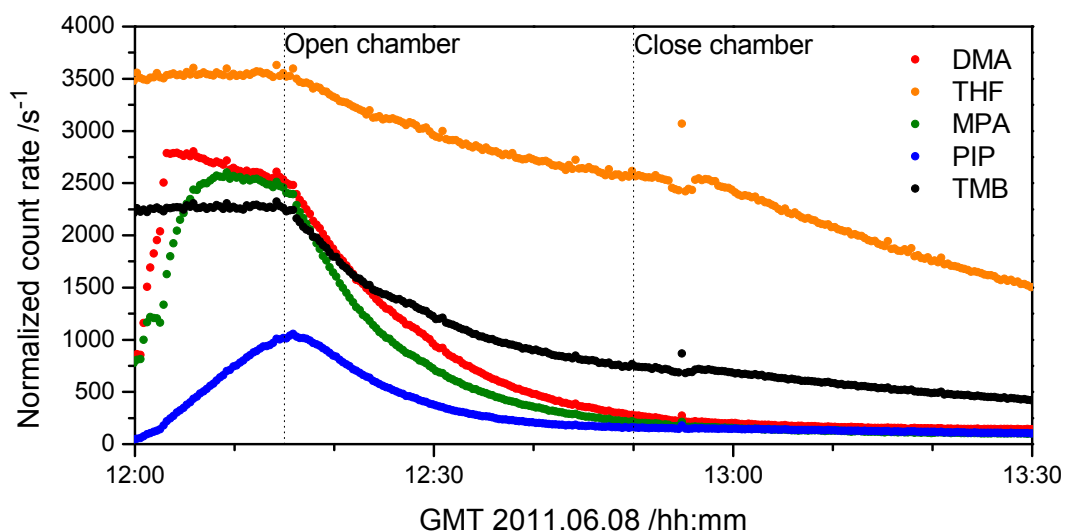


Figure C.7. The decays of $(\text{CH}_3)_2\text{NH}$, $\text{CH}_3\text{NHCH}_2\text{CH}_2\text{CH}_3$, piperidine, tetrahydrofuran and 1,3,5-trimethylbenzene as a function of time in the presence OH radicals at 1013 hPa and 298 K.

The decays of $(\text{CH}_3)_2\text{NH}$, $\text{CH}_3\text{NHCH}_2\text{CH}_2\text{CH}_3$, piperidine and TMB in the presence of OH radicals are plotted as $\ln\{[\text{Substrate}]_0/[\text{Substrate}]_t\}$ vs. $\ln\{[\text{THF}]_0/[\text{THF}]_t\}$ in Figure C.8.

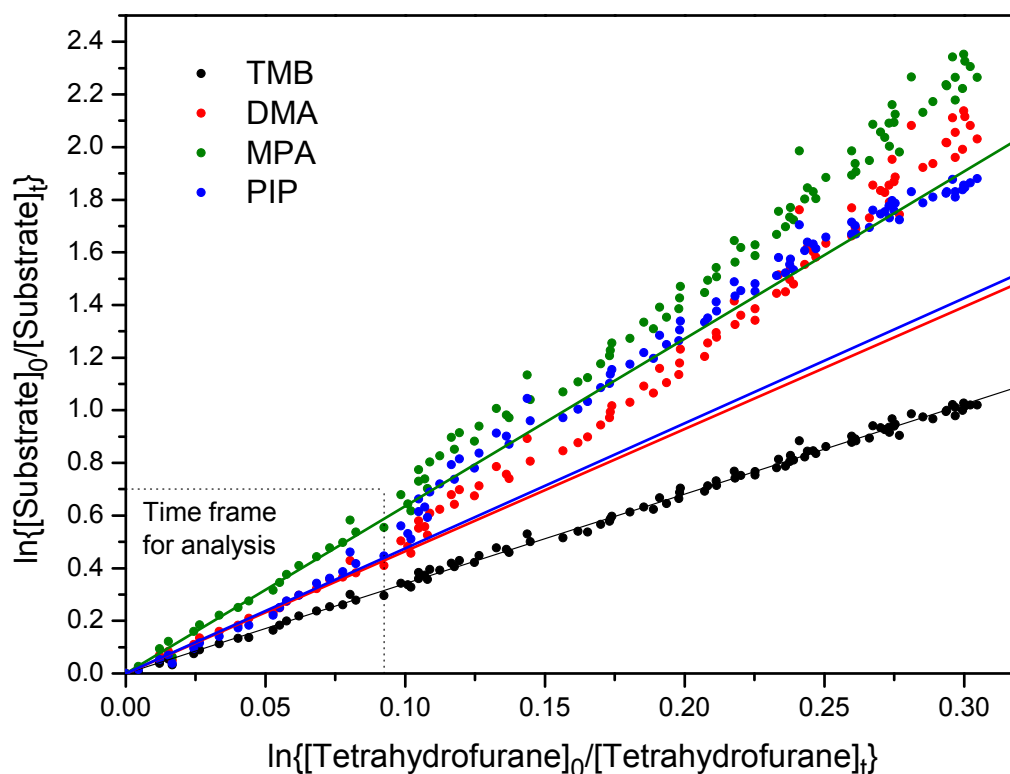


Figure C.8. Relative rate plots for the OH reactions with $(\text{CH}_3)_2\text{NH}$, $\text{CH}_3\text{NHCH}_2\text{CH}_2\text{CH}_3$, piperidine and TMB versus THF at 1013 hPa and 298 K.

It is clear from Figure C.7 that only the first part of the experiment is suited for gas phase kinetics analysis. This is also obvious from Figure C.8, in which the data sub-set to be analysed is indicated. It can be seen that there is an excellent correlation between the THF and TMB data throughout the experiment. For the amines, however, there are systematic curvatures, which, again, tentatively are ascribed to particle formation and addition amine uptake on these particles. The first third of the experiment is apparently not severely affected, and data from this part was subsequently used in the final analyses. The relative-rate plots, based on this data range, are presented in Figure C.9 (DMA), Figure C.10 (MPA) and Figure C.11 (PIP). The results are included in Table 2.1, page 17.

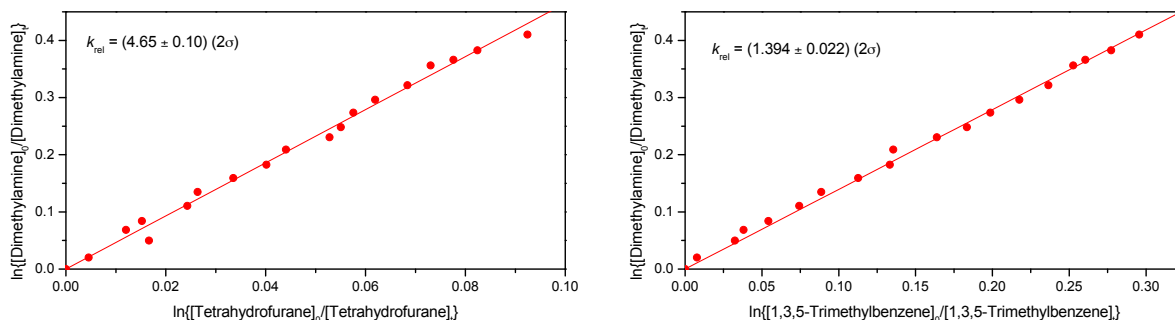


Figure C.9. Relative rate plots showing the decays of $(\text{CH}_3)_2\text{NH}$ versus Tetrahydrofuran (left) and 1,3,5-trimethylbenzene (right) during reactions with OH radicals at 1013 hPa and 298 K.

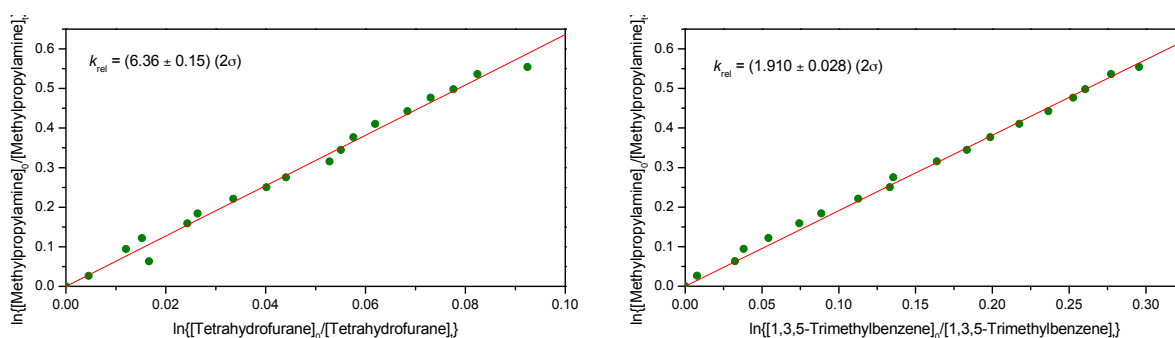


Figure C.10. Relative rate plots showing the decays of $\text{CH}_3(\text{CH}_3\text{CH}_2)\text{NH}$ versus Tetrahydrofuran (left) and 1,3,5-trimethylbenzene (right) during reactions with OH radicals at 1013 hPa and 298 K.

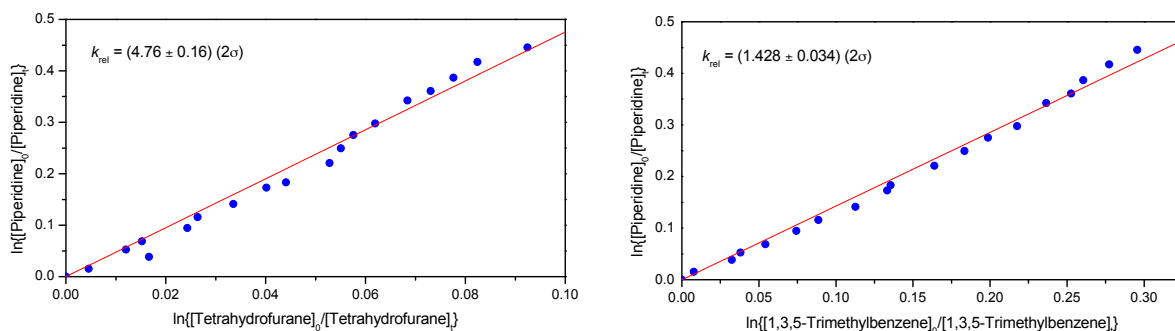


Figure C.11. Relative rate plots showing the decays of $\text{CH}_3(\text{CH}_3\text{CH}_2\text{CH}_2)\text{NH}$ versus Tetrahydrofuran (left) and 1,3,5-trimethylbenzene (right) during reactions with OH radicals at 1013 hPa and 298 K.

Experiment #4. A relative-rate kinetics study of OH radical reactions with 3 amines ($(\text{CH}_3)_2\text{NH}$ (DMA), $\text{CH}_3\text{NHCH}_2\text{CH}_3$ (MeEtA) and $\text{CH}_3\text{NHCH}_2\text{CH}_2\text{CH}_3$ (MePrA)) was carried out in the morning of 2011.06.10. Tetrahydrofuran (THF) and 1,3,5-Trimethylbenzene (TMB) were used as reference compounds and IPN was injected as OH precursor. Figure C.12 shows the PTR-TOF-MS ion signals of the 6 compounds during the photo-oxidation experiment.

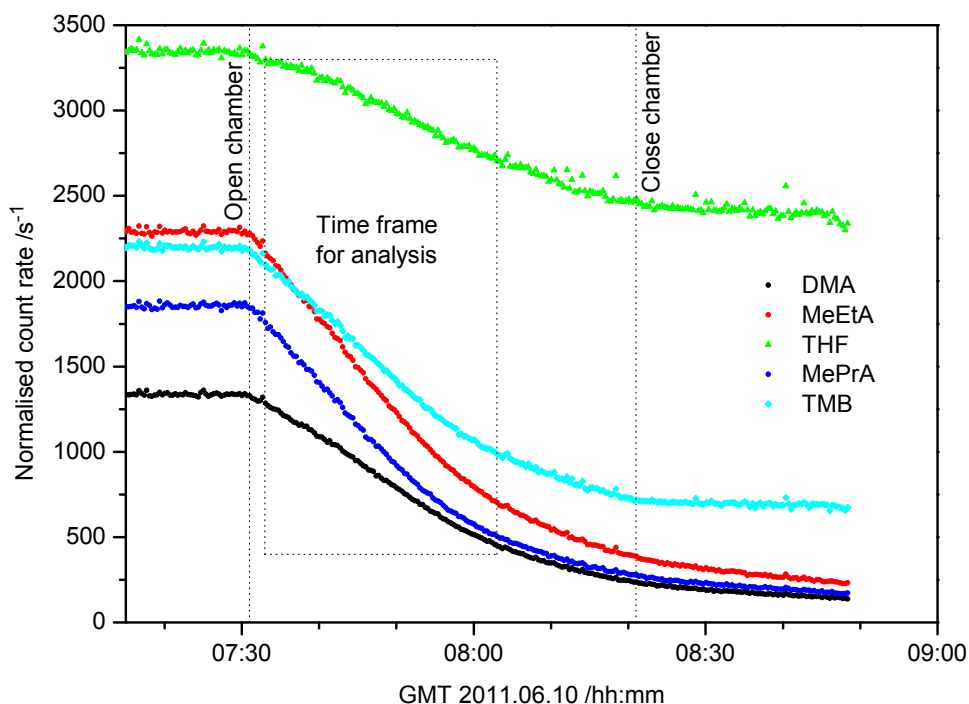


Figure C.12. The decays of $(\text{CH}_3)_2\text{NH}$, $\text{CH}_3(\text{CH}_3\text{CH}_2)\text{NH}$, $\text{CH}_3(\text{CH}_3\text{CH}_2\text{CH}_2)\text{NH}$, piperidine, tetrahydrofuran and 1,3,5-trimethylbenzene as a function of time in the presence OH radicals at 1013 hPa and 298 K.

Relative-rate plots, based on the indicated time span (Figure C.12) are presented in Figure C.13 (DMA), Figure C.14 (MeEtA) and Figure C.15 (MePrA). The results are included in Table 2.1, page 17.

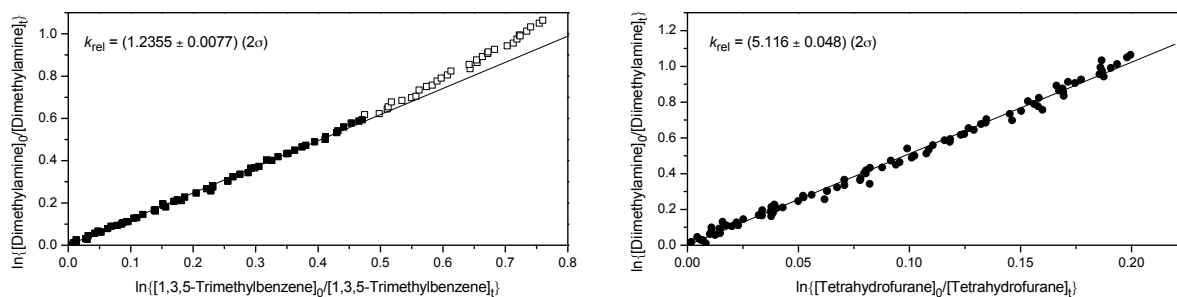


Figure C.13. Relative rate plots showing the decays of $(\text{CH}_3)_2\text{NH}$ versus 1,3,5-trimethylbenzene (left) and Tetrahydrofuran (right) during reactions with OH radicals at 1013 hPa and 298 K.

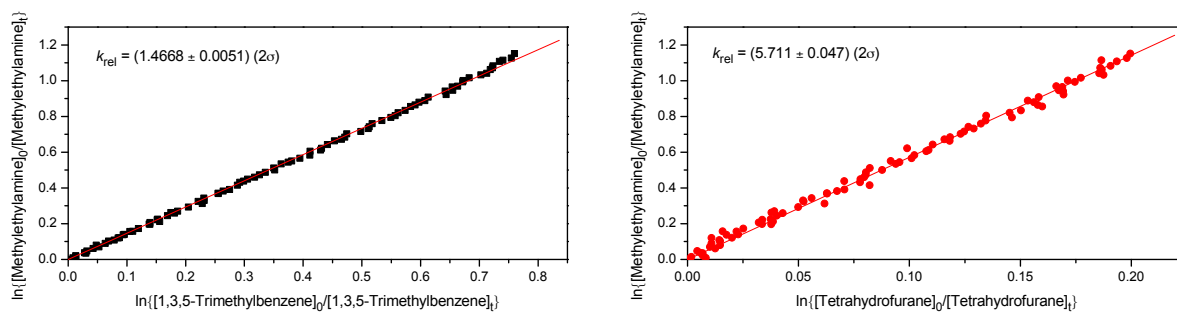


Figure C.14. Relative rate plots showing the decays of $\text{CH}_3(\text{CH}_3\text{CH}_2)\text{NH}$ versus 1,3,5-trimethylbenzene (left) and Tetrahydrofuran (right) during reactions with OH radicals at 1013 hPa and 298 K.

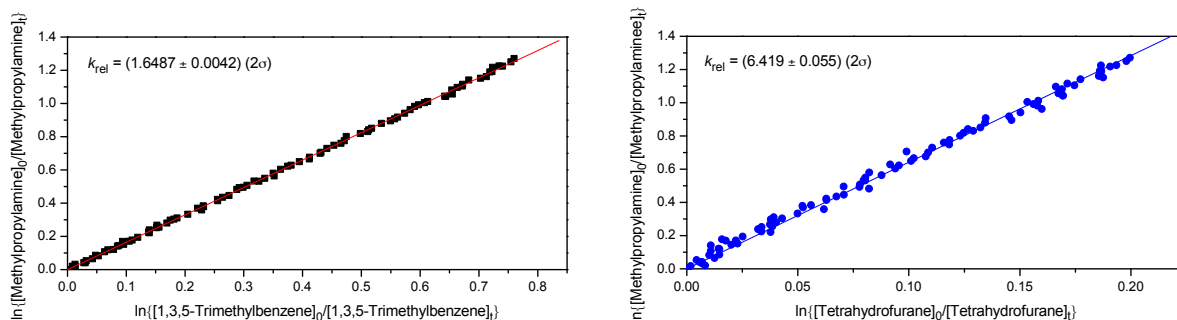


Figure C.15. Relative rate plots showing the decays of $\text{CH}_3(\text{CH}_3\text{CH}_2\text{CH}_2)\text{NH}$ versus 1,3,5-trimethylbenzene (left) and Tetrahydrofuran (right) during reactions with OH radicals at 1013 hPa and 298 K.

Experiment #5. A relative-rate kinetics study of OH radical reactions with 3 amines ($(\text{CH}_3)_2\text{NH}$ (DMA), $\text{CH}_3\text{NHCH}_2\text{CH}_3$ (MeEtA) and $\text{CH}_3\text{NHCH}_2\text{CH}_2\text{CH}_3$ (MePrA)) was carried out around noon on 2011.06.10. Tetrahydrofuran (THF) and 1,3,5-Trimethylbenzene (TMB) were used as reference compounds and IPN was injected as OH precursor. Figure C.16 shows the PTR-TOF-MS ion signals of the 6 compounds during the photo-oxidation experiment. The figure also includes an indication of the time span selected for analysis.

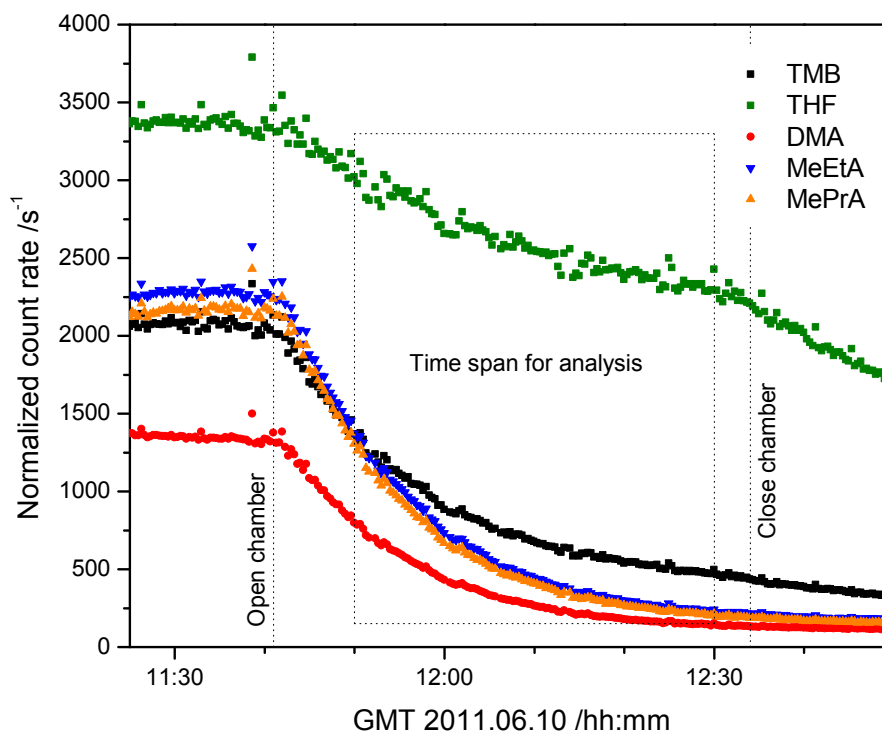


Figure C.16. The decays of $(\text{CH}_3)_2\text{NH}$, $\text{CH}_3(\text{CH}_3\text{CH}_2)\text{NH}$, $\text{CH}_3(\text{CH}_3\text{CH}_2\text{CH}_2)\text{NH}$, tetrahydrofuran and 1,3,5-trimethylbenzene as a function of time in the presence OH radicals at 1013 hPa and 298 K.

The decays of $(\text{CH}_3)_2\text{NH}$, $\text{CH}_3\text{NHCH}_2\text{CH}_3$, $\text{CH}_3\text{NHCH}_2\text{CH}_2\text{CH}_3$ and TMB in the presence of OH radicals are plotted as $\ln\{[\text{Substrate}]_0/[\text{Substrate}]_t\}$ vs. $\ln\{[\text{THF}]_0/[\text{THF}]_t\}$ in Figure C.17. There is an excellent correlation between the THF and TMB data throughout the experiment. For the amines, again, there are systematic curvatures, which, as also mentioned above, tentatively are ascribed to particle formation and addition amine uptake on these particles.

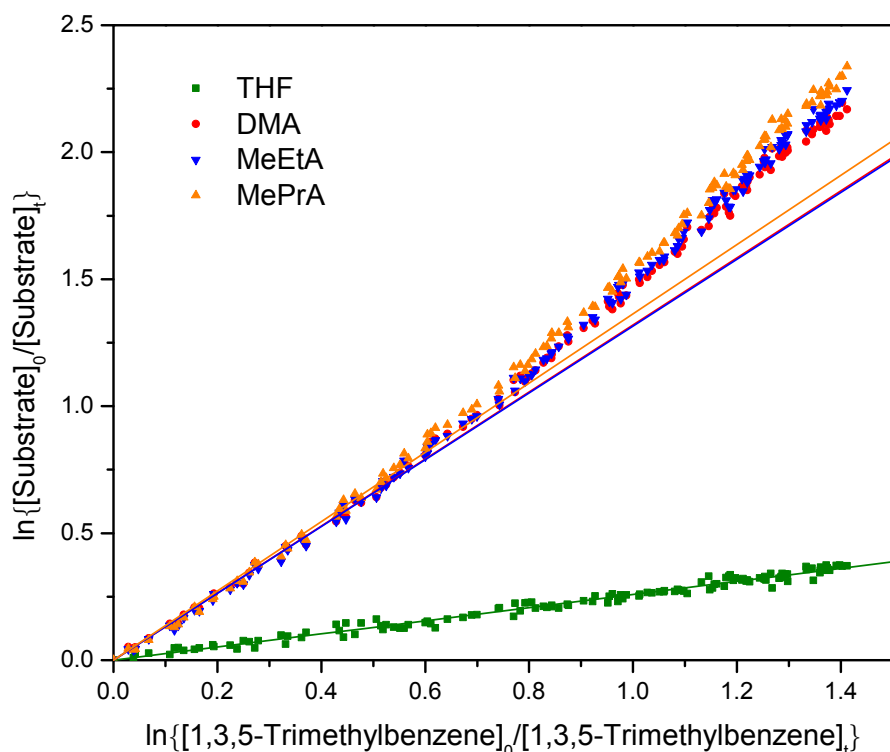


Figure C.17. Relative rate plots for the OH reactions with $(\text{CH}_3)_2\text{NH}$, $\text{CH}_3(\text{CH}_3\text{CH}_2)\text{NH}$, $\text{CH}_3(\text{CH}_3\text{CH}_2\text{CH}_2)\text{NH}$, and THF versus TMB at 1013 hPa and 298 K.

Relative-rate plots, based on the indicated time span (Figure C.17) are presented in Figure C.18 (DMA), Figure C.19 (MeEtA) and Figure C.20 (MePrA). The results obtained are included in Table 2.1, page 17.

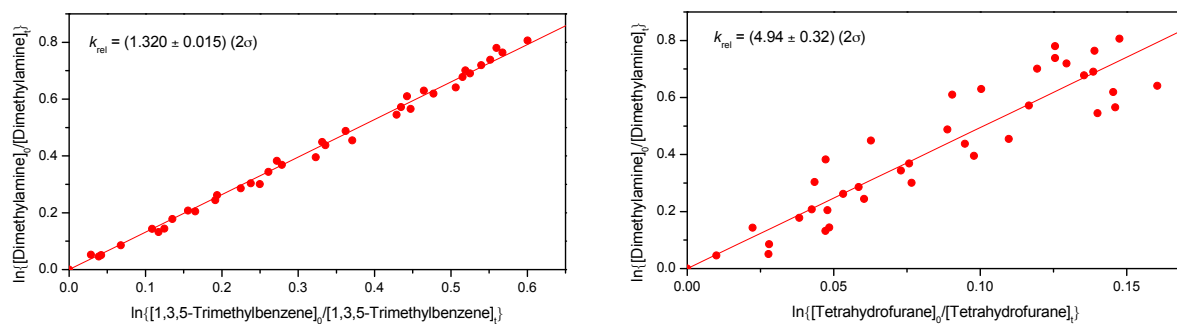


Figure C.18. Relative rate plots showing the decays of $(\text{CH}_3)_2\text{NH}$ versus 1,3,5-trimethylbenzene (left) and Tetrahydrofurane (right) during reactions with OH radicals at 1013 hPa and 298 K.

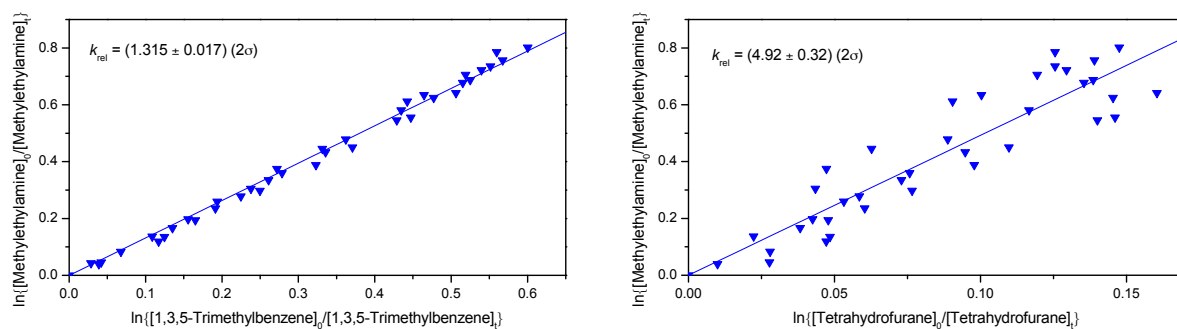


Figure C.19. Relative rate plots showing the decays of $\text{CH}_3(\text{CH}_3\text{CH}_2)\text{NH}$ versus 1,3,5-trimethylbenzene (left) and Tetrahydrofuran (right) during reactions with OH radicals at 1013 hPa and 298 K.

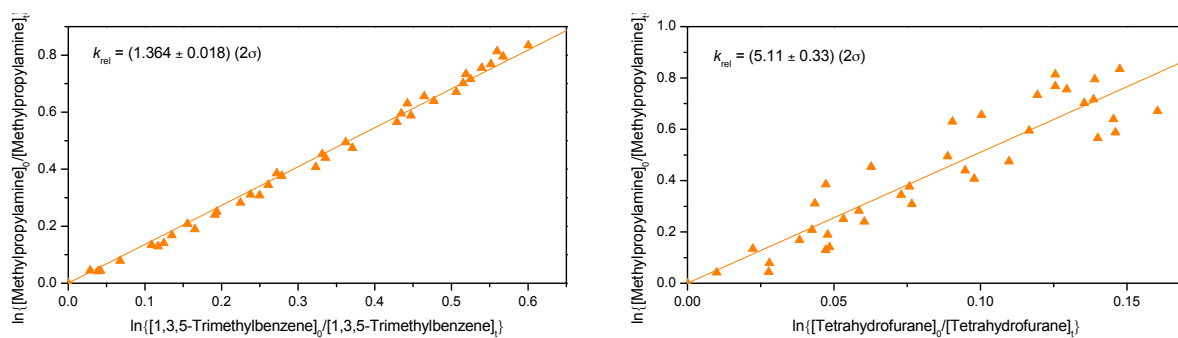


Figure C.20. Relative rate plots showing the decays of $\text{CH}_3(\text{CH}_3\text{CH}_2\text{CH}_2)\text{NH}$ versus 1,3,5-trimethylbenzene (left) and Tetrahydrofuran (right) during reactions with OH radicals at 1013 hPa and 298 K.

D. Additional results from Aerosol Studies

D1. Relative Ion Efficiency (RIE) of the organic fraction of pure aminium nitrate salts.

Accurate identification and quantification of the primary aminium nitrate salts by the AMS is possible by analysis of synthesized ethyl-, diethyl-, triethyl- and piperazine-aminium nitrate salts. This procedure allows the determination of the Relative Ionization Efficiency (RIE) of the organic fraction (Table D.1).

Table D.1. The RIE determined for the dimethyl-, diethyl, triethyl- and piperazine- aminium nitrate salts. All derived RIE are within 30%.

m/z	compound	RIE 70 eV	RIE 30 eV
45	EA	4.12	4.45
73	DEA	4.9	6.09
101	TEA	4.49	6.3
86	PZ *	2.7	3.5

*The primary aminium salt has two possible forms (a mononitrate and a dinitrate depending on the available nitrate).

D2. Photooxidation experiments

Diethylamine (DEA).

Figure D.1 illustrates the evolution of the AMS and SMPS loadings during the photo-oxidation experiment of diethylamine (DEA) under low NO_x conditions. 200 μl of DEA were injected in the chamber at 6:58, the roof was opened at 7:37 and closed at 9:32, flushing started at 11:01. A maximum aerosol mass loading of approximately 65 μg/m³ was detected around 10:20. The aerosol was composed by nitrate (blue), organic (green) and traces of water (light blue). The SMPS mass loadings were calculated using the number of particles and the derived effective density ($\rho = 1.3 \text{ g/cm}^3$) and are shown in red in Figure E.1 (line with dots).

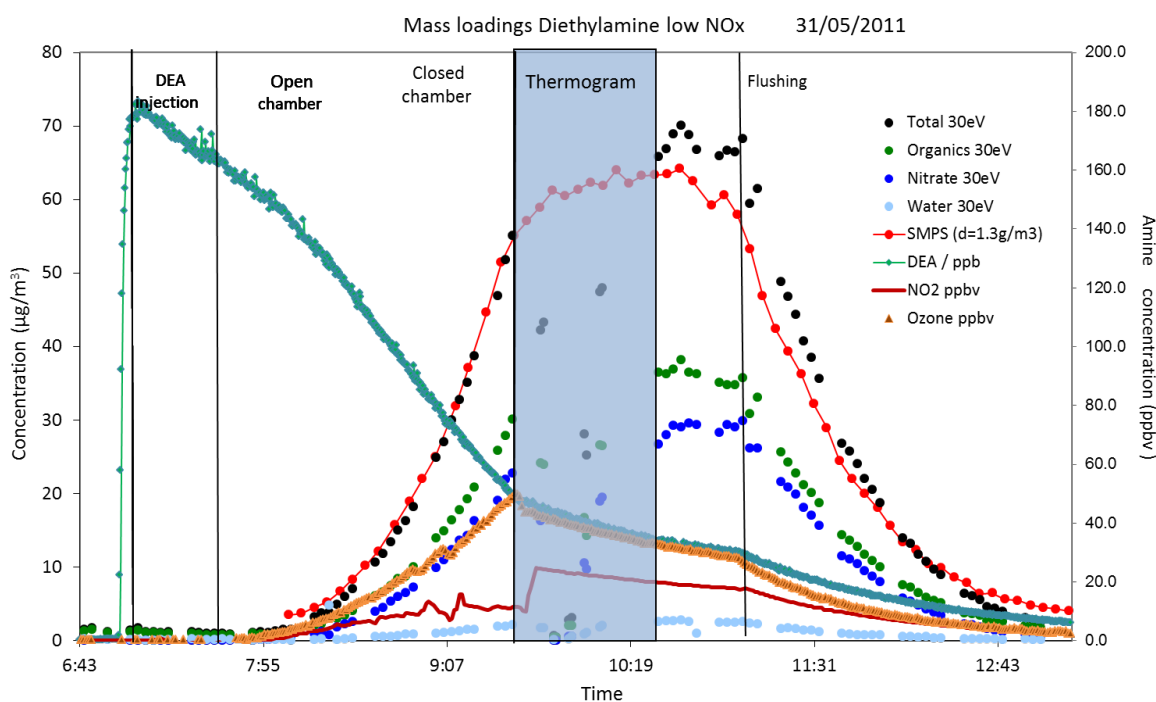


Figure D.1. Temporal evolution of Diethylamine, ozone, NO₂ and aerosol mass monitored by the SMPS and AMS during the 2011.05.31 low NO_x experiment.

A very good quantitative agreement was observed between the SMPS and the AMS data until 9:32 when the aerosol was formed by EANO_3 ; later on some secondary products were formed and some discrepancy was observed between AMS and SMPS data. A plausible reason is that the ionisation efficiency in the AMS has some uncertainties regarding the secondary products. In the present quantification the same ionisation efficiency as for the ethylammonium fraction was applied.

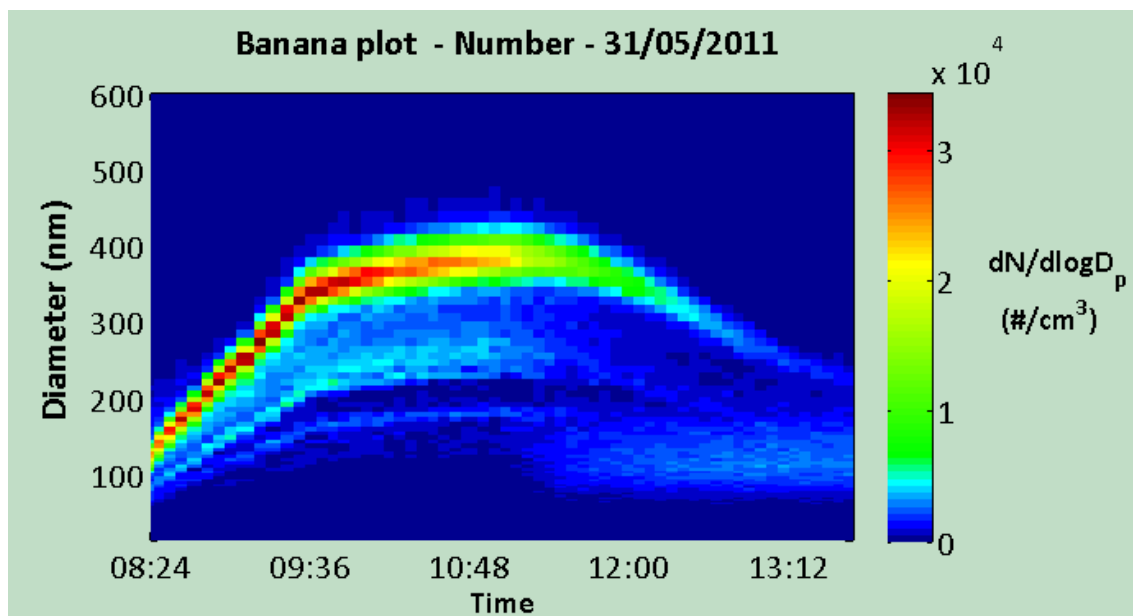


Figure D.2. Temporal evolution of aerosol diameter as a function of time from the SMPS data during the 2011.05.31 low NO_x experiment.

Most experiments were conducted without any seed and Figure E.2 shows how the number and size of the particles evolves during the photo-oxidation of DEA under low NO_x conditions. There was a clear nucleation followed by intense growth of the particles while the roof was open. When the roof was closed the growth subsides and a stable aerosol was formed. During the flushing period where the aerosol was diluted a clear evaporation of existing aerosol were observed with a decrease in particle size with time.

The AMS provided information on the fragmentation pattern and the time trend of the most significant fragments associated with diethylammonium nitrate are shown in Figure D.3. They were derived by comparison with DEANO_3 reference mass spectra. The major fragments associated to primary aminium nitrate salt are $\text{C}_4\text{H}_{11}\text{N}^+$, $\text{C}_4\text{H}_9\text{N}^+$, $\text{C}_3\text{H}_8\text{N}^+$, $\text{C}_3\text{H}_6\text{N}^+$, $\text{C}_2\text{H}_6\text{N}^+$, $\text{C}_2\text{H}_4\text{N}^+$ and CH_4N^+ . Some of the reaction products, however, form the same fragment ions as the primary amine ($\text{C}_4\text{H}_9\text{N}^+$, $\text{C}_3\text{H}_6\text{N}^+$, $\text{C}_2\text{H}_4\text{N}^+$ and $\text{C}_2\text{H}_6\text{N}^+$). Using the DEANO_3 reference spectra it was possible to discriminate between the contribution of the primary amine salt and the reaction products. Figure D.4. shows a comparison between the spectra of the reference diethylammonium nitrate salt (top panel) and from the photooxidation experiment of diethylammonium at 10:30. The index "a" indicates the fraction of the ion fragment arising from the primary amine.

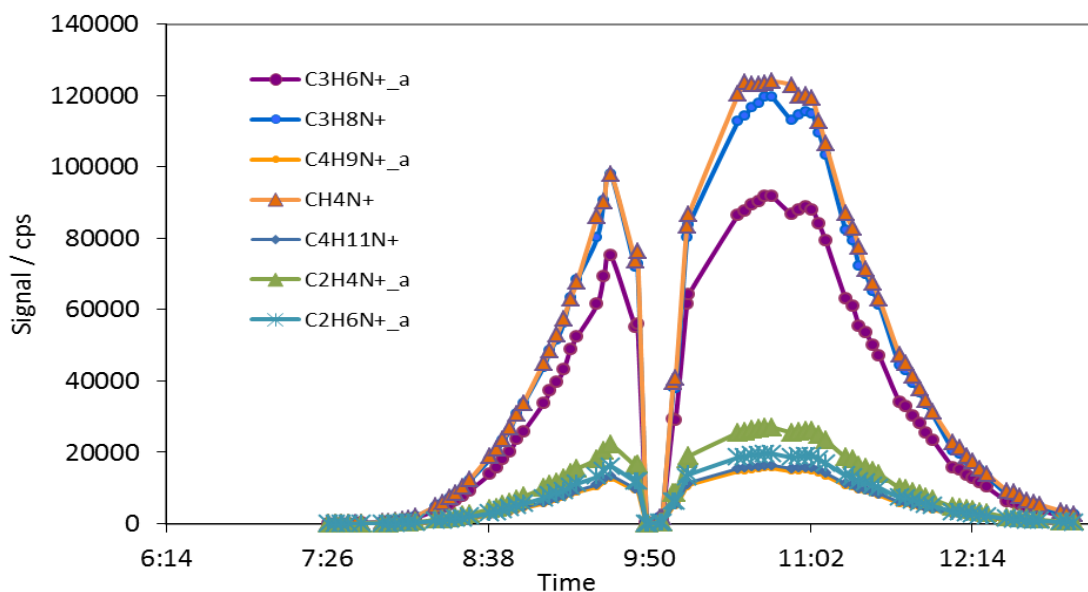


Figure D.3. Major identified fragments associated to diethylammonium nitrate salt (index “a” indicated the fraction of the ion fragment derived exclusively from primary amine).

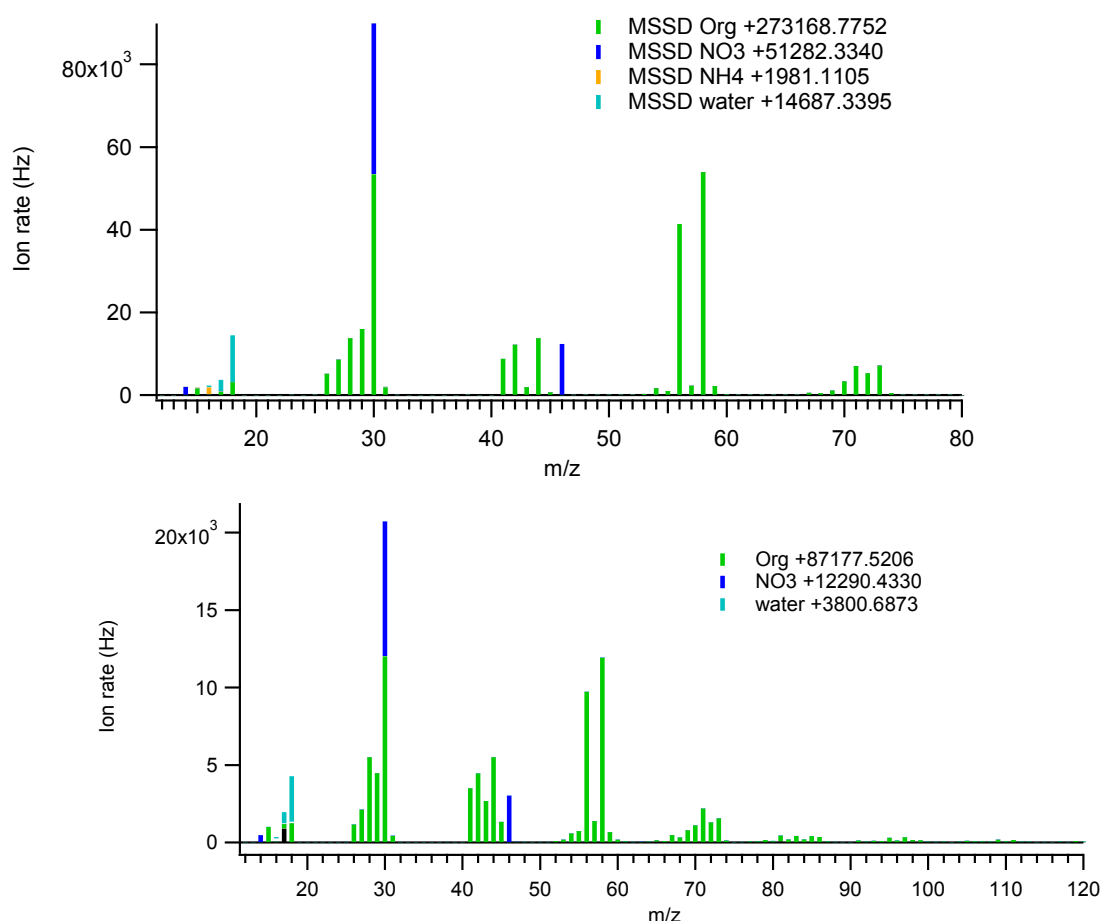


Figure D.4. AMS spectra acquired at 30 eV of the DEANO_3 (top panel) and the aerosol during the photo-oxidation of DEA of the 2011.05.31 at 11:48 (bottom panel).

From the fragmentation patterns and the ionisation efficiency one can derive the amount of nitrate associated to the primary DEA salt, which is shown in Figure D.5. Most of the nitrate was associated

to the primary DEANO₃ salt and towards the end of the experiment a maximum of about 15% could be associated to nitrates from DEA photo-oxidation products.

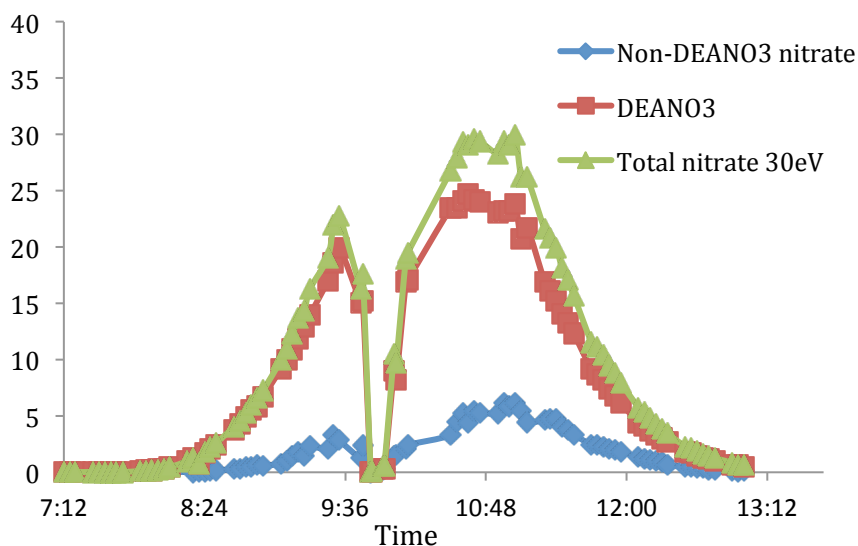


Figure D.5. Measured total nitrate (green line) and nitrate associated to diethylammonium nitrate salt (brown line) and remaining nitrate (blue line).

Figure D.6. shows the time trend of selected fragments (ion signals) associated to other products than the primary nitrate salt from the photo-oxidation experiment of DEA. Some of the reaction products form the same fragment ions that the primary amine ($C_3H_6N^+$, $C_2H_6N^+$ and $C_2H_4N^+$) but the signal shown in Figure D.6 takes only into account the secondary product contribution to this signal. A summary of a number of fragments from the DEA experiment are tabulated in Table D.2. This can be compared to the compound and fragments identified using off-line qTOF-MS analysis of the aerosol Table D.4.

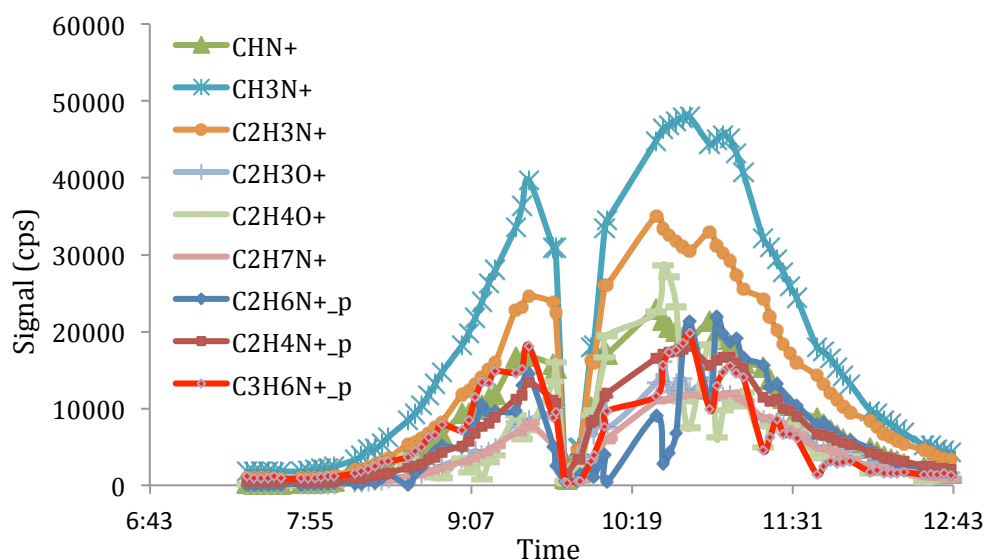


Figure D.6. Most abundant fragments associated to the remaining organic fraction in the particle phase. The index "p" indicates the secondary product contribution to this signal.

Table D.2. Some of the major ion signals observed in the particle phase during the photo-oxidation of diethylamine photo-oxidation experiments in May 2011.

Ion sum formula	2011.05.31	2011.06.01	Comments
	Low NOx	Low NOx	
CHN ⁺	27.011	27.011	diethylaminium salt
CH ₂ N ⁺ *			diethylaminium salt +product
CH ₃ N ⁺	29.010	26.009	diethylaminium salt + product
NO ⁺	29.997	29.997	nitrate
CH ₄ N ⁺	30.034	30.034	diethylaminium salt
C ₂ H ₃ N ⁺	41.029	41.029	diethylaminium salt + reaction product
C ₂ H ₄ N ⁺	42.035	42.035	diethylaminium salt + reaction product
C ₂ H ₃ O ⁺	43.018	43.018	reaction product
C ₂ H ₅ N ⁺	43.042	43.042	reaction product (ethaniminium salt?)
CO ₂ ⁺	43.992	43.992	reaction product
C ₂ H ₄ O ⁺	44.025	44.025	reaction product
C ₂ H ₆ N ⁺	44.049	44.049	diethylaminium salt + reaction product (ethaniminium salt?)
C ₂ H ₇ N ⁺	45.050	45.048	reaction product
NO ₂ ⁺	45.993	45.993	nitrate
C ₃ H ₆ N ⁺	56.050	56.050	diethylamine+ reaction product
C ₃ H ₈ N ⁺	58.060	58.065	diethylaminium salt
C ₄ H ₉ N ⁺	71.074	71.073	diethylaminium salt +reaction product #
C ₄ H ₁₁ N ⁺	73.080	73.080	diethylaminium salt

CH₃CH=NH+CH₃CH₂NH₂→ CH₃CH=NCH₂CH₃+NH₃. * Contribution calculated by subtracting the contribution of N₂⁺ signal, its exact m/z cannot be determined.

Table D.3. Major compounds detected in diethylamine photooxidation by off-line qTOF-MS analysis

2011.05.31 (low NOx)	2011.06.01 (low NOx)	Suggested molecular formula	Mol. Mass
m/z+	m/z+		
71.11	71.11	-	
74.12		C ₄ H ₁₁ N	73.09
	98.10	C ₆ H ₁₁ N	97.09
	99.08	-	
99.11	99.11	C ₆ H ₁₂ N	98.10
101.09		-	
111.13			
112.12			
115.12		C ₆ H ₁₄ N ₂	114.12
120.10		C ₄ H ₁₁ N ₂ O ₂	119.08
126.13			

Due to differences in ionization energy between the methods, ions in Table D.2 are generally of lower mass than ions listed in Table D.3.

Using the information as described above the total mass aerosol and organic yields were calculated and are shown in Figure D.7. The yields increases with time and it is linked to availability of HNO₃ and the photo-oxidation of the precursor amine.

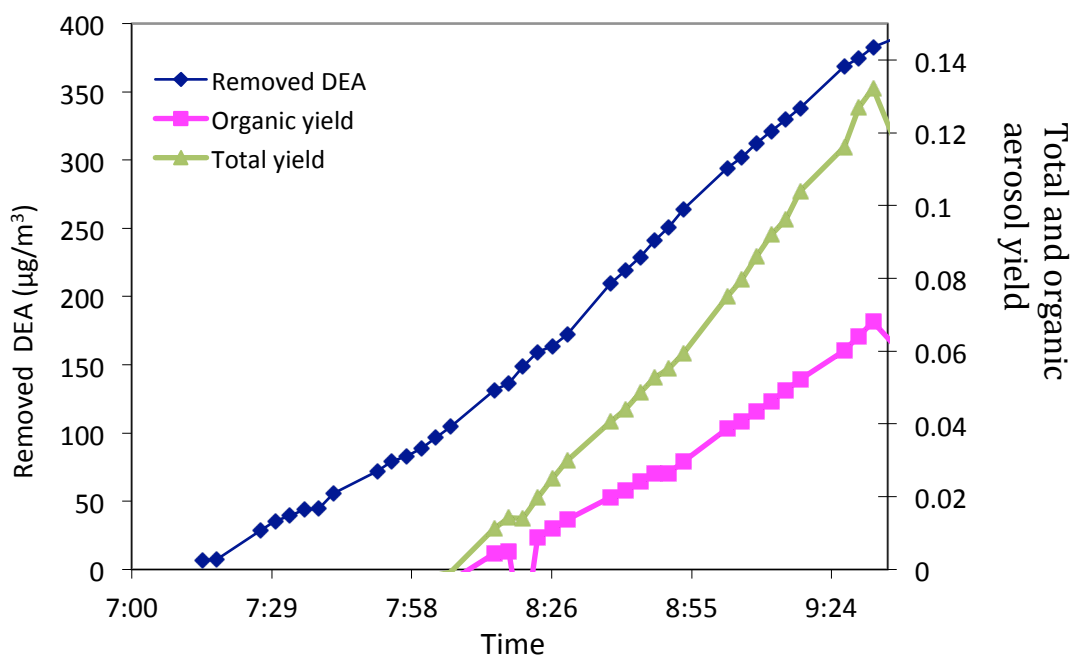


Figure D.7. Mass yields (total and organic) calculated towards the removed DEA from the gas phase.

For the particles formed from the photo-oxidation of DEA under low NO_x conditions the volatility, as expected, were going from being rather volatile in the beginning of the experiment to become less volatile with age, Figure D.8. This trend is associated to the increase in organic yield with time as illustrated in Figure D.7. Even if the total amount of secondary organics were below 10% it may still have an influence on the physical properties of the aerosol by reducing evaporation. However, the aerosol at the end of the experiment is still regarded as semi-volatile, which is illustrated by the observed shrink of particle diameter during the flushing of the chamber Figure D.2.

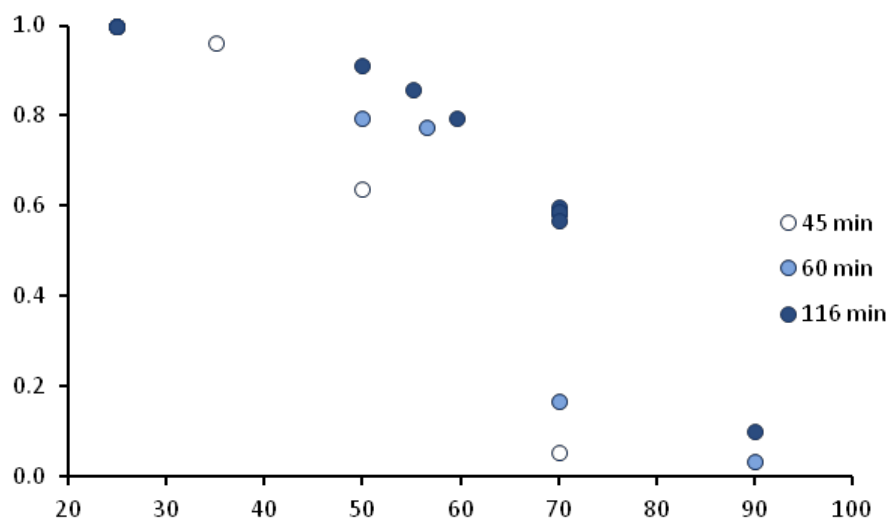


Figure D.8. The volume fraction remaining at selected temperatures for DEA particles in a low- NO_x experiment (2011-05-31), samples were collected at three times after the opening of the roof, time equals zero.

Triethylamine (TEA) Photo-oxidation

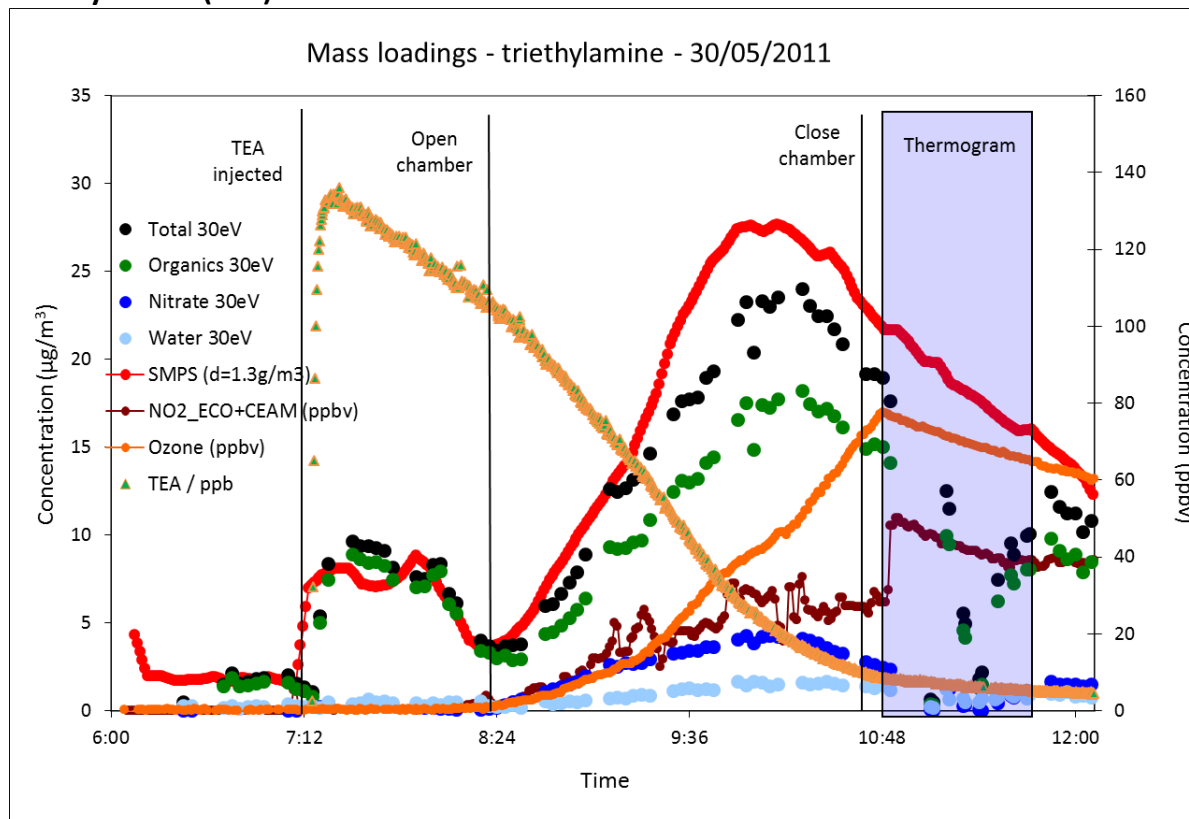


Figure D.9. Temporal evolution of triethylamine, ozone, NO_2 and aerosol mass monitored by the SMPS and AMS during the 2011.05.30 low NO_x experiment.

Figure D.9 depicts the evolution of the AMS, SMPS and TEOM loadings during the photo-oxidation of triethylamine (TEA). TEA (200 μL) was injected in the chamber at 7:16 under low NO_x condition. The roof was opened at 7:51 and closed at 10:43. A maximum aerosol mass loading of 20-25 $\mu\text{g}/\text{m}^3$ was observed around 10:10. Both 70 and 30 eV electron impact ionization energy AMS data were analysed but only the results from the 30 eV are presented here. The aerosol was composed of nitrate (blue), organic (green) and traces of water (light blue). The SMPS mass loadings were calculated using the number of particles and the derived effective density ($\rho = 1.2 \text{ g}/\text{cm}^3$) and are shown in red (line with dots). During the experiment a very fast first nucleation event was observed just few minutes after the injection of TEA in the chamber at 7:15. When the roof was open the photochemistry started and most of the pre-existing aerosol disappeared and a new size fraction of the aerosol started to grow Figure D.10.

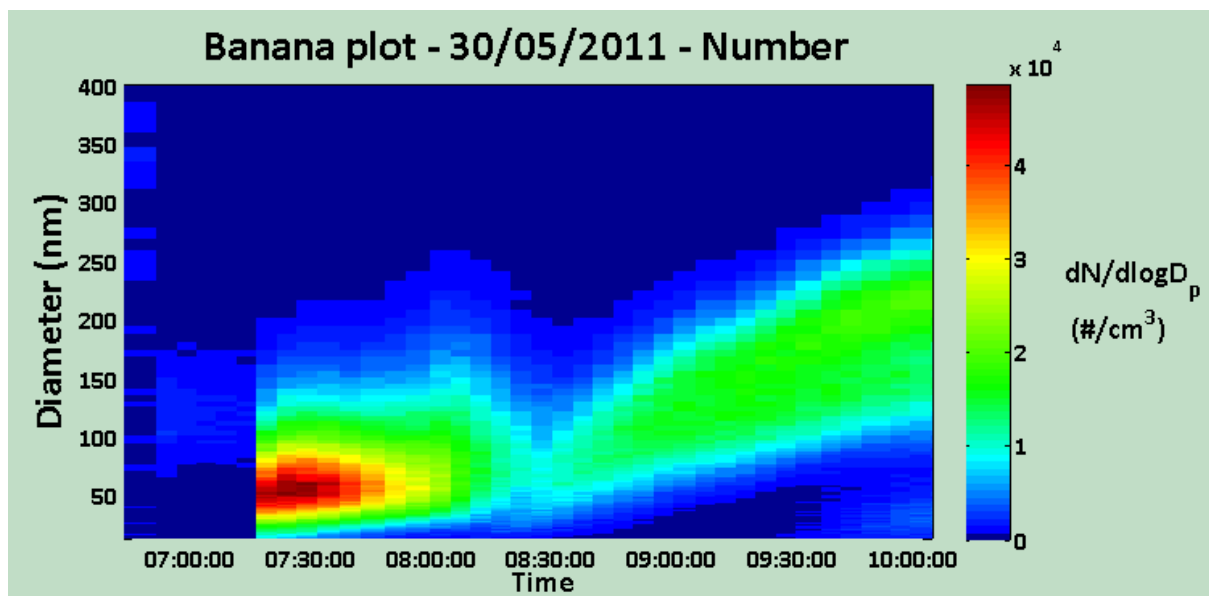


Figure D.10. Temporal evolution of the number of particles from the SMPS measurements during the 2011/05/30 low NO_x experiment.

Figure D.11 illustrates the reference spectrum of triethylammonium nitrate salt acquired at 30eV (top panel) and the aerosol composition of the TEA experiment at 10:15. Here it is clearly visible that a more important fraction with organic fragments (green colour) was formed during the photo-oxidation of TEA compared to the triethylammonium nitrate salt.

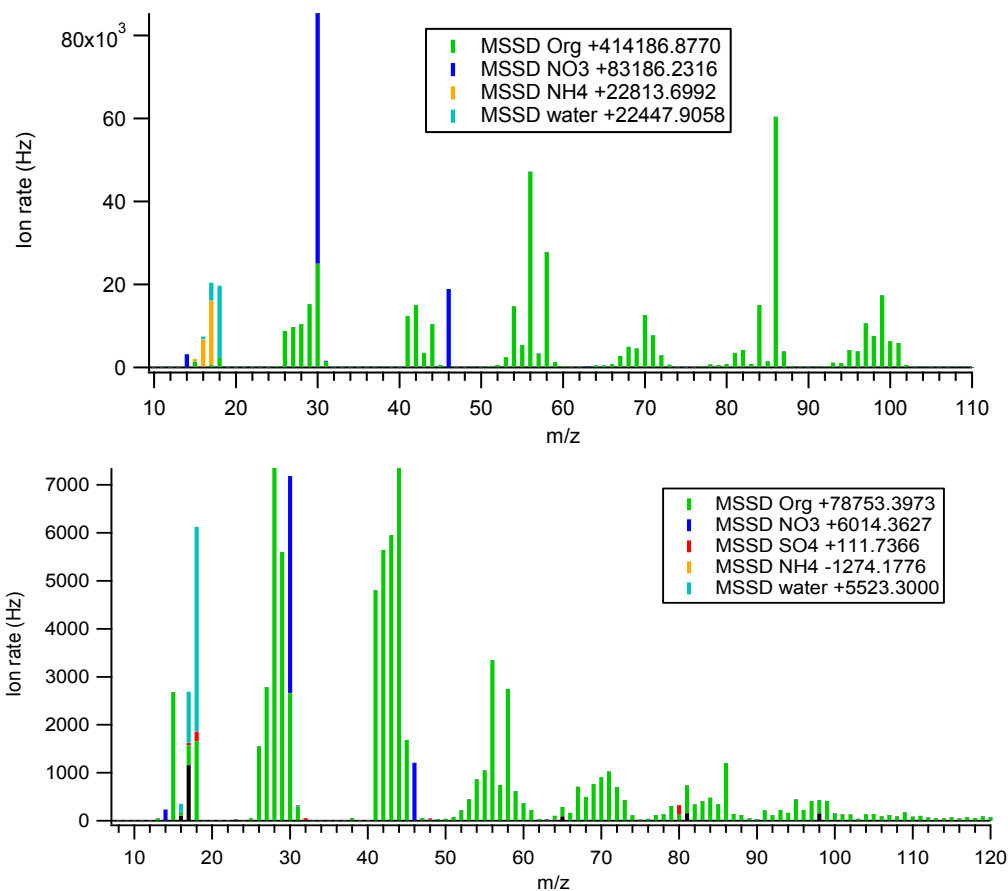


Figure D.11. AMS spectra acquired at 30eV of the TEA NO₃ (top panel) and the aerosol during the photo-oxidation of TEA of the 2011.05.30 at 10:15 (bottom panel).

The time trends of the most significant fragments associated with the triethylammonium fraction are shown in Figure D.12. The selection of these fragments was derived by comparison with a TEANO₃ reference mass spectrum taken in March 2011. The major fragments associated to the primary aminium nitrate salt are C₆H₁₅N⁺, C₆H₁₃N⁺ and C₅H₁₂N⁺. Some of products from the amine photo-oxidation form the same fragment ions as the primary amine (CH₄N⁺, C₃H₆N⁺ and C₃H₇N⁺). Using TEANO₃ reference spectra it was however, possible to discriminate their respective contribution to the primary amine salt and to reaction products of TEA-photo-oxidation. It is worth to note that the first nucleation event in the dark takes independently on acid-base reaction (availability of HNO₃), indeed between 7:20 and 8:24 the aerosol is formed by organic fraction (from the TEA). Figure D.12 shows the fragments of the triethylammonium salt while Figure D.14 shows the time trends of the fragments associated to the products. Table D.4 presents the major ion signals observed in the particle phase during the photo-oxidation of TEA (data from both 26th and 30th May 2011). This can be compared to the compound and fragments identified using off-line qTOF-MS analysis of the aerosol Figure D.5.

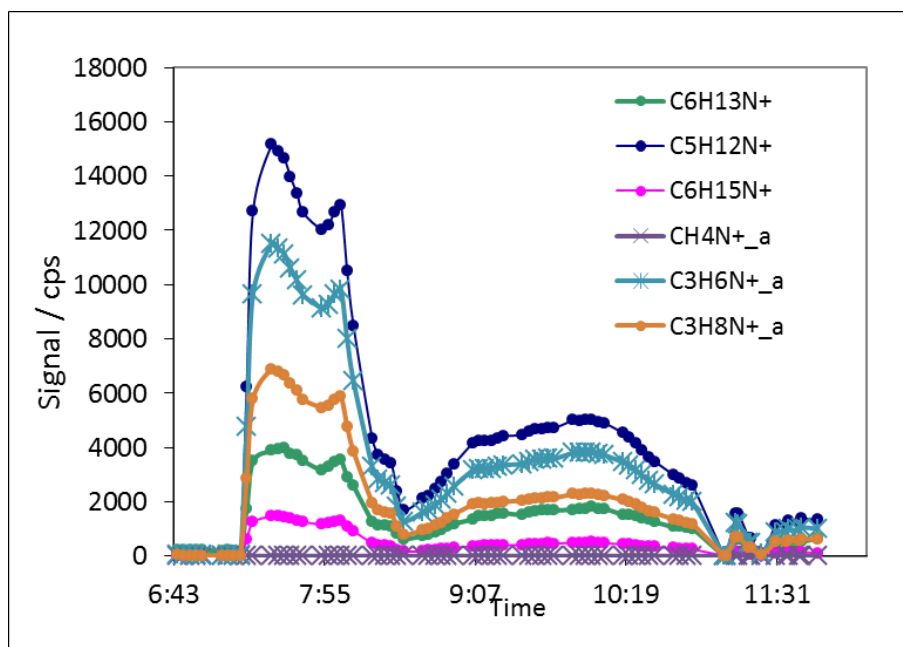


Figure D.12. Major identified fragments associated to triethylammonium nitrate salt.

The amount of nitrate associated to the primary TEA salt during the experiments is shown in Figure D.13. The nitrate is shown as total nitrate (blue line), nitrate associated to the triethylammonium nitrate salt (brown line) and the remaining nitrate (green line). At 10:00 approximately only 35% of the nitrate was from the TEANO₃ salt, the remaining nitrate was associated to an organic fraction which was partly oxygenated. TEA clearly tends to undergo important photo-oxidation and the acid-base reaction (path 1) is not the dominant one for particle formation.

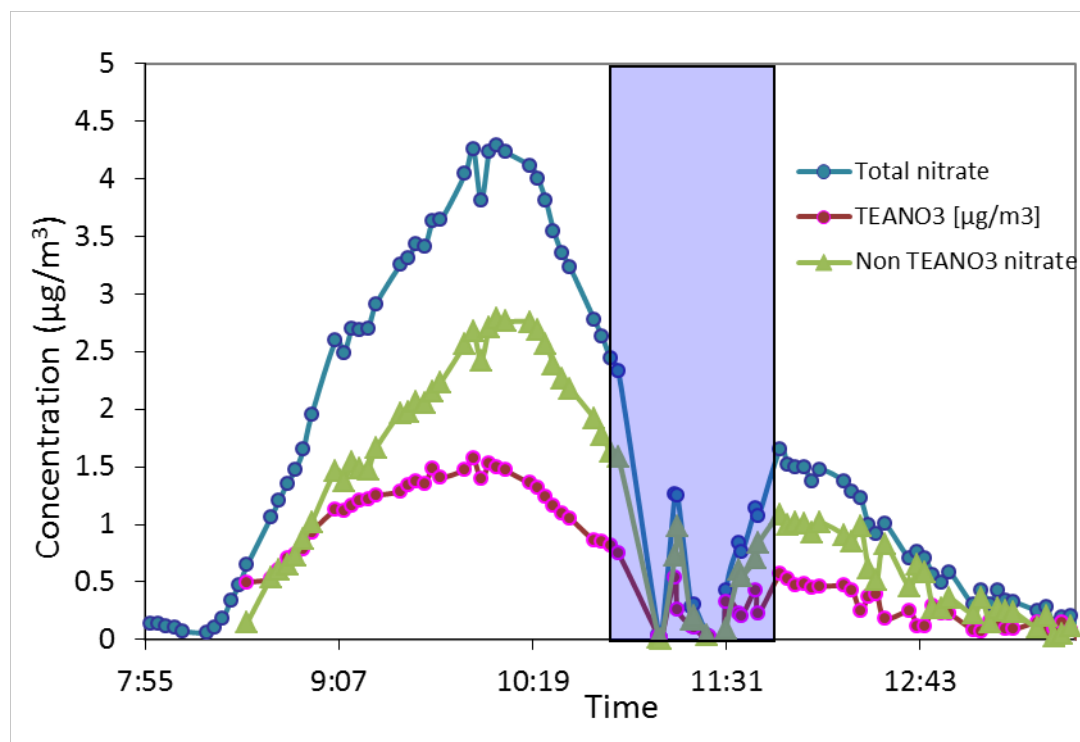


Figure D.13. Measured total nitrate (blue line) and nitrate associated to triethylammonium nitrate salt (brown line) and remaining nitrate (green line).

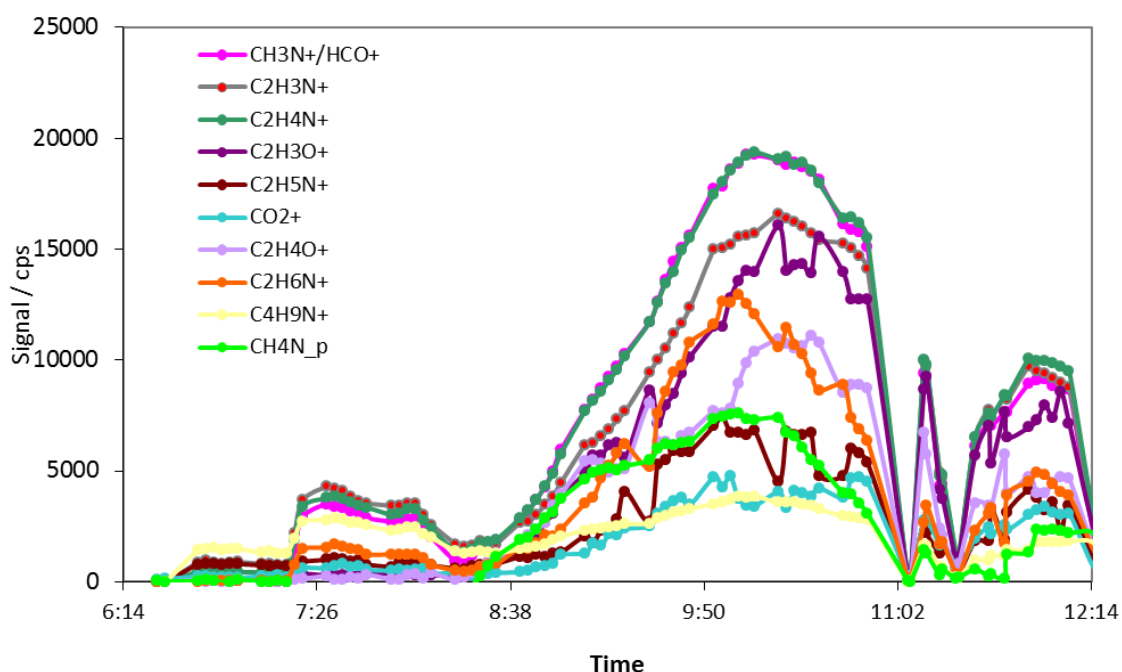


Figure D.14: Most abundant fragments associated to the remaining organic fraction.

Figure D.15 shows two interesting features: the ratio organic/nitrate increase considerably with time, after the first aerosol formation the aerosol evolved by adding mostly organics to the pre-existing seeds. The second part of Figure D.15 shows the O/C ratio an increase from 0.05 to 0.35, suggesting the importance of oxygenated products. The additional reaction of TEA with the O_3 formed during the photo-oxidation could be an explanation for the formation of the oxygenated species.

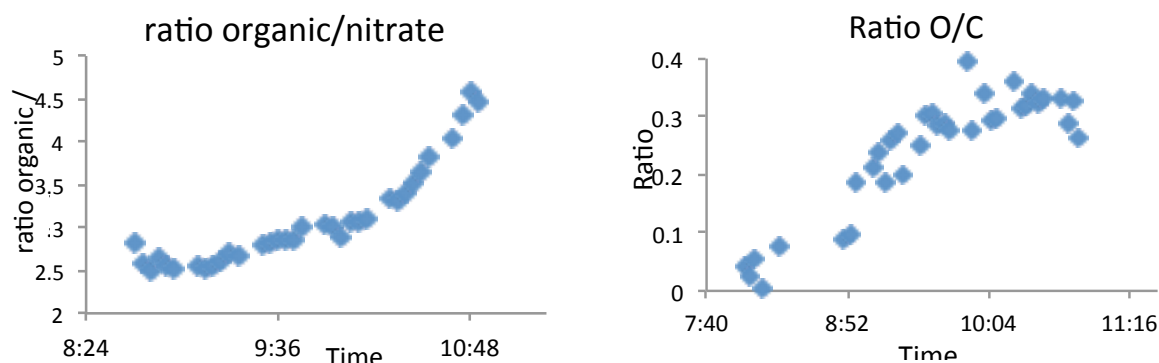


Figure D.15. Left plot: time evolution of the ratio organic/nitrate; right plot: time evolution of the ratio O/C.

Table D.4. Some of the major ion signals observed in the particle phase during the photo-oxidation of Triethylamine in May 2011.

Ion sum formula	2011.05.26 Low NOx	2011.05.30 Low NOx	Comments
CN ⁺	26.008	26.008	reaction product
CHN ⁺	27.011	27.011	reaction product
CO ⁺ /CH ₂ N ⁺ *			reaction product
HCO ⁺ /CH ₃ N ⁺	29.010	29.008	reaction product
NO ⁺	29.997	29.997	nitrate
CH ₄ N ⁺	30.034	30.034	triethylamine + product
C ₂ H ₃ N ⁺	41.029	41.029	triethylamine + reaction product
C ₂ H ₄ N ⁺	42.035	42.035	triethylamine + reaction product
C ₂ H ₃ O ⁺	43.018	43.018	reaction product
CO ₂ ⁺	43.992	43.992	reaction product
C ₂ H ₄ O ⁺	44.025	44.025	reaction product
C ₂ H ₆ N ⁺	44.049	44.049	triethylamine +reaction product
CH ₃ NO ⁺	45.021	45.021	oxidation product
NO ₂ ⁺	45.993	45.993	Nitrate
C ₃ H ₅ N ⁺	55.047	55.047	mostly reaction product
C ₃ H ₆ N ⁺	56.054	56.052	triethylamine +reaction product
C ₃ H ₈ N ⁺	58.060	58.065	triethylamine +reaction product
C ₄ H ₈ N ⁺	70.066	70.066	triethylamine +reaction product
C ₄ H ₉ N ⁺	71.075	71.075	Triethylamine salt+reaction product
C ₃ H ₆ NO ⁺	72.035	72.035	reaction product
C ₄ H ₁₀ N ⁺	72.080	72.080	triethylamine
C ₅ H ₇ N ⁺	81.069	81.069	Reaction product
C ₅ H ₉ N ⁺	83.082	83.082	Reaction product
C ₅ H ₁₀ N ⁺	84.096	84.092	triethylamine +reaction product
C ₅ H ₁₂ N ⁺	86.092	86.092	triethylamine
C ₆ H ₁₃ N ⁺	99.109	99.109	triethylamine
C ₆ H ₁₅ N ⁺	101.118	101.118	triethylamine

*Contribution calculated by subtracting the contribution of N₂⁺ signal, its exact m/z cannot be determined.

Table D.5. Major compounds detected in triethylamine photo-oxidation 2011.05.30 (low NO_x) by off-line qTOF-MS analysis

2011.05.30			
m/z+	Mol. Mass	Mol. Formula	Mol. Mass
71.11	70.10	-	
73.05	72.04	C ₃ H ₆ NO	72.04
81.09	80.08	-	
85.12	84.11		
101.09	100.08	C ₅ H ₁₀ NO	100.08
108.11	107.10	-	
112.12	111.11		
122.12	121.11	-	-
129.10	128.09	C ₆ H ₁₂ N ₂ O	128.09
135.14	134.13		

Figure D.16 show the calculated organic and total yield. For the calculation we took into account the aerosol formed after the roof was open, therefore we took into account only gas-to-particle conversion during the photo-oxidation of amine. We therefore ignored the first rapid nucleation event occurred in the dark when TEA was injected in the chamber.

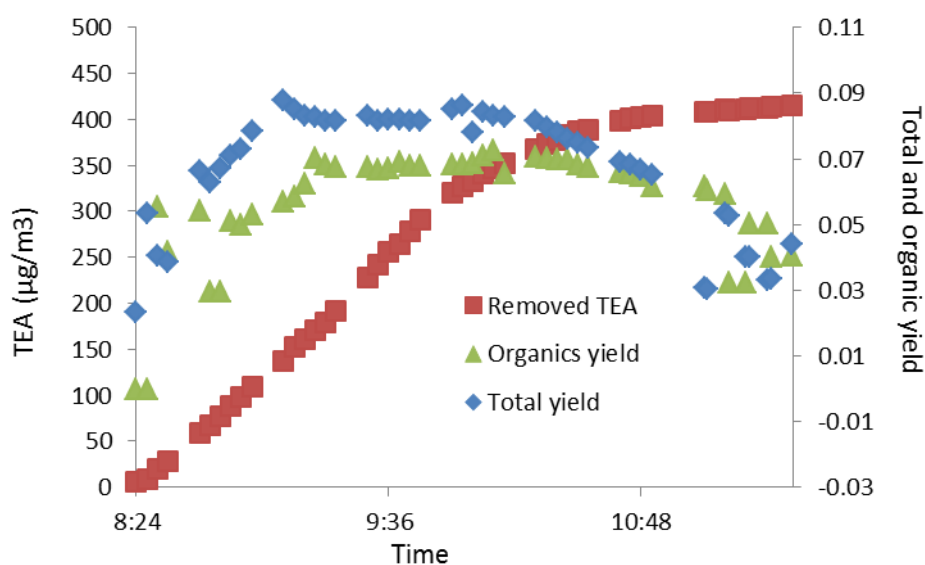


Figure D.16. TEA removal from the gas phase (red squares), and total aerosol yield (blue diamonds) and organic aerosol yield (green triangles).

The thermal properties of the produced aerosol are illustrated in Figure D.17. The particles formed in the photo-oxidation experiment of triethylamine during low NO_x conditions became less volatile with time, indicating transformation into particles with lower salt content. During the photo-oxidation of TEA a large fraction of secondary organic products were formed, some of those were oxygenated and they were probably responsible for the lower volatility that the TEANO₃.

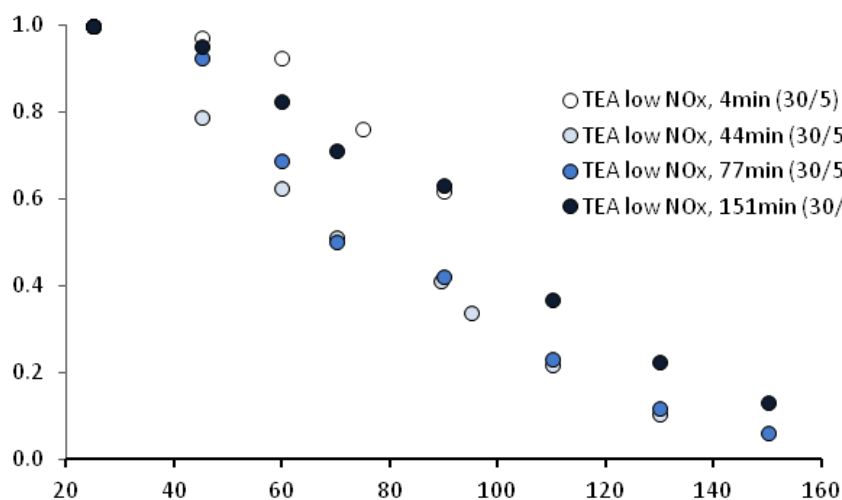


Figure D.17. The volume fraction remaining at selected temperatures for TEA particles in a low-NO_x experiment (2011-05-30), samples were collected at three times after the opening of the roof, time equals zero.

Piperazine photo-oxidation

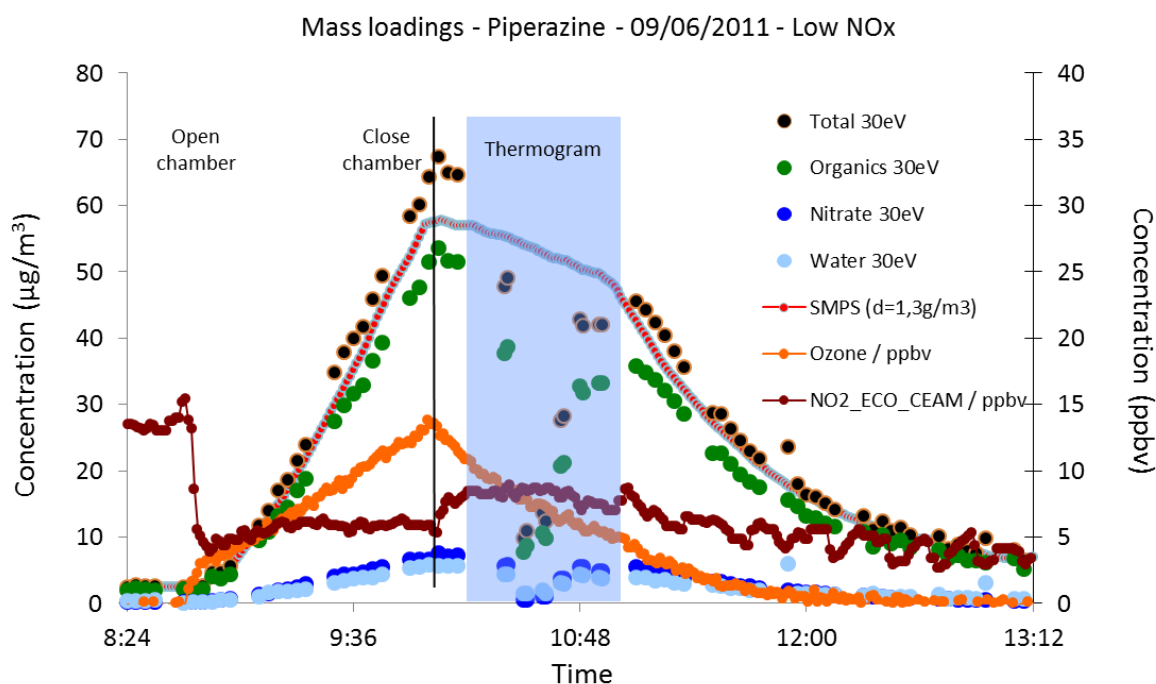


Figure D.18. Temporal evolution of ozone (orange), NO₂ (brown) concentrations and aerosol mass monitored by the SMPS (red dots) and AMS during the piperazine = low NO_x experiment (2011.06.09). AMS data: total aerosol (black dots and full lines), nitrate (blue dots and full lines), organic (green dots and full lines) and organic-water (light blue dots and full lines).

Figure D.18 depicts the evolution of the ozone, NO₂ and aerosol loading (total, organic and nitrate) during the experiment. Piperazine and NO_x have been injected at 6:44 in the chamber; the canopy was opened at 8:00 and closed at 10:00. A maximum aerosol mass loading of approximately 60µg/m³

was detected by the SMPS at 9:57, nearly 2 hours after the canopy was opened. The SMPS mass loadings are calculated using the number of particles and the derived effective density ($\rho = 1.3 \text{ g/cm}^3$) and are shown in red (line with dots). A discrepancy of about 15-20% between SMPS data was observed in this experiment.

The amount of nitrate associated to the primary Piperazine salt during the experiment is shown in Figure D.19. The nitrate is shown as total nitrate (blue line), nitrate associated to the Piperazine nitrate salt (brown line) and the remaining nitrate (green line). At 10:00 approximately only 55% of the nitrate was from the PipNO_3 salt, the remaining nitrate was associated to an organic fraction, which was partly oxygenated.

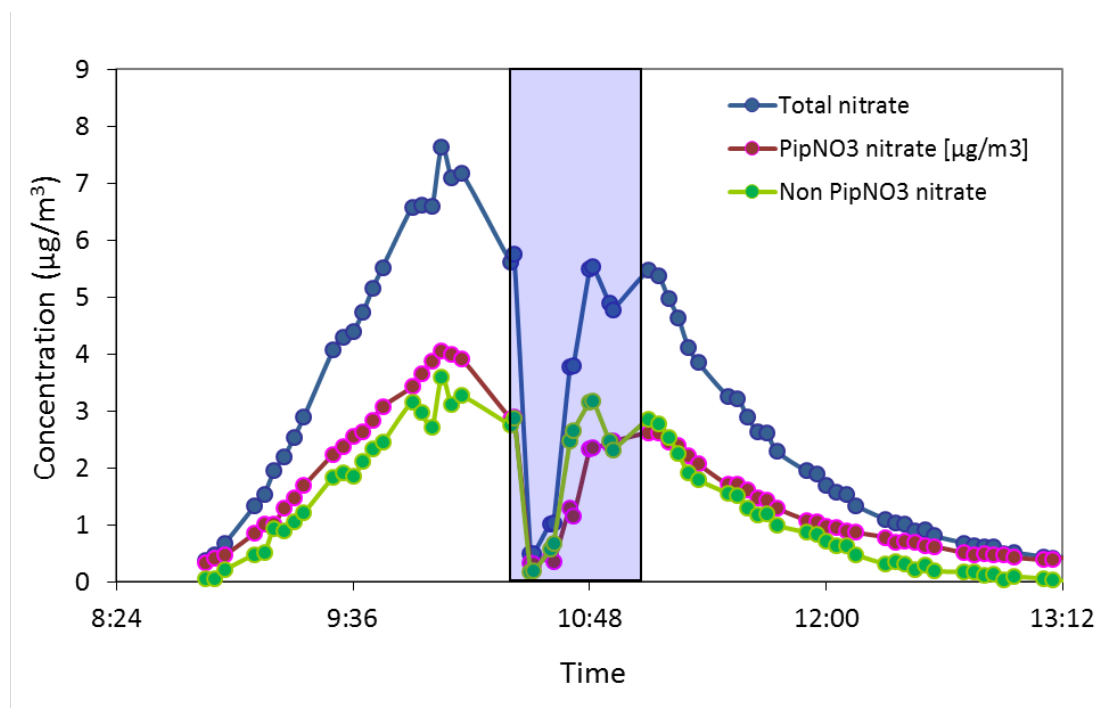


Figure D.19. Measured total nitrate (blue line) and nitrate associated to Piperazine nitrate salt (brown line) and remaining nitrate (green line).

The thermal properties of aerosol produced during the photo-oxidation of piperazine at low and high NO_x conditions are shown in Figure D.20 and Figure D.21. In all piperazine photo-oxidation experiments the initial aerosols was much less volatile than for the other amines studied. This is also reflected in the ageing of the aerosol for which volatility did only slightly changed with time (Figure D.20. and Figure D.21). In addition there was no significant difference between high and low NO_x experiments.

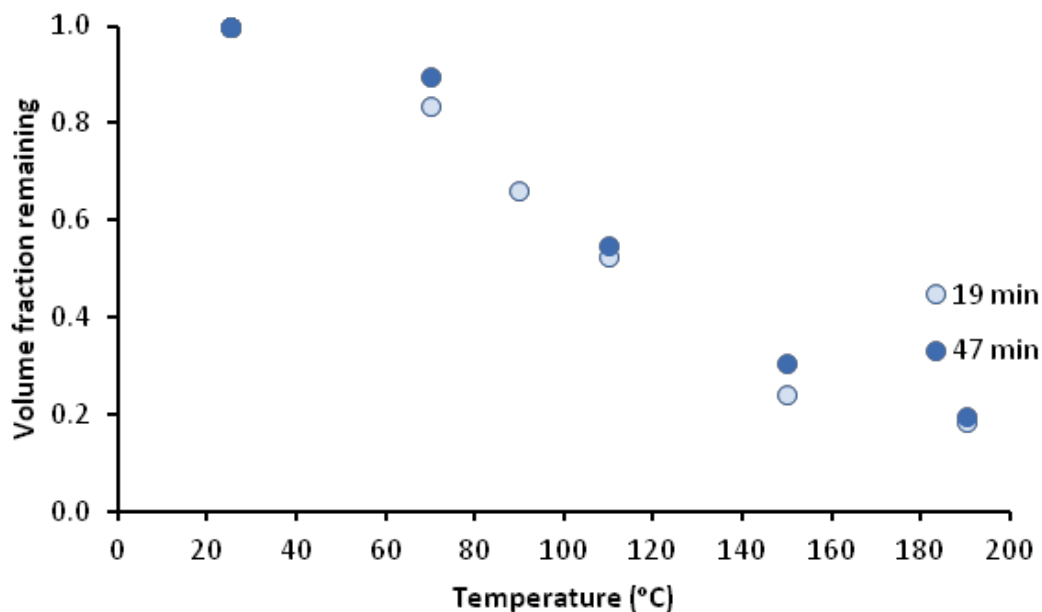


Figure D.20. Piperazine low NOx (2011-06-09_morning experiment)

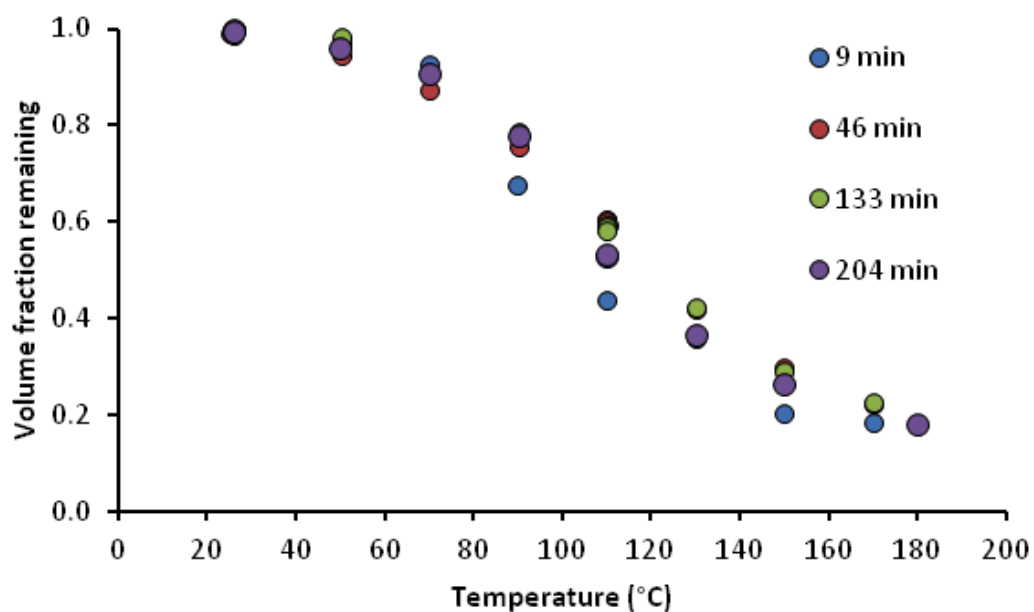


Figure D.21. Piperazine high-NOx (2011-04-06), the volume fraction remaining at selected temperatures measured at three occasions during the experiment.

Analysis of aerosol samples by qTOF-MS generally shows the same compounds at both high and low NO_x conditions (Table D.6) in agreement with the volatility properties. The parent compound, piperazine is observed here because it condenses on the aerosol maybe as the dinitrate salt. Pyrazine seems to be produced as an oxidation product of piperazine. The products in Table D.6 were formed through both gas-phase oxidation and condensed phase processes.

Table D.6. Some of the major ions observed in off-line analysis of piperazine photo-oxidation aerosol samples.

2010.07.20	2010.07.21	2010.07.22	2011.04.05	20110406	20110609			
	High NOx	High NOx	High NOx	High NOx	Low NOx	Suggested		Suggested
m/z +	m/z +	m/z +	m/z +	m/z +	m/z +	Formula	Molar mass	ion m/z
44.046	44.046							
56.046	56.046	56.046				-	-	
72.041	72.041	72.041	72.033			C2H3N2O	71.025	72.032
			81.051	81.052	81.055	C4H4N2 pyrazine	80.037	81.045
			85.070	85.077		C4H8N2	84.069	85.077
87.089	87.089	87.089	87.077	87.075	87.075	C4H10N2 piperazine	86.081	87.089
99.078	99.078		99.072			C4H8N3	98.072	99.080
				100.062	100.069	C4H7N2O	99.056	100.064
			109.090	109.090	109.087			
			114.081	114.081	114.084	C5H9N2O	113.071	114.079
115.083	115.083	115.083	115.077	115.077	115.077	C4H8N3O	114.067	115.075
116.082	116.082					C4H9N3O or C4H7N2O2	115,075 or 115.074	116,083 or 116,082
117.065	117.065	117.065	117.058			C4H8N2O2	116.057	117.065
		158.096			123.104	C3H12N3O2	122.093	123.101
				125.108		C7H12N2	124.000	125.008
				128.096	128.099	C6H11N2O	127.087	128.095

E3. Analysis of nitramines and nitrosamines in aerosol samples

Aerosol filter samples were analysed for formamides, nitramines and nitrosamines using GC-MS. Results are listed in Table D.7. Generally the concentrations are low compared to gas phase concentrations, which was also expected. However, it should be noted that adsorption of gas phase compounds cannot be excluded, which is also indicated by the presence of detected compounds on both the upper and lower filter in the dual filter sampler.

Table D.7. Formamides, nitramines and nitrosamines in aerosol filter samples. F1 up is the first filter in dual filter sampler, while F1 down is the second filter. F2 is a filter in the second sampling unit.

Date	ID	Objective	Compound ($\mu\text{g}/\text{m}^3$)						
			Dimethyl-formamide Me ₂ NNO ₂	Nitromethyl-amine MeNNO ₂	Nitroethyl-amine EthNNO ₂	Diethyl-nitrosamine Eth ₂ NNO	Methyl-Formamide MeNHCHO	Dimethyl-Formamide Me ₂ NCHO	
21-03-2011	F1-DOWN	Dimethylamine + NOx	0,12	0,32	-	0,11	1,77	0,45	
21-03-2011	F1-UP	Dimethylamine + NOx	-	0,63	-	0,11	1,22	0,27	
21-03-2011	F2	Dimethylamine + NOx	-	1,07	-	0,20	3,81	0,98	
22-03-2011	F1-DOWN	Methylamine + NOx	-	0,61	-	0,11	0,73	0,15	
22-03-2011	F1-UP	Methylamine + NOx	-	0,40	-	0,11	0,58	0,12	
22-03-2011	F2	Methylamine + NOx	-	1,05	-	0,22	1,58	0,25	
25-03-2011	F1-DOWN	Photooxidation of ethylamine	-	0,36	0,72	0,11	0,34	0,11	
25-03-2011	F1-UP	Photooxidation of ethylamine	-	0,23	0,24	0,10	0,26	0,10	
25-03-2011	F2	Photooxidation of ethylamine	-	0,56	0,81	0,22	-	0,21	
28-03-2011	F1-DOWN	Diethylamine	-	0,20	0,21	0,11	-	-	
28-03-2011	F1-UP	Diethylamine	-	0,20	0,19	0,11	-	-	
28-03-2011	F2	Diethylamine	-	0,41	0,43	0,22	-	-	
28-03-2011	F1-DOWN (tarde)	Dimethylamine + NOx	-	0,28	0,52	0,11	-	-	
28-03-2011	F1-UP (tarde)	Dimethylamine + NOx	-	0,22	0,25	0,11	-	-	
28-03-2011	F2 (tarde)	Dimethylamine + NOx	-	0,51	0,74	0,22	-	-	
29-03-2011	F1-DOWN	Diethylamine + NO ₂ + IPN-D6	-	0,21	0,19	0,11	-	-	
29-03-2011	F1-UP	Diethylamine + NO ₂ + IPN-D6	-	0,21	0,19	0,11	-	-	
29-03-2011	F2	Diethylamine + NO ₂ + IPN-D6	-	0,44	0,44	0,23	-	-	
30-03-2011	F1-DOWN	Diethylamine + NO ₂	-	0,21	0,21	0,11	-	-	
30-03-2011	F1-UP	Diethylamine + NO ₂	-	0,21	0,20	0,11	-	-	
30-03-2011	F2	Diethylamine + NO ₂	-	0,42	0,40	0,22	-	-	
31-03-2011	F1-DOWN	Triethylamine + NOx	-	-	0,43	-	-	-	
31-03-2011	F1-UP	Triethylamine + NOx	-	0,50	0,43	-	0,93	-	
31-03-2011	F2	Triethylamine + NOx	-	-	0,93	-	2,54	-	
01-04-2011	F1-DOWN	Triethylamine + NOx	-	0,59	0,44	-	0,55	-	
01-04-2011	F1-UP	Triethylamine + NOx	-	0,43	0,44	-	1,08	-	
01-04-2011	F2	Triethylamine + NOx	-	1,13	0,92	-	1,36	-	

E. Infrared absorption cross-sections

Infrared reference spectra of compounds with vapour pressures above 0.2 mbar were obtained of the pure gases at 295 ± 2 K in cells of 10.0 ± 0.1 and $23.0 \text{ cm} \pm 0.1$ length equipped with windows of CsI and KBr, respectively. The spectra were recorded in the 4000-400 wavenumber region using a Bruker IFS 66v FTIR spectrometer employing a nominal resolution of 0.5 cm^{-1} . Single channel spectra (background or sample) were recorded averaging 128 interferograms and applying a Boxcar apodization. A Ge/KBr beam splitter was used to cover the spectral region. To ensure optical linearity a DTGS detector was used.

The partial pressures of the gases in the cell ranged from 0.1 to 5 hPa and were measured using a CERVAC CTR 100 pressure transducers with a stated accuracy of $\pm 0.2\%$. The absorption cross-sections were obtained from the absorbance spectra assuming that the gas was ideal.

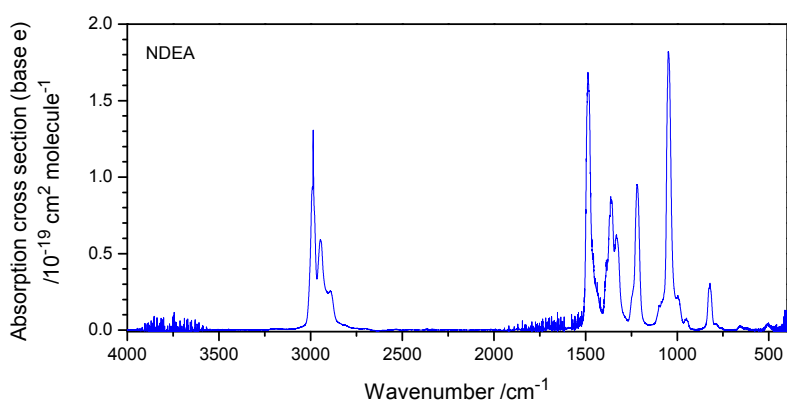


Figure E.1. Infrared absorption cross-section of *N*-nitroso diethylamine.

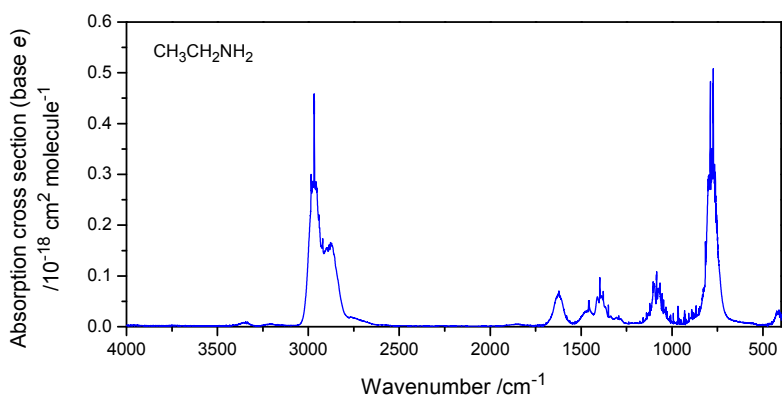


Figure E.2. Infrared absorption cross-section of ethylamine.

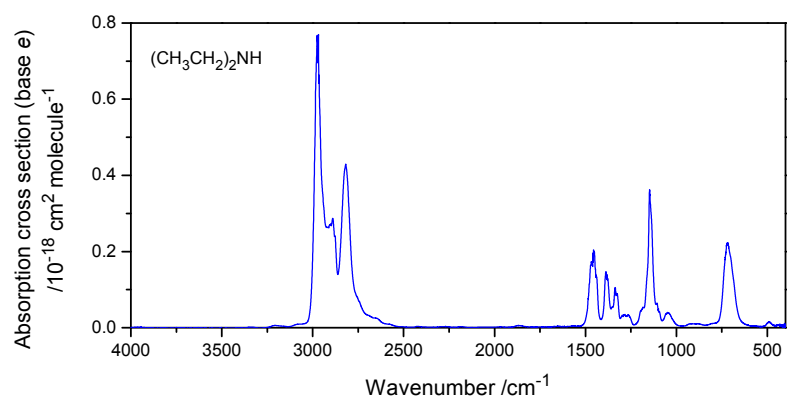


Figure E.3. Infrared absorption cross-section of diethylamine.

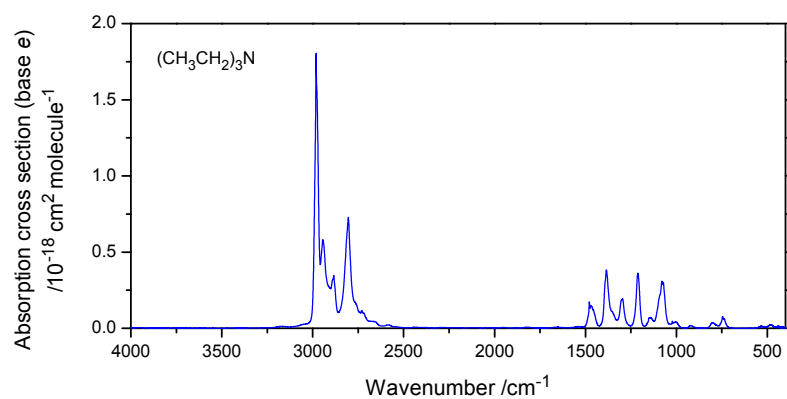


Figure E.4. Infrared absorption cross-section of triethylamine.

F. Dipole moments and isotropic polarizabilities from Quantum Chemical Calculations

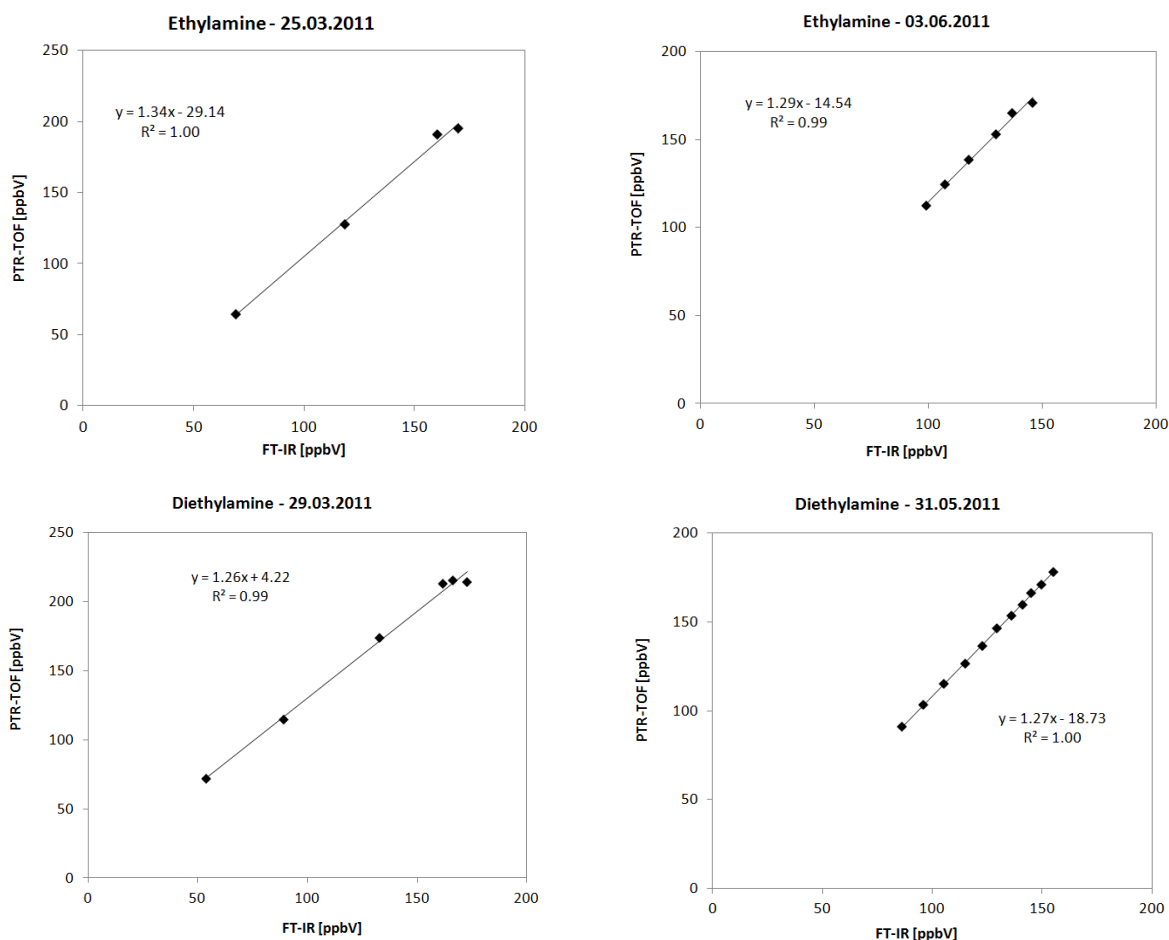
Dipole moments and isotropic polarizabilities were obtained in DFT calculations using B3LYP functional⁹²⁻⁹⁵ and the aug-cc-pVTZ basis set.⁹⁶ All calculations were performed in Gaussian 09.³⁷

Table F.1. Dipole moments (μ /D) and isotropic polarizabilities (α /Å³).

Molecule	μ_{calc}	μ_{exp}	α_{calc}	α_{exp}
CH ₃ CH ₂ NH ₂	1.27	1.01 ⁹⁷	5.79	
CH ₃ CH=NH	2.57		5.32	
CH ₃ CH ₂ N=CHCH ₃	1.43		9.44	
CH ₃ N=CHCH ₃	1.49		7.51	
CH ₃ CH ₂ NHNO ₂	4.52		8.11	
CH ₃ C(O)NH ₂	1.75		5.92	
CHONH ₂				
CHOCH ₂ NH ₂	3.92		5.91	
(CH ₃ CH ₂) ₂ NH	0.79		9.44	
(CH ₃ CH ₂) ₂ NNO	4.36		10.99	
(CH ₃ CH ₂) ₂ NNO ₂	4.91		11.70	
CH ₃ CH ₂ N=CHCH ₃	1.96		9.23	
CH ₃ CH ₃ NHCHO	4.45		7.88	
CH ₃ CH ₂ NHCH ₂ CHO	2.07		9.52	
(CH ₃ CH ₂) ₃ N	0.52		13.33	
(CH ₃ CH ₂) ₂ NCHO	4.21		11.35	
(CH ₃ CH ₂) ₂ NC(O)CH ₃	3.98		13.09	
(CH ₃ CH ₂) ₂ NCH ₂ CHO	3.19		13.16	
c(-CH ₂ CH ₂ OCH ₂ CH ₂ NH-)	1.56		9.28	
c(-CH ₂ CH ₂ OCH ₂ CH=N-)	1.12		8.80	
c(-CH ₂ CH ₂ OCH ₂ CH ₂ N(NO)-)	3.10		11.10	
c(-CH ₂ CH ₂ OCH ₂ CH ₂ N(NO ₂)-)	3.41		11.61	
c(-CH ₂ CH ₂ CH ₂ CH ₂ CH ₂ NH-)	0.83		10.37	
c(-CH ₂ CH ₂ CH ₂ CH ₂ CH=N-)	2.25		9.85	
c(-CH ₂ CH ₂ CH ₂ CH ₂ CH ₂ N(NO)-)	4.71		12.16	
c(-CH ₂ CH ₂ CH ₂ CH ₂ CH ₂ N(NO ₂)-)	4.95		12.63	
c(-CH ₂ CH ₂ CH ₂ CH ₂ NH-)	1.29		8.52	
c(-CH ₂ CH ₂ CH ₂ CH=N-)	2.23		8.04	
c(-CH ₂ CH ₂ CH ₂ CH ₂ N(NO)-)	5.06		10.22	
c(-CH ₂ CH ₂ CH ₂ CH ₂ N(NO ₂)-)	5.61		11.03	
c(-CH ₂ CH ₂ CH ₂ CH ₂ CH ₂ C(O)-)	3.42	2.87 ⁹⁸	10.86	

G. PTR-TOF-MS data validation

The generation of quantitative PTR-TOF-MS data is based on accurate peak area quantification and a conversion of obtained peak areas from normalized ion counts per second (ncps) into volume mixing ratios (ppbV). This conversion involves a calculation of specific ion-molecule capture rates using quantum chemically calculated molecular properties and corrections of instrumental effects (mass discrimination and detector saturation). This analysis procedure is complicated and prone to errors, and validation of the obtained results is highly desirable. It was beyond the scope and timescales of this project to conduct a formal and extensive method validation. A limited FT-IR dataset was, however, obtained to validate the PTR-TOF-MS data. FT-IR is an absolute method and quantification is fully independent from the PTR-TOF-MS calibration. In addition, the two instruments operate on different measurement principles: the FT-IR is based on optical spectroscopy while the PTR-TOF-MS is a mass spectrometry based method. FT-IR data of ethylamine, diethylamine, triethylamine and N-nitroso diethylamine were obtained from selected experiments, i.e. one experiment per compound from the spring campaign and one experiment per compound from the summer campaign. For data intercomparison, we only used the data obtained when the chamber was kept in the dark or from the initial phase of photo-oxidation when FT-IR spectral interferences from reaction products were small. The regression plots of the alkylamine data (PTR-TOF data vs. FT-IR data) are shown in **Error! Reference source not found..** The PTR-TOF derived ethylamine and diethylamine data were 26-34% higher than the FT-IR data. The discrepancy is slightly higher than the combined error of the two instruments, i.e. $\pm 15\%$ for the PTR-TOF-MS and $\pm 10\%$ for the FT-IR. The agreement is considered to be satisfactory, but any quantitative data interpretation based on PTR-TOF ethylamine and diethylamine data should consider a +30% uncertainty. The PTR-TOF derived triethylamine data are lower for the spring experiment (-8%) and higher for the summer experiment (+ 11%). The agreement is considered to be good.



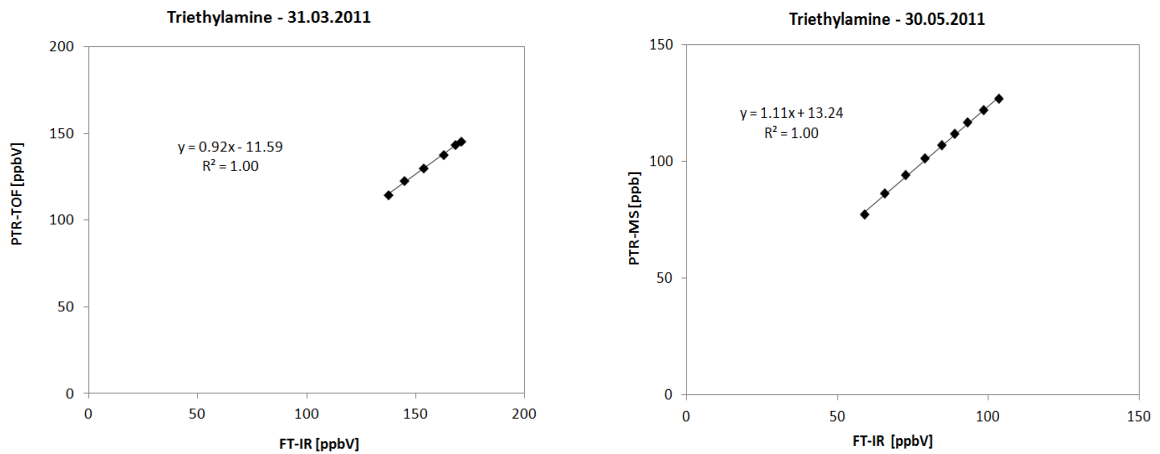


Figure G.1. Regression plots of alkylamine data (PTR-TOF-MS vs. FT-IR)

Error! Reference source not found. shows the mixing ratio of ammonia (NH_3) as measured by PTR-TOF-MS and FT-IR on 2011.6.03. The PTR-TOF underestimates NH_3 mixing ratios above 20 ppbV. The discrepancy is caused by saturation effects in the PTR-TOF detector. A correction via the ^{15}N -isotope at m/z 19 was not possible due to interferences from the large H_3O^+ signal. For quantitative analyses, the FT-IR data should be used. The same holds for formaldehyde (HCHO) data.

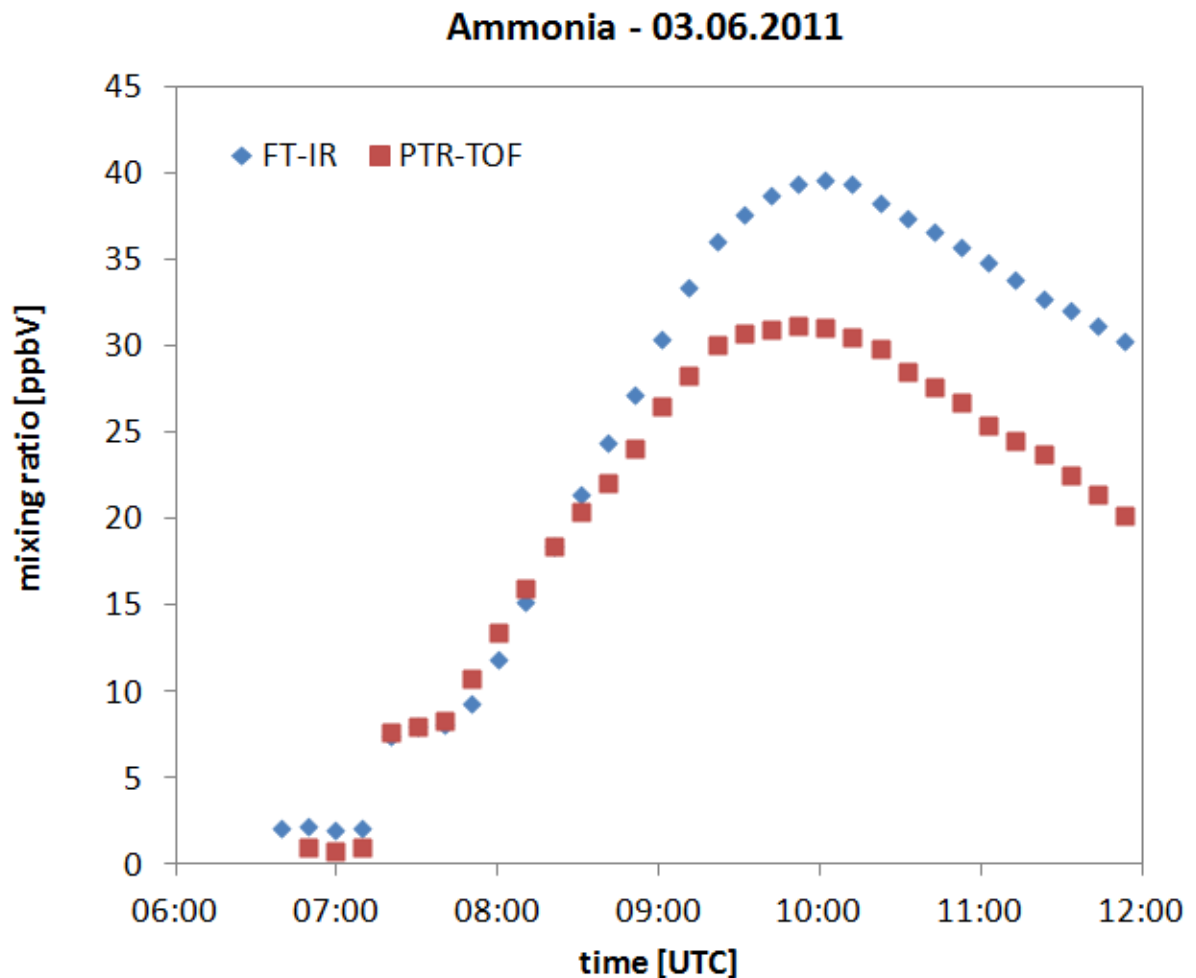


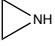
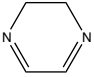
Figure G.2. Mixing ratio of ammonia (NH_3) as measured by PTR-TOF-MS and FT-IR on June 3

Only two FT-IR data points of N-nitroso diethylamine were obtained during the period when the chamber was closed. After chamber opening, the nitrosamine was rapidly lost. The obtained FT-IR data, the corresponding average of the PTR-TOF-MS data and the ratio of PTR-TOF-MS to FT-IR data is reported in **Error! Reference source not found.** For the spring experiment, the PTR-TOF data were lower (10-14%). Data were in excellent agreement (better than 1%) for the summer experiment.

01.04.2011	FT-IR	PTR-TOF	PTR-TOF/FT-IR
15:28:40	212.5	191.2	0.90
15:38:48	223.3	191.3	0.86
26.05.2011	FT-IR	PTR-TOF	PTR-TOF/FT-IR
15:14:24	155.6	157.0	1.01
15:24:33	156.1	156.8	1.00

Table G.1. N-nitroso diethylamine data as measured by PTR-TOF-MS an FT-IR on April 4 and May 26.

H. Chemical formulas, compound names, structures and CAS numbers

Formula	Structure	Name	CAS
CHNO	H-N=C=O	Isocyanic acid	75-13-8
CH ₂ O	H ₂ C=O	Formaldehyde	50-00-0
CH ₂ O ₂	HC(O)OH	Formic acid	64-18-6
CH ₄ O	CH ₃ OH	Methanol	67-56-1
C ₂ H ₃ N	CH ₃ CN	Acetonitrile	75-05-8
CH ₃ NO	H ₂ NCHO	Formamide	75-12-7
CH ₃ NO ₂	CH ₃ NO ₂	Nitromethane	75-52-5
CH ₄ N ₂ O ₂	CH ₃ NHNO ₂	<i>N</i> -Nitro methanamine	598-57-2
C ₂ H ₃ NO	CH ₂ =N-CHO	<i>N</i> -Methylene formamide	83442-29-9
C ₂ H ₃ NO	CH ₃ -N=C=O	Isocyanato methane	624-83-9
C ₂ H ₄ O	CH ₃ CHO	Acetaldehyde	75-07-0
C ₂ H ₄ O ₂	CH ₃ C(O)OH	Acetic acid	64-19-7
C ₂ H ₅ N	CH ₃ -N=CH ₂	<i>N</i> -Methylene methanamine	1761-67-7
C ₂ H ₅ N	CH ₃ -CH=NH (Z,E)	Ethanimine	20729-41-3
C ₂ H ₅ N	CH ₂ =CH-NH ₂	Ethenamine	593-67-9
C ₂ H ₅ N		Aziridine	151-56-4
C ₂ H ₅ NO	H ₂ NC(O)CH ₃	Acetamide	60-35-5
C ₂ H ₅ NO	CH ₃ NHCHO	<i>N</i> -Methyl formamide	123-39-7
C ₂ H ₅ NO	H ₂ NCH ₂ CHO	Amino acetaldehyde	6542-88-7
C ₂ H ₅ NO ₂	CH ₃ CH ₂ NO ₂	Nitroethane	79-24-3
C ₂ H ₆ N ₂ O	(CH ₃) ₂ N-NO	<i>N</i> -Methyl- <i>N</i> -nitroso methanamine	62-75-9
C ₂ H ₆ N ₂ O ₂	(CH ₃) ₂ N-NO ₂	<i>N</i> -Methyl- <i>N</i> -nitro methanamine	4164-28-7
C ₂ H ₆ N ₂ O ₂	CH ₃ CH ₂ NHNO ₂	<i>N</i> -Nitro ethanamine	19091-98-6
C ₂ H ₇ N	(CH ₃) ₂ NH	<i>N</i> -Methyl methanamine	124-40-3
C ₂ H ₇ N	CH ₃ CH ₂ NH ₂	Ethanamine	75-04-7
C ₃ H ₃ O	CH ₃ C(O)CH ₃	Acetone	67-64-1
C ₃ H ₅ NO ₂	CH ₃ C(O)NHCHO	<i>N</i> -Formyl acetamide	21163-79-1
C ₃ H ₇ N	CH ₃ -N=CHCH ₃	<i>N</i> -Ethylidene methanamine	6896-67-5
C ₃ H ₇ N	CH ₂ =N-CH ₂ CH ₃	<i>N</i> -Methylene ethanamine	43729-97-1
C ₃ H ₇ NO	CH ₃ NHC(O)CH ₃	<i>N</i> -Methyl acetamide	79-16-3
C ₄ H ₅ NO ₂	HOCH=CHN=CHCHO	(2-[(2-hydroxyethenyl)imino]-acetaldehyde)	151589-06-9
C ₄ H ₆ N		2,3-Dihydro pyrazine	93591-56-1

C ₄ H ₆ N		2,5-Dihydro pyrazine	5725-79-0
C ₄ H ₇ N		3,4-Dihydro-2H-pyrrole	5724-81-2
C ₄ H ₇ NO	CH ₃ C(O)-N=CHCH ₃ (Z,E)	<i>N</i> -Ethylidene acetamide	70603-39-3
C ₄ H ₇ NO		3,6-Dihydro-2H-1,4-oxazine	15601-95-3
C ₄ H ₇ NO ₂	CH ₃ C(O)NHC(O)CH ₃	<i>N</i> -Acetyl acetamide	625-77-4
C ₄ H ₇ NO ₂	CH ₃ C(O)NHCH ₂ CHO	<i>N</i> -(2-Oxoethyl) acetamide	64790-08-5
C ₄ H ₈ N		1,2,3,6-Tetrahydro pyrazine	77253-83-9
C ₄ H ₈ N ₂ O		1-Nitroso pyrrolidine	930-55-2
C ₄ H ₈ N ₂ O		2-Piperazinone	5625-67-2
C ₄ H ₈ N ₂ O ₂		1-Nitro pyrrolidine	3760-55-2
C ₄ H ₉ N	CH ₃ CH ₂ -N=CHCH ₃	<i>N</i> -Ethylidene ethanamine	1190-79-0
C ₄ H ₉ N		Pyrrolidine	123-75-1
C ₄ H ₉ NO	CH ₃ CH ₂ NHC(O)CH ₃	<i>N</i> -Ethyl acetamide	625-50-3
C ₄ H ₉ NO	CH ₃ CH ₂ NHCH ₂ CHO	2-(Ethylamino) acetaldehyde	1262944-47-7
C ₄ H ₉ N ₂ O		1-Nitroso piperazine	5632-47-3
C ₄ H ₉ N ₂ O ₂		1-Nitro piperazine	42499-41-2
C ₄ H ₁₀ N		Piperazine	110-85-0
C ₄ H ₁₀ N ₂ O	(CH ₃ CH ₂) ₂ N-NO	<i>N</i> -Ethyl- <i>N</i> -nitroso ethanamine	55-18-5
C ₄ H ₁₀ N ₂ O ₂	(CH ₃ CH ₂) ₂ N-NO ₂	<i>N</i> -Ethyl- <i>N</i> -nitro ethanamine	7119-92-8
C ₄ H ₁₁ N	(CH ₃ CH ₂) ₂ NH	<i>N</i> -Ethyl ethanamine	109-89-7
C ₅ H ₉ N		2,3,4,5-Tetrahydro pyridine	505-18-0
C ₅ H ₁₀ N ₂ O		1-Nitroso piperidine	100-75-4
C ₅ H ₁₀ N ₂ O ₂		1-Nitro piperidine	7119-94-0
C ₅ H ₁₁ NO	(CH ₃ CH ₂) ₂ NCHO	<i>N,N</i> -Diethyl formamide	617-84-5
C ₆ H ₁₃ NO	(CH ₃ CH ₂) ₂ NC(O)CH ₃	<i>N,N</i> -Diethyl acetamide	685-91-6
C ₆ H ₁₃ NO	(CH ₃ CH ₂) ₂ NCH ₂ CHO	2-(diethylamino) acetaldehyde	32314-21-9
C ₆ H ₁₅ N	(CH ₃ CH ₂) ₃ N	<i>N,N</i> -Diethyl ethanamine	121-44-8

ISBN 978-82-992954-7-5